



**Universitat Ramon Llull**

## **TESI DOCTORAL**

Títol	Cardiomyogenic potentiality of somatic and stem cells when cultured in the three-dimensional peptide scaffold RAD16-I
Realitzada per	Verònica Puig Sanvicens
en el Centre	Institut Químic de Sarrià – School of Engineering
i en el Departament	Bioenginyeria
Dirigida per	Dr. Carlos E. Semino Dra. Nicole I. zur Nieden

*C. Claravall, 1-3  
08022 Barcelona  
Tel. 936 022 200  
Fax 936 022 249  
E-mail: [urisc@sec.url.es](mailto:urisc@sec.url.es)  
[www.url.es](http://www.url.es)*



**Als meus pares,  
Al Carles i  
Al Rory**





*Genius is one percent inspiration, ninety-nine percent perspiration.*

*Thomas Alva Edison (1847 - 1931)*

*El geni és u percent inspiració, noranta-nou percent perspiració.*

*Thomas Alva Edison (1847 - 1931)*



## ACKNOWLEDGEMENTS

Arribat aquest punt, només queda fer balanç dels últims quatre anys. La Tesis Doctoral no ha estat un camí fàcil i com sempre dic, no ho recomano però ho tornaria a fer. Com en qualsevol experiència en la vida, hi han hagut bons i mals moments, alegries i enrabiades, recompenses i frustracions. Ha estat una etapa que m'ha fet créixer immensament, tant personal com professionalment, i he après a mirar endavant quan tot semblava negre. Afortunadament, he estat sempre envoltada de persones magnífiques que m'han acompanyat al llarg d'aquest camí i és a tota aquesta gent que vull esmentar seguidament.

Primer de tot, vull agrair al M. I. Govern d'Andorra i a la Fundació Crèdit Andorrà per la beca (BTC2009/2010-0010-AND) que se'm va concedir al 2010 per fer realitat un somni. Res va ser fàcil des d'un principi i valoro el suport rebut per fer front als entrebancs causats per persones indesitjables. Inclús d'aquella angoixa generada aleshores en treure alguna cosa positiva, una bonica amistat amb l'Helena Solé a qui vull donar les gràcies per la seva empatia i per tota l'ajuda que m'ha ofert sempre.

Al meu co-director de Tesis, Dr. Carlos Semino, li agraeixo haver-me donat l'oportunitat de formar part del seu equip. *Gracias Carlos por introducirme a la investigación, por guiarme en los proyectos, por compartir ideas, por darme consejos y sobretodo por creer en mí.* Vull aprofitar aquest paràgraf per incloure a totes les teixidores en els agraïments: Mire, Patri, Cris, Núria, Lourdes, Caterina, Desi... i Tere. *A ti te dejo para el final como todo lo bueno, gracias por ser como una hermana mayor.*

*To the other co-advisor of my Thesis, Dr. Nicole zur Nieden, I would like to thank you for welcoming me to UCR, for all your friendly support and for making me feel like part of your family. I sincerely appreciate your mentoring, scientific and personal. I also want to acknowledge my colleagues and lab mates for helping me to make myself at home in NzN's lab: Darcie, Tiffany, Devon, Ivann, Beatriz, and especially Dorota, Kevin and Nicole S.*

Aquesta Tesis no hauria estat possible sense un dels pilars fonamentals dels projectes: les cèl·lules. Gràcies al Dr. Antoni Bayés-Genís i al seu equip de l'IGTP de Can Ruti per les cèl·lules porcines i per acollir-me càlidament en el seu laboratori: Aida, Santi, Carol S. i especialment a la Cris i a la Carol G. per la seva empenta i

bon humor. *Quisiera dar las gracias también al Dr. Jesús Otero del Hospital Universitario Central de Asturias en Oviedo por proporcionarnos los fibroblastos humanos. In addition, I am grateful to Dr. Duncan Chee Liew for generously providing the hiPSCs. Thank you as well to the Core Facilities (Stem Cell and Genomics) of the UCR for letting me use their equipments and to Dr. Emma Wilson and Kathryn for letting me use the cytospin.*

A més a més, vull agrair a molta altra gent que m'ha envoltat al llarg dels últims quatre anys i ha fet la meva estada a l'IQS divertida i inoblidable. Gràcies als meus companys de Biomaterials per l'alegria i el bon ambient generat al laboratori: Oscar, Joan, Pri, Pam, Greg, Jose, Víctor, Nathaly i Djamila. Gràcies també als nostres veïns de Bioquímica per ser sempre servicials i mostrar companyerisme: Magda, Carlitos, Patri, Xevi, Victòria, i molts altres. Voldria destacar al meu bio-friki preferit, l'Albert G. amb qui vam compartir dinars memorables al Mero. A la Mar, gràcies per moments de riure sense parar que feien els dies durs més amés. També aprecio els somriures de molta altra gent de l'IQS: Santi N., Merche, els del bar, Iolanda i altres que segurament oblidó.

Em reservo aquestes línies per donar les gràcies als meus amics, que m'han fet costat i m'han donat dosis d'alegria i d'optimisme. Gràcies a les meves estimades Meninas (Ana, Carol, Lúdia, Vane i Vir) per ser la meva segona família. Gràcies a la Rosa i a l'Anto per mantenir una fidel amistat. Gràcies al Benja per ser honest, divertit i una bellíssima persona. Gràcies a les nenes biòlogues pels brain-stormings sobre la vida: Yara, Alba i Cris. *Thank you to all my friends in California, "the Internationals", I am so grateful to have you all in my daily basis: Laetitia, Jorge, Patty, Adam, Alberto, Carol, Elizabeth, Grette, Dani, Alba, Anita, Maureen, Brad, Diana, Polo, Marco, Rubén. Thank you to Chantal and Kassy for helping me to immerse myself in the real American adventure and for being my perfect roommates. Gracias a Maria A. por ser maravillosa!*

Per acabar, he volgut guardar les paraules més emotives i dolces per la meva família. No s'ha descrit la paraula que defineixi lo immensament agraïda que estic als meus pares, Feli i Víctor. El títol de Doctor és compartit entre els tres. Gràcies per confiar en mi i per donar-me llibertat per convertir-me en qui sóc, tot i la tristesa d'estar separats. Vull donar les gràcies al Carles per ser el meu confident i per ser un germà protector i orgullós de mi. Em falta agrair a les meves àvies, tieta, i altres familiars el seu suport incondicional. *Finally, I owe many thanks to Rory. Thank you*

*babes for being my best friend, mentor, life partner, soul mate, English teacher, and reviewer. I feel very lucky to have met you and I cannot wait to start the next chapter of my life with you. Thank you also to my sweet Irish family for making me feel like a Mc Donnell.*



## ABSTRACT

Cardiac failure is the primary cause of mortality throughout the world. One of the leading causes of heart failure is myocardial infarction, which results from a reduced flow of blood to a part of the heart. This leads to cardiomyocyte death and myocardial necrosis. In the past decade, various strategies for cardiac reparative medicine have been investigated, from tissue engineering to stem cell-based therapy. Herein, we characterized the cardiac potential of different cell types cultured in three-dimensional (3D) scaffolds based on the peptide hydrogel RAD16-I. Firstly, we studied the mesenchymal potential acquisition of human Normal Dermal Fibroblasts (hNDFs) in 3D cultures and further commitment into adipogenic and cardiogenic lineages. We suggest that only hNDFs cultured in RAD16-I hydrogels undergo a mesenchymal potentiation. Cells spontaneously acquired mesenchymal stem cell-like properties whereas they required induction media to differentiate into adipogenic- and cardiogenic-like lineages. Secondly, we compared the degree of cardiac commitment of human induced Pluripotent Stem Cells (hiPSCs) when cultured in 2D *versus* 3D and the effect of ascorbic acid (AA), which has been proven to promote cardiac differentiation, on the process. In fact, AA seemed to accelerate and improve the cardiac commitment of hiPSCs in 2D cultures. Results suggested that hiPSCs in 3D cultures displayed an increased level of differentiation and acquired  $10^5$ -fold more cardiogenic potential than cells cultured in 2D. Thirdly, we designed a cardiac patch based on 3D cultures of adult porcine Mediastinal Adipose Tissue Progenitor Cells (pMATPCs) injected into natural matrices (decellularized human pericardium). We implanted the myocardial bioprosthesis *in vivo* and determined that the bioscaffold supported cell migration and regeneration into the infarcted area in swine. In summary, we studied the cardiogenic potential of adult somatic cells (hNDFs), adult stem cells (pMATPCs) and pluripotent stem cells (hiPSCs) in 3D cultures based on RAD16-I hydrogels for potential future applications in the treatment of heart disease.





## RESUM

Les malalties cardiovasculars són una de les majors causes de mortalitat a escala mundial. L'infart de miocardi és el principal responsable de les cardiopaties isquèmiques. La irrigació sanguínia al cor es veu bloquejada degut a una oclusió en un capil·lar sanguini provocant mort cel·lular massiva que genera una zona miocardiaca necròtica. En la última dècada, la medicina cardíaca regenerativa s'ha focalitzat en estratègies fonamentades en l'enginyeria de teixits i la teràpia cel·lular basada en cèl·lules mare. En aquest treball, hem caracteritzat el potencial cardíac de diferents tipus cel·lulars cultivats en bastides tri-dimensionals (3D) generades a partir de l'hidrogel peptídic RAD16-I. En primer lloc, hem estudiat l'adquisició de potencial mesenquimàtic de fibroblasts humans de dermis (hNDFs) en cultius 3D i la seva diferenciació subseqüent a llinatges adipogènic i cardiogènic. Únicament els hNDFs cultivats en hidrogels de RAD16-I adquireixen una potenciació mesenquimàtica. Les cèl·lules adopten espontàniament propietats semblants a les cèl·lules mare mesenquimàtiques mentre que la diferenciació a adipogènesis i cardiogènesis requereix medi d'inducció. En segon lloc, hem comparat el grau de diferenciació cardíaca de cèl·lules mare humanes pluripotents induïdes (hiPSCs) cultivades en ambients 2D *versus* 3D i hem avaluat l'efecte de l'àcid ascòrbic (AA) en el procés. En el nostre treball i com ja s'havia demostrat en publicacions prèvies, l'AA va resultar accelerar i millorar la diferenciació cardíaca de hiPSCs en cultius 2D. A més, els resultats presentats suggereixen que les hiPSCs cultivades en 3D augmenten el seu grau de diferenciació i adquireixen un potencial cardiogènic  $10^5$  vegades més elevat que en els cultius 2D. En tercer lloc, hem dissenyat un pegat cardíac basat en cultius 3D de cèl·lules adultes porcines progenitores del teixit adipós del mediastí (pMATPCs) injectats en matrius naturals (pericardi humà descel·lularitzat). Hem implantat la bio-pròtesis miocardiaca *in vivo* i hem determinat que la bio-bastida afavoreix la migració cel·lular i la regeneració de la zona infartada en el model porcí. En conclusió, hem analitzat el potencial cardiogènic de cèl·lules adultes somàtiques (hNDFs), cèl·lules mare adultes (pMATPCs) i cèl·lules mare pluripotents (hiPSCs) en cultius 3D basats en hidrogels de RAD16-I per a futures aplicacions en el tractament de malalties cardíques.



## RESUMEN

Las enfermedades cardiovasculares son una de las mayores causas de mortalidad a escala mundial. El infarto de miocardio es el principal responsable de las cardiopatías isquémicas. La irrigación sanguínea al corazón se ve bloqueada debido a una oclusión en un capilar sanguíneo provocando muerte celular masiva que genera una zona miocárdica necrótica. En la última década, la medicina cardíaca regenerativa se ha focalizado en estrategias fundamentadas en la ingeniería de tejidos y la terapia celular basada en células madre. Es este trabajo, hemos caracterizado el potencial cardíaco de distintos tipos celulares cultivados en andamios tridimensionales (3D) generados a partir del hidrogel peptídico RAD16-I. En primer lugar, hemos estudiado la adquisición de potencial mesenquimático de fibroblastos humanos de dermis (hNDFs) en cultivos 3D y su diferenciación subsecuente a linajes adipogénico y cardiogénico. Únicamente los hNDFs cultivados en hidrogeles de RAD16-I adquieren una potenciación mesenquimática. Las células adoptan espontáneamente propiedades parecidas a las células madre mesenquimáticas mientras que la diferenciación a adipogénesis y cardiogénesis requiere medio de inducción. En segundo lugar, hemos comparado el grado de diferenciación cardíaca de células madre humanas pluripotentes inducidas (hiPSCs) cultivadas en ambientes 2D *versus* 3D y hemos evaluado el efecto del ácido ascórbico (AA) en el proceso. En nuestro trabajo y como ya se había demostrado en publicaciones previas, el AA resultó acelerar y mejorar la diferenciación cardíaca de hiPSCs en cultivos 2D. A demás, los resultados presentados sugieren que las hiPSCs cultivadas en 3D aumentan su grado de diferenciación y adquieren un potencial cardiogénico  $10^5$  veces más elevado que en los cultivos 2D. En tercer lugar, hemos diseñado un parche cardíaco basado en cultivos 3D de células adultas porcinas progenitoras del tejido adiposo del mediastino (pMATPCs) inyectados en matrices naturales (pericardio humano descelularizado). Hemos implantado la bio-prótesis miocárdica *in vivo* y hemos determinado que el bio-andamio favorece la migración celular y la regeneración de la zona infartada en el modelo porcino. En conclusión, hemos analizado el potencial cardiogénico de células adultas somáticas (hNDFs), células madre adultas (pMATPCs) y células madre pluripotentes (hiPSCs) en cultivos 3D basados en hidrogeles de RAD16-I para futuras aplicaciones en el tratamiento de enfermedades cardíacas.



# TABLE OF CONTENTS

<b>ACKNOWLEDGEMENTS</b> .....	vii
<b>ABSTRACT</b> .....	xi
<b>RESUM</b> .....	xiii
<b>RESUMEN</b> .....	xv
<b>TABLE OF CONTENTS</b> .....	xvii
<b>LIST OF FIGURES</b> .....	xxi
<b>LIST OF TABLES</b> .....	xxiii
<b>LIST OF ABBREVIATIONS</b> .....	xxv
<b>CHAPTER 1. INTRODUCTION</b> .....	<b>1</b>
1.1. <i>Cardiac tissue engineering</i> .....	3
1.2. <i>Myocardial infarction and therapeutic perspectives: a worldwide health concern</i> .....	4
1.3. <i>Three-dimensional cultures: scaffolds used to mimic an in vivo extracellular matrix</i> .....	7
1.4. <i>Self-assembling peptides, a promising strategy for cell and drug delivery</i> .....	10
1.5. <i>Cells full of hope</i> .....	14
1.6. <i>Fibroblasts and Reprogramming, a route to personalized cell therapy</i> .....	18
1.7. <i>Summary of the Thesis</i> .....	21
1.8. <i>Objectives</i> .....	22
1.9. <i>References</i> .....	22
<b>CHAPTER 2. MATERIALS AND METHODS</b> .....	<b>33</b>
2.1. <i>2D Culture of human Normal Dermal Fibroblasts (hNDFs)</i> .....	35
2.2. <i>2D Culture of human induced Pluripotent Stem Cells (hiPSCs) Riv9</i> ...	36
2.3. <i>3D Culture of human Normal Dermal Fibroblasts (hNDFs) in RAD16-I</i> .....	37
2.4. <i>3D Culture of human Embryonic Stem Cells (hESCs) H9 in RAD16-I</i> .....	38
2.5. <i>3D Culture of human induced Pluripotent Stem Cells (hiPSCs) Riv9 in RAD16-I</i> .....	40

2.6.	<i>3D Culture of porcine Mediastinal Adipose Tissue Progenitor Cells (pMATPCs) in RAD16-I</i>	40
2.7.	<i>3D Culture of human Normal Dermal Fibroblasts (hNDFs) in Collagen I</i>	41
2.8.	<i>DAPI and Phalloidin staining</i>	42
2.9.	<i>Live/Dead assay</i>	43
2.9.1.	<i>Human Normal Dermal Fibroblasts (hNDFs)</i>	43
2.9.2.	<i>Human Embryonic Stem Cells (hESCs) H9 and human induced Pluripotent Stem Cells (hiPSCs) Riv9</i>	43
2.10.	<i>Differentiation of human Normal Dermal Fibroblasts (hNDFs) in 3D cultures</i>	44
2.10.1.	<i>Adipogenesis induction</i>	44
2.10.2.	<i>Cardiogenesis induction</i>	45
2.11.	<i>Cardiogenic differentiation of human induced Pluripotent Stem Cells (hiPSCs) Riv9</i>	45
2.11.1.	<i>2D cultures</i>	45
2.11.2.	<i>3D cultures</i>	46
2.12.	<i>Human pericardium decellularization</i>	46
2.13.	<i>Self-assembling peptide scaffold RAD16-I combined to NanoGold</i>	47
2.14.	<i>Porcine cardiac smart patch</i>	47
2.15.	<i>Immunocytochemistry (ICC)</i>	48
2.15.1.	<i>Fluorescence-tag immunocytochemistry</i>	48
2.15.2.	<i>Enzyme-tag immunocytochemistry</i>	49
2.16.	<i>Nile red staining</i>	51
2.17.	<i>Congo red staining</i>	51
2.18.	<i>Design of primers</i>	51
2.19.	<i>RNA extraction</i>	53
2.19.1.	<i>Human Normal Dermal Fibroblasts (hNDFs)</i>	54
2.19.2.	<i>Human Embryonic Stem Cells (hESCs) H9 and human induced Pluripotent Stem Cells (hiPSCs) Riv9 in 2D cultures</i>	54
2.19.3.	<i>Human induced Pluripotent Stem Cells (hiPSCs) Riv9 in 3D cultures</i>	55
2.20.	<i>cDNA synthesis</i>	56
2.20.1.	<i>Human Normal Dermal Fibroblasts (hNDFs)</i>	56
2.20.2.	<i>Human Embryonic Stem Cells (hESCs) H9 and human induced Pluripotent Stem Cells (hiPSCs) Riv9</i>	56

2.21.	<i>Polymerase Chain Reaction (PCR)</i> .....	57
2.21.1.	<i>Human Normal Dermal Fibroblasts (hNDFs)</i> .....	57
2.21.2.	<i>Human Embryonic Stem Cells (hESCs) H9 and human induced Pluripotent Stem Cells (hiPSCs) Riv9</i> .....	57
2.22.	<i>Agarose gel electrophoresis</i> .....	58
2.22.1.	<i>Agarose gel electrophoresis preparation</i> .....	58
2.22.2.	<i>Samples preparation</i> .....	59
2.23.	<i>Quantitative Polymerase Chain Reaction (qPCR) of human Embryonic Stem Cells (hESCs) H9 and human induced Pluripotent Stem Cells (hiPSCs) Riv9</i> .....	59
2.24.	<i>Cytospin</i> .....	60
2.25.	<i>References</i> .....	61

**CHAPTER 3. MESENCHYMAL POTENTIAL OF HUMAN NORMAL DERMAL  
FIBROBLASTS IN THE THREE-DIMENSIONAL PEPTIDE SCAFFOLD RAD16-I .... 63**

3.1.	<i>Introduction</i> .....	65
3.2.	<i>Hypothesis and specific aims</i> .....	65
3.3.	<i>Results</i> .....	66
3.3.1.	<i>Confirmation of the cellular phenotype of hNDFs in 2D cultures</i> .....	66
3.3.2.	<i>Mesenchymal phenotype acquisition of hNDFs cultured in RAD16-I and Collagen I scaffolds</i> .....	68
3.3.3.	<i>Study of the effect of fetal bovine serum on the expression of early differentiation markers of hNDFs cultured in RAD16-I</i> .....	72
3.3.4.	<i>Adipogenic lineage commitment of hNDFs cultured in RAD16-I</i> .....	76
3.3.5.	<i>Cardiogenic lineage commitment of hNDFs cultured in RAD16-I</i> .....	79
3.4.	<i>Discussion</i> .....	84
3.5.	<i>Concluding remarks</i> .....	90
3.6.	<i>References</i> .....	91

**CHAPTER 4. COMPARISON OF THE CARDIAC DIFFERENTIATION POTENTIAL OF HUMAN INDUCED PLURIPOTENT STEM CELLS IN 2D AND IN 3D CULTURES BASED ON RAD16-I HYDROGELS AND THE EFFECT OF ASCORBIC ACID ON CARIOGENESIS ..... 95**

4.1. *Introduction* ..... 97

4.2. *Hypothesis and specific aims* ..... 99

4.3. *Results* ..... 99

4.3.1. *Cardiac induction of hiPSCs in 2D cultures and the effect of AA on cardiogenesis* ..... 99

4.3.2. *Setting up the 3D culture protocol based on RAD16-I with hESCs* ..... 108

4.3.3. *Cardiac induction of hiPSCs cultured in RAD16-I and the effect of AA on cardiogenesis* ..... 111

4.4. *Discussion* ..... 119

4.5. *Concluding remarks* ..... 125

4.6. *References* ..... 126

**CHAPTER 5. DEVELOPMENT OF BIOLOGICAL SCAFFOLDS FOR POST-INFARCTION SCAR REPAIR ..... 129**

5.1. *Introduction* ..... 131

5.2. *Hypothesis and specific aims* ..... 132

5.3. *Results* ..... 133

5.3.1. *Cardiogenic potential of pMATPCs in 2D and 3D cultures based on RAD16-I* ..... 133

5.3.2. *Preparation of the biological macro-scaffold based on decellularized human pericardium* ..... 134

5.3.3. *Tailoring of RAD16-I with NanoGold particles* ..... 137

5.3.4. *Implant in vivo of the cardiac smart patch into swine* ..... 138

5.4. *Discussion* ..... 141

5.5. *Concluding remarks* ..... 143

5.6. *References* ..... 144

**CONCLUSIONS ..... 147**

**APPENDIX ..... 151**



## LIST OF FIGURES

<b>Figure 1.</b> Time line of crucial discoveries in cardiac TE .....	4
<b>Figure 2.</b> Strategies applied for MI treatment .....	7
<b>Figure 3.</b> Amino acid sequence and structural model of a RAD16-I nanofiber .....	12
<b>Figure 4.</b> Scheme of the patient-specific cardiomyocytes generation .....	17
<b>Figure 5.</b> Table summarizing the SWOT of different stem cell types used in cardiac TE .....	18
<b>Figure 6.</b> The three routes to regeneration .....	21
<b>Figure 7.</b> DAPI and Phalloidin staining of hNDFs cultured in 2D with control medium .....	66
<b>Figure 8.</b> Immunostaining for mesenchymal, cardiac progenitor and mature cardiomyocyte markers of hNDFs cultured in 2D with control medium .....	68
<b>Figure 9.</b> Macroscopic observation of the construct contraction of hNDFs cultured in different 3D conditions .....	70
<b>Figure 10.</b> Scheme representing the construct contraction and the dome-shape of 3D cultures based on RAD16-I .....	70
<b>Figure 11.</b> Microscopic observation of 3D cultures of hNDFs embedded in Collagen I and RAD16-I at day 5 and 10 .....	71
<b>Figure 12.</b> Immunostaining for mesenchymal markers of hNDFs cultured in RAD16-I <i>versus</i> Collagen I for 5 and 10 days in control medium .....	72
<b>Figure 13.</b> Microscopic observation of hNDFs cultured in RAD16-I for 5 and 10 days and in 2D .....	73
<b>Figure 14.</b> Live/Dead assay of hNDFs cultured in RAD16-I for 20 days with different media .....	74
<b>Figure 15.</b> DAPI and Phalloidin staining of hNDFs cultured in RAD16-I for 20 days with different media ...	75
<b>Figure 16.</b> Immunostaining for mesenchymal markers of hNDFs cultured in RAD16-I for 5 and 10 days with control and defined media .....	76
<b>Figure 17.</b> Stereoscopic and microscopic observation of hNDFs cultured for 20 days in RAD16-I with control and adipogenic media .....	77
<b>Figure 18.</b> DAPI and Nile red staining of hNDFs cultured in 2D and in RAD16-I for 20 days with control and adipogenic media .....	78
<b>Figure 19.</b> Agarose gel of specific bands for PPAR $\gamma$ amplified with PCR from hNDFs cultured in 2D and in RAD16-I for 20 days with control and adipogenic media .....	79
<b>Figure 20.</b> Stereoscopic and microscopic observation of hNDFs cultured in RAD16-I with control and cardiogenic media for 20 days .....	80
<b>Figure 21.</b> Agarose gel of specific bands for cardiac progenitor and mature cardiomyocyte genes amplified with PCR from hNDFs cultured in 2D and in RAD16-I for 20 days with control and cardiogenic media .....	82
<b>Figure 22.</b> Immunostaining for cardiac progenitor and mature cardiomyocyte proteins of hNDFs cultured in RAD16-I with control and cardiogenic media for 20 days .....	83
<b>Figure 23.</b> Diagram representing sequential steps in the cardiac differentiation of pluripotent stem cells as hiPSCs .....	98
<b>Figure 24.</b> Schematic representation of the induced cardiac differentiation protocol used with hiPSCs in 2D cultures .....	100
<b>Figure 25.</b> Microscopic observation of hiPSCs at confluence in 2D cultures .....	100
<b>Figure 26.</b> Cellular morphology of hiPSCs differentiated in 2D cultures into cardiac lineage in a medium with and without AA over 25 days .....	102

<b>Figure 27.</b> Agarose gel showing the PCR amplicons of RNA extracts from hiPSCs cultured with and without AA from day 0 to 25 .....	104
<b>Figure 28.</b> Quantitative PCR analysis for pluripotent, early differentiation, cardiac progenitor and mature cardiomyocyte markers of hiPSCs cultured in 2D with and without AA for 25 days .....	106
<b>Figure 29.</b> Immunostaining with FITC-conjugated secondary antibodies of hiPSCs cultured in 2D with and without AA .....	107
<b>Figure 30.</b> Comparison of the number of functional cardiomyocytes (beating clusters) obtained from hiPSCs with and without AA in 2D .....	108
<b>Figure 31.</b> Observation under the phase microscope of 3D cultures of hESCs embedded in RAD16-I at three different cell densities for 1 and 3 days .....	109
<b>Figure 32.</b> Viability assay of hESCs cultured in 3D at three different cell concentrations for 1 and 3 days .....	110
<b>Figure 33.</b> 3D constructs of hESCs disrupted with accutase, collagenase IV and trypsin .....	111
<b>Figure 34.</b> Observation under the phase microscope of hiPSCs cultured in RAD16-I with and without AA for 20 days .....	112
<b>Figure 35.</b> Live/Dead assay of hiPSCs cultured in 3D for 20 days with and without AA .....	113
<b>Figure 36.</b> DAPI/Phalloidin staining of hiPSCs cultured in 3D with and without AA for 20 days .....	114
<b>Figure 37.</b> Quantitative PCR for pluripotent, early differentiation and cardiac progenitor markers showing gene expression in 3D cultures of hiPSCs with and without AA .....	115
<b>Figure 38.</b> Immunostaining of hiPSCs in 3D cultured with and without AA for 3 and 10 days .....	117
<b>Figure 39.</b> Immunostaining with HRP-conjugated secondary antibodies of hiPSCs cultured in 3D for 15 days with and without AA .....	117
<b>Figure 40.</b> Fluorescent immunocytochemistry of cytospin samples of hiPSCs cultured in 3D with and without AA .....	118
<b>Figure 41.</b> Immunocytochemistry for mesenchymal and mature cardiomyocyte markers of pMATPCs cultured in RAD16-I for 7 days .....	134
<b>Figure 42.</b> Macroscopic morphology of lyophilized human pericardia under stereoscope .....	135
<b>Figure 43.</b> Congo red staining of decellularized and lyophilized human pericardia .....	136
<b>Figure 44.</b> DAPI staining of decellularized and lyophilized human pericardia .....	136
<b>Figure 45.</b> Scanning Electron Microscopy photographs of human decellularized pericardium .....	137
<b>Figure 46.</b> Scheme of Biotin-RAD16-I binding to Streptavidin-NanoGold .....	138
<b>Figure 47.</b> Myocardial bioprosthesis assembling and implantation .....	140
<b>Figure 48.</b> Macroscopic appearance and histological examination of myocardial bioprostheses in porcine hearts .....	141

## LIST OF TABLES

<b>Table 1.</b> List of primary and secondary antibodies used in this Thesis .....	50
<b>Table 2.</b> List of designed primers used in this Thesis .....	53



## LIST OF ABBREVIATIONS

2D	Two-dimensional	END2	visceral endoderm-like cell
3D	Three-dimensional		
αMEM	alpha Modification of Eagle's Medium	EthD-1	Ethidium Homodimer-1
AA	Ascorbic Acid	FACS	Fluorescent Activated Cell Sorting
ACTC1	Actin, alpha Cardiac Muscle 1	FBS	Fetal Bovine Serum
BB	Blocking Buffer	FITC	Fluorescein Isothiocyanate
BSA	Bovine Serum Albumin	GF	Growth Factor
Calcein AM	Calcein Acetoxymethyl	GFP	Green Fluorescent Protein
cDNA	complementary DNA		
CDS	Coding DNA Sequence	hESC	human Embryonic Stem Cell
CHF	Congestive Heart Failure		
CM	Cardiomyocyte	hiPSC	human induced Pluripotent Stem Cell
CPC	Cardiac Progenitor Cell		
C <sub>T</sub>	Threshold Cycle	hNDF	human Normal Dermal Fibroblast
Cx43	Connexin 43		
DAB	3,3-diaminobenzidine	HRP	Horseradish Peroxidase
DAPI	4'-6-diamidino-2-phenylindole	ICC	Immunocytochemistry
DEPC	Diethylpyrocarbonate	IgG	Immunoglobulin G
DMEM	Dulbecco's Modified Eagle's Medium	IGTP	Institut Germans Trias i Pujol
DMSO	Dimethyl Sulfoxide	IQS	Institut Químic de Sarrià
DNA	Deoxyribonucleic Acid	LV	Left Ventricular
dNTP	Deoxynucleotide Triphosphate	MACS	Magnetic Affinity Cell Sorting
EB	Embryoid Body	MCSC	Marrow-derived Cardiac Stem Cell
ECM	Extracellular Matrix	MEF	Mouse Embryonic Fibroblast
EDTA	Ethylenediamine-tetraacetic Acid	mESC	mouse Embryonic Stem Cell
EIS	Electrochemical Impedance Spectroscopy	MHC/MYH	Myosin Heavy Chain
		MI	Myocardial Infarction

mRFP	monomeric Red Fluorescent Protein	RGD	Arginine-Glycine- Aspartic Acid
mRNA	messenger Ribonucleic Acid	RI RNA	ROCK Inhibitor Ribonucleic Acid
MSC	Mesenchymal Stem Cell	ROCK	Rho-associated protein Kinase
NCBI	National Center for Biotechnology Information	RT RT	Room Temperature Reverse Transcriptase
NEAA	Non-Essential Amino Acids	SC SEM	Stem Cell Scanning Electron Microscopy
NIPAAm	N-isopropylacrylamide		
OD	Optical Density	SYBR Green	DNA intercalating green fluorescent dye
ON	Overnight		
PBS	Phosphate Buffered Saline	TAE TE	Tris-Acetate-EDTA Tissue Engineering
PCR	Polymerase Chain Reaction	TF Tm	Transcription Factor melting Temperature
PDGF	Platelet-Derived Growth Factor	TRITC	Tetramethylrhodamine Isothiocyanate
PEG	Polyethylene Glycol	Trop I/cTnI	Troponin I
PFA	Paraformaldehyde	UPC	Universitat Politècnica de Catalunya
PGA	Polyglycolic Acid		
Ph	Phase contrast		
PLA	Polylactic Acid		
PLG	Poly lactide-co-glycolide		
PLGA	Poly lactic-co-glycolic Acid		
PLLA	Poly-L-lactic Acid		
pMATPC	porcine Mediastinal Adipose Tissue Progenitor Cell		
PPAR $\gamma$	Peroxisome Proliferator- Activated Receptor $\gamma$		
qPCR	quantitative Polymerase Chain Reaction		
RAD	Arginine-Alanine- Aspartic Acid		

## Chapter 1: Introduction





## CHAPTER 1. INTRODUCTION

### 1.1. *Cardiac tissue engineering*

Tissue Engineering (TE) combines biomaterials science with cell biology. The European Commission on Health and Consumer Protection defined TE as “the persuasion of the body to heal itself through the delivery, to the appropriate site, independently or in synergy, of cells, biomolecules and supporting structures”<sup>1</sup>. Thus, it has been shown to be a powerful tool to replace or rebuild damaged tissues and organs<sup>2</sup>. This Thesis focuses on cardiac TE that aims to restore myocardial tissue. Indeed, heart failure is one of the main causes of mortality throughout the world. In the past decade, various strategies for cardiac reparative medicine have been investigated, from TE to stem cell-based therapy<sup>3</sup> (**Figure 1**). There are primarily four mechanisms of myocardial regeneration in TE: induction or stimulation of endogenous cardiac progenitor cells; transplantation of isolated exogenous cells; myocardial implantation of tissue created *ex vivo*; and design of biomaterials<sup>1</sup>. Cardiac TE represents a promising pathway to apply fundamental myocardial biology to *in vitro* models of human cardiac tissue, with the goal of treating ischemic heart diseases. The majority of such models are based on a variety of cell sources pre-seeded on engineered scaffolds allowing cell maturation *in vitro*. In addition, cell-based cardiac grafts have been surgically attached to the damaged myocardium<sup>4</sup>. Recently, approaches have focused on *in vitro* engineered myocardial tissue (cultured *in vitro* and then implanted *in vivo*) and *in situ* engineered myocardial tissue (injected directly into the myocardium)<sup>5</sup>. The critical aspects that cardiac TE considers are: cell anchorage in the scaffold; diffusion of nutrients and other small molecules; vascular integration; cellular organization; and tissue vascularization of the engineered tissue<sup>6</sup>. Furthermore, there are other techniques that do not use pre-formed scaffolds but instead use mixtures of cells and liquid matrices to create engineered heart tissue<sup>7-9</sup>. Indeed, the methods are unlimited whereas there is a common goal: restore damaged cardiac tissue. This chapter introduces the key challenges in cardiac TE<sup>10</sup> that are the basis of the research presented: cardiac diseases to be treated; biomimetic platforms; 3D cultures establishing correspondence between *in vitro* and *in vivo* studies; cells used as “tissue engineers”; and reprogramming for personalized cellular therapy.

## INTRODUCTION

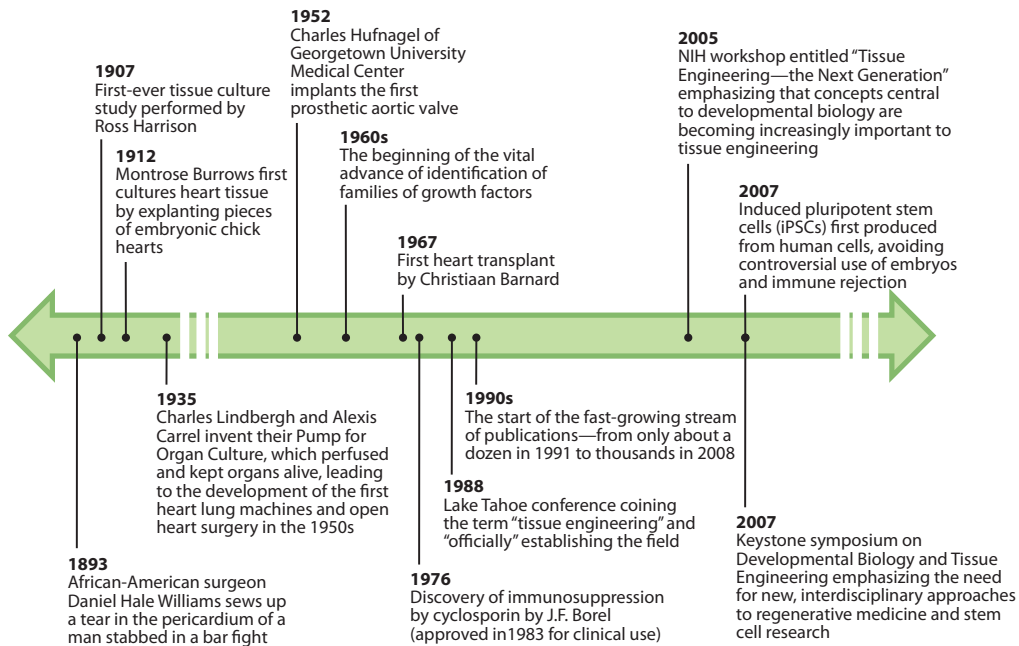


**Figure 1.** Time line of crucial discoveries in cardiac TE<sup>44</sup>. Tissue Engineering is a novel science that dates from 1988.

### 1.2. Myocardial infarction and therapeutic perspectives: a worldwide health concern

Currently there are 16.8 million people with coronary heart diseases in the United States of America (<http://www.americanheart.org>)<sup>11</sup>. In 2011, ischemic heart disease accounted for 12.8% of global deaths, according to the World Health Organization. In the USA, 40% of all deaths are due to cardiovascular disease; one person dies every 39 seconds because of a heart disease, which equates to 800,000 deaths per year. According to the *Fundación española del Corazón*, the mortality rate due to cardiovascular diseases in Spain was 32.2% in 2007. All in all, cardiac failure is the primary cause of death in the world<sup>12</sup>. To better understand the origin of the cardiac failure, it is necessary to review heart development and structure.

Cardiac development starts with the commitment of undifferentiated pluripotent stem cells of the inner cell mass of blastocysts to mesodermal restricted derivatives during embryonic development. Cell reorganization, cross talk and proliferation lead to highly specialized myocardial cells, which include cardiomyocytes, endothelial cells, smooth muscle cells and fibroblasts. Fibroblasts play a key role in the cardiac tissue as they secrete important cardio instructive extracellular matrix (ECM) components (growth factors and cytokines) for the differentiation of the cardiogenic

niche (progenitors, stromal cells and ECM)<sup>13</sup>.

As mentioned above, heart failure is a major modern health concern. One of the leading causes of heart failure is Myocardial Infarction (MI), which results from a reduced flow of blood to a part of the heart. This leads to cardiomyocyte death and myocardial necrosis. Evidence of a MI includes: ventricular dilation and scar formation. The ventricular dilation is caused by a succession of events. First, there is an inflammatory response due to the massive migration of macrophages, monocytes and neutrophils to the infarcted area. Then, metalloproteases degrade the ECM causing myocyte slippage and the expansion of the infarct. As a result, the collagen scaffold weakens as the heart wall. After the initial inflammatory response, there is an increase in fibrillar, cross-linked collagen deposition, which resists deformation and smooth beating. The death of cardiomyocytes results in negative left ventricular (LV) remodeling causing wall stress in the remaining viable myocardium. The final consequence is ventricular dilation<sup>5</sup>. Furthermore, the narrowing and/or occlusion of coronary arteries (by atherosclerosis, spasm of major or intramural arterial branches of the coronary vasculature, or alterations of the microcirculation) block the blood supply provoking drastic decrease in nutrients and oxygen. The clinical spectrum ranges from acute myocardial infarction to chronic ischemic cardiomyopathy depending on the degree of ischemia and tissue injury<sup>14</sup>. As mentioned above, MI results in the development of a necrotic area in the heart that causes the second characteristic symptom: scar formation. This cell death in the myocardium results in the development of a rigid area that compromises the contractile, mechanical and electrical properties of normal myocardium. By consequence, cardiac output is reduced and the heart loses the ability to supply blood efficiently<sup>15</sup>.

Currently, the most common treatment for severe Congestive Heart Failure (CHF) is surgical heart transplantation. Christian Barnard was the first surgeon to perform a human heart transplant on the 3<sup>rd</sup> December 1967 in Cape Town, South Africa. Experimental surgery pioneers such as Norman Shumway, Donald Lower and Adrian Kantrowitz developed the techniques used to carry out the surgical intervention. A few days later, Kantrowitz performed the world's second transplant in Brooklyn, New York. During the coming decades, Shumway and his team would complete hundreds of transplants in Stanford, California<sup>16</sup>. Nevertheless, this technique has always been restricted by a shortage of donors. Other strategies to treat CHF are coronary artery bypass grafting, ventricular remodeling, dynamic *latissimus dorsi* cardiomyoplasty, cardiac bio-assist mechanical support and

## INTRODUCTION

pharmacological intervention. There are two promising pathways to cure CHF: direct implantation of progenitor cells into the injured heart and replacement of portions of heart muscle with tissue-engineered bio-artificial grafts. This last approach is being widely studied and includes three different biomaterial approaches for the treatment of MI. The first is based on polymeric LV restraints in the prevention of ventricular dilation and heart failure. The second involves *in vivo* implantation of *in vitro* engineered cardiac tissue. The third entails injection of cells and/or a scaffold into the damaged myocardium to create *in situ* engineered cardiac tissue<sup>11</sup>.

The main goal of cardiac TE is to deliver in a defined and organized manner living cells and/or other important agents to the injured cardiac area. For this, different strategies include tissue printing technology<sup>17</sup>, direct cell injection, direct tissue replacement, embryonic and adult stem cell therapy<sup>15</sup>, etc. Basically, the strategies can be divided into two main groups: cellular transplantation and cardiac TE (**Figure 2**). Cellular transplantation is also called *in situ* cellular cardiomyoplasty. It entails the direct delivery of cells into the infarcted myocardium<sup>18</sup> and it influences myogenesis, angiogenesis and paracrine effects. The main disadvantage of cellular cardiomyoplasty is limited cell retention caused by the pumping of blood, which washes out most of the injected cells from the target site. Other disadvantages that compromise the viability of the injected cells are poor nutrition supply in the ischemic heart and immune rejection by the host. However, cardiac TE provides alternatives to overcome these technical problems. Strategies based on cardiac TE combine cells with biomaterials (hydrogels or 3D scaffolds). There are three primary approaches: *in situ* TE (cells are combined with biomaterial and injected into the infarcted myocardium); *in vitro* TE of cardiac tissue constructs (cells are embedded in 3D scaffolds to develop tissue constructs, which are implanted for *in vivo* regeneration of myocardium); and scaffold free TE (cell sheets<sup>19,20</sup>, cell bodies<sup>21</sup>, core-shell cell bodies<sup>22</sup> and aggregates are injected into the damaged myocardium)<sup>23</sup>. *In situ* TE has been widely used and researchers have developed a diverse range of options. In fact, the parameters (type of cell, type of biomaterial) can be modified and the possibilities become countless. Some interesting examples include: (1) injection of only biomaterial (platelet gel<sup>24,25</sup>, hydrogel PEG<sup>26</sup>, gels derived from small intestinal submucosa ECM<sup>27</sup>); (2) injection of seeded cells on construct<sup>28</sup>; (3) injection of cells and biomaterial (porous beads with synthetic polymer and cells<sup>29</sup>, cells and hydrogel<sup>30,31</sup>, polymer-transfected cells<sup>32</sup>). Interestingly, *in vitro* TE includes the generation of cell delivery patches for cardiac regeneration of infarcted myocardium<sup>33-38</sup>. Nonetheless, some approaches describe acellular polymeric

patches for ventricular restraint<sup>39,40</sup>.

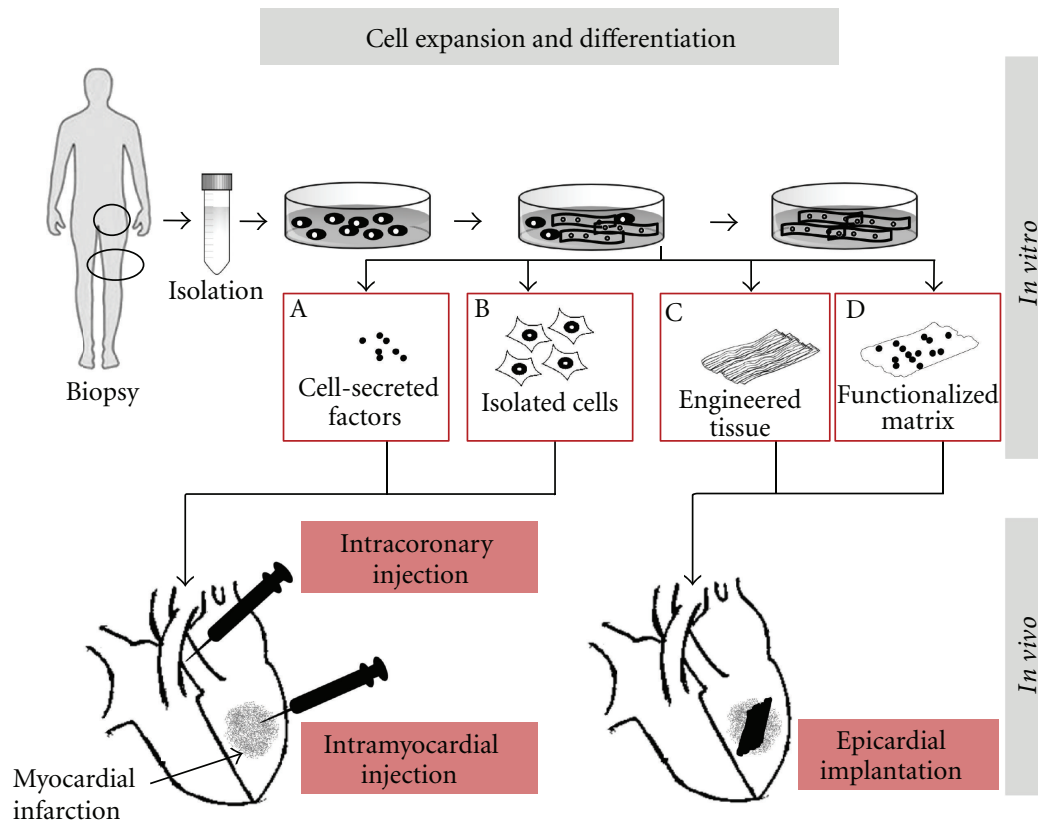


**Figure 2.** Strategies applied for MI treatment. All approaches start with cell isolation and expansion from a patient biopsy. Then, cell-secreted factors (A) or isolated cells (B) can directly be injected into damaged myocardium or cells can be embedded into an engineered tissue (C) or a functionalized matrix (D) and implanted as a patch *in vivo*<sup>132</sup>.

### 1.3. Three-dimensional cultures: scaffolds used to mimic an *in vivo* extracellular matrix

The most promising strategy in cardiac TE is embedding cells in three-dimensional cultures *in vitro* and engrafting the constructs *in vivo*. Although several biomaterials have been studied in TE, all of the constructs should fulfill basic requirements. The biomaterial has to be biocompatible (no rejection nor immune response *in vivo*), mechanically compatible (it should match the mechanical properties of the myocardium and provide mechanical support), biodegradable (its degradation rate should match the regeneration rate of the cardiac tissue and its degradation by-products must be non-toxic and readily removed from the body), cell-friendly (enhance cell survival and adhesion), biomimetic (mimic the ECM of the host

## INTRODUCTION

tissue) and cost-effective (easily accessible and reasonably affordable). Essentially, the biomaterial must encourage cell proliferation and maturation into cardiomyocytes in order to re-populate the necrotic tissue *in vivo* and improve the contractility of the graft. Another important requirement specific for cardiac tissue regeneration is that the biomaterial must integrate with the endogenous electrical pattern of the heart, never compromise it and propagate the internal wave front. Importantly, the construct must encourage vascularization to enhance cell survival of the engrafted cells<sup>41</sup>. In addition, a TE scaffold should be highly porous (to allow nutrients and gas exchange<sup>42</sup>), hydrophilic (to facilitate cell attachment), structurally stable (to resist the shearing forces of the heartbeats) and elastic (to transmit contractile forces)<sup>11</sup>.

Three-dimensional engineered scaffolds can be scaffold-free tissue constructs, repopulated decellularized native organs<sup>43</sup>, cells mechanically stimulated in hydrogels, cells cultured in perfused channeled scaffolds, cells electrically stimulated in porous scaffolds or cell delivered in injectable hydrogels<sup>44</sup>. Most approaches involve the generation of cardiac micro-tissues, which are micro-scale constructs of cardiac cells embedded in 3D matrices<sup>4</sup>. Another strategy is the use of perfusion bioreactors<sup>45,46</sup>. All in all, it has been proven that 3D scaffolds promote cell attachment, proliferation, organization and differentiation (osteogenic, hematopoietic, neural and chondrogenic)<sup>42</sup>. Other examples in bibliography apply acellular extracellular scaffolds for tissue engineering or regeneration purposes<sup>47-51</sup>. The aim of obtaining totally decellularized matrices is to use the mechanical and morphological properties of these macro-scaffolds to support cells or bioengineered patches. It is of critical importance to remove all the endogenous cells of the bioscaffold in order to avoid any immunological rejection during the implantation of the patch *in vivo*. Several decellularization protocols have been described in literature including physical, chemical and enzymatic approaches<sup>52</sup>. Some examples of effective chemical decellularization are based on ionic detergents<sup>53</sup>. A research group developed the complete decellularization of human myocardium and impregnated it with human mesenchymal stem cells embedded in fibrin hydrogel. They implanted the composite onto the infarcted myocardium of rat model<sup>54</sup>. Another related approach is to use decellularized porcine myocardium scaffold seeded with bone marrow mononuclear cells<sup>55</sup>.

During the past decades, several types of biomaterials have been tested in order to elucidate the best three-dimensional scaffold for TE. These artificial microenvironments can be divided into two groups depending on their origin: natural

(e.g. collagen<sup>56</sup>, alginate, gelatin, matrigel<sup>57</sup>, fibrin) and synthetic (e.g. PGA, PLA, PLGA<sup>29</sup>, PLG, PEG)<sup>58,59</sup>. Despite their promising characteristics, major drawbacks had to be overcome. For example, natural materials are undefined and instructive structures whereas synthetic ones are not always sufficiently bioactive. Scaffolds releasing cells, drugs or Growth Factors (GFs) are a spotlight for cardiac regenerative therapy<sup>60</sup>. The goal is to increase survival of engrafted cells, guide cell differentiation and migration. To accomplish it, scaffolds should be non-cytotoxic, biodegradable, porous, permeable and flexible<sup>61</sup>. First attempts at drug and cell delivery for MI repair<sup>62</sup> were based on tailoring natural and synthetic biomaterials with the integrin adhesion peptide sequence RGD (Arginine-Glycine-Aspartic Acid), GFs<sup>63</sup>, hormones, and other proteins. Furthermore, GFs are involved in cell survival, growth, differentiation, mobility and communication processes. For instance, the gold standard collagen, which has convenient mechanical properties, has been conjugated with polysaccharides<sup>64–66</sup>, RGD<sup>67</sup>, GFs (Vascular Endothelial GF<sup>68</sup>) and specific antibodies<sup>69</sup>. Additional examples reported in literature are based on gelatin<sup>70</sup>, alginate (functionalized with RGD<sup>71</sup>, extracellular matrix peptides<sup>72</sup>, Placental GF<sup>73</sup>, Insulin-like GF-1<sup>74</sup>, Hepatocyte GF<sup>74</sup>) and chitosan<sup>75</sup>. Other attempts include b-Fibroblast GF-loaded NIPAAm thermosensitive hydrogels<sup>76</sup> and modified PEG<sup>77,78</sup>. All scaffolds were seeded with cells in order to promote cardiac regeneration<sup>79</sup>.

Collagen is the major component of the extracellular matrix (ECM) of many tissues. It generates an extracellular anchor for the cells as it contains cellular specific binding sites. Therefore, these trails allow cells to attach and migrate. Cells modulate the collagen's composition of their ECM by degrading it (collagenases). For all its properties, hydrogels of collagen have been widely used as tissue-derived natural polymer to study reconstruction of organs, bone regeneration, etc. However, the polymerization of the collagen can influence cell morphology and cellular protein localization. Indeed, some factors should be taken into account such as collagen concentration, method used to build the 3D construct and conditions of collagen's polymerization. Collagen extractions are usually prepared by dissolving native fibrillar collagen at pH 2 and 4°C in order to preserve the terminal groups of the molecule (basically non-helical telopeptides, responsible for the collagen fibril alignment). Thus, collagen molecules are mostly acid-soluble. Conversely, collagen fibrils polymerize in heterogeneous cross-linked structures at physiological conditions of neutral pH 7 and 37°C<sup>80</sup>. The polymerization can be described in two phases: first, a nucleation phase where the molecules assemble; and second, a rapid growth phase

## INTRODUCTION

where the molecules cross-link. The nucleation phase lasts longer at both low temperature and low pH, which generates thicker collagen fibers before reaching the final thickness (>200 nm wide)<sup>81</sup>. Regarding the concentration of the collagen, the higher it is the denser is the matrix. Moreover, a variety of cells have been cultured either in a *sandwich* shape construct<sup>82-84</sup> or embedded directly in collagen<sup>81,85-88</sup>.

### 1.4. *Self-assembling peptides, a promising strategy for cell and drug delivery*

The discovery and development of self-assembling peptides revolutionized the TE community. An *in vivo* example of self-assembling is that of phospholipids in aqueous solution, which form micelles, vesicles and tubules<sup>89</sup>. By definition, molecular self-assembly is the spontaneous organization under thermodynamic equilibrium conditions of molecules into regular structures linked by non-covalent bonds. Indeed, the oligopeptides self-assemble at physiological conditions into nanofibers recreating biological *in vivo* processes<sup>89</sup>. The nanofibers are 1000-fold smaller than synthetic polymer microfibers and similar in scale to ECM. The first self-assembling peptide discovered was EAK16-II, a 16 amino acid peptide found as a segment in a yeast protein, Zuotin. The latter is a protein with 433 residues, which was initially characterized by its preferential binding to left-handed Z- DNA. Its peculiarity is the domain consisting of 34 amino acid residues (305-339) with alternating alanines and alternating charges of glutamates and lysines with an interesting regularity: AGARAEAEAKAKAEAEAKAKAESEAKANASAKAD (A: Alanine; E: Glutamic Acid; K: Lysine; G: Glycine; R: Arginine; D: Aspartic Acid; S: Serine)<sup>90</sup>. The peptide solution of EAK16-II exposed to a physiological medium or a salt solution was found to form well-ordered nanofiber scaffolds with high water content (99%). The peptidic chains form  $\beta$ -sheet structures due to internal periodic repeats of alternating ionic hydrophilic and hydrophobic amino acids. This creates polar and non-polar surfaces<sup>91</sup>. There are three different types of self-assembling peptides: type I (form  $\beta$ - sheet structures), type II (form both  $\beta$ -sheet and  $\alpha$ -helix) and type III (form monolayers on surfaces). Self-assembling peptides included in type I are classified according to the scheme of moduli based on the hydrophilic surface of the molecules. Depending on the alternating positively and negatively charged arrangement of amino acids, peptides are included in several moduli: modulus I encloses peptides with -+-+--+-, modulus II encloses those with --+--+ and so on. The number following the peptide name is the modulus that it belongs to<sup>89</sup>. The most



hopeful property of the scaffold built by EAK16-II when it was discovered in the medium of a PC12 (noradrenergic cell line derived from rat adrenal gland pheochromocytoma) culture was its apparent lack of toxicity. Other variants from this self-assembling peptide model have been discovered, all of them with the same properties as their ancestor. The one that interests us is RAD16-I (RADARADARADARADADA) in which arginine and aspartic acid residues substitute lysine and glutamate (R: Arginine; A: Alanine; D: Aspartic Acid)<sup>91-96</sup> (**Figure 3**). As with EAK16, RAD16 also spontaneously self-assembles in physiological salt-containing solutions and forms  $\beta$ -sheet structures in aqueous solution with hydrophilic and hydrophobic surfaces. As mentioned previously, self-assembling is based on the chemical complementarity and structural compatibility of the molecules. The interactions are weak and non-covalent (hydrogen bonds, ionic bonds, hydrophobic interactions, van der Waals interactions and water-mediated hydrogen bonds). This type of peptide is stable under changes in temperature, pH, concentration of denaturing agents (urea, guanidium hydrochloride) and degradation by proteolytic enzymes *in vitro*. Moreover, the RAD motif (Arginine-Alanine-Aspartic Acid) is similar to the ubiquitous integrin receptor-binding site RGD (Arginine-Glycine-Aspartic Acid) that renders the matrix adhesive to the cells. RAD16 produces no noticeable immune response, nor inflammatory reactions in animals, nor cytotoxicity<sup>95</sup>. Furthermore, several cell types from established cell lines and cells derived from primary cultures were found to attach to both RAD16 and EAK16<sup>93</sup>. Critically, greater than 95% of the content of the hydrogel formed by the self-assembling peptide is water. This is important because the peptide material has no detectable swelling effect when it is in contact with a saline solution. This property renders the material a potentially viable option for cellular therapy. These peptides also have the ability to reassemble, which has been observed by applying cycles of sonication. This trait is important to understand the process, design better biological materials and find correlations with pathological similarities<sup>96</sup>. However, the unregulated expansion of the scaffold once implanted in the tissue could lead to adverse physiological effects<sup>97</sup>.

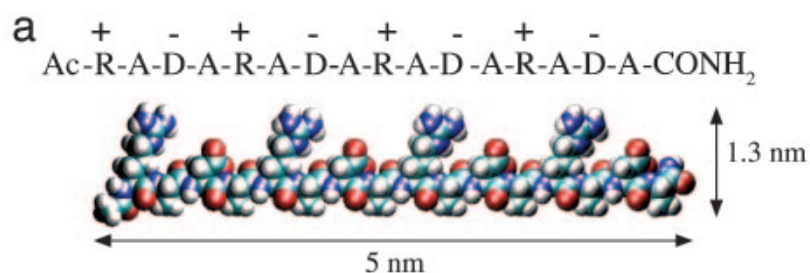


**Figure 3.** Amino acid sequence and structural model of a RAD16-I nanofiber<sup>96</sup>.

Self-assembling peptides type II (DAR16-IV: n- ADADADADARARARAR (D: Aspartic Acid; A: Alanine; R: Arginine)) can undergo a secondary structure switch from a  $\beta$ -sheet structure to a  $\alpha$ -helix as the charge distribution (negatively charged residues in the N-terminus and positively ones in the C-terminus) reminds the  $\alpha$ -helical dipole moment (C $\rightarrow$ N)<sup>97</sup>. The environment dictates the balance between both secondary structures and the temperature increase causes the transition. The process is energetically inaccessible in the other direction (from  $\alpha$ -helix to  $\beta$ -sheet). This remarkable discovery ruined the theory that secondary structures are relatively static in proteins in comparison to the tertiary ones that change dramatically. In spite of that, RAD16-I is extremely stable under a  $\beta$ -sheet structure regardless of the environment. Even when it is used with extended incubation times or higher temperatures (up to 90°C), it retains its structure and remains stable. This phenomenon correlates with the formation *in vivo* of amyloid proteins in Alzheimer disease<sup>98</sup>, which is one of the most evident examples of salt-induced peptide aggregation. The plaques of insoluble filaments found in the neurofibrillary tangles consist of  $\beta$ -amyloid protein, a 43-amino acid residue protein highly soluble in water but poorly soluble in phosphate-buffered saline solution (physiological conditions). The filaments of the salt-dependent aggregates from  $\beta$ -amyloid protein with an extremely stable  $\beta$ -sheet structure (stained with Congo Red) have a diameter similar to the EAK16 filaments (10-15 nm). Therefore, investigation of EAK16 could elucidate many questions about Alzheimer disease and serve as a system model for exploring treatments<sup>90</sup>.

Admittedly, combinations of peptides, derivatives, natural basement membranes and other techniques might be infinite. For example, *Genové et al.* designed a RAD16-I scaffold functionalized with laminin and collagen motifs in order to render the microenvironment more receptive to endothelial cells<sup>94</sup>. Other attempts combine

self-assembling oligopeptides (type III) and microcontact printing<sup>97</sup>. The cell pattern formation also has potential application in electronics sensors, surface catalysis, microseparation, adsorption of protein and adhesion of cells to surfaces<sup>89,99,100</sup>. The micropatterns can be created by photolithography plus adsorption of proteins and cells to the solid surface.

In the last years, *Semino et al.* have been applying the 3D culture technique based on RAD16-I using mouse cells as a mammal model<sup>92,101–103</sup>. Indeed, *Garreta et al.* cultured mESCs (pluripotent mouse Embryonic Stem Cells derived from the inner cell mass of blastocysts) and MEFs (Mouse Embryonic Fibroblasts isolated from 12- to 14-day mid-gestation mouse embryos) in 3D with RAD16-I in order to study the differentiation into osteoblast-like cells (the 2D culture served as control). In 2006, they demonstrated that mESCs acquired an osteoblast-like phenotype (expression of bone markers such as Ca<sup>2+</sup> mineralization, alkaline phosphatase activity, osteopontin and collagen I expression) when cultured in 2D and in 3D conditions whereas MEFs only underwent osteoblast differentiation when cultured in 3D RAD16-I and induced with osteogenic medium. So, the authors concluded that not only were the osteogenic supplements needed to induce the osteogenic commitment but also, the 3D-environment was essential<sup>101</sup>. *Genové et al.* also assessed a new way to culture rat hepatocytes preserving their specific functionality. They compared hepatocyte cultures in peptide sandwich *versus* in collagen sandwich (considered the gold standard in hepatocyte *in vitro* culture) and concluded that hepatocytes behaved similar in both materials (similar gene expression profile, both secreted proteome of hepatocytes in culture and had comparable albumin secretory capacity). The main advantage of culturing cells in this peptide scaffold was that it was completely synthetic and defined<sup>92</sup>. Another approach using this peptide scaffold is the one proposed by *Quintana et al.* who studied the de-differentiation of MEFs. Cells seemed to undergo a process that came close to many aspects of animal development. Following *Garreta et al.*'s work, they cultured MEFs in RAD16-I and discovered that MEFs only underwent osteogenesis after osteogenic induction with supplements whereas adipogenesis and chondrogenesis occurred with and without adipogenic/chondrogenic induction. Therefore, MEFs cultured in 3D lost their fibroblastic phenotype (lost the capacity to synthesize collagen I) and became chondrocyte-like cells (expressing collagen II, Runx2 and Sox9)<sup>102</sup>.

Nevertheless, biomaterial science has taken a step forward with designed nanofibers to render the scaffold more biomimetic. Indeed, tailored self-assembling

## INTRODUCTION

peptides have been designed to restore cardiac tissue after Myocardium Infarction (MI). Finally, a novel and promising strategy combines self-assembling peptides with functional motifs. These hydrogels have been modified with dextran macromolecules<sup>104</sup>, laminin and collagen motifs<sup>94</sup>, integrin-binding sequence, laminin receptor binding sequence and heparin binding sequence<sup>92</sup>. It is strongly believed that the attachment of functional motifs to the nanofibers of the engrafted scaffold combined with cell delivery could have a beneficial effect on cardiac regeneration after MI. The best-established system involves the attachment of the cell-adhesion motif RGD. Thus, modified self-assembling peptide RAD16 presenting RGDSP (adhesion sequence Arginine-Glycine-Aspartic Acid-Serine-Proline) promotes survival, growth and differentiation of encapsulated Marrow-derived Cardiac Stem Cells (MCSCs). This represents an excellent approach for stem cell transplantation into damaged tissue<sup>105</sup>.

### 1.5. *Cells full of hope*

Cell therapy is crucial in cardiac repair attempts. Indeed, massive cell death occurs after infarction leading to a necrotic area that generates a scar formation. Several types of cells have been used in cardiac regeneration approaches. As discussed above, cardiac TE encloses two major components: cells and biomaterials. Herein, we review what cells have been reported to be appropriate candidates for cardiac repair. These include fetal cardiomyocytes, Embryonic Stem Cells (ESCs), bone marrow-derived stromal and Mesenchymal Stem Cells (MSCs), skeletal myoblasts, endothelial precursor stem cells, etc. The list of cells is extensive and ranges from embryonic to adult cells, from stem to somatic cells. Some of them have shown promising results in preclinical protocols. Indeed, skeletal myoblasts and bone marrow-derived stem cells are currently being assessed in phase 2 clinical trials for the treatment of ischemic cardiomyopathies<sup>1</sup>. As previously stated, the major concern is that few transplanted cells can survive injection into the myocardium probably due to paracrine effects, transdifferentiation or high oxidative stress. Cardiac TE focuses on designing a beneficial scaffold that recruits endogenous cells and induces cell survival of the engrafted cells to the injected scaffold. Microenvironments themselves, without any coupled biological signal, can promote vascular cell recruitment in the myocardium. For instance, endothelial cells are able to invade the injected scaffold, self-organize and mature in it. Moreover, it has been observed that potential myocyte progenitors populate the microenvironment as well. In spite of the innate potential to attract cells of the peptide scaffold, the combination

of self-assembling microenvironment with exogenous cells (neonatal cardiac myocytes or embryonic stem cells) increases the recruitment of endogenous cardiac progenitors and promotes their spontaneous differentiation into myocytes. It is thought that non-surviving injected cardiomyocytes release recruitment signals for endogenous cardiac progenitors<sup>106</sup>.

Although adult cells such as differentiated cardiomyocytes have been implanted in the myocardium in order to increase cardiac muscle mass<sup>107</sup>, progenitor cells seem to be the best choice to repair damaged cardiac tissue. Currently, there are two major stem cell sources for generating cardiomyocytes: Cardiac Progenitor Cells (CPCs) and Embryonic Stem Cells (ESCs), adult and embryonic stem cells respectively. On the one hand, CPCs are tissue-specific progenitors that reside in the heart and are responsible for its regeneration. They were first identified in the murine heart in 1999 although they were not isolated and characterized as CPCs until 2004<sup>108</sup>. It was *Messina et al.* who isolated CPCs from very small fragments of human myocardium and expanded them *in vitro* many-fold without losing their multipotentiality<sup>109</sup>. Indeed, cardiac tissue self-regenerates although it does so at a very slow speed<sup>110</sup>. It is thought that resident CPCs need a stimulus to migrate to the damaged area. Trials have been reported to accelerate this natural regeneration led by the migration of CPCs and restore the loss of cardiomyocytes and vascular structures in the infarcted zone. In addition, it appears that the distribution of human CPCs in the compartments of the heart is different. The highest concentration of cardiac resident stem cells is in the atria and not in the ventricle. Therefore, CPCs can be explanted and isolated from the atria<sup>111</sup>. Importantly, adult stem cells do not raise any philosophical, social, political, religious or ethical concern because they are derived from adult tissue sources.

Another important source of adult stem cells to treat infarcted myocardium is the hematopoietic lineage (cells present in the bone marrow and peripheral circulation). The two major subtypes of bone marrow-derived stem cells with cardiac regenerative potential are: hematopoietic progenitor cells and Mesenchymal Stem Cells (MSCs)<sup>16</sup>. MSCs appear to be specially attractive for cell therapy and TE studies because they can be isolated, expanded *ex vivo*, used in autologous mode and do not exhibit allogeneic rejection in human and animal models<sup>112</sup>.

Adipose tissue is also a source of adult stem cells. Indeed, fat is an abundant tissue in any individual, it is simple and efficient to harvest and it has a higher stem

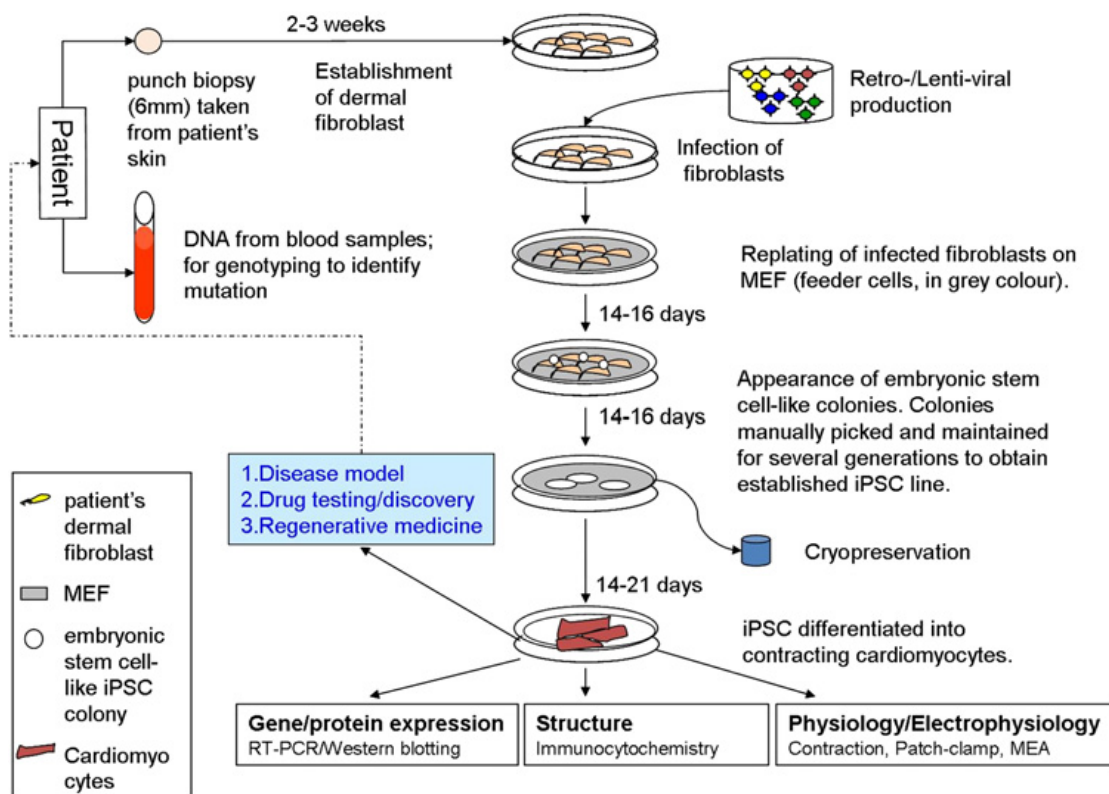
## INTRODUCTION

cell yield than bone marrow. Adipose-derived stem cells can easily be isolated and cultured *ex vivo*<sup>11</sup>. Progenitor cells derived from adipose tissue have been shown to have a MSC-like pattern and an inherent cardiomyogenic potential<sup>113,114</sup>. Fat is believed to be a protective cushion but also a source of hormones, cytokines and chemokines that create the perfect environment for stem cells to reside in. All in all, adult stem cells are a valuable source of stem cells because they are patient-specific (no immune rejection) although it usually requires surgery to harvest them. Also, they are tissue-specific, which means that their differentiation capacity is limited to the tissue where they reside in and they can only commit to that tissue lineage.

On the other hand, Embryonic Stem Cells (ESCs) have a vast pluripotent capacity. They can expand unlimitedly and generate cells of all three germ layers (endoderm, mesoderm and ectoderm) that can further differentiate into specific cell lineages. They derive from the inner cell mass of pre-implanted blastocysts. Human ESCs have been widely used for cardiac regeneration studies due to their potential to differentiate into cardiomyocytes. It is known that hESCs can spontaneously differentiate *in vitro* into functional beating cardiomyocytes although the efficiency is very low. The main goal is to generate cardiac cells *in vitro* and implant them in the damaged myocardium. For this, several strategies have been developed (cardiac patches, cell injection, etc.). Indeed, many tissue engineers are realizing the importance of an *in vitro* environment that mimics the *in vivo* ECM. Human ESCs have been cultured in 2D (in adherent static cultures) and compared to 3D cultures (cell aggregates called embryoid bodies in suspension). Researchers have proven that cells cultured in 3D have a better efficiency of cardiac differentiation (better rate, extend and consistency of beating activity)<sup>115</sup>. In addition, some groups have created reporter cell lines of hESCs to assess the cardiac differentiation in real-time. The objective is to identify and track the implanted stem cells that have migrated or committed into cardiomyocytes. Molecular and cloning techniques have permitted the design of stable cell lines containing cardiac gene promoters driving the expression of fluorescent proteins (green GFP, red mRFP and mCherry). Also, the fluorescence can be coupled to drug-selectable markers that permit isolation of pure populations of labeled stem cells and hESC-derived cardiomyocytes<sup>116-119</sup>.










A recently discovered generation of stem cells that has opened the doors of personalized cell therapy is the induced Pluripotent Stem Cells (iPSCs). In 2007, Dr. Yamanaka and his group created a patient-specific embryonic stem cell line called iPSCs. Taking into account the ethical controversies that hinder the use of hESCs

and human embryos, they induced pluripotency in somatic cells by direct reprogramming. After demonstrating that the phenomenon was feasible with Mouse Embryonic Fibroblasts (MEFs) and adult mouse tail-tip fibroblasts<sup>120</sup>, they reproduced it with human somatic cells. They used human dermal fibroblasts derived from facial dermis of a Caucasian female and introduced the retroviruses containing human Oct3/4, Sox2, Klf4, and c-Myc into the cell line. They showed that the hiPSCs expressed hESCs markers, differentiated into neural and cardiac cells *in vitro* and formed teratoma<sup>121</sup>. This finding suggested that a generation of patient-specific stem cell lines could be possible (**Figure 4**). Despite the recent impact of hiPSCs, more and more researchers are focusing on using hiPSCs for cardiac TE purposes. Some approaches describe 3D cultures of hiPSCs in scalable stirred-suspension bioreactors as aggregates<sup>122</sup>, hydrogels<sup>123</sup>, etc. All in all, pros and cons of each cell type used in cardiac TE must be taken into account to design suitable regeneration strategies (**Figure 5**).



**Figure 4.** Scheme of the patient-specific cardiomyocytes generation: first, explant of human dermal fibroblasts; second, reprogramming into hiPSCs; third, cardiac differentiation<sup>124</sup>.

## INTRODUCTION

Cell Type	Strengths	Weaknesses	Opportunities	Threats	Clinical Trial
 Embryonic	<ul style="list-style-type: none"> <li>-Pluripotent</li> <li>-High quantities</li> </ul>	<ul style="list-style-type: none"> <li>-Allogeneic</li> <li>-Uncontrolled proliferation</li> <li>-Controlling commitment</li> <li>-Ethical/Political concerns</li> </ul>	<ul style="list-style-type: none"> <li>-Useful scientific model for basic research</li> </ul>	<ul style="list-style-type: none"> <li>-Rise of iPSCs</li> <li>-Shift in laws and political parties</li> </ul>	 No <sup>37,38</sup>
 Induced Pluripotent (iPSC)	<ul style="list-style-type: none"> <li>-Autologous</li> <li>-Pluripotent</li> <li>-High quantities</li> <li>-Non-invasive acquisition</li> </ul>	<ul style="list-style-type: none"> <li>-Lack of homogeneity in the cell population</li> <li>-Uncontrolled proliferation</li> <li>-Chromatin modification</li> <li>-Epigenetic reprogramming</li> <li>-Potential immunogenicity</li> </ul>	<ul style="list-style-type: none"> <li>-Directed differentiation</li> <li>-Avoids ethical dilemma's</li> <li>-Highly fundable</li> </ul>	<ul style="list-style-type: none"> <li>-Clinical application of adult cardiac stem cells</li> <li>-Oversold potential may increase public frustration</li> </ul>	 No <sup>29,38,40</sup>
 Bone Marrow-derived/ Mesenchymal	<ul style="list-style-type: none"> <li>-Autologous,</li> <li>-Readily procured</li> <li>-Decades of clinical experience</li> <li>-Potential for allogenic use</li> </ul>	<ul style="list-style-type: none"> <li>-Low quantities</li> <li>-Limited efficacy</li> <li>-Low survival, persistence, and commitment</li> </ul>	<ul style="list-style-type: none"> <li>-Harvesting and purification protocols well established</li> </ul>	<ul style="list-style-type: none"> <li>-Development of tissue-specific progenitor cells (CPCs, ESCs, iPSCs)</li> </ul>	 Yes <sup>34-36</sup>
 Adult Cardiac	<ul style="list-style-type: none"> <li>-Autologous</li> <li>-Proven cardiogenic potential</li> </ul>	<ul style="list-style-type: none"> <li>-Limited proliferation and durability</li> <li>-Stressed/Aged source</li> <li>-Patient variability</li> <li>-Invasive harvesting procedure</li> </ul>	<ul style="list-style-type: none"> <li>-Safety</li> <li>-Selective enrichment to enhance specificity</li> <li>-Detailed molecular biology established</li> </ul>	<ul style="list-style-type: none"> <li>-Focus upon iPSCs</li> <li>-Relative ease to produce ESCs, iPSCs and BMSCs</li> </ul>	 In Progress <sup>14,33</sup>
 Cardiosphere-derived	<ul style="list-style-type: none"> <li>-Autologous</li> <li>-Rapid expansion in culture</li> <li>-Mixed population</li> </ul>	<ul style="list-style-type: none"> <li>-Poorly-defined cellular biology</li> <li>-Technical aspects of culture</li> <li>-Low efficacy</li> <li>-Low survival, persistence, and commitment</li> <li>-Mixed population</li> </ul>	<ul style="list-style-type: none"> <li>-Unique culture environment may enhance cardiogenic potential</li> </ul>	<ul style="list-style-type: none"> <li>-Controlled mixtures of other stem cell types</li> <li>-The relative ease to produce ESCs, iPSCs, and BMSCs</li> </ul>	 In Progress <sup>41</sup>

**Figure 5.** Table summarizing the SWOT (Strengths, Weaknesses, Opportunities and Threats) of different stem cell types used in cardiac TE<sup>133</sup>.

### 1.6. Fibroblasts and Reprogramming, a route to personalized cell therapy

Following a MI, heart-resident fibroblasts divide and migrate into the damaged myocardium to heal the scar caused by cell necrosis. Formation of a fibroblastic scar initiates remodeling, hypertrophy, and ultimately heart failure and cell death. Therefore, fibroblasts play a key role in cardiac dysfunction. Fibroblasts are somatic cells, very abundant in several tissues and easy to harvest. For these reasons, they have been targeted by many studies including reprogramming methods.

Nuclear reprogramming is the natural phenomenon that occurs after fertilization. Indeed, the fusion of two differentiated cells (gametes) gives rise to embryonic stem cells through epigenetic alterations of the zygote's genome during development. Thus, reprogramming can be defined as an alteration of a differentiated nucleus into a totipotent or multipotent state. Reprogramming of somatic cells is accompanied by demethylation of critical pluripotency genes promoters. To date, mouse<sup>120</sup> and human<sup>121</sup> fibroblasts have been successfully reprogrammed using a combination of



transgenes including Oct3/4, Sox2, Klf4, and cMyc; or Oct3/4, Sox2, Nanog, and Lin28. Interestingly, neonatal and fetal cells are easier to reprogram than adult cells although researchers are improving the yield of reprogramming adult somatic cell (mostly dermal fibroblasts) for personalized cell therapy purposes<sup>12</sup>. Indeed, reprogramming methods could generate patient-specific stem cells (induced Pluripotent Stem Cells iPSCs). There are two main techniques used to reprogram somatic cells into iPSCs: integrating and non-integrating methods. Integrating methods involve viral delivery (retro- or lentiviruses) and integration of the Yamanaka factors (Oct3/4, Sox2, Klf4, and c-Myc) into the host genome of the somatic cell. Non-integrating methods do not involve genomic integration of the transgenes but transient expression of reprogramming factors (episomal plasmid vectors, minicircle vectors, RNA and protein delivery). Nevertheless, the main disadvantage of the genomic integration is that it can cause development of a tumorigenic phenotype due to random integration into the host genome that can induce the expression of endogenous silenced pro-oncogenes. This may not be a major issue if the iPSCs are used for *in vitro* research, but presents a major barrier to use these cells as a therapeutic option. Therefore, cells derived from this method should be exhaustively tested for tumorigenic markers before being defined as stable cell lines and implanted *in vivo*. Moreover, non-integrating methods would be a suitable alternative for iPSC-based therapeutic applications. The involvement of industry collaborators to create commercial and large-scale production of human iPSC-cardiomyocytes that can be used clinically for drug testing and therapeutics is a promising fast-approaching reality<sup>124</sup>. In addition, there are two types of reprogramming: direct and partial reprogramming. On one hand, direct reprogramming is the process by which differentiated cells are directly reprogrammed (with specific transgene viral infection) into another somatic cell type without going through the pluripotent stage. At present, the main drawbacks of this technique are its low efficiency rate (only 5% of fibroblasts are successfully reprogrammed), the random integration of the transgenes and its experimental complexity. On the other hand, partial reprogramming generates partially reprogrammed cells from fibroblasts that can be fully differentiated to the desired cell type. Both techniques offer exciting prospects for drug screening and disease modeling.

Direct reprogramming could potentially be applied *in vivo* without the formation of teratomas as it does not go through the pluripotent stage. However, direct *in vivo* reprogramming could lead to ectopic myocardium in scar tissue causing arrhythmias post-infarct in humans. Another major concern is how to control the quiescence of *in*

## INTRODUCTION

*vivo* partially reprogrammed cells to prevent the risk of tumor formation<sup>125</sup>. Nonetheless, iPSCs are the most promising method to create patient-specific stem cells to treat diseases and screen drugs. Cells can easily be harvested from a biopsy or blood sample. After cell explant and derivation, hiPSCs must be extensively tested for pluripotency characteristics and then established as a cell line. A related problem is that long-latency diseases (Alzheimer, Parkinson) cannot be studied with derived-iPSCs because the *in vitro* model does not correlate with the dynamics of progression of the illness. Other diseases related to epigenetic alterations also cannot be studied because reprogramming of hiPSCs removes epigenetic components. In spite of the disadvantages, several hiPSCs lines have been generated *in vitro* from different cell sources (human umbilical cord mononuclear blood cells, neonatal human dermal fibroblasts<sup>126</sup>, differentiated fibroblast derivatives of hESCs, primary fetal tissues (lung, skin), neonatal fibroblasts and adult fibroblasts, MSCs<sup>127</sup>). All in all, direct reprogramming is the technique that has been used the most to generate cardiomyocytes *in vitro*. Although no “master regulator” has been identified for cardiac transdifferentiation, three key developmental cardiac regulators (Gata4, Mef2c, and Tbx5) have been found to reprogram cardiac fibroblasts into cardiomyocytes. The combination of these three defined transcription factors (TFs) was sufficient to generate functional beating cardiomyocytes from postnatal cardiac or dermal fibroblasts. It is thought that TFs interact and co-activate cardiac gene expression: Gata4 opens the chromatin structure in cardiac *loci* and allows the binding of Mef2c and Tbx5 to their target sites leading to the full activation of the cardiac cascade differentiation<sup>128,129</sup>. More recently, *Efe et al.* have shown that brief reactivation of reprogramming factors in mouse embryonic and adult fibroblasts is enough to generate functional cardiomyocytes without going through a pluripotent intermediate. Their protocol is much faster than the traditional direct reprogramming and it is based on transdifferentiation by overexpression of lineage-specific factors. Furthermore, their model resembles blastema formation in zebrafish and frogs where regeneration is driven by transient low-level expression of pluripotency factors rather than full re-establishment of pluripotency<sup>130</sup>. Natural transdifferentiation involves dedifferentiation of a cell without reaching a pluripotent stage (like reprogramming) and further differentiation into a new lineage<sup>131</sup> (**Figure 6**).

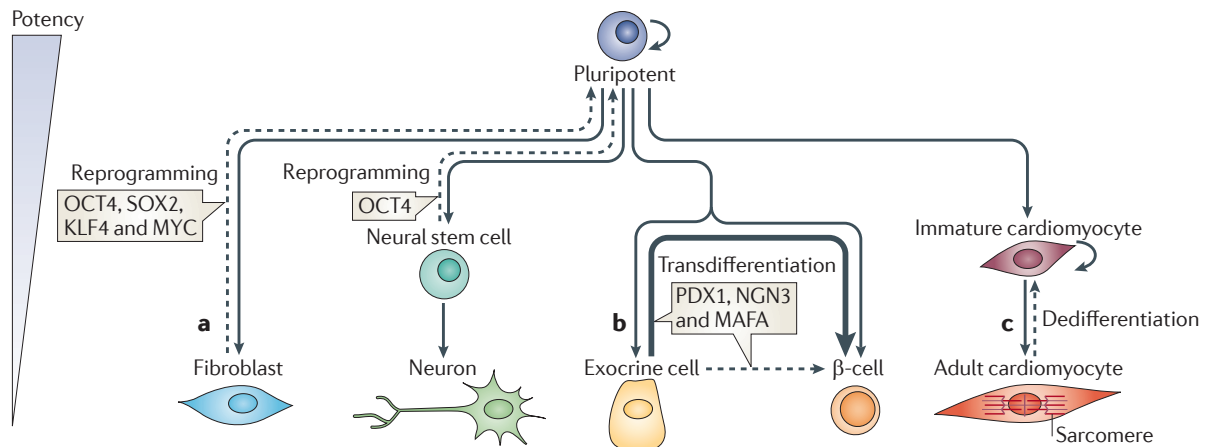


**Figure 6.** The three routes to regeneration: (a) reprogramming, (b) transdifferentiation and (c) dedifferentiation<sup>131</sup>.

### 1.7. Summary of the Thesis

This Thesis includes three experimental parts, which compare and characterize the cardiogenic potential of different cell types when cultured in three-dimensional cultures (3D) based on the neutral peptide scaffold RAD16-I. Firstly, we studied the mesenchymal potential acquisition of human Normal Dermal Fibroblasts (hNDFs) in 3D cultures and future commitment into adipogenic and cardiogenic lineages. We believe that cells cultured in neutral 3D conditions acquire a naïve stage and spontaneously attain a MSC-like phenotype. At this point, cells express a battery of embryonic-related proteins that they do not translate when maintained in traditional two-dimensional cultures (2D). Thus, chemical inducers can drive their further differentiation into adipogenic and cardiogenic lineages. We suggest that hNDFs spontaneously acquire mesenchymal potentiality whereas they require induction media to differentiate into adipogenic and cardiogenic lineages. Secondly, we compared the cardiac differentiation potential of human induced Pluripotent Stem Cells (hiPSCs) when cultured in 2D *versus* 3D environments. This section also considers the effect of ascorbic acid (AA) on cardiogenic induction. This compound has been proven to promote cardiac differentiation among different hiPSCs lines including those without spontaneous cardiogenic potential. We studied the stepwise process of the cardiogenic commitment of hiPSCs cultured in 2D with and without AA: pluripotency, early differentiation, cardiac progenitors and mature cardiomyocytes. Results suggest that AA accelerates and improves the cardiac commitment of hiPSCs in 2D cultures. Furthermore, hiPSCs embedded in RAD16-I

## INTRODUCTION

hydrogels displayed an increased level of cardiac differentiation. The neutral 3D milieu promotes hiPSCs to acquire a strong pre-differentiation into cardiomyocyte-like cells with high potential to commit into cardiac lineage. Third, we cultured adult adipose tissue-resident stem cells (pMATPCs) from porcine heart and designed a cardiac patch based on natural matrices (decellularized human pericardium). We implanted the designed cardiac patch *in vivo* in swine. This section demonstrates the applicability of our system *in vivo*. In summary, we studied the cardiogenic potential of adult somatic cells (hNDFs), adult stem cells (pMATPCs) and pluripotent stem cells (hiPSCs) in 3D cultures based on RAD16-I for potential future applications in the treatment of heart disease.

### 1.8. Objectives

Herein are introduced the general goals of this Thesis although each chapter contains specific objectives for the research presented.

- Compare the mesenchymal potential of human adult somatic cells (hNDFs) when cultured in 3D cultures at different conditions. Evaluate the adipogenic and cardiogenic commitment of hNDFs cultured in RAD16-I.
- Compare the cardiogenic potential of hiPSCs in 2D *versus* 3D cultures and study the effect of ascorbic acid in cardiac differentiation. Identify the cardiogenic pathway step by step from pluripotency to mature cardiomyocytes.
- Preparation of a biological matrix scaffold from human pericardium to develop a porcine cardiac patch based on porcine resident stem cells (pMATPCs) embedded in hydrogel RAD16-I. Implantation of the patch *in vivo* and future applications.

### 1.9. References

1. Giraud, M.-N., Armbruster, C., Carrel, T. & Tevæearai, H. T. Current state of the art in myocardial tissue engineering. *Tissue Eng.* **13**, 1825–36 (2007).
2. Atala, A. Regenerative medicine strategies. *J. Pediatr. Surg.* **47**, 17–28 (2012).
3. Giraud, M.-N., Guex, A. G. & Tevæearai, H. T. Cell therapies for heart function recovery: focus on myocardial tissue engineering and nanotechnologies. *Cardiol. Res. Pract.* **2012**, 971614 (2012).

4. Boudou, T. *et al.* A Microfabricated Platform to Measure and Manipulate the Mechanics of Engineered Cardiac Microtissues. *Tissue Eng. Part A* **18**, 910–919 (2012).
5. Christman, K. L. & Lee, R. J. Biomaterials for the treatment of myocardial infarction. *J. Am. Coll. Cardiol.* **48**, 907–13 (2006).
6. Curtis, M. W. & Russell, B. Cardiac tissue engineering. *J. Cardiovasc. Nurs.* **24**, 87–92 (2009).
7. Eschenhagen, T., Didié, M., Heubach, J., Ravens, U. & Zimmermann, W.-H. Cardiac tissue engineering. *Transpl. Immunol.* **9**, 315–21 (2002).
8. Zimmermann, W.-H., Melnychenko, I. & Eschenhagen, T. Engineered heart tissue for regeneration of diseased hearts. *Biomaterials* **25**, 1639–1647 (2004).
9. Zimmermann, W.-H. & Eschenhagen, T. Cardiac tissue engineering for replacement therapy. *Heart Fail. Rev.* **8**, 259–69 (2003).
10. Vunjak-Novakovic, G. *et al.* Challenges in cardiac tissue engineering. *Tissue Eng. Part B. Rev.* **16**, 169–87 (2010).
11. Venugopal, J. R. *et al.* Biomaterial strategies for alleviation of myocardial infarction. *J. R. Soc. Interface* **9**, 1–19 (2012).
12. Lui, K. O., Bu, L., Li, R. A. & Chan, C. W. Pluripotent stem cell-based heart regeneration: from the developmental and immunological perspectives. *Birth Defects Res. C. Embryo Today* **96**, 98–108 (2012).
13. Christalla, P., Hudson, J. E. & Zimmermann, W.-H. The cardiogenic niche as a fundamental building block of engineered myocardium. *Cells. Tissues. Organs* **195**, 82–93 (2012).
14. Beltrami, C. A. *et al.* Structural basis of end-stage failure in ischemic cardiomyopathy in humans. *Circulation* **89**, 151–163 (1994).
15. Nunes, S. S., Song, H., Chiang, C. K. & Radisic, M. Stem cell-based cardiac tissue engineering. *J. Cardiovasc. Transl. Res.* **4**, 592–602 (2011).
16. Mullenix, P. S., Huddleston, S. J., Stojadinovic, A., Trachiotis, G. D. & Alexander, E. P. A new heart: somatic stem cells and myocardial regeneration. *J. Surg. Oncol.* **105**, 475–80 (2012).
17. Gaetani, R. *et al.* Cardiac tissue engineering using tissue printing technology and human cardiac progenitor cells. *Biomaterials* **33**, 1782–90 (2012).
18. Song, H. *et al.* Interrogating functional integration between injected pluripotent stem cell-derived cells and surrogate cardiac tissue. *Proc. Natl. Acad. Sci. U. S. A.* **107**, 3329–34 (2010).

## INTRODUCTION

19. Sekine, H. *et al.* Cardiac cell sheet transplantation improves damaged heart function via superior cell survival in comparison with dissociated cell injection. *Tissue Eng. Part A* **17**, 2973–80 (2011).
20. Yeh, Y.-C. *et al.* Cardiac repair with injectable cell sheet fragments of human amniotic fluid stem cells in an immune-suppressed rat model. *Biomaterials* **31**, 6444–53 (2010).
21. Lee, W.-Y. *et al.* Enhancement of cell retention and functional benefits in myocardial infarction using human amniotic-fluid stem-cell bodies enriched with endogenous ECM. *Biomaterials* **32**, 5558–67 (2011).
22. Lee, W.-Y. *et al.* Vascularization and restoration of heart function in rat myocardial infarction using transplantation of human cbMSC/HUVEC core-shell bodies. *Biomaterials* **33**, 2127–36 (2012).
23. Wang, F. & Guan, J. Cellular cardiomyoplasty and cardiac tissue engineering for myocardial therapy. *Adv. Drug Deliv. Rev.* **62**, 784–97 (2010).
24. Cheng, K. *et al.* Transplantation of platelet gel spiked with cardiosphere-derived cells boosts structural and functional benefits relative to gel transplantation alone in rats with myocardial infarction. *Biomaterials* **33**, 2872–9 (2012).
25. Cheng, K. *et al.* Intramyocardial injection of platelet gel promotes endogenous repair and augments cardiac function in rats with myocardial infarction. *J. Am. Coll. Cardiol.* **59**, 256–64 (2012).
26. Kadner, K. *et al.* The beneficial effects of deferred delivery on the efficiency of hydrogel therapy post myocardial infarction. *Biomaterials* **33**, 2060–6 (2012).
27. Okada, M. *et al.* Differential efficacy of gels derived from small intestinal submucosa as an injectable biomaterial for myocardial infarct repair. *Biomaterials* **31**, 7678–83 (2010).
28. Dengler, J. *et al.* Engineered heart tissue enables study of residual undifferentiated embryonic stem cell activity in a cardiac environment. *Biotechnol. Bioeng.* **108**, 704–19 (2011).
29. Huang, C. *et al.* Injectable PLGA porous beads cellularized by hAFSCs for cellular cardiomyoplasty. *Biomaterials* **33**, 4069–4077 (2012).
30. Habib, M. *et al.* A combined cell therapy and in-situ tissue-engineering approach for myocardial repair. *Biomaterials* **32**, 7514–23 (2011).
31. Martens, T. P. *et al.* Percutaneous cell delivery into the heart using hydrogels polymerizing in situ. *Natl. Institutes Heal.* **18**, 297–304 (2009).
32. McGinn, A. N. *et al.* Bioreducible polymer-transfected skeletal myoblasts for VEGF delivery to acutely ischemic myocardium. *Natl. Institutes Heal.* **32**, 942–949 (2012).

33. Chen, Q.-Z. *et al.* An elastomeric patch derived from poly(glycerol sebacate) for delivery of embryonic stem cells to the heart. *Biomaterials* **31**, 3885–93 (2010).
34. Freytes, D. O., Santambrogio, L. & Vunjak-Novakovic, G. Optimizing dynamic interactions between a cardiac patch and inflammatory host cells. *Cells. Tissues. Organs* **195**, 171–82 (2012).
35. Liao, B., Christoforou, N., Leong, K. W. & Bursac, N. Pluripotent stem cell-derived cardiac tissue patch with advanced structure and function. *Biomaterials* **32**, 9180–7 (2011).
36. Piao, H. *et al.* Effects of cardiac patches engineered with bone marrow-derived mononuclear cells and PGCL scaffolds in a rat myocardial infarction model. *Biomaterials* **28**, 641–9 (2007).
37. Wei, H.-J. *et al.* Bioengineered cardiac patch constructed from multilayered mesenchymal stem cells for myocardial repair. *Biomaterials* **29**, 3547–56 (2008).
38. Yang, M.-C. *et al.* The cardiomyogenic differentiation of rat mesenchymal stem cells on silk fibroin-polysaccharide cardiac patches in vitro. *Biomaterials* **30**, 3757–65 (2009).
39. Chen, Q.-Z. *et al.* Characterisation of a soft elastomer poly(glycerol sebacate) designed to match the mechanical properties of myocardial tissue. *Biomaterials* **29**, 47–57 (2008).
40. Fujimoto, K. L. *et al.* An elastic, biodegradable cardiac patch induces contractile smooth muscle and improves cardiac remodeling and function in subacute myocardial infarction. *J. Am. Coll. Cardiol.* **49**, 2292–300 (2007).
41. Jawad, H., Lyon, A. R., Harding, S. E., Ali, N. N. & Boccaccini, A. R. Myocardial tissue engineering. *Br. Med. Bull.* **87**, 31–47 (2008).
42. Naderi, H., Matin, M. M. & Bahrami, A. R. Review paper: critical issues in tissue engineering: biomaterials, cell sources, angiogenesis, and drug delivery systems. *J. Biomater. Appl.* **26**, 383–417 (2011).
43. Chachques, J. C. Development of bioartificial myocardium using stem cells and nanobiotechnology templates. *Cardiol. Res. Pract.* **2011**, 806795 (2010).
44. Vunjak-Novakovic, G., Lui, K. O., Tandon, N. & Chien, K. R. Bioengineering heart muscle: a paradigm for regenerative medicine. *Annu. Rev. Biomed. Eng.* **13**, 245–67 (2011).
45. Radisic, M., Marsano, A., Maidhof, R., Wang, Y. & Vunjak-Novakovic, G. Cardiac tissue engineering using perfusion bioreactor systems. *Nat. Protoc.* **3**, 719–38 (2008).
46. Radisic, M. *et al.* Biomimetic approach to cardiac tissue engineering. *Philos. Trans. R. Soc. Lond. B. Biol. Sci.* **362**, 1357–68 (2007).

## INTRODUCTION

47. Chen, F., Yoo, J. J. & Atala, a. Acellular collagen matrix as a possible “off the shelf” biomaterial for urethral repair. *Urology* **54**, 407–10 (1999).
48. Lichtenberg, A. *et al.* In vitro re-endothelialization of detergent decellularized heart valves under simulated physiological dynamic conditions. *Biomaterials* **27**, 4221–9 (2006).
49. Lichtenberg, A., Breymann, T., Cebotari, S. & Haverich, A. Cell seeded tissue engineered cardiac valves based on allograft and xenograft scaffolds. *Prog. Pediatr. Cardiol.* **21**, 211–217 (2006).
50. Seif-Naraghi, S. B., Salvatore, M. a, Schup-Magoffin, P. J., Hu, D. P. & Christman, K. L. Design and characterization of an injectable pericardial matrix gel: a potentially autologous scaffold for cardiac tissue engineering. *Tissue Eng. Part A* **16**, 2017–27 (2010).
51. Seif-Naraghi, S. B., Horn, D., Schup-Magoffin, P. J. & Christman, K. L. Injectable extracellular matrix derived hydrogel provides a platform for enhanced retention and delivery of a heparin-binding growth factor. *Acta Biomater.* **8**, 3695–703 (2012).
52. Gilbert, T. W., Sellaro, T. L. & Badylak, S. F. Decellularization of tissues and organs. *Biomaterials* **27**, 3675–83 (2006).
53. Ng, S. L. J., Narayanan, K., Gao, S. & Wan, A. C. A. Lineage restricted progenitors for the repopulation of decellularized heart. *Biomaterials* **32**, 7571–80 (2011).
54. Godier-Furnémont, A. F. G. *et al.* Composite scaffold provides a cell delivery platform for cardiovascular repair. *Proc. Natl. Acad. Sci. U. S. A.* **108**, 7974–7979 (2011).
55. Wang, B. *et al.* Fabrication of cardiac patch with decellularized porcine myocardial scaffold and bone marrow mononuclear cells. *J. Biomed. Mater. Res. A* **94**, 1100–10 (2010).
56. Valarmathi, M. T. *et al.* A 3-D cardiac muscle construct for exploring adult marrow stem cell based myocardial regeneration. *Biomaterials* **31**, 3185–3200 (2010).
57. Naderi, H., Matin, M. M. & Bahrami, A. R. Review paper: critical issues in tissue engineering: biomaterials, cell sources, angiogenesis, and drug delivery systems. *J. Biomater. Appl.* **26**, 383–417 (2011).
58. Chen, Q.-Z., Harding, S. E., Ali, N. N., Lyon, A. R. & Boccaccini, A. R. Biomaterials in cardiac tissue engineering : Ten years of research survey. *Mater. Sci. Eng.* **59**, 1–37 (2008).
59. Rane, A. a & Christman, K. L. Biomaterials for the treatment of myocardial infarction: a 5-year update. *J. Am. Coll. Cardiol.* **58**, 2615–29 (2011).



60. Ptaszek, L. M., Mansour, M., Ruskin, J. N. & Chien, K. R. Towards regenerative therapy for cardiac disease. *Ser. Stem Cells* **1** **379**, 933–942 (2012).
61. Karam, J.-P., Muscari, C. & Montero-Menei, C. N. Combining adult stem cells and polymeric devices for tissue engineering in infarcted myocardium. *Biomaterials* **33**, 5683–95 (2012).
62. Nelson, D. M., Ma, Z., Fujimoto, K. L., Hashizume, R. & Wagner, W. R. Intra-myocardial biomaterial injection therapy in the treatment of heart failure : Materials , outcomes and challenges. *Acta Biomater.* **7**, 1–15 (2011).
63. Chiu, L. L. Y., Radisic, M. & Vunjak-novakovic, G. Bioactive Scaffolds for Engineering Vascularized Cardiac Tissues. *Macromol. Biosci.* **10**, 1286–1301 (2010).
64. Reis, L. a *et al.* A peptide-modified chitosan-collagen hydrogel for cardiac cell culture and delivery. *Acta Biomater.* **8**, 1022–1036 (2012).
65. Xiang, Z., Liao, R., Kelly, M. S. & Spector, M. Collagen – GAG Scaffolds Grafted onto Myocardial Infarcts in a Rat Model : A Delivery Vehicle for Mesenchymal Stem Cells. *Tissue Eng.* **12**, (2006).
66. Chiu, L. L. Y. & Radisic, M. Controlled release of thymosin  $\beta$ 4 using collagen – chitosan composite hydrogels promotes epicardial cell migration and angiogenesis. *J. Control. Release* **155**, 376–385 (2011).
67. Chimenti, I. *et al.* Human cardiosphere-seeded gelatin and collagen scaffolds as cardiogenic engineered bioconstructs. *Biomaterials* **32**, 9271–9281 (2011).
68. Gao, J. *et al.* A Myocardial Patch Made of Collagen Membranes Loaded with Collagen-Binding Human Vascular Endothelial Growth Factor Accelerates Healing of the Injured Rabbit Heart. *Tissue Eng.* **17**, (2011).
69. Shi, C. *et al.* Stem-cell-capturing collagen scaffold promotes cardiac tissue regeneration. *Biomaterials* **32**, 2508–2515 (2011).
70. Cheng, K. *et al.* Functional performance of human cardiosphere-derived cells delivered in an in situ polymerizable hyaluronan-gelatin hydrogel. *Biomaterials* **33**, 5317–24 (2012).
71. Shachar, M., Tsur-gang, O., Dvir, T., Leor, J. & Cohen, S. The effect of immobilized RGD peptide in alginate scaffolds on cardiac tissue engineering. *Acta Biomater.* **7**, 152–162 (2011).
72. Sapir, Y., Kryukov, O. & Cohen, S. Integration of multiple cell-matrix interactions into alginate scaffolds for promoting cardiac tissue regeneration. *Biomaterials* **32**, 1838–1847 (2011).
73. Binsalamah, Z. M., Paul, A., Khan, A. A., Prakash, S. & Shum-Tim, D. Intramyocardial sustained delivery of placental growth factor using nanoparticles as a vehicle for delivery in the rat infarct model. *Int. J. Nanomedicine* **6**, 2667–78 (2011).

## INTRODUCTION

74. Ruvinov, E., Leor, J. & Cohen, S. The promotion of myocardial repair by the sequential delivery of IGF-1 and HGF from an injectable alginate biomaterial in a model of acute myocardial infarction. *Biomaterials* **32**, 565–578 (2011).
75. Liu, Z. *et al.* The influence of chitosan hydrogel on stem cell engraftment, survival and homing in the ischemic myocardial microenvironment. *Biomaterials* **33**, 3093–3106 (2012).
76. Li, Z., Guo, X. & Guan, J. A Thermosensitive Hydrogel Capable of Releasing bFGF for Enhanced Differentiation of Mesenchymal Stem Cell into Cardiomyocyte-like Cells under Ischemic Conditions. *Biomacromolecules* (2012).
77. Baumann, L. *et al.* A novel, biased-like SDF-1 derivative acts synergistically with starPEG-based heparin hydrogels and improves eEPC migration in vitro. *J. Control. Release* **162**, 68–75 (2012).
78. Kraehenbuehl, T. P. *et al.* Three-dimensional extracellular matrix-directed cardioprogenitor differentiation: Systematic modulation of a synthetic cell-responsive PEG-hydrogel. *Biomaterials* **29**, 2757–2766 (2008).
79. Puig-Sanvicens, V. A. C. & Semino, C. E. Self-assembling peptide scaffolds as innovative platforms for drug and cell delivery systems in cardiac regeneration. *Drug Deliv. Transl. Res.* **3**, 330–335 (2013).
80. Artym, V. V & Matsumoto, K. Imaging cells in three-dimensional collagen matrix. *Natl. Institutes Heal.* 1–23 (2011).  
doi:10.1002/0471143030.cb1018s48.Imaging
81. Sung, K. E. *et al.* Control of 3-dimensional collagen matrix polymerization for reproducible Human Mammary Fibroblasts cell culture in microfluidic devices. *Natl. Institutes Heal.* **30**, 4833–4841 (2010).
82. Hakkinen, K. M., Harunaga, J. S., Doyle, A. D. & Yamada, K. M. Direct comparisons of the morphology, migration, cell adhesions, and actin cytoskeleton of fibroblasts in four different three-dimensional extracellular matrices. *Tissue Eng.* **17**, (2011).
83. Hesse, E. *et al.* Collagen type I hydrogel allows migration, proliferation and osteogenic differentiation of rat bone marrow stromal cells. *Natl. Institutes Heal.* **94**, 442–449 (2011).
84. Miron-Mendoza, M., Seemann, J. & Grinnell, F. THE DIFFERENTIAL REGULATION OF CELL MOTILE ACTIVITY THROUGH MATRIX STIFFNESS AND POROSITY IN THREE DIMENSIONAL COLLAGEN MATRICES. *Natl. Institutes Heal.* **31**, 6425–6435 (2011).
85. Hong, H. & Stegemann, J. P. 2D and 3D collagen and fibrin biopolymers promote specific ECM and integrin gene expression by vascular smooth muscle cells. *Natl. Institutes Heal.* **19**, 1279–1293 (2009).

86. Kreger, S. T. & Voytik-Harbin, S. L. Hyaluronan concentration within a 3D collagen matrix modulates matrix viscoelasticity, but not fibroblast response. *Natl. Institutes Heal.* **28**, 336–346 (2010).
87. Lund, A. W., Stegemann, J. P. & Plopper, G. E. Inhibition of ERK promotes collagen gel compaction and fibrillogenesis to amplify the osteogenesis of human mesenchymal stem cells in three-dimensional collagen I culture. *Stem Cells Dev.* **18**, 331–41 (2009).
88. Provenzano, P. P., Inman, D. R., Eliceiri, K. W., Trier, S. M. & Keely, P. J. Contact guidance mediated three-dimensional cell migration is regulated by Rho/ROCK-dependent matrix reorganization. *Biophys. J.* **95**, 5374–84 (2008).
89. Zhang, S. Fabrication of novel biomaterials through molecular self-assembly. *Nat. Biotechnol.* **21**, 1171–1178 (2003).
90. Zhang, S., Holmes, T., Lockshin, C. & Rich, A. Spontaneous assembly of a self-complementary oligopeptide to form a stable macroscopic membrane. *Proc. Natl. Acad. Sci. U. S. A.* **90**, 3334–8 (1993).
91. Zhang, S., Gelain, F. & Zhao, X. Designer self-assembling peptide nanofiber scaffolds for 3D tissue cell cultures. *Semin. Cancer Biol.* **15**, 413–420 (2005).
92. Genové, E. *et al.* Functionalized self-assembling peptide hydrogel enhance maintenance of hepatocyte activity in vitro. *J. Cell. Mol. Med.* **XX**, 1–12 (2009).
93. Zhang, S. *et al.* Self-complementary oligopeptide matrices support mammalian cell attachment. *Biomaterials* **16**, 1385–93 (1995).
94. Genové, E., Shen, C., Zhang, S. & Semino, C. E. The effect of functionalized self-assembling peptide scaffolds on human aortic endothelial cell function. *Biomaterials* **26**, 3341–3351 (2005).
95. Holmes, T. C. *et al.* Extensive neurite outgrowth and active synapse formation on self-assembling peptide scaffolds. *Proc. Natl. Acad. Sci. U. S. A.* **97**, 6728–33 (2000).
96. Yokoi, H., Kinoshita, T. & Zhang, S. Dynamic reassembly of peptide RADA16 nanofiber scaffold. *Proc. Natl. Acad. Sci. U. S. A.* **102**, 8414–9 (2005).
97. Zhang, S. & Altman, M. Peptide self-assembly in functional polymer science and engineering. *React. Funct. Polym.* **41**, 91–102 (1999).
98. Altman, M., Lee, P., Rich, A. & Zhang, S. Conformational behavior of ionic self-complementary peptides. *Protein Sci.* **9**, 1095–105 (2000).
99. Liu, W. F. & Chen, C. S. Engineering biomaterials to control cell function. *Mater. today* **8**, 28–35 (2005).
100. Zhang, S. *et al.* Biological surface engineering: a simple system for cell pattern formation. *Biomaterials* **20**, 1213–20 (1999).

## INTRODUCTION

101. Garreta, E., Genove, E., Borros, S. & Semino, C. E. Osteogenic differentiation of mouse embryonic stem cells and mouse embryonic fibroblasts in a three-dimensional self-assembling peptide scaffold. *Tissue Eng.* **12**, 1–14 (2006).
102. Quintana, L. *et al.* Early Tissue Patterning Recreated by Mouse Embryonic Fibroblasts in a Three-Dimensional Environment. *Tissue Eng.* **15**, (2009).
103. Semino, C. E., Merok, J. R., Crane, G. G., Panagiotakos, G. & Zhang, S. Functional differentiation of hepatocyte-like spheroid structures from putative liver progenitor cells in three-dimensional peptide scaffolds. *Differentiation.* **71**, 262–70 (2003).
104. Branco, M. C., Pochan, D. J., Wagner, N. J. & Schneider, J. P. Macromolecular diffusion and release from self-assembled b-hairpin peptide hydrogels. *Natl. Institutes Heal.* **30**, 1339–1347 (2010).
105. Guo, H., Cui, G., Wang, H. & Tan, Y. Transplantation of marrow-derived cardiac stem cells carried in designer self-assembling peptide nanofibers improves cardiac function after myocardial infarction. *Biochem. Biophys. Res. Commun.* **399**, 42–8 (2010).
106. Davis, M. E. *et al.* Injectable self-assembling peptide nanofibers create intramyocardial microenvironments for endothelial cells. *Natl. Institutes Heal.* **111**, 442–450 (2009).
107. Jawad, H. *et al.* Myocardial tissue engineering : a review. *J. Tissue Eng. Regen. Med.* **1**, 327–342 (2007).
108. Oldroyd, K. G., Berry, C. & Bartunek, J. Myocardial repair and regeneration: bone marrow or cardiac stem cells? *Mol. Ther.* **20**, 1102–5 (2012).
109. Messina, E. *et al.* Isolation and expansion of adult cardiac stem cells from human and murine heart. *Circ. Res.* **95**, 911–21 (2004).
110. Bergmann, O. *et al.* Evidence for cardiomyocyte renewal in humans. *Natl. Institutes Heal.* **324**, 98–102 (2010).
111. Arsalan, M. *et al.* Distribution of cardiac stem cells in the human heart. *ISRN Cardiol.* **2012**, 483407 (2012).
112. Gneccchi, M., Danieli, P. & Cervio, E. Mesenchymal stem cell therapy for heart disease. *Vascul. Pharmacol.* **57**, 48–55 (2012).
113. Bayes-Genis, A. *et al.* Human progenitor cells derived from cardiac adipose tissue ameliorate myocardial infarction in rodents. *J. Mol. Cell. Cardiol.* **49**, 771–80 (2010).
114. Bayes-Genis, A., Gálvez-Montón, C., Prat-Vidal, C. & Soler-Botija, C. Cardiac adipose tissue: A new frontier for cardiac regeneration? *Int. J. Cardiol.* (2012). doi:10.1016/j.ijcard.2012.05.082

115. Pal, R., Mamidi, M. K., Das, A. K. & Bhonde, R. Comparative analysis of cardiomyocyte differentiation from human embryonic stem cells under 3-D and 2-D culture conditions. *J. Biosci. Bioeng.* **115**, 200–6 (2013).
116. Anderson, D. *et al.* Transgenic enrichment of cardiomyocytes from human embryonic stem cells. *Mol. Ther.* **15**, 2027–36 (2007).
117. Dixon, J. E., Dick, E., Rajamohan, D., Shakesheff, K. M. & Denning, C. Directed differentiation of human embryonic stem cells to interrogate the cardiac gene regulatory network. *Mol. Ther.* **19**, 1695–703 (2011).
118. Kita-Matsuo, H. *et al.* Lentiviral vectors and protocols for creation of stable hESC lines for fluorescent tracking and drug resistance selection of cardiomyocytes. *PLoS One* **4**, e5046 (2009).
119. Ritner, C. *et al.* An engineered cardiac reporter cell line identifies human embryonic stem cell-derived myocardial precursors. *PLoS One* **6**, e16004 (2011).
120. Takahashi, K. & Yamanaka, S. Induction of pluripotent stem cells from mouse embryonic and adult fibroblast cultures by defined factors. *Cell* **126**, 663–76 (2006).
121. Takahashi, K. *et al.* Induction of pluripotent stem cells from adult human fibroblasts by defined factors. *Cell* **131**, 861–72 (2007).
122. Kehoe, D. E., Jing, D., Lock, L. T. & Tzanakakis, E. S. Scalable stirred-suspension bioreactor culture of human pluripotent stem cells. *Tissue Eng. Part A* **16**, 405–421 (2010).
123. Hazeltine, L. B. *et al.* Effects of substrate mechanics on contractility of cardiomyocytes generated from human pluripotent stem cells. *Int. J. Cell Biol.* **2012**, 508294 (2012).
124. Oh, Y., Wei, H., Ma, D., Sun, X. & Liew, R. Clinical applications of patient-specific induced pluripotent stem cells in cardiovascular medicine. *Heart* **98**, 443–9 (2012).
125. Burridge, P. W., Keller, G. M., Gold, J. D. & Wu, J. C. Production of de novo cardiomyocytes: human pluripotent stem cells differentiation and direct reprogramming. *Natl. Institutes Heal.* **10**, 16–28 (2013).
126. Ye, L. *et al.* Effective cardiac myocyte differentiation of human induced pluripotent stem cells requires VEGF. *PLoS One* **8**, e53764 (2013).
127. Park, I.-H. *et al.* Reprogramming of human somatic cells to pluripotency with defined factors. *Nature* **451**, 141–6 (2008).
128. Ieda, M. *et al.* Direct reprogramming of fibroblasts into functional cardiomyocytes by defined factors. *Cell* **142**, 375–86 (2010).

## INTRODUCTION

129. Takeuchi, J. K. & Bruneau, B. G. Directed transdifferentiation of mouse mesoderm to heart tissue by defined factors. *Natl. Institutes Heal.* **459**, 708–711 (2009).
130. Efe, J. A. *et al.* Conversion of mouse fibroblasts into cardiomyocytes using a direct reprogramming strategy. *Nat. Cell Biol.* **13**, 215–22 (2011).
131. Jopling, C., Boue, S. & Izpisua Belmonte, J. C. Dedifferentiation, transdifferentiation and reprogramming: three routes to regeneration. *Nat. Rev. Mol. Cell Biol.* **12**, 79–89 (2011).
132. Giraud, M.-N., Guex, A. G. & Tevæearai, H. T. Cell therapies for heart function recovery: focus on myocardial tissue engineering and nanotechnologies. *Cardiol. Res. Pract.* **2012**, 971614 (2012).
133. Mohsin, S., Siddiqi, S., Collins, B. & Sussman, M. A. EMPOWERING ADULT STEM CELLS FOR MYOCARDIAL REGENERATION. *Natl. Institutes Heal.* **109**, 1415–1428 (2012).

## Chapter 2: Materials and Methods





## **CHAPTER 2. MATERIALS AND METHODS**

### *2.1. 2D Culture of human Normal Dermal Fibroblasts (hNDFs)*

Human Normal Dermal Fibroblasts (hNDFs), isolated from the skin of anonymous adult patients, were sent from our collaborator Dr. Jesús Otero (*Hospital Universitario Central de Asturias*, Oviedo, Spain). These cells (approximate 7 passages) passed the Ethical Committee protocol from the hospital where pertinent biohazard controls were tested in order to ensure the experimenter's safety (human immunodeficiency virus and hepatitis infection test). The cells were cultured at 37°C under 5% CO<sub>2</sub> in 75 cm<sup>2</sup> flasks. The medium used was DMEM (Dulbecco's Modified Eagle's Medium (DMEM), high Glucose (4.5 g/l), without L-Glutamine – PAA – E15-009) supplemented with 10% Fetal Bovine Serum (FBS, Sigma – F7524), 2 mM L-glutamine (L-Glutamine 200 mM (100X) – PAA – M11-004) and 50 U penicillin – 0.05 mg/ml streptomycin (Penicillin – Streptomycin – Sigma – P4458).

Human NDFs were expanded in 75 cm<sup>2</sup> flasks (2D cultures) and cultured in the control medium described above. Before reaching a high cellular passage (below 20), cells were frozen in liquid nitrogen and kept as stocks of cells for future experiments. Fibroblasts were cryopreserved at a final concentration of 10<sup>6</sup> cells/0.5 ml per cryotube. The freezing medium was based on FBS (Sigma – F7524) with 5% dimethyl sulfoxide (DMSO, Dimethyl sulfoxide – Sigma – D2650). The DMSO acts as a cryoprotector to avoid cellular fracture by reducing the formation of intracellular water crystals. The freezing process was performed *slowly* by decreasing the temperature of cells suspended in freezing medium from 4°C to -80°C in several hours (24 hours). Therefore, hNDFs were re-suspended in cold freezing medium, aliquoted in cryotubes that were placed in an ice container and immediately stored at -80°C. The following day, cells were submerged in liquid nitrogen until the next programmed culture.

On the other hand, the thaw process was performed *quickly*. Indeed, cryotubes were defrosted by fast submersion in a bath at 37°C until the cell suspension was liquid. Thermic shock has been shown to improve cell survival as it avoids the explosion of cells related to water crystal formation and osmotic exchanges through the plasmatic membrane. Then, the cell content of each cryotube was mixed with 10 ml of control medium pre-warmed at 37°C in order to wash out the DMSO as it is very cytotoxic. After centrifuging the cells at 1000 rpm for 5 minutes, the pellet was re-suspended in 1 ml of control medium and added to a 75 cm<sup>2</sup> flask already containing 9

## MATERIALS AND METHODS

ml of medium (flasks were equilibrated beforehand with medium and placed in the incubator for 30 minutes before seeding the cells). Indeed, the final cellular concentration was  $10^6$  cells/75 cm<sup>2</sup>.

Cells were passaged at a ratio of 1:2 when they reached around 80% confluence. Thus, cells were washed once with PBS 1X and treated with 2 ml of porcine trypsin (Trypsin – EDTA solution – Sigma – T4299) at 37°C for 3 – 4 minutes. The enzymatic digestion is an aggressive process and must be stopped quickly with FBS (naturally containing trypsin inhibitors) as soon as > 50% of the cells are detached. The trypsin is a serine protease that catalyzes the hydrolysis of peptide bonds, degrading the main anchor sites of the cell to its substrate, the flask surface. Therefore, the reaction was stopped with control medium by doubling the trypsin's volume added (4 ml). The cellular suspension was centrifuged at 1000 rpm for 5 minutes and cells were seeded as explained above.

### 2.2. 2D Culture of human induced Pluripotent Stem Cells (hiPSCs) Riv9

Human induced Pluripotent Stem Cells (hiPSCs) Riv9 were generously provided by Dr. Duncan Chee Liew from the Stem Cell Core Facilities at the University of California Riverside, Riverside, California, USA. Cells were cultured in 6-well-plates, which were pre-coated with matrigel (BD Matrigel Basement Membrane Matrix – Fisher Scientific – 356234) for 30 minutes at 37°C and 5% CO<sub>2</sub>. Matrigel is a commercial gelatinous protein mixture extracted from Engelbreth-Holm-Swarm mouse sarcoma cells. According to the manufacturers, matrigel contains high amounts of laminin (55%), collagen IV (30%), entactin (10%), heparin sulfate proteoglycan (5%), insulin-like growth factor 1 (11-24 ng/ml) and other growth factors. Indeed, due to its rich content in components of basement membranes enriched with laminin, collagen, other extracellular matrix proteins and some growth factors, matrigel covers and renders plastic surfaces cell friendly for hiPSCs. The concentrated matrigel was diluted with DMEM F12 (1/50, DMEM/F-12, GlutaMAX™ – Gibco® – 10565-018) and the mixture was added to each well. Cells were seeded on matrigel pre-coated wells and cultured with supplemented mTeSR (mTeSR™1 – Stem Cell Technologies – 5850).

Furthermore, hiPSCs grew forming colonies attached to the pre-coated well surface. Confluent cells were passaged at a ratio of 1:3 to 1:6 depending on their growth speed and the size of the colonies. It has been observed that the larger is the colony, the more differentiated the cells appear to be. For each passage, cells were

incubated with 1 ml accutase (Accutase™ – Stem Cell Technologies – 7920) for 1 minute at room temperature. Accutase is a cell detachment solution of proteolytic and collagenolytic enzymes from invertebrate species. Due to its non-mammalian source, accutase is guaranteed free of parvovirus and other viruses common in trypsin. Afterwards accutase was removed, fresh supplemented mTeSR was added (taking into account the ratio of passaging) and with the help of a scraper, colonies were detached from the surface. It is important to keep the cells in colonies during the passaging in order to increase their viability and this is why the pipetting should be gentle. Then, cells were seeded on new pre-coated wells. The volume of medium per well was 1 ml to allow an easier and quicker precipitation of the colonies on the well's surface. After 2 days, 1 ml of fresh medium was added and from then onwards the whole medium was changed every two days (2 ml).

Interestingly, hiPSCs were treated with ROCK inhibitor (RI, Inhibitor Y-27632 – VWR – 80511-062) in the first passage after thawing them. RI inactivates the ROCK pathway, which leads to cell death. Cells frozen in 90% FBS (PAA – A15-204 Lot A20410-7002) and 10% dimethyl sulfoxide (DMSO, Fisher Scientific – BP231-100) could be vulnerable after defrosting and this is why it is strongly recommended to treat them with RI to increase the cell survival at the first passage. Human iPSCs have been shown to die as single cells whereas treated cells with RI for one hour at 37°C before trypsinization appeared to survive.

### 2.3. 3D Culture of human Normal Dermal Fibroblasts (hNDFs) in RAD16-I

To carry out three-dimensional cultures, an appropriate scaffold should be chosen to allow cell integration. In this work, the peptide solution RAD16-I (PuraMatrix™ Peptide Hydrogel – BD Bioscience – 354250) has been used. The nanofibers of RAD16-I self-assemble and form a network with a pore diameter ranging from 50 to 150 nm and a fiber diameter ranging from 1 to 10 nm. This pore size allows easy molecule diffusion (i.e. growth factors, nutrients, toxins, and gasses). The nanoscaffold assembling is based on weak interactions, which facilitate cellular growth, migration and interaction. The nanofiber density correlates positively with the concentration of self-assembling peptide solution used. The self-assembling process rapidly occurs in the presence of millimolar concentrations of monovalent salts at levels that are found in physiological conditions.

## MATERIALS AND METHODS

Human NDFs expanded in 2D cultures (flasks) were washed once with PBS 1X and treated with porcine trypsin (Trypsin – EDTA solution – Sigma – T4299) at 37°C for 3 – 4 minutes (see Materials and Methods 2.1). Cells were counted and re-suspended in sucrose 10% at  $4 \cdot 10^6$  cells/ml. On the other hand, the peptide solution RAD16-I was diluted at 0.3% in sucrose 10%. When mixing both suspensions, peptide (1/2) and cells (1/2), the final peptide concentration was 0.15% and the cellular concentration was  $2 \cdot 10^6$  cells/ml. The suspension (40  $\mu$ l) containing  $8 \cdot 10^5$  cells and RAD16-I solution was loaded into 9 mm diameter cell culture inserts (Millicell Cell Culture Insert – Millipore – PICM01250) previously placed in 6-well culture plates and equilibrated with medium DMEM (Dulbecco's Modified Eagle's Medium (DMEM), high Glucose (4.5 g/l), without L-Glutamine – PAA – E15-009) supplemented with 15% Fetal Bovine Serum (FBS, Sigma – F7524), 2 mM L-glutamine (L-Glutamine 200 mM (100X) – PAA – M11-004) and 50 U penicillin – 0.05 mg/ml streptomycin (Penicillin – Streptomycin – Sigma – P4458) at 37°C. Thus, when RAD16-I self-assembled, a hydrogel was formed with hNDFs dispersed inside the scaffold. After the gel was built, the medium was added slowly in aliquots of 50  $\mu$ l at a time. Afterwards, 500  $\mu$ l of medium was placed inside the insert and 2.5 ml outside it (in the well). Constructs were incubated at 37°C with 5% CO<sub>2</sub> and the medium was changed every day (500  $\mu$ l of medium was replaced by removing this volume from the well and adding 500  $\mu$ l of fresh medium inside the insert). In resume, cells were cultured in a truly 3D environment that resembled their real *in vivo* milieu. This biological analogue scaffold is a good approach to mimic the extracellular matrix counterpart<sup>1</sup>.

In addition, hNDFs were embedded in RAD16-I 0.15% (as explained above) in defined medium containing DMEM (Dulbecco's Modified Eagle's Medium (DMEM), high Glucose (4.5 g/l), without L-Glutamine – PAA – E15-009), 2 mM L-glutamine (L-Glutamine 200 mM (100X) – PAA – M11-004), 50 U penicillin – 0.05 mg/ml streptomycin (Penicillin – Streptomycin – Sigma – P4458) and 20 nM Platelet-Derived Growth Factor (PDGF, Platelet-Derived Growth Factor-BB from rat – Sigma – P4056). Indeed, the effect of FBS on the 3D cultures was assessed. Finally, the cellular behavior of hNDFs was compared when cells were cultured in complex medium (rich in FBS) and defined medium (lacking FBS and rich in PDGF).

### 2.4. 3D Culture of human Embryonic Stem Cells (hESCs) H9 in RAD16-I

In stem cell biology research, many human Embryonic Stem Cell (hESC) lines have been developed and widely used in differentiation assays. Among all of them, hESCs

line H9 is the one that has been reported the most frequently in literature by the end of 2008 (36.7% of published studies)<sup>2</sup>. H9 cell line was provided by Dr. Duncan Chee Liew from the Stem Cell Core Facilities at the University of California Riverside, Riverside, California, USA.

In this thesis, hESCs H9 were used to establish the adequate conditions to embed human stem cells in the peptide scaffold RAD16-I (PuraMatrix™ Peptide Hydrogel – BD Bioscience – 354250). Cells were expanded in 2D cultures (following the same protocol as with hiPSCs Riv9, see Materials and Methods 2.2), on matrigel (BD Matrigel Basement Membrane Matrix – Fisher Scientific – 356234) pre-coated 6-well-dishes. At confluence, H9 cells were pre-treated with ROCK inhibitor (RI, Inhibitor Y-27632 – VWR – 80511-062) at 37°C and 5% CO<sub>2</sub> for one hour. Human ESCs cultured as single cells seem to activate a ROCK pathway that brings them to apoptosis. Therefore, this response was inhibited using a ROCK inhibitor before trypsinizing and individualizing cells in order to keep them alive. Thus, hESCs were washed once with PBS 1X and incubated with trypsin (0.25% Trypsin-EDTA (1X), Phenol Red – Gibco – 25200-056) at 37°C and 5% CO<sub>2</sub> for 4 minutes. The enzymatic reaction was stopped with culture medium mTeSR (mTeSR™1 – Stem Cell Technologies – 5850). The 3D encapsulation protocol followed as explained above for hNDFs (see Materials and Methods 2.3). Cells H9 were cultured in RAD16-I 0.15% at three different concentrations: 2·10<sup>6</sup> cells/ml, 4·10<sup>6</sup> cells/ml and 8·10<sup>6</sup> cells/ml. The goal was to establish the appropriate cell concentration in RAD16-I.

On the other hand, one of the downstream experiments regarding cardiac differentiation of human induced Pluripotent Stem Cells (hiPSCs), was to disrupt the constructs for subsequent assays. The conditions of the experiment were established using hESCs. Thus, different enzymatic treatments were evaluated to collect individual cells from the 3D scaffold. Three enzymes were used: collagenase IV (protease that degrades extracellular matrix, Collagenase IV – Sigma – C5138), accutase (proteolytic and collagenolytic enzyme, mainly used for cell detachment, Accutase™ – Stem Cell Technologies – 7920) and trypsin (very strong serine protease that cleaves peptides on the C-terminal side of lysine and arginine). Therefore, hESCs were cultured in 3D in mTeSR medium. After 3 days, cells were pre-treated with RI as explained above, washed once with PBS 1X and incubated for 4 minutes at 37°C and 5% CO<sub>2</sub> with each corresponding enzyme. The mixture of cells and enzyme was gently pipetted and split in 3 assays: suspension of cells after disruption, 2D culture on matrigel and 3D culture

## MATERIALS AND METHODS

with RAD16-I 0.15%. Cell viability was assessed in cells suspended just after each enzymatic treatment (see Materials and Methods 2.9.2).

### 2.5. 3D Culture of human induced Pluripotent Stem Cells (hiPSCs) Riv9 in RAD16-I

Human induced Pluripotent Stem Cells (hiPSCs) Riv9 were cultured in a 3D environment based on RAD16-I (PuraMatrix™ Peptide Hydrogel – BD Bioscience – 354250). First of all, cells were treated with ROCK inhibitor (RI, Inhibitor Y-27632 – VWR – 80511-062) for one hour at 37°C and 5% CO<sub>2</sub> in order to keep them alive in the subsequent step of trypsinization (0.25% Trypsin-EDTA (1X), Phenol Red – Gibco – 25200-056). Single cells were counted and re-suspended in sucrose 10% at a final concentration of  $8 \cdot 10^6$  cells/ml. The cellular suspension was then mixed with RAD16-I diluted in sucrose 10% to 0.3%. Afterwards, 40 µl of the solution was loaded on the membrane of each cell culture insert, which diameter was 12 mm (Millicell Cell Culture Insert – Millipore – PICM01250). Cell culture inserts with a wider diameter (30 mm, Millicell Cell Culture Insert – Millipore – PICM03050) were also used in experiments requiring a pool of 3D cultures (3 constructs/insert were loaded). In all the cases, the final cell concentration was  $4 \cdot 10^6$  cells/ml and 0.15% RAD16-I. The protocol followed as defined beforehand with hNDFs (see Materials and Methods 2.3). Cells were cultured with supplemented mTeSR (mTeSR™1 – Stem Cell Technologies – 5850). Regarding the three constructs cultured per big cell culture insert, the volumes of medium added after the encapsulation were three times the volumes added in small inserts containing one single 3D construct. The medium was changed every day as explained above (see Materials and Methods 2.3): 500 µl were replaced in the case of small cell culture inserts and 1.5 ml in the big ones.

### 2.6. 3D Culture of porcine Mediastinal Adipose Tissue Progenitor Cells (pMATPCs) in RAD16-I

Porcine Mediastinal Adipose Tissue Progenitor Cells (pMATPCs) were isolated from mediastinum in swine (by the collaborator group from *Institut Germans Trias i Pujol*). The porcine stem cells were embedded in the peptide 3D scaffold RAD16-I (PuraMatrix™ Peptide Hydrogel – BD Bioscience – 354250)<sup>3</sup>. To obtain the cell population required to create the 3D constructs, cells were first expanded in culture flasks (2D cultures). At confluence, cells were trypsinized (Trypsin – EDTA solution – Sigma – T4299), washed with PBS and suspended in sucrose 10% at a final

concentration of  $8 \cdot 10^6$  cells/ml. The cell suspension was mixed with an equal volume of RAD16-I 0.3% in sucrose 10%. As a result, the final concentration was  $4 \cdot 10^6$  cells/ml in RAD16-I 0.15% in sucrose 10%. Then, 40  $\mu$ l of the mixture was loaded into cell culture inserts (Millicell Cell Culture Insert – Millipore – PICM01250) placed in 6-well-plates. Culture medium was added progressively:  $\alpha$ MEM (MEM alpha Modified Liquid with Nucleosides with L-Glutamine – PAA – E15-862) supplemented with 15% Fetal Bovine Serum (FBS, Sigma – F7524), 50 U penicillin – 0.05 mg/ml streptomycin (Penicillin – Streptomycin – Sigma – P4458) and 10  $\mu$ l Plasmocin (Plasmocin™ treatment – Invitrogen – ant-mpt). The slow addition of medium washed out the sucrose from the cells, which was crucial for cell survival. Finally, the medium was removed from the wells and fresh medium was added into the cell culture inserts (0.5 ml) containing the gelified constructs and into the well (2.5 ml). Every day, 0.5 ml of medium from the well was removed and 0.5 ml of fresh medium was added into the cell culture insert<sup>1</sup>.

### 2.7. 3D Culture of human Normal Dermal Fibroblasts (hNDFs) in Collagen I

Hydrogels of collagen have been widely used as tissue-derived natural polymer to generate three-dimensional cultures. Moreover, a variety of cells have been cultured either in a *sandwich* shape construct or embedded directly in collagen. Indeed, culture techniques based on collagen are nowadays the gold standard and this is why 3D constructs based on Collagen I were used as a benchmark for RAD16-I constructs.

The Collagen type I (BD™ Collagen I, Rat Tail – BD Biosciences – 354236) substrate was prepared at a final concentration of 2.8 mg/ml (0.28%) following the manufacturer's instructions. Indeed, the concentrated Collagen I solution was diluted in a mixture of 10% PBS 10X (Dulbecco's PBS 10X without Ca & Mg- PAA – H15-011) containing 5  $\mu$ g/ml phenol red (Phenol red solution – Sigma – P0290) and 90% water (Sterile Water EP Grade – PAA – S21-012). Afterwards, the solution was kept in ice and neutralized with 1 M NaOH until reaching neutral pH 7 (the pink color of the pH indicator given by the phenol red became yellow). The polymerization of Collagen I occurs by increasing the temperature and the pH to a neutral level. This is why at this point of the protocol cells had to be ready to mix with the solution in order to create the 3D culture. Thus, hNDFs were trypsinized in parallel, re-suspended in cold PBS 1X, counted and mixed with neutralized Collagen I at a final concentration of  $2 \cdot 10^6$  cells/ml and 0.14% Collagen I. A volume of 40  $\mu$ l of the mixture was loaded in each non-treated well. In this thesis, 48-well-plates were coated with 1% sterile cell culture warmed agarose (100  $\mu$ l/well, Agarose low gelling temperature – Sigma – A9045). The pre-

coating avoids the constructs to attach to the plastic surface and it also prevents the cells to migrate from the 3D collagen construct to the surface of the well and settle on it. The constructs were incubated for 30 minutes at 37°C and 5% CO<sub>2</sub> to allow the spontaneous gelification of the matrix. Certainly, collagen fibrils polymerize in heterogeneous cross-linked structures at physiological conditions of neutral pH 7 and 37°C<sup>4</sup>. Finally, embedded hNDFs in Collagen I were maintained with control medium (see Materials and Methods 2.3). The medium was carefully changed every day<sup>5</sup>.

### 2.8. DAPI and Phalloidin staining

To have an insight into the cellular cytoskeleton, a rapid assay was carried out: a staining with two fluorescent dyes, DAPI (4'-6-Diamidino-2-Phenylindole – Sigma – D9542) and phalloidin (Phalloidin–Tetramethylrhodamine B Isothiocyanate – Sigma – P1951). DAPI is a fluorescent probe that binds strongly to nucleic acids (dsDNA and RNA) whereas phalloidin stains actin microfilaments. Phalloidin inhibits microfilament de-polymerization and in this case, it is attached to TRITC that has its maximum excitation at 540 – 545 nm and emission at 570 – 573 nm (red region). DAPI is excited at 364 nm and emits at 454 nm (blue region) when it forms the DAPI-DNA complex.

First of all, hNDFs were fixed with 1% paraformaldehyde (PFA, Paraformaldehyde powder 95% – Sigma – 158127) for one hour at room temperature. PFA was previously filtered at 0.45 µm to avoid contaminations and clumps. After the fixation protocol, cells were washed three times with PBS 1X, incubated with 0.1% Triton X-100 (Triton™ X-100 – Sigma – X100) in PBS 1X for 30 minutes to permeabilize the cellular membrane, 25 minutes with 0.1 µg/ml phalloidin-TRITC in PBS 1X and 5 minutes with 0.1 µg/ml DAPI. Samples were washed with PBS 1X in order to remove dyes' excess and then examined under the inverted fluorescent microscope (Axiovert 200M – Carl Zeiss) using its ApoTome (Carl Zeiss) application. The concentration and incubation time of the DAPI dye are crucial for an optimal staining. If these are not respected, DAPI not only binds to DNA in the nucleus, but also to RNA in the cytoplasm. As a result, nuclei cannot be distinguished, which is the aim of the technique, and the background interferes with the phalloidin-TRITC staining.

Regarding the human induced Pluripotent Stem Cells, 2D cultures as well as 3D constructs were washed once with PBS 1X and fixed for 30 minutes with 4% PFA (PFA 40% – Electron Microscopy Sciences – 15715-S) at 4°C. Thus, cells were treated as mentioned before and incubated with 20 µg/ml DAPI (4'-6-Diamidino-2-Phenylindole –



Sigma – D9542) and 0.1 µg/ml phalloidin-TRITC (Phalloidin–Tetramethylrhodamine B Isothiocyanate – Sigma – P1951) in PBS 1X for 30 minutes. After having conveniently washed the cultures with PBS 1X, cells were observed under the fluorescent microscope Nikon Eclipse TI. The quality of the pictures was objectively improved using the deconvolution option of the NIS elements program, which decreases the background by concentrating and averaging the fluorescent noise surrounding the cells.

## 2.9. *Live/Dead assay*

### 2.9.1. *Human Normal Dermal Fibroblasts (hNDFs)*

This assay is a quick technique to measure cellular viability in 2D and 3D cultures. The live/dead assay (LIVE/DEAD Viability/Cytotoxicity Kit for mammalian cells – Invitrogen – L-3224) is a two-color fluorescence assay that simultaneously determines living (green) and dead (red) cells. Calcein acetoxymethyl (Calcein AM) is a cell-permeable and non-fluorescent compound that in contact with intracellular esterases becomes intensely fluorescent (in the green spectrum zone). So, it renders green, under the fluorescent microscope, all the living cells because they have intracellular esterase activity. On the other hand, ethidium homodimer-1 (EthD-1) appears fluorescent when bound to nucleic acids and produces a bright red fluorescence in dead cells that have their plasmatic membrane damaged, which allows the entrance of the compound.

Thus, both compounds (EthD-1 and Calcein AM) were mixed at a final concentration of 2 µM each in PBS 1X. This was called the working solution. Moreover, cells were washed three times with PBS 1X for 30 minutes and then incubated in the dark with the working solution for 15 minutes and washed again in order to remove any excess of fluorescent compounds. Then the samples were ready to analyze under the fluorescent microscope.

### 2.9.2. *Human Embryonic Stem Cells (hESCs) H9 and human induced Pluripotent Stem Cells (hiPSCs) Riv9*

In this case, the technique was based on the same principle as explained before but instead of using a kit including both dyes, the staining chemicals

were purchased separately. Indeed, hESCs were incubated with green calcein (CellTrace™ Calcein Green, AM – Invitrogen – C34852) at 2  $\mu$ M in PBS 1X for 15 minutes in the dark. Regarding the hiPSCs, these were incubated with the green dye mentioned above and ethidium homodimer-1 (Ethidium Homodimer-1 – Invitrogen – E1169) at 1  $\mu$ M in PBS 1X for 15 minutes. Afterwards, cells were washed in PBS 1X and observed under the inverted fluorescent microscope.

### 2.10. Differentiation of human Normal Dermal Fibroblasts (hNDFs) in 3D cultures

#### 2.10.1. Adipogenesis induction

Human Normal Dermal Fibroblasts (hNDFs) have a mesodermal origin as well as adipocytes. It has been shown that human Mesenchymal Stem Cells (hMSCs) can be chemically differentiated into adipocytes *in vitro*<sup>6</sup>.

Fibroblasts were embedded in RAD16-I 0.15% and cultured in 3D as explained above (see Materials and Methods 2.3). Human NDFs were cultured for 20 days in adipogenic induction medium containing DMEM (Dulbecco's Modified Eagle's Medium (DMEM), high Glucose (4.5 g/l), without L-Glutamine – PAA – E15-009), 10% fetal bovine serum (FBS, Sigma – F7524), 2 mM L-glutamine (L-Glutamine 200 mM (100X) – PAA – M11-004), 50 U penicillin – 0.05 mg/ml streptomycin (Penicillin – Streptomycin – Sigma – P4458), 0.5 mM isobutylmethylxanthine (3-Isobutyl-1-methylxanthine – Sigma – I5879), 100  $\mu$ M indomethacin (Indomethacin – Sigma – I7378), 10  $\mu$ g/ml insulin (Insulin solution human – Sigma – I9278) and 1  $\mu$ M dexamethasone (Dexamethasone – Sigma – D8893). Control constructs were cultured for 20 days in control medium containing DMEM (Dulbecco's Modified Eagle's Medium (DMEM), high Glucose (4.5 g/l), without L-Glutamine – PAA – E15-009) supplemented with 15% Fetal Bovine Serum (FBS, Sigma – F7524), 2 mM L-glutamine (L-Glutamine 200 mM (100X) – PAA – M11-004) and 50 U penicillin – 0.05 mg/ml streptomycin (Penicillin – Streptomycin – Sigma – P4458).

Cells were observed every day under the light phase microscope in order to analyze their morphology (cells cultured with control medium were used to compare the degree of adipogenic differentiation) and droplet lipid formation.

### 2.10.2. Cardiogenesis induction

Cardiomyocytes and dermal fibroblasts have a common mesodermal ancestor. Human Embryonic Stem Cells (hESCs) spontaneously differentiate into cardiomyocyte cells *in vitro*. This commitment can be accelerated and increased with chemical inductors. Indeed, ascorbic acid (AA) is an anti-oxidant that plays a key role in cardiogenesis. Although its role is unknown, it has been proved that it does not act as an anti-oxidant itself<sup>7</sup>.

Human NDFs were embedded in RAD16-I 0.15% at a final concentration of  $2 \cdot 10^6$  cells/ml and cultured for 20 days. The culture medium used contained cardiogenic inductors and its composition was 47% Iscove's Modified Dulbecco's Medium (IMDM – Gibco® – 21980-032), 47% Ham's F-12 Nutrient Mixture (Ham's F-12 Nutrient Mix, GlutaMAX™ – Gibco® – 31765-027), 4% horse serum (Sigma – H1138), 1%  $\alpha$ MEM (MEM alpha Modified Liquid with Nucleosides with L-Glutamine – PAA – E15-862), 50 U penicillin – 0.05 mg/ml streptomycin (Penicillin – Streptomycin – Sigma – P4458), 10  $\mu$ g/ml insulin (Insulin solution human – Sigma – I9278), 20 ng/ml Transforming Growth Factor- $\beta$ 1 (TGF- $\beta$ 1 from porcine platelets – Sigma – T5050) and 10  $\mu$ g/ml ascorbic acid (AA, L-Ascorbic acid 2-phosphate sesquimagnesium salt hydrate – Sigma – A8960)<sup>8</sup>. Control constructs were cultured for 20 days in control medium (DMEM (Dulbecco's Modified Eagle's Medium (DMEM), high Glucose (4.5 g/l), without L-Glutamine – PAA – E15-009) supplemented with 15% Fetal Bovine Serum (FBS, Sigma – F7524), 2 mM L-glutamine (L-Glutamine 200 mM (100X) – PAA – M11-004) and 50 U penicillin – 0.05 mg/ml streptomycin (Penicillin – Streptomycin – Sigma – P4458)).

## 2.11. Cardiogenic differentiation of human induced Pluripotent Stem Cells (hiPSCs) Riv9

### 2.11.1. 2D cultures

Human induced Pluripotent Stem Cells (hiPSCs) were cultured with control medium mTeSR (mTeSR™1 – Stem Cell Technologies – 5850) on pre-coated matrigel (BD Matrigel Basement Membrane Matrix – Fisher Scientific – 356234) wells as explained in section 2.2. Day 0 of the cardiogenic differentiation experiment was defined as the day when cells reached confluence. At this

point, control medium was replaced by induction medium DMEM (Dulbecco's Modification of Eagle's Medium, DMEM, Cellgro – 10-013-CV), 15% fetal bovine serum (FBS, PAA – A15-204 Lot A20410-7002), 1% non-essential amino acids (MEM NEAA, Cellgro – 25-025-CI), 0.5% penicillin-streptomycin (Penicillin-Streptomycin Solution, 100X – Cellgro – 30-002-CI) and 0.1 mM  $\beta$ -mercaptoethanol (2-mercaptoethanol, 55 mM – Gibco® – 21985-023). Cells were cultured for 25 days in cardiogenic medium. Furthermore, hiPSCs were induced with two cardiogenic media: with and without ascorbic acid (AA 50  $\mu$ g/ml, L-Ascorbic acid – Sigma – A4544). Medium was replaced every day (1 ml/24-well and 3 ml/6-well).

### 2.11.2. 3D cultures

In this case, human induced Pluripotent Stem Cells (hiPSCs) were expanded in 2D cultures and embedded afterwards in RAD16-I (see Materials and Methods 2.5). From the beginning of the 3D construct formation, cells were cultured with the induction medium mentioned above (with and without ascorbic acid). Day 0 corresponded to cell confluence in 2D cultures, when cells were harvested and embedded in the peptide scaffold. Four inserts (1 construct/cell culture insert (Millicell Cell Culture Insert – Millipore – PICM01250)) were placed in each well (6-well-plates). Each cell culture insert contained one construct submerged in 500  $\mu$ l of induction medium. Medium was added in each well (1 ml). Two milliliters of medium was removed from the well every day whereas 500  $\mu$ l of fresh medium was carefully added in each cell culture insert.

### 2.12. Human pericardium decellularization

Human pericardium is an avascular structure rich in collagen fibrils and small elastic fibers. Thus, it was used as a biological patch for cell release in the porcine infarcted area. In order to avoid any immunological rejection of the xenograft, an exhaustive wash out of the endogenous human pericardial cells was carried out<sup>9</sup>.

Human pericardium was used as a macro-scaffold support for the 3D micro-scaffold based on RAD16-I. Thus, pieces of pericardium were collected from the cardiology operation room at the *Germans Trias i Pujol* Hospital. All the samples were extracted from cardiac surgeries with the previous agreement and signed consent of the patients. Pericardia were washed for 10 minutes three times with dH<sub>2</sub>O in order to remove the

blood. Then, the endogenous pericardial cells were disrupted with 1% sodium dodecyl sulfate (SDS, Sigma – L5750) in dH<sub>2</sub>O for at least 72 hours with stirring. Afterwards, pericardia were washed again with dH<sub>2</sub>O as explained beforehand. Consecutively, they were incubated with 1% Triton-X100 (Triton™ X-100 – Sigma – X100) in dH<sub>2</sub>O with stirring for at least 24 hours to remove cell traces<sup>9,10</sup>. An extensive perfusion was carried out to wash out all the endogenous cells. For this, a vacuum system was used. Pericardia were placed on a filter paper and 100 ml of 1% Triton-X100 in dH<sub>2</sub>O were poured through them and then 100 ml of PBS 1X. Finally, pericardia were kept in PBS 1X for 24 hours before lyophilization at -80°C for 24 hours. The pieces of pericardium were sterilized with gamma ray at high dose.

### 2.13. *Self-assembling peptide scaffold RAD16-I combined to NanoGold*

A mixture of RAD16-I solution and nanoparticles of NanoGold (Nanogold®-Streptavidin conjugate – Nanoprobes – 2016) was prepared to make the micro-scaffold more electrically conductive. Indeed, pre-synthesized lyophilized Biotin-RAD16-I was solubilized in dH<sub>2</sub>O at a final concentration of 0.15%. Therefore, 9 µl Biotin-RAD16-I at 0.15% was mixed with 1 µl Streptavidin-NanoGold ( $5.5 \times 10^5$  particles). After 20 minutes, the specific binding occurred. Then, 90 µl of RAD16-I 0.15% in dH<sub>2</sub>O were added and the mixture was gently pipetted. The final working solution contained 1% NanoGold (at a final concentration of  $5.5 \times 10^7$  particles/µl) and 99% RAD16-I (PuraMatrix™ Peptide Hydrogel – BD Bioscience – 354250) in dH<sub>2</sub>O at 0.15% (9% of it was Biotin-RAD16-I).

### 2.14. *Porcine cardiac smart patch*

The *smart patch* that was placed on the infarcted myocardium of a porcine model was combined as it follows. First, the decellularized, lyophilized and sterilized pericardium (see Materials and Methods 2.12) was cut with a scalpel (2 x 1 cm) and Lead Coupler stainless steel electrodes (Data Sciences International – Kit 276-0031-001) were connected at both extremes. Afterwards, the joints were embedded with 10 µl of the NanoGold solution (see Materials and Methods 2.13) and 20 minutes later the mixture gellified in between the pericardium's fibers surrounding the electrodes. The electrodes were connected to a measurement system device coated with biocompatible silicone that was implanted under the skin of the porcine nape. This device recorded swine electrocardiograms (ECG) and sent the information via Zigbee to a computer (on line monitoring). Then, porcine Mediastinal Adipose Tissue

Progenitor Cells (pMATPCs) were embedded with RAD16-I following the protocol explained above (see Materials and Methods 2.6) at a final concentration of  $10 \times 10^6$  cells/ml and 0.15% hydrogel. This mixture was seeded in the middle of the pericardium, in between the two NanoGold drops. After 20 minutes, the designed scaffold was implanted on the porcine infarcted myocardium<sup>11</sup>.

### 2.15. Immunocytochemistry (ICC)

Immunocytochemistry (ICC) technique consists in detecting the presence of target proteins. In this thesis, indirect ICC has been applied (use of primary specific antibodies and secondary tagged ones). All the 2D cultures (and cytopspin samples) have been tested using fluorescent ICC whereas all the 3D constructs have been stained using enzyme-tag ICC based on Horseradish Peroxidase (HRP) activity.

#### 2.15.1. Fluorescence-tag immunocytochemistry

First of all, cells (in 2D cultures and cytopspin (see Materials and Methods 2.24) on slides) were washed with PBS 1X and fixed with 4% paraformaldehyde (PFA 40% – Electron Microscopy Sciences – 15715-S) at 4°C for 30 minutes. Then, cells were washed three times with PBS 1X for 5 minutes (without stirring, cells shouldn't be stirred at any time during this protocol to avoid cell detachment). The next step was to permeabilize the cellular membrane with 0.1% Triton X-100 (Triton X-100 – Fisher Scientific – BP-151-100) in PBS 1X for 15 minutes at room temperature (RT) to allow the further diffusion of molecules (antibodies). Cells were washed again three times with PBS 1X. Afterwards, the cells were incubated in a blocking solution for one hour at RT. The blocking buffer (BB) contained 10% fetal bovine serum (FBS, PAA – A15-204 Lot A20410-7002) and 0.5% bovine serum albumin (BSA, Fisher Scientific – BP1600-100) in PBS 1X. The convenient dilution of primary antibodies (**Table 1**) was prepared in BB and cells were incubated with the antibodies at 4°C overnight (ON). The following day, cells were washed three times with PBS 1X and incubated with secondary antibodies (diluted in BB) and 20 µg/ml DAPI (4'-6-Diamidino-2-Phenylindole – Sigma – D9542) for two hours at RT. Finally, cells were washed with PBS 1X three times in order to eliminate fluorescent antibodies not specifically bound. The 2D samples were kept in PBS 1X and observed under the inverted fluorescence microscope Nikon Eclipse TI. The slides obtained after cytopinning, were mounted with coverslips and mounting

medium (Permount™ Mounting Media – Fisher Scientific – SP15-100) and observed under the microscope after being completely dried.

### 2.15.2. Enzyme-tag immunocytochemistry

The different types of cells described above were cultured in the 3D peptide scaffold RAD16-I. At each time point specified, constructs were washed with PBS 1X and fixed with 1% paraformaldehyde (PFA, Paraformaldehyde powder 95% – Sigma – 158127) for 30 minutes at 4°C. Then, cells were washed three times with PBS 1X for 10 minutes each with stirring (all the steps of this protocol included stirring). Consecutively, cells were incubated with 0.1% H<sub>2</sub>O<sub>2</sub> in methanol for 45 minutes in order to block endogenous peroxidases. Afterwards, air bubbles inside the constructs generated by the peroxidases were removed by gently pipetting with PBS 1X. Cells were blocked in filtered (0.45 µm) blocking buffer (BB) (PBS 1X + 20% fetal bovine serum (FBS, Sigma – F7524) + 1% dimethyl sulfoxide (DMSO, Sigma – D8418) + 0.1% Triton-X100 (Triton™ X-100 – Sigma – X100)) for 2 hours at room temperature (RT) with stirring. The constructs were incubated with primary antibodies for 1.5 hours at RT (**Table 1**). After washing with BB two times, cells were kept in BB overnight (ON) at 4°C. The following day, the constructs were washed with BB and incubated with secondary antibodies conjugated to Horseradish Peroxidase (HRP) for 1.5 hours at RT. Cells were washed with BB and kept in BB ON. The third day, cells were washed with PBS 1X and the enzymatic reaction of the secondary antibodies was initiated with 3,3-diaminobenzidine 1X (DAB Substrate – Roche – 11718096001) until a brown precipitate was observed. Indeed, the specific bound of DAB to its enzyme HRP generates a brown precipitate that can be visually observed. Pictures were taken under the stereoscope.

<b>Antibody</b>	<b>Host</b>	<b>IgG Class</b>	<b>Reactivity</b>	<b>Concentration (Working Dilution)</b>	<b>Company</b>	<b>Catalog Number</b>
<b>Brachyury (hiPSCs)</b>	Goat	IgG	Mouse / Human	0.2 mg/mL (1:200)	R&D system	AF2085
<b>Nanog</b>	Rabbit	IgG	Mouse / Human	(1:250)	Millipore	AB9220
<b>MHC (hiPSCs)</b>	Mouse	IgG1	Mouse / Rabbit / Human	1 mg/mL (1:500)	Abcam	ab15

MATERIALS AND METHODS

<b>Troponin I</b>	Rabbit	IgG	Mouse / Rat / Human	200 µg/mL (1:200)	Santa Cruz	sc-15368
<b>Connexin 43</b>	Rabbit	IgG	Mouse / Rat / Human	200 µg/mL (1:1000)	Santa Cruz	sc-9059
<b>Nkx2.5</b>	Rabbit	IgG	Mouse / Rat / Human	200 µg/mL (1:1000)	Santa Cruz	sc-14033
<b>TBX5</b>	Rabbit	IgG	Mouse / Rat / Human	200 µg/mL (1:200)	Santa Cruz	sc-48782
<b>MYH (hNDFs)</b>	Rabbit	IgG	Mouse / Rat / Human	200 µg/mL (1:200)	Santa Cruz	sc-20641
<b>HNF-3β – FOXA2</b>	Goat	IgG	Mouse / Rat / Human	200 µg/mL (1:200)	Santa Cruz	sc-6554
<b>Brachyury (hNDFs)</b>	Goat	IgG	Mouse / Rat / Human	200 µg/mL (1:200)	Santa Cruz	sc-17743
<b>GATA4</b>	Rabbit	IgG	Mouse / Rat / Human	200 µg/mL (1:200)	Santa Cruz	sc-9053
<b>Rabbit-HRP</b>	Donkey	IgG	Rabbit	400 µg/mL (1:400)	Santa Cruz	sc-2317
<b>Goat-HRP</b>	Donkey	IgG	Goat	400 µg/mL (1:400)	Santa Cruz	sc-2020
<b>Mouse-HRP</b>	Goat	IgG1	Mouse	400 µg/mL (1/200)	Santa Cruz	sc-2060
<b>Rabbit-488</b>	Donkey	IgG	Rabbit	2 mg/mL (1/200)	Invitrogen	A21206
<b>Goat-488</b>	Donkey	IgG	Goat	2 mg/mL (1/200)	Invitrogen	A11055
<b>Mouse-488</b>	Donkey	IgG	Mouse	2 mg/mL (1/200)	Invitrogen	A21202
<b>Goat-546</b>	Donkey	IgG	Goat	2 mg/mL (1/200)	Invitrogen	A11056
<b>Rabbit-546</b>	Donkey	IgG	Rabbit	2 mg/mL (1/200)	Invitrogen	A10040

**Table 1.** List of primary and secondary antibodies used in this Thesis.



### 2.16. Nile red staining

Nile red is a lipophilic stain that specifically detects intracellular lipid droplets. In a lipid-rich environment, Nile red fluoresces red. It has been used to stain lipid droplet formation in adipogenic differentiation experiments.

Indeed, human Normal Dermal Fibroblasts (hNDFs) were cultured either in 2D or 3D environments. Then, cells were washed three times for 5 minutes with PBS 1X, then with deionized water and finally stained with Nile red (2.5 µg/ml in 75% glycerol, Nile red – Sigma – 19123) for 10 minutes in the dark. Afterwards, cells were washed again with MilliQ water before being stained with DAPI (0.1 µg/ml in PBS 1X, 4'-6-Diamidino-2-Phenylindole – Sigma – D9542) for 5 minutes. Nile red and DAPI are fluorescent dyes and therefore, cells should be hidden from the light during the protocol. Finally, cells were washed three times for 5 minutes with PBS 1X and observed under the inverted fluorescent microscope.

### 2.17. Congo red staining

Congo red binds to amyloid-like peptides having a  $\beta$ -sheet conformation. This staining shows the deposition of amyloid plaques in tissues mostly observed in Alzheimer disease<sup>12,13</sup>. Indeed, gelified RAD16-I is rich in  $\beta$ -sheet structures and appears highly positive when stained with this dye. Conversely, the pericardium's matrix is mostly composed of collagens enclosing  $\alpha$ -helix structures.

Human pericardia were soaked with dH<sub>2</sub>O (control) and with 0.15% RAD16-I (PuraMatrix™ Peptide Hydrogel – BD Bioscience – 354250). Afterwards, they were stained with Congo red (Fisher Scientific – C580-25) overnight at room temperature and stirring. In the following two days, pericardia were exhaustively washed with PBS 1X (several washes with stirring). When the dye was totally washed out, pericardia were transversally cut with a scalpel and observed under the stereoscope.

### 2.18. Design of primers

Nowadays, *computational biology* known as bioinformatics plays a key role in understanding biological processes and predicting molecular biology pathways. Among the numerous areas of bioinformatics, DNA sequence analysis is widely used to scan genetic profiles. Indeed, the gold standard tool of molecular biology is the Polymerase

## MATERIALS AND METHODS

Chain Reaction (PCR), which is based on the amplification of a concrete DNA sequence. The extremes flanking this region are guided by the bound of a primer's pair that consists in a nucleic acid sequence complementary to the gene of interest. Furthermore, the primers can be designed thanks to bioinformatics tools, as it was done in this thesis.

Furthermore, the gene of interest was browsed in the National Center for Biotechnology Information (NCBI) on line. The mRNA sequence was selected and its coding sequence (CDS) was analyzed by the Consensus CDS (CCDS) at the NCBI website. Once the sequence was picked up, the primer's pair was obtained using the program Primer 3 Input (version 0.4.0). Afterwards, the promiscuity of the primers was predicted using the Electronic PCR (Reverse ePCR) of NCBI. This website lists all the genes potentially amplified by specific primer pairs. The size of the amplicon should be around 200bp and the melting temperature ( $T_m$ ) of the primers 60°C. Finally, the primer's specificity was double-checked by doing a BLAST at NCBI.

Primer	Tissue	Tm	Amplicon	Efficiency (Time point)	Sequence (FW/RV)
<b>Oct4</b>	Pluripotency	60°C	110	2,05	AGTGAGAGGCAACCTGGAGA
					ACACTCGGACCACATCCTTC
<b>FoxA2</b>	Endoderm	60°C	120	2,37	CCCGGTTTTATCCCTTGAAT
					CCTGCAACCAGACAGGGTAT
<b>ACTC1</b>	Late cardiogenesis	60°C	136	2,08 (d30)	GCCCTGGATTTTGAGAATGA
					AGGGCTGGAAGAGTGTCTCA
<b>GATA4</b>	Cardiac Progenitor	60°C	194	2,5 (d15)	TCCCTCTTCCCTCCTCAAAT
					TCAGCGTGTAAGGCATCTG
<b>MEF2C</b>	Cardiac Progenitor	65°C	139	2,34 (d30)	CCATTGGACTCACCAGACCT
					AGCACACACACACTGCAA
<b>Tbx5</b>	Cardiac Progenitor	60°C	169	2,05 (d15)	CATGGAGACATCACCCAGTG
					GCAGCTGATGTCCTCTAGGC
<b>Brachyury</b>	Mesendoderm	65°C	274	2,2 (d3)	GCCCTCTCCCTCCCCTCCACGCACAG
					CGGCGCCGTTGCTCACAGACCACAGG
<b>PPAR<math>\gamma</math><sup>14</sup></b>	Adipogenesis	60°C	225		GCTGTGCAGGAGATCACAGA
					GGGCTCCATAAAGTCACCAA
<b>18S</b>	Housekeeper	60°C	245	2,06 (d15)	GCTACCACATCCAAGGAAGGCAG
					CGCTCCCAAGATCCAACACTACGAG

**Table 2.** List of designed primers used in this Thesis.

### 2.19. RNA extraction

In molecular biology, RNA extraction is widely used to study gene expression profiles. Thus, unmethylated DNA is first transcribed into mRNA, which is later translated into proteins. Specific cell types express specific genes, whereas all the cells contain the same genome and DNA sequence. This is why, the transcriptome (set of all the RNAs in a cell) is an indirect method used to analyze gene expression.

### 2.19.1. Human Normal Dermal Fibroblasts (hNDFs)

Cells were cultured either in 2D or 3D environments. To carry out the RNA extraction and purification of human Normal Dermal Fibroblasts (hNDFs), a commercial kit (peqGOLD Total RNA kit – Peqlab – 12-6634-01) was used and the instruction of its manual was followed according to its manufacturer. Cells were first washed with PBS 1X and then 0.2 ml TRK lysis buffer was added. The lysate was mixed by gently pipetting and transferred into a nuclease-free tube. An equal volume (0.2 ml) of 70% ethanol was added to precipitate the RNA. The mixture was transferred into a HiBind RNA spin column and centrifuged at 10000 x g for 1 minute. After this step, RNA was retained in the membrane of the column and ready to be washed and dried. Then, 500 µl of RNA wash buffer I were added and the mixture was centrifuged at 10000 x g for 1 minute. Samples were washed twice with 600 µl of ethanolic RNA wash buffer II and centrifuged at 10000 x g for 30 seconds. To completely dry the column matrix, samples were centrifuged at 10000 x g for 1 minute. Finally, RNA was eluted at 5000 x g for 1 minute with 30 µl of nuclease-free water into a new tube. The RNA concentration and purity were quantified with OD lecture at 230, 260, 280 and 320 nm.

RNA concentration:  $[RNA] \text{ (mg/mL)} = (A_{260} - A_{320}) \times 40 \times 10 \times \text{dilution factor}$

RNA Purity:  $A_{260/280} = (A_{260} - A_{280}) / (A_{260} - A_{280})$

$A_{260/230} = (A_{260} - A_{230}) / (A_{230} - A_{230})$

The ratio  $A_{260/280}$  gives information about protein contamination and should be around 2.  $A_{260/230}$  tells us about chemical contamination and again, it should range between 2 – 2.4. The samples were stored at -80°C.

### 2.19.2. Human Embryonic Stem Cells (hESCs) H9 and human induced Pluripotent Stem Cells (hiPSCs) Riv9 in 2D cultures

This protocol is based on a commercial kit (RNeasy Mini Kit – Qiagen – 74106). Cells grown in monolayer on matrigel were washed with PBS 1X, disrupted with 600 µl of RLT buffer and 6 µl of β-mercaptoethanol (2-mercaptoethanol, 55 mM – Gibco® - 21985-023) and homogenized. Then, an equal volume of ethanol 70% was added in order to precipitate the RNA. Samples were loaded in RNeasy mini spin columns sitting on collection tubes and centrifuged for 15 seconds at 10000 rpm. After binding the RNA to the membrane, 700 µl of buffer RW1 were added and

samples were centrifuged at 10000 rpm for 15 seconds. Next, 500 µl of buffer RPE were pipetted onto each RNeasy column, which were centrifuged again as done previously. The last step was repeated, samples were centrifuged at 10000 rpm for 2 minutes and centrifuged again for 1 minute to totally dry the membrane. Finally, RNeasy columns were transferred into new tubes and the RNA was eluted with 60 µl of nuclease-free water and centrifugation at 10000 rpm for 1 minute. RNA samples were frozen at -80°C.

### *2.19.3. Human induced Pluripotent Stem Cells (hiPSCs) Riv9 in 3D cultures*

The RNA extraction was performed using TRIzol<sup>®</sup> Reagent (Ambion<sup>®</sup> – 15596-018), which is a ready-to-use product based on a monophasic solution of phenol and guanidine isothiocyanate. During sample lysis, TRIzol<sup>®</sup> Reagent maintains the integrity of the RNA, while disrupting cells and dissolving cell components.

At each specific time point, cells were washed with PBS 1X and incubated for 5 minutes at room temperature (RT) with 400 µl of TRIzol<sup>®</sup> Reagent. Afterwards, each mixture was gently pipetted in order to completely dissociate nucleoprotein complexes. Then, 0.2 ml of chloroform were added, tubes were shaken vigorously for 15 seconds and incubated for 3 minutes at RT. Samples were centrifuged at 14000 rpm for 15 minutes at 4°C. Following centrifugation, the mixture separates into a lower red phenol-chloroform phase, an interphase and a colorless upper aqueous phase. RNA remains exclusively in the aqueous phase. This first part of the protocol is basically RNA extraction. Consecutively, supernatants were transferred into clean tubes (the organic phase can be saved for isolation of DNA or protein) and the next step was to precipitate RNA. Therefore 400 µl of 100% isopropanol were added, samples were mixed by vortex and incubated for 5 minutes at RT. Then, samples were centrifuged at 14000 rpm for 20 minutes at 4°C. After having precipitated the RNA, it was washed and dried by washing the pellet with 500 µl of 75% cold ethanol, without mixing. Samples were centrifuged at 7600 rpm for 5 minutes at 4°C. Then, all the ethanol was carefully removed and the pellets were let to dry in the air for an hour. Once all the ethanol was evaporated, pellets were dissolved in 30 µl of nuclease-free water (UltraPure<sup>™</sup> DEPC-Treated Water – Invitrogen<sup>™</sup> – 750023). Finally, OD values were read at 230, 260 and 280 nm and the RNA concentration and purity were calculated (NanoDrop 2000c – Thermo Scientific). Samples were stored at -80°C.

### 2.20. *cDNA synthesis*

This technique is based on the enzyme reverse transcriptase (RT) first discovered and isolated from viruses in 1970 by Howard Temin and David Baltimore. Indeed, RT transcribes RNA molecules into complementary DNA (cDNA), which is used by retroviruses to replicate. RT creates single-stranded DNA from an RNA template. Complementary DNA is used as an initial material for PCR and for the construction of cDNA banks.

#### 2.20.1. *Human Normal Dermal Fibroblasts (hNDFs)*

After the extraction, purification and quantification of RNA (see Materials and Methods 2.19.1), 150 ng of RNA were transcribed. Nuclease-free water was added to a final volume of 12  $\mu$ l. For the cDNA synthesis, a commercial kit was used (QuantiTect Reverse Transcription Kit – Qiagen – 205311). Indeed, RNA templates were mixed with 2  $\mu$ l of gDNA Wipeout buffer 7X and incubated at 42°C for 2 minutes. This reaction degrades the remaining genomic DNA in the samples. At the same time, a pool was prepared for each sample: 1  $\mu$ l Quantiscript reverse transcriptase (RT), 4  $\mu$ l Quantiscript RT buffer 5X and 1  $\mu$ l RT primer mix. Finally the pool (6  $\mu$ l) was added to the RNA templates (14  $\mu$ l). The reactions were incubated at 42°C for 15 minutes (synthesis reaction) and at 95°C for 3 minutes (RT inactivation). Samples were kept at -20°C until future analysis.

#### 2.20.2. *Human Embryonic Stem Cells (hESCs) H9 and human induced Pluripotent Stem Cells (hiPSCs) Riv9*

Extraction RNA samples (see Materials and Methods 2.19.2 and 2.19.3) were defrosted at room temperature. At the same time, a reaction pool was prepared: RT buffer 5X (5  $\mu$ l), 0.4  $\mu$ M random primers (0.1  $\mu$ l, Random Hexamer Primer 100  $\mu$ M – Fermentas – S0142), 5 mM deoxynucleotide triphosphate (dNTPs, 1.25  $\mu$ l, dNTP set 100 mM Solutions – Fermentas – R0181), 50 Units RNase inhibitor (1.25  $\mu$ l, RiboLock™ Ribonuclease Inhibitor 40 U/ $\mu$ l – Fermentas – E00382), 80 Units reverse transcriptase enzyme (0.4  $\mu$ l, RevertAid Reverse Transcriptase 200 U/ $\mu$ l – Fermentas – EP0441) and nuclease-free water (UltraPure™ DEPC-Treated Water – Invitrogen™ – 750023). Finally, 625 ng of RNA were added to each tube. The final volume of each sample was 25  $\mu$ l. Then, the program of the thermo cycler was: 10 minutes at 25°C (extension of the random primers), 50 minutes at 42°C

(synthesis reaction) and 15 minutes at 70°C (RT inactivation). The product was frozen at -20°C and stored for further analysis.

### 2.21. Polymerase Chain Reaction (PCR)

The polymerase Chain Reaction (PCR) is the most powerful technique that has been developed in molecular biology with major impact on molecular cloning and genetics. The *in vitro* procedure permits amplifying a DNA fragment a billion-fold in several hours. PCR is based on the DNA polymerase activity, which synthesizes complementary DNA strands in between two specific primers that flank the target sequence. The reaction consists in several cycles of three steps: denaturation, annealing of primers and primer extension.

#### 2.21.1. Human Normal Dermal Fibroblasts (hNDFs)

Polymerase Chain Reaction (PCR) was carried out with the cDNA templates processed previously (see Materials and Methods 2.20.1). Indeed, the reaction pool contained: 10X Reaction Buffer (5 µl, BioLabs – M0254S), 2 mM deoxynucleotide triphosphate (dNTPS, 1 µl, dNTP MIX 100 mM total – Ecogen – BIO39028), 1 µM forward primer (2.5 µl), 1 µM reverse primer (2.5 µl), 2 Units Deep Vent polymerase (1 µl, Vent<sub>R</sub>® DNA Polymerase 2000 U/ml – BioLabs – M0254S), nuclease-free water (34.67 µl, Nuclease-Free Water not DEPC-treated – Ambion® – AM9938) and 25 ng cDNA (3.33 µl). The PCR (Veriti™ Thermal Cycler – Applied Biosystems) program used was:

- (1x) 3 minutes at 95°C: exhaustive initial denaturation
- (35x) 15 seconds at 95°C: denaturation
- 15 seconds at T<sub>m</sub> (specific for each primer pair): annealing
- 1 minute at 72°C: extension of primers
- (1x) 7 minutes at 72°C: exhaustive final extension

#### 2.21.2. Human Embryonic Stem Cells (hESCs) H9 and human induced Pluripotent Stem Cells (hiPSCs) Riv9

The cDNA samples previously obtained (see Materials and Methods 2.20.2) by retro-transcription were used for Polymerase Chain Reaction (PCR) assays. The goal was to analyze and compare gene profiles of stem cells. Thus, each sample

## MATERIALS AND METHODS

contained: PCR buffer 10X (2.5  $\mu$ l, 10X *Taq* Buffer with KCl – Fermentas – B38), 2 Units *Taq* polymerase (0.4  $\mu$ l, *Taq* DNA Polymerase 5 U/ $\mu$ l – Fermentas – EP0402), 2 mM MgCl<sub>2</sub> (2  $\mu$ l, 25 mM MgCl<sub>2</sub> – Fermentas – R0971), 1 mM deoxynucleotide triphosphate (dNTPs, 0.25  $\mu$ l, dNTP set 100 mM Solutions – Fermentas – R0181), 0.2  $\mu$ M forward primer (0.5  $\mu$ l), 0.2  $\mu$ M reverse primer (0.5  $\mu$ l), nuclease-free water (17.85  $\mu$ l, UltraPure™ DEPC-Treated Water – Invitrogen™ – 750023) and 25 ng cDNA (1  $\mu$ l). The final volume of the reaction was 25  $\mu$ l. The program of the thermocycler (Mastercycler® Pro – Eppendorf) was a three step PCR based on 35 cycles. Each cycle consisted on: 45 seconds at 94°C (denaturation), 45 seconds at the melting temperature (T<sub>m</sub>) of the primers (annealing) and 1 minute at 72°C (extension).

### 2.22. *Agarose gel electrophoresis*

Agarose gel electrophoresis is the most common and easiest method to separate DNA by size. Agarose acts as a molecular sieve, through which nucleic acids are driven by an electric field. DNA is negatively charged at neutral pH (because of the phosphate groups), so it migrates toward the positive pole. The pore size is determined by the agarose concentration: the higher the concentration is, the smaller the pore is. Migration rate of DNA in agarose gel depends on agarose concentration, molecular size of the DNA fragments, conformation of the DNA and applied voltage.

#### 2.22.1. *Agarose gel electrophoresis preparation*

In the experiments presented in this Thesis, the size of all the amplicons was around 200 bp. Therefore, the agarose concentration chosen was 3%. The agarose gel consisted in 100 ml TAE 1X buffer (Tris-Acetate-EDTA 50X: 242 g Tris base in 750 ml deionized H<sub>2</sub>O, 57.1 ml glacial acid and 100 ml 0.5 M EDTA pH 8, adjusted to a final volume of 1 l; dilutions of the buffer were prepared with dH<sub>2</sub>O) and 3 g of agarose (peqGOLD Universal-Agarose – Peqlab – 35-1020). The mixture was warmed up in the microwave until the agarose powder was totally dissolved. After cooling it down, 0.3  $\mu$ g/ml ethidium bromide (3  $\mu$ l, Ethidium Bromide 1% solution – Fisher Scientific – BP1302-10) were added to the solution. The mixture was poured into the gelification plate with the comb and let it gelify for 20 minutes. Finally, the comb was carefully removed from the gel (the wells were already formed) and the agarose gel was immersed in the electrophoresis cuvette full of TAE 1X.



### 2.22.2. Samples preparation

The PCR samples (see Materials and Methods 2.21), which had a final volume of 25  $\mu$ l, were spun down. Then, 5  $\mu$ l of loading buffer 6X (6X Loading Dye Solution – Fermentas – R0611) were added in each tube. The mixtures were shaken using a vortex, spun down again and 10  $\mu$ l of each sample were loaded in each well of the agarose gel electrophoresis. In addition, a DNA ladder was loaded in the first well of the gel in order to have a DNA length size reference. O'GeneRuler 50 – 1000 bp (O'GeneRuler DNA ladder – Thermo Scientific – SM1133) was used for hESCs and hiPSCs DNA samples. Regarding the hNDFs DNA samples, Marker V (Roche Applied Science – 10821705001) and Marker VI (Roche Applied Science – 11062590001) were used depending on the size of the amplicons. Once the gel was loaded with the convenient samples, the electrophoresis cuvette was plugged in at 120 V and unlimited amperage for 30 – 45 minutes.

### 2.23. *Quantitative Polymerase Chain Reaction (qPCR) of human Embryonic Stem Cells (hESCs) H9 and human induced Pluripotent Stem Cells (hiPSCs) Riv9*

Quantitative (or Real Time) Polymerase Chain Reaction (qPCR) is a fluorescence-based PCR. Unlike conventional PCR, qPCR monitors fluorescent reporter molecules and allows accurate quantification of DNA in real time, during the exponential phase of the reaction. The fluorescent dye (SYBR Green) intercalates between base pairs and fluoresces only when it is specifically bound to double-stranded DNA. At the exponential phase of the reaction, the target gene flanked by designed primer pairs will be the major fluorescent signal detected by the laser of the thermocycler. Indeed, the signal of different samples can be compared and plotted. All in all, the expression of a specific gene can be quantified.

Each qPCR sample contained 10  $\mu$ l SYBR Green buffer (IQ™ SYBR® Green Supermix – BioRad – 170-8882), 0.05  $\mu$ M forward primer (0.4  $\mu$ l), 0.05  $\mu$ M reverse primer (0.4  $\mu$ l), nuclease-free water (7.2  $\mu$ l, UltraPure™ DEPC-Treated Water – Invitrogen™ – 750023) and 50 ng cDNA (2  $\mu$ l). The qPCR program set up in the thermocycler was a two-step run:

## MATERIALS AND METHODS

- (1x) 3 minutes at 95°C: exhaustive initial denaturation
- (35x) 10 seconds at 95°C: denaturation
- 30 seconds at T<sub>m</sub> (specific for each primer pair): annealing

Furthermore, each sample consisted on three biological triplicates and three technical triplicates (9 reactions/gene in total). Regarding the analysis of the data, n-fold expression of genes of interest was calculated according to the  $\Delta\Delta C_T$  method<sup>15</sup> using correction for PCR efficiency (see below). All values represented n-fold expression over undifferentiated cells (d0) cultured in 2D and normalized to the housekeeper gene 18S.

On the other hand, the PCR efficiency was assessed for each pair of primers designed. The samples used for this were cDNAs from human induced Pluripotent Stem Cells (hiPSCs) Riv9 cultured in cardiogenic medium in 2D cultures. Thus, each sample consisted on a pool of the three biological triplicates. The time point chosen to establish the efficiency of the primers for each gene was the one that appeared to have the maximum gene expression peak in the agarose gel electrophoresis run previously (**Table 2**). Then, the samples were diluted 1/1 (50 ng), 1/10 (5 ng) and 1/100 (0.5 ng). Three technical triplicates for each diluted sample were loaded in a PCR plate. The qPCR program selected in the thermocycler was identical to the one used for conventional qPCR despite instead of heating at a specific melting temperature (T<sub>m</sub>), it ran a gradient of temperatures. Afterwards, the threshold cycle (C<sub>T</sub>) averages were plotted for each biological triplicate in function of the cDNA concentration (0.5 – 5 – 50 ng). The slope of the chart represented the efficiency of the primer pair:

$$\text{Efficiency} = 10^{-1/\text{slope}}$$

Acceptable PCR efficiencies concerning the primer pairs should range between 2 – 2.5. This concept is very important because it defines how specific and suitable the primer pairs are for qPCR assays (**Table 2**).

### 2.24. *Cytospin*

The cytospin is a technique that uses a high-speed centrifuge to concentrate the cells on a slide in a uniform monolayer. The method consists in spinning a cellular suspension through a funnel placed on a microscopy slide. A tinny hole located at the bottom of the funnel enforces the cells to concentrate and spread on the slide. In

between the funnel and the slide, there is a filter paper that absorbs the liquid in which the cells are suspended. Therefore, cells stick to the surface of the slide. Cytospinning is widely used in clinical analysis of blood, urine, sperm and other corporal fluids.

First of all, the parameters to cytospin human induced Pluripotent Stem Cells (hiPSCs) were established (centrifuge speed and time, and cell concentration). Cells can expel the nucleus if the spinning speed is too high or too long. It is important to set up the right conditions of the experiment to obtain suitable cytological preparations. Thus, hiPSCs were cultured in 3D as explained above (see Materials and Methods 2.5). At a given time point, three constructs were pre-treated with ROCK Inhibitor (RI, Inhibitor Y-27632 – VWR – 80511-062) for one hour at 37°C. Cells were then washed with PBS 1X and trypsinized (0.25% Trypsin-EDTA (1X), Phenol Red – Gibco – 25200-056) for 4 – 5 minutes at 37°C until the constructs were totally disrupted. Gentle pipetting helped to their complete disruption. Cells were counted and re-suspended in PBS 1X at a final concentration of  $5 \cdot 10^5$  cells/ml. For each sample, a metallic support (Shandon Cytoclip Stainless-Steel Slide Clip – Thermo Scientific Shandon – 59910052), a slide (Cytoslide single circle coated – Thermo Scientific Shandon – 5991056) and a funnel (Single Cytology Funnels – Fisherbrand – 10-354) bound to a filter paper were assembled and placed in the cytospin (Shandon Cytospin 3 – Shandon). Afterwards, 100  $\mu$ l of the cellular suspension containing 50000 cells were loaded in each cytospin funnel and centrifuged at 500 rpm for 4 minutes. The slides were air-dried, fixed (Safetex Cytology Fixative – Andwin Scientific – 930022-C12) and air-dried again with the fixative. Samples were washed with distilled water to remove the excess of fixative. Finally, the slides were air-dried and kept at room temperature ready to be stained<sup>16</sup>.

### 2.25. References

1. Quintana, L. *et al.* Early Tissue Patterning Recreated by Mouse Embryonic Fibroblasts in a Three-Dimensional Environment. *Tissue Engineering* **15**, (2009).
2. Löser, P., Schirm, J., Guhr, A., Wobus, A. M. & Kurtz, A. Human embryonic stem cell lines and their use in international research. *Stem cells (Dayton, Ohio)* **28**, 240–6 (2010).
3. Zhang, S., Gelain, F. & Zhao, X. Designer self-assembling peptide nanofiber scaffolds for 3D tissue cell cultures. *Seminars in cancer biology* **15**, 413–420 (2005).

## MATERIALS AND METHODS

4. Artym, V. V & Matsumoto, K. Imaging cells in three-dimensional collagen matrix. *National Institutes of Health* 1–23 (2011).  
doi:10.1002/0471143030.cb1018s48.Imaging
5. Genové, E. *et al.* Functionalized self-assembling peptide hydrogel enhance maintenance of hepatocyte activity in vitro. *Journal of Cellular and Molecular Medicine* **XX**, 1–12 (2009).
6. Blasi, A. *et al.* Dermal fibroblasts display similar phenotypic and differentiation capacity to fat-derived mesenchymal stem cells, but differ in anti-inflammatory and angiogenic potential. *Vascular cell* **3**, 5 (2011).
7. Cao, N. *et al.* Ascorbic acid enhances the cardiac differentiation of induced pluripotent stem cells through promoting the proliferation of cardiac progenitor cells. *Cell research* **22**, 219–36 (2012).
8. Smits, A. M. *et al.* Human cardiomyocyte progenitor cells differentiate into functional mature cardiomyocytes: an in vitro model for studying human cardiac physiology and pathophysiology. *Nature protocols* **4**, 232–43 (2009).
9. Ott, H. C. *et al.* Perfusion-decellularized matrix: using nature's platform to engineer a bioartificial heart. *Nature medicine* **14**, 213–21 (2008).
10. Pasquino, E. *et al.* Bovine pericardium for heart valve bioprotheses: in vitro and in vivo characterization of new chemical treatments. *Journal of Materials Science: Materials in Medicine* **5**, 850–854 (1994).
11. Sanchez, B. *et al.* Towards on line monitoring the evolution of the myocardium infarction scar with an implantable electrical impedance spectrum monitoring system. *34th Annual International Conference of the IEEE Engineering in Medicine and Biology Society* **2012**, 3223–6 (2012).
12. Zhang, S. *et al.* Self-complementary oligopeptide matrices support mammalian cell attachment. *Biomaterials* **16**, 1385–93 (1995).
13. Zhang, S., Holmes, T., Lockshin, C. & Rich, A. Spontaneous assembly of a self-complementary oligopeptide to form a stable macroscopic membrane. *Proceedings of the National Academy of Sciences of the United States of America* **90**, 3334–8 (1993).
14. Loviscach, M. *et al.* Distribution of peroxisome proliferator-activated receptors (PPARs) in human skeletal muscle and adipose tissue: relation to insulin action. *Diabetologia* **43**, 304–11 (2000).
15. Zhang, J. D., Ruschhaupt, M. & Biczok, R. ddCt method for qRT – PCR data analysis. *Bioconductor* 1–8 (2013).
16. Choi, K.-D., Vodyanik, M. & Slukvin, I. I. The hematopoietic differentiation and production of mature myeloid cells from human pluripotent stem cells. *National Institutes of Health* **6**, 296–313 (2012).

*Chapter 3: Mesenchymal potential of human  
Normal Dermal Fibroblasts in the three-  
dimensional peptide scaffold RAD16-I*



## **CHAPTER 3. MESENCHYMAL POTENTIAL OF HUMAN NORMAL DERMAL FIBROBLASTS IN THE THREE-DIMENSIONAL PEPTIDE SCAFFOLD RAD16-I**

### *3.1. Introduction*

Adult cardiomyocytes are terminally differentiated cells with a very low rate of proliferation. Indeed, radioactivity assays show that this type of human cell has a turnover of less than 1% per year<sup>1</sup>. Due to the particularly limited regenerative capacity of adult cardiac tissue, many strategies have risen to restore damaged heart tissue. Recently, it has been demonstrated that dermal fibroblasts, which are the major cell type in dermis, have differentiation potential similar to Mesenchymal Stem Cells (MSCs). Populations of fibroblasts are heterogeneous and contain progenitors with various levels of differentiation potentials. Therefore, fibroblasts are considered to be partially multipotent and a promising cell source for autologous regenerative medicine purposes. Some approaches have shown their potential to differentiate into other mesodermal (osteoblast-like, adipocyte-like and chondrocyte-like cells<sup>2</sup>) and endodermal (hepatocyte-like cells<sup>3</sup>) lineages when cultured in the presence of different chemical inductors. Nevertheless, it is unknown if the process is due to transdifferentiation of committed fibroblasts or to differentiation of resident progenitors. Three-dimensional (3D) cultures of fibroblasts have indicated that cells might undergo chondrogenesis<sup>4</sup> and osteogenesis<sup>5</sup> under specific culture conditions. Human dermal fibroblasts cultured in RAD16-I create cell network and tensional forces, which lead to global contraction of the construct. This morphological process is similar to mesenchymal condensation during embryonic development<sup>6</sup>. Here we present spontaneous mesenchymal phenotype acquisition by the expression of primitive markers (Brachyury, FoxA2 and Gata4) and induced adipogenic and cardiogenic differentiation of adult human Normal Dermal Fibroblasts (hNDFs) when cultured in RAD16-I (3D cultures).

### *3.2. Hypothesis and specific aims*

Dermal fibroblasts are an important cell source for tissue engineering applications. They could be used for future regeneration assays because they are known to be partially multipotent. The main goal of this chapter was to assess the mesenchymal potential of hNDFs in 3D cultures and their commitment to other mesodermal

lineages (adipogenic and cardiogenic) under induction conditions.

Hypothesis: When hNDFs are grown in RAD16-I, they acquire mesenchymal phenotype that induces them to differentiate into adipogenic and cardiogenic lineages mimicking a three-dimensional tissue-like structure.

Specific aims:

- Assess the mesenchymal potential acquisition of hNDFs in 3D cultures under different culture conditions such as scaffold type (RAD16-I *versus* Collagen I) and medium composition (presence or absence of FBS and PDGF).
- Study the adipogenic and cardiogenic commitment of hNDFs cultured in RAD16-I with control and induction media.

### 3.3. Results

#### 3.3.1. Confirmation of the cellular phenotype of hNDFs in 2D cultures

Human Normal Dermal Fibroblasts (hNDFs) were expanded in regular two-dimensional cultures (2D cultures in flasks or culture-wells). Indeed, the cells grew attached to the plastic surface of the flask. Fibroblasts extended filopodia, which were responsible for the cellular adhesion to the substratum and migration<sup>7</sup>. Cells had particular spindle-shaped morphologies (**Figure 7**) with size ranging from 150 to 200  $\mu\text{m}$ , one nucleus (blue staining, DAPI) per cell and multiple elongated and parallel actin microfilaments (red staining, phalloidin). The cytoskeleton of this type of cell was abundant.

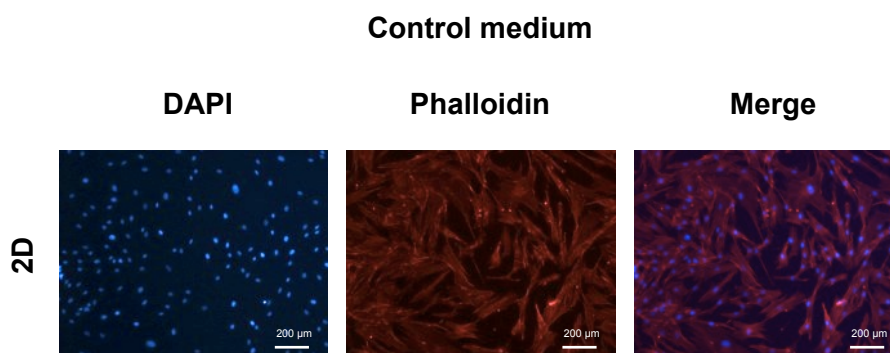


**Figure 7.** DAPI (nuclei, blue) and Phalloidin (actin microfilaments, red) staining of hNDFs cultured in 2D with control medium.



Survival of cells in 2D was easily assessed using a microscope and without staining because when cells died, they detached and floated. During this research, cell viability in 2D cultures was high because most of the hNDFs remained attached to the plastic surface and very few were dead and floating.

This chapter is based on increasing mesenchymal lineage potentiality of hNDFs by culturing them in a neutral biomaterial, which recreates a true three-dimensional environment. Hence, 2D cultures were used as a control for all of the experiments in order to assess the effect of three-dimensionality (3D scaffold) on the morphogenetic process. It is important to consider that the rigidity of both 2D and 3D systems is highly different, which could indicate that the observed effect might be associated in part to the mechanical difference of the materials. During the course of experiments, hNDFs cultured in 2D presented a clear fibroblastic phenotype. Moreover, hNDFs were stained using fluorescent immunocytochemistry to confirm that the target cells did not express certain cardiogenic markers. The proteins of interest were related to early differentiation (Brachyury, Gata4), cardiac progenitors (Nkx2.5, Tbx5) and mature cardiomyocyte (Connexin 43) markers. The hNDFs cultured in 2D did not express any of these markers (**Figure 8**). The characterization of hNDFs in 2D was extremely important, since these were the same cells used for subsequent 3D experiments.

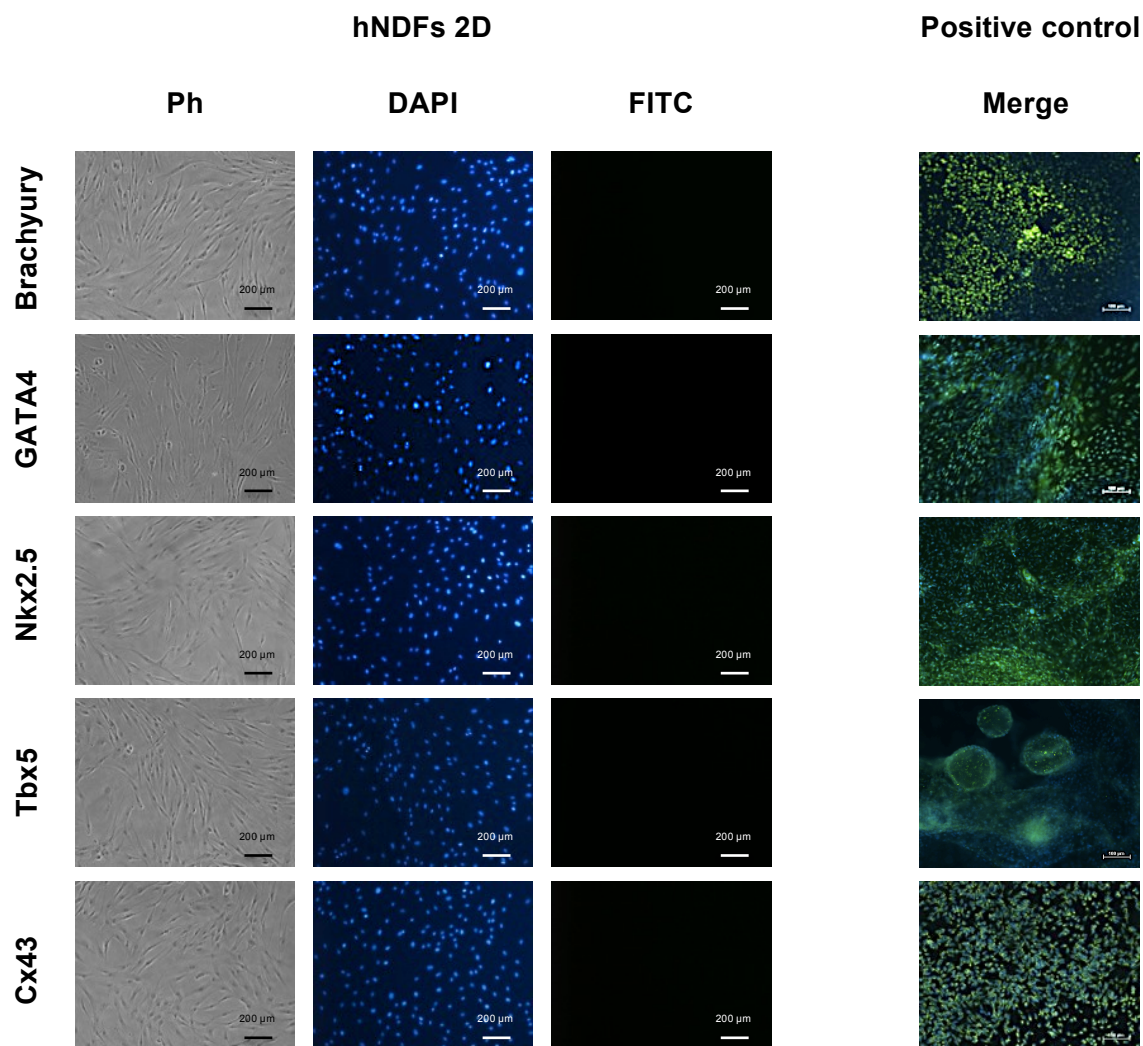


**Figure 8.** Immunostaining for mesenchymal (Brachyury and Gata4), cardiac progenitor (Nkx2.5 and Tbx5) and mature cardiomyocyte (Cx43) markers of hNDFs cultured in 2D with control medium. The right column shows merge pictures of positive immunostaining for each marker of differentiated hiPSCs cultured in 2D with cardiogenic medium. Secondary antibodies were bound to FITC that fluoresces green under blue excitation.

### 3.3.2. Mesenchymal phenotype acquisition of hNDFs cultured in RAD16-I and Collagen I scaffolds

Human NDFs were cultured in RAD16-I and Collagen I scaffolds in parallel. Both biomaterials have been widely used in 3D cultures approaches but in terms of origin they are very different: RAD16-I is a neutral synthetic biomaterial whereas Collagen I is a natural biomaterial extracted from animal tissues. Moreover, 3D environments based on collagen are considered for many applications the gold standard in tissue engineering<sup>8</sup>. For this reason, the cells embedded in Collagen I were used as a benchmark for those cultured in RAD16-I. Collagen constructs allowed the

comparison and understanding of what were the differences in cellular behavior of hNDFs cultured in other scaffolds such as RAD16-I. The main goal was to evaluate if the 3D scaffold based on RAD16-I played a role in the acquisition of the mesenchymal phenotype of hNDFs; or if the process was simply caused by the 3D environment, independently of its nature.

Human NDFs cultured in RAD16-I created a dense intercellular network. The connections were so tight and strong that cells pulled the surrounding matrix towards them. The tensions resulted in the contraction of the whole construct (**Figure 9**). Thus, constructs acquired a dome-shaped morphology due to the tensional stress generated: cells created an outer dense layer that surrendered to forces and lifted up (**Figure 10**). Regarding the cellular morphology, hNDFs encapsulated in RAD16-I lost their spindle-shaped morphology and appeared elongated. During the course of the experiment, cells became more compacted with increasing intercellular connections (**Figure 11**). Regardless, cells were less spread in 3D than in 2D cultures.

Similarly, fibroblasts embedded in Collagen I also contracted the whole construct although they did it faster than in RAD16-I. The contraction forces were so tense that the construct appeared extremely compacted at day 5 (**Figure 9**). Cells generated a denser intercellular network than in RAD16-I (**Figure 11**). Interestingly, hNDFs were successfully encapsulated in both scaffolds and remained entrapped in the matrix. Indeed, cells did not migrate out of the matrix, which suggests that both biomaterials (RAD16-I and Collagen I) were cell friendly.

MESENCHYMAL POTENTIAL OF HUMAN NORMAL DERMAL FIBROBLASTS IN THE THREE-DIMENSIONAL PEPTIDE SCAFFOLD RAD16-I

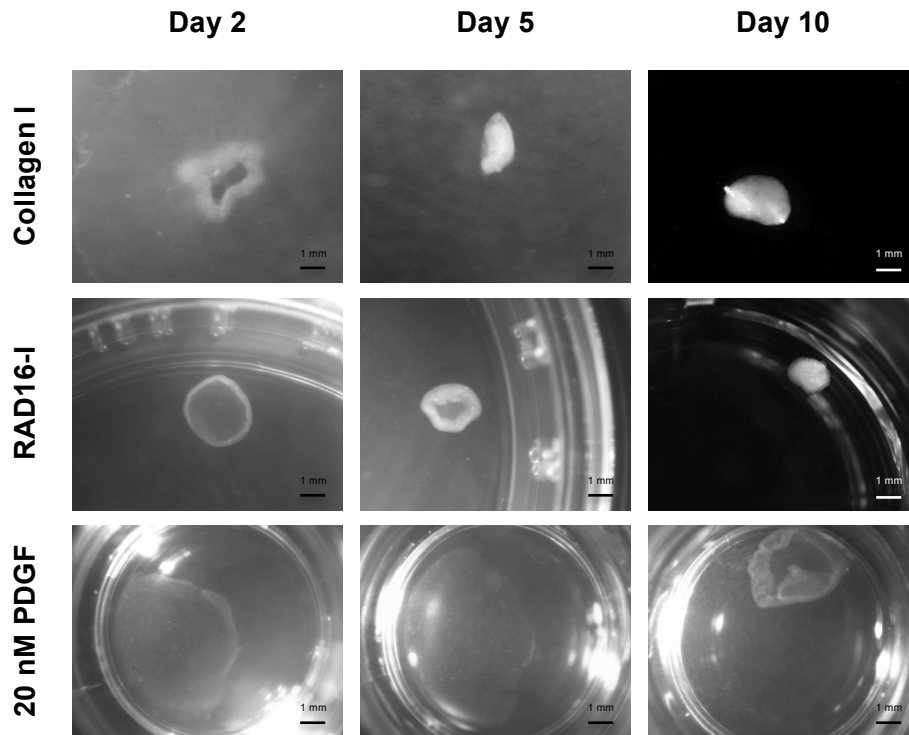


**Figure 9.** Macroscopic observation of the construct contraction of hNDFs cultured in different 3D conditions: Collagen I with control medium; RAD16-I with control medium; and RAD16-I with defined medium (without FBS and supplemented with PDGF).

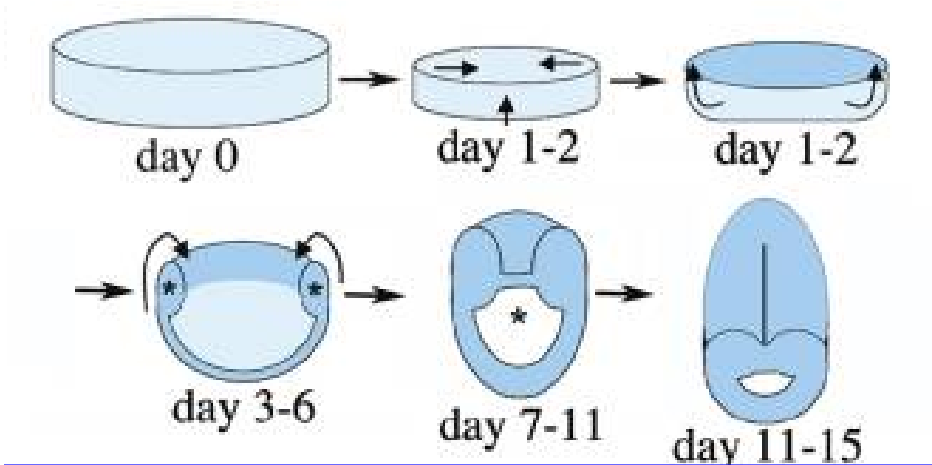


**Figure 10.** Scheme representing the construct contraction and the dome-shape of 3D cultures based on RAD16-I<sup>4</sup>.

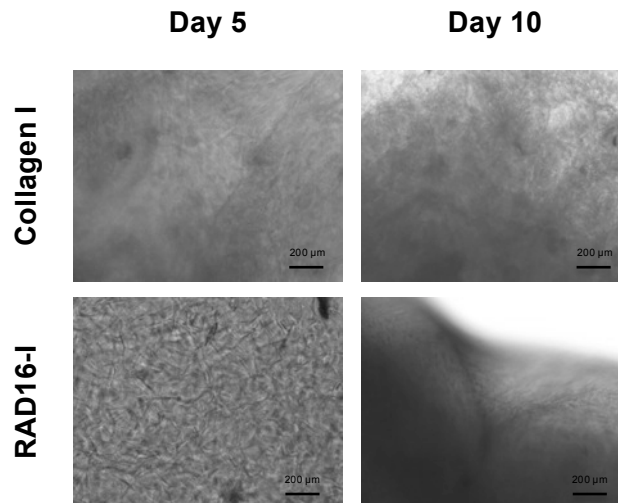


**Figure 11.** Microscopic observation of 3D cultures of hNDFs embedded in Collagen I and RAD16-I at day 5 and 10.

On the other hand, the global contraction of RAD16-I constructs into compacted disc-shaped structures resembled the mesenchymal condensation during development. Mouse embryonic fibroblasts cultured in 3D are known to acquire mesenchymal potentiality<sup>4</sup> and consequently the potential of hNDFs to undergo the same lineage commitment was determined in this study. Thus, the presence of markers related to early differentiation during embryonic development was assessed: Brachyury (mesendoderm), FoxA2 (endoderm) and Gata4 (mesoderm). Surprisingly, hNDFs cultured in RAD16-I for 10 days seemed to express these embryonic proteins (**Figure 12**), which implied that the cells displayed a primitive phenotype. However, hNDFs embedded in Collagen I did not express any of these markers (**Figure 12**).

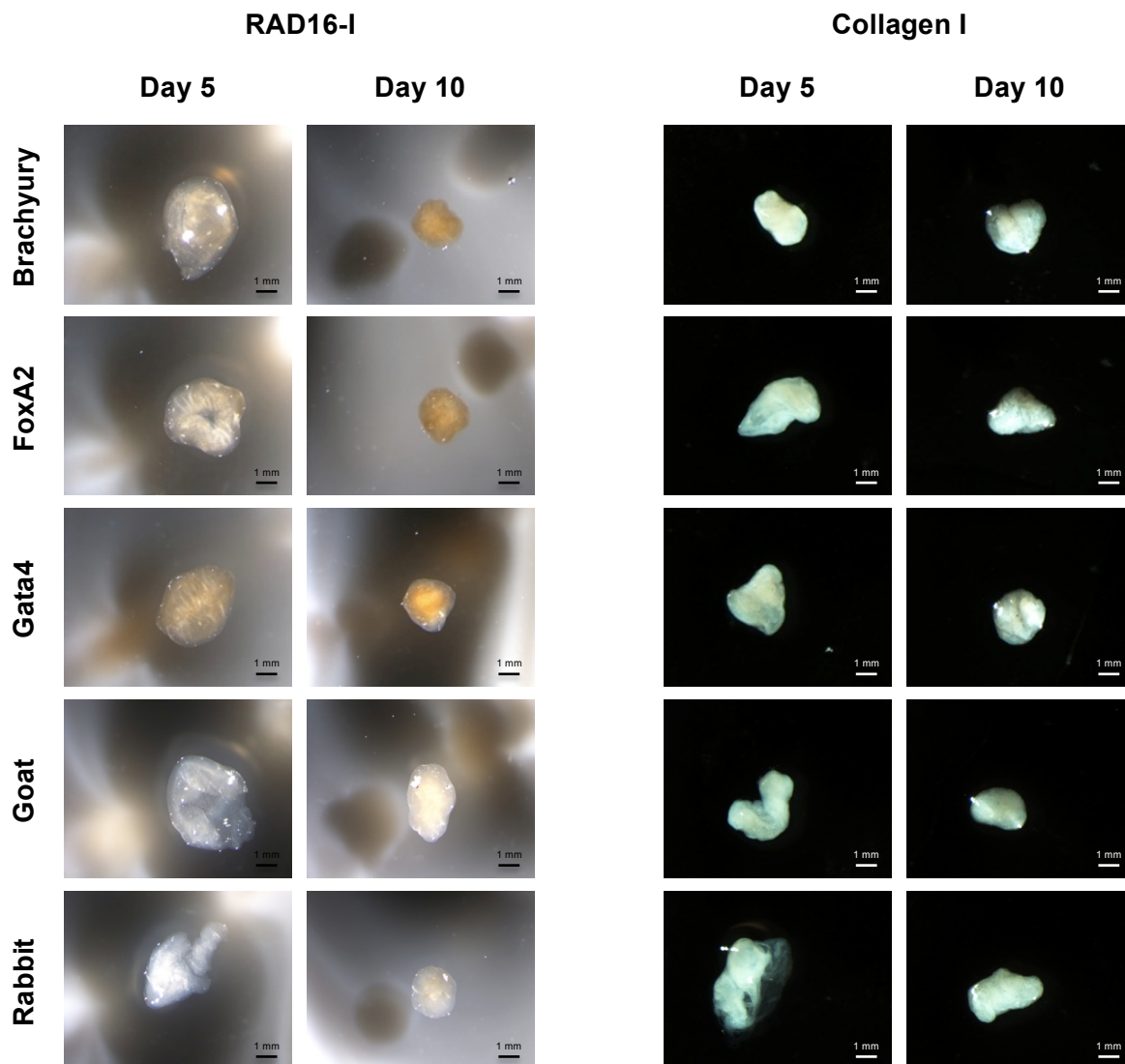


**Figure 12.** Immunostaining for mesenchymal markers (Brachyury, FoxA2 and Gata4) of hNDFs cultured in RAD16-I *versus* Collagen I for 5 and 10 days in control medium. Secondary antibodies were bound to HRP and the samples were positive when a brown precipitate appeared. Secondary antibodies anti-Goat (Brachyury and FoxA2) and anti-Rabbit (Gata4) represent negative controls without primary antibodies and they were white.

### 3.3.3. Study of the effect of fetal bovine serum on the expression of early differentiation markers of hNDFs cultured in RAD16-I

The following experiments were carried out to study the effect of Fetal Bovine Serum (FBS) on the expression of early differentiation markers. Human Normal Dermal Fibroblasts (hNDFs) were cultured in RAD16-I with control (plus FBS) and defined (minus FBS and supplemented with Platelet-Derived Growth Factor, PDGF) media. Fetal Bovine Serum is used in the vast majority of cell cultures even though its composition is variable and undefined. The goal was to study how the culture medium modulated the acquisition of the mesenchymal-like phenotype of hNDFs

cultured in RAD16-I. As expected, many hNDFs cultured in 2D without FBS and with PDGF detached from the plastic surface and died. The few cells that remained attached had an unusual round shape (**Figure 13**). Cells cultured in 3D with PDGF appeared sparse in the bioscaffold, also had rounded morphologies and created few cell-cell connections (**Figure 13**). Therefore, the cellular network described above and responsible for the contraction of the construct was less evident in 3D cultures without FBS than with it. As a result, constructs maintained with defined medium were soft and fragile. The characteristic dense cellular outer layer observed in constructs cultured with FBS could also be distinguished but to a lesser extent in those without FBS. Thus, the contractive forces appeared to be less intense in the absence of FBS resulting in a circular flat morphology of the construct instead of a dome-shape one (**Figure 9**). Independently of the culture medium used (with or without FBS), cells remained inside the biomaterial scaffold and did not migrate out of it.

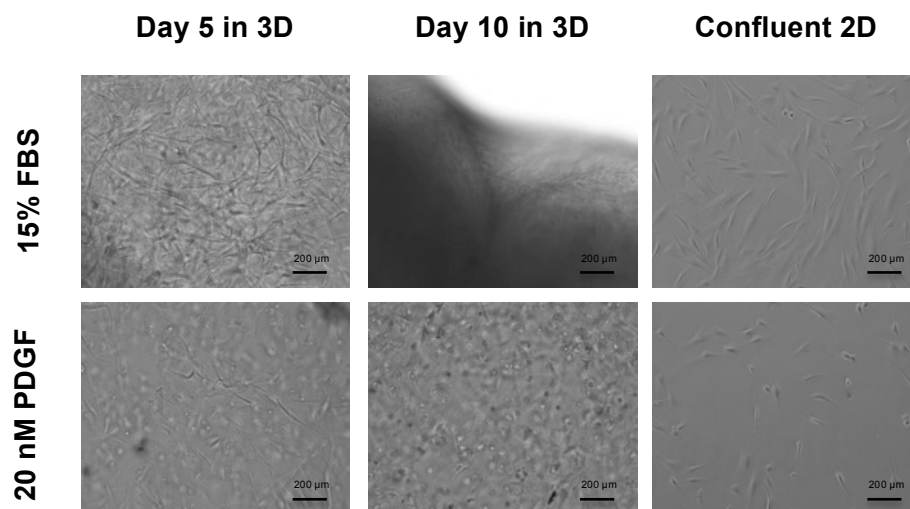


**Figure 13.** Microscopic observation of hNDFs cultured in RAD16-I for 5 and 10 days and in 2D. Cells were maintained in a control medium rich in FBS and in a defined medium lacking FBS but containing PDGF.

**Figure 14** shows living (green, stained with Green Calcein) and dead (red, stained with Ethidium Homodimer-1) hNDFs cultured in RAD16-I with and without FBS (complemented with PDGF). The cellular viability was very high (almost no dead/red cells) after 20 days in hNDFs cultured in RAD16-I with 15% FBS (control medium). Surprisingly, most of the cells cultured in 3D in the absence of FBS (PDGF complemented medium) were alive at the end of the experiment (day 20). Some dead cells, however, were detected in the outer layer of the construct (**Figure 14**:



**20nM PDGF and EthD-1**). Overall, the results suggested that the bioscaffold was not cytotoxic for the hNDFs and that the 3D environment based on RAD16-I promoted cell survival without FBS.

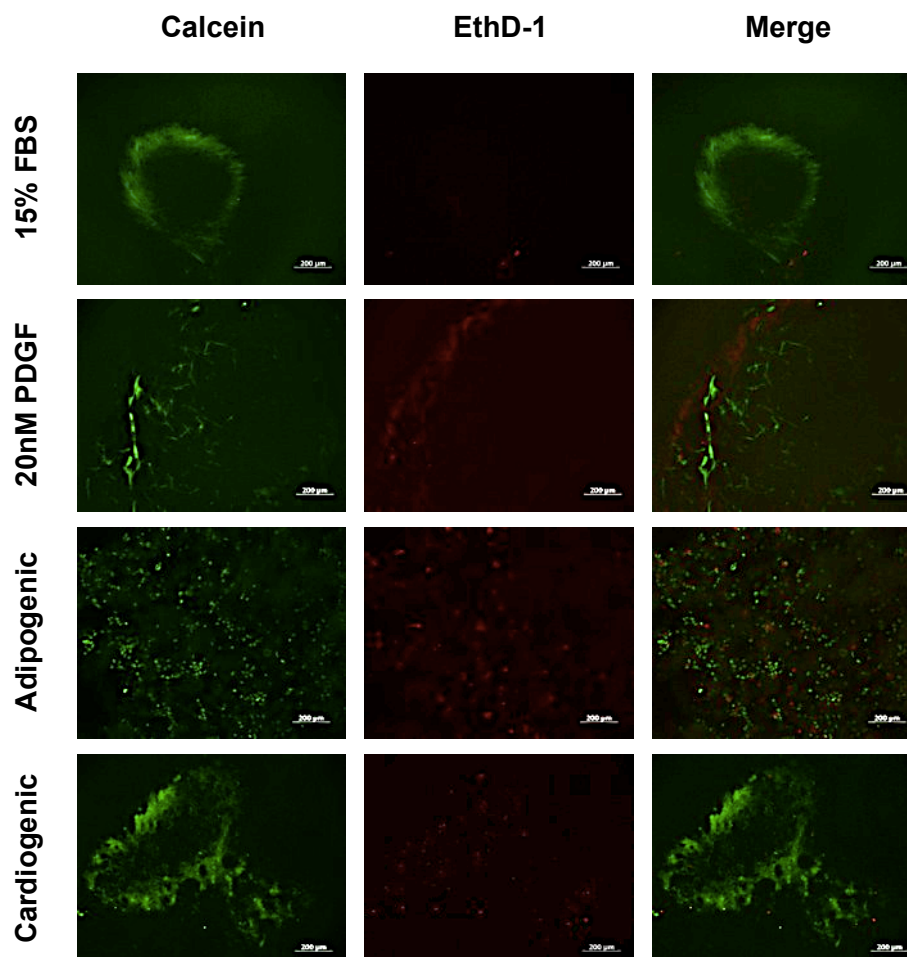


**Figure 14.** Live/Dead assay of hNDFs cultured in RAD16-I for 20 days with different media: control (15% FBS), defined (no FBS but 20nM PDGF), adipogenic and cardiogenic. Green calcein stains living cells (green) whereas EthD-1 stains dead cells (red).

Staining of the cytoskeleton showed that hNDFs embedded in RAD16-I and cultured with FBS had a dense intercellular network (**Figure 15: 15% FBS and Phalloidin**). Actin filaments were present among the cell body. Each cell was oriented differently in the construct and that explained the appearance of the cytoskeleton (of all the cells), which seemed to be overlapping in all directions creating a dense 3D cellular network. Indeed, cells were distributed homogeneously among the construct. The cell density was so high that cells seemed highly compacted. Conversely, hNDFs cultured without FBS were scattered throughout the



scaffold. Their cytoskeleton was also elongated, although it was wider than in cells cultured with FBS (**Figure 15: 20 nM PDGF and Phalloidin**).

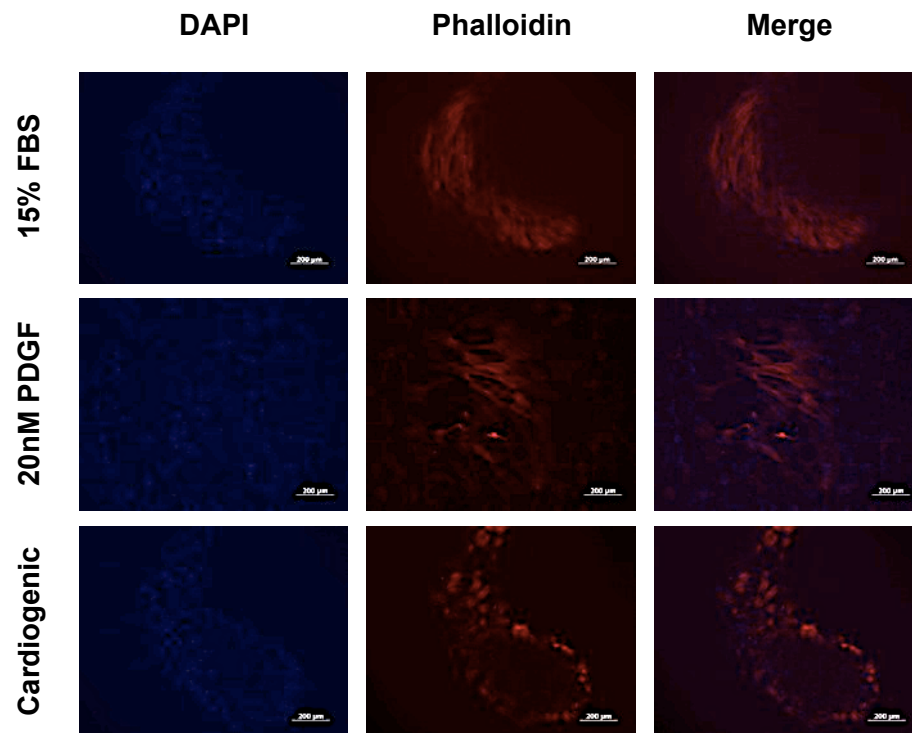


**Figure 15.** DAPI (nuclei, blue) and Phalloidin (actin microfilaments, red) staining of hNDFs cultured in RAD16-I for 20 days with different media: control (15% FBS), defined (no FBS but 20nM PDGF) and cardiogenic.

As previously mentioned, immunocytochemistry (ICC) for early differentiation markers (Brachyury and FoxA2) of hNDFs cultured in RAD16-I with FBS was slightly positive at day 5 and highly positive at day 10 (**Figure 12**). These results seem to be corroborated here. Human NDFs contained embryonic-related proteins when cultured in RAD16-I for 10 days with and without FBS. Moreover, ICCs of hNDFs cultured in the neutral peptide scaffold independent of the culture medium were positive for Brachyury and FoxA2 (**Figure 16**).

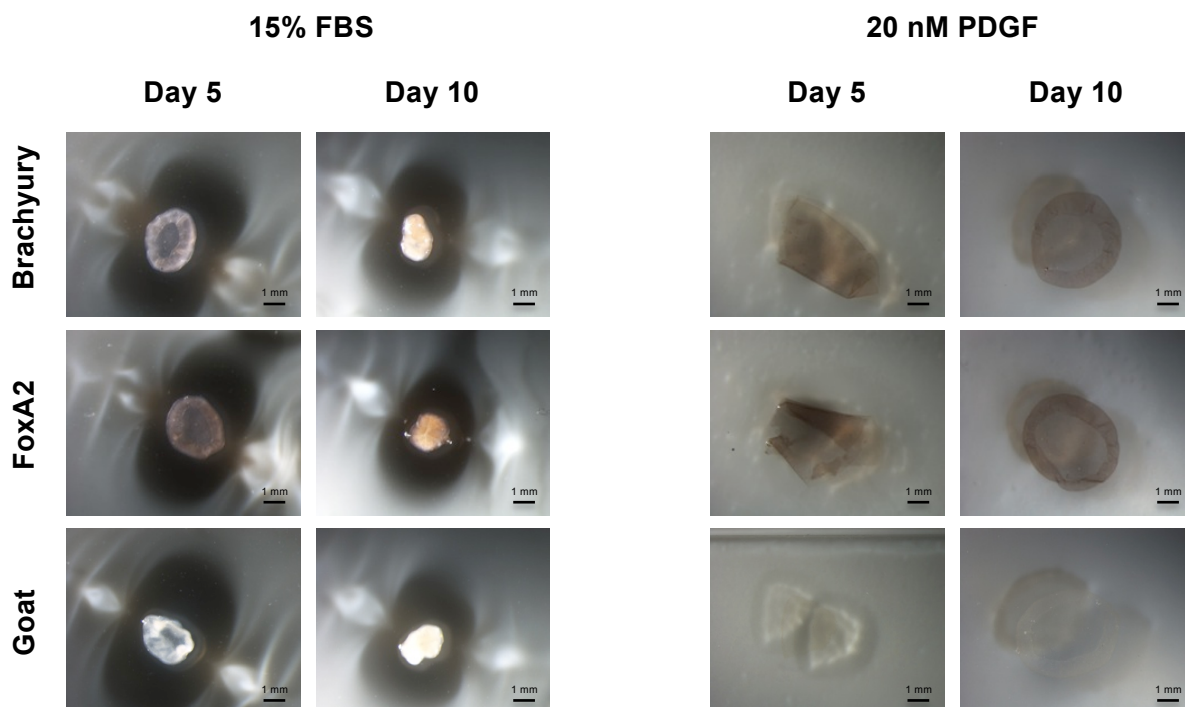


**Figure 16.** Immunostaining for mesenchymal markers (Brachyury and FoxA2) of hNDFs cultured in RAD16-I for 5 and 10 days with control (15% FBS) and defined (no FBS but 20nM PDGF) media. Secondary antibodies were bound to HRP and the samples were positive when a brown precipitate appeared. Secondary antibody anti-Goat represents negative controls, which were white in all cases.

#### 3.3.4. Adipogenic lineage commitment of hNDFs cultured in RAD16-I

The main characteristic of adipocytes is the formation of cytoplasmic lipid droplets. Indeed, the lipids were easily observed with brightfield microscopy and with specific fluorescent staining using a hydrophobic dye (Nile red). Human Normal Dermal Fibroblasts (hNDFs) were first embedded in RAD16-I in order to mimic a cellular 3D environment and cultured with adipogenic induction medium. A batch of cells was cultured in parallel with control medium lacking chemical inductors. Observation under the phase contrast microscope showed that control constructs contracted as described above from day 5 onwards whereas chemically induced ones did not contract and looked very soft, porous and spongy (**Figure 17**). The cellular morphology was also very different: control cells looked elongated while induced cells were rounded. Cytoplasmic lipid droplets were observed inside the hNDFs (**Figure 17**) cultured with adipogenic medium (from day 15 to 20). Interestingly, cytosolic lipid droplets resembled clusters throughout the cytoplasm (see arrows and magnified photographs in the **Figure 17**). Nonetheless, hNDFs in RAD16-I and cultured with control medium never developed any cytoplasmic lipid droplets.

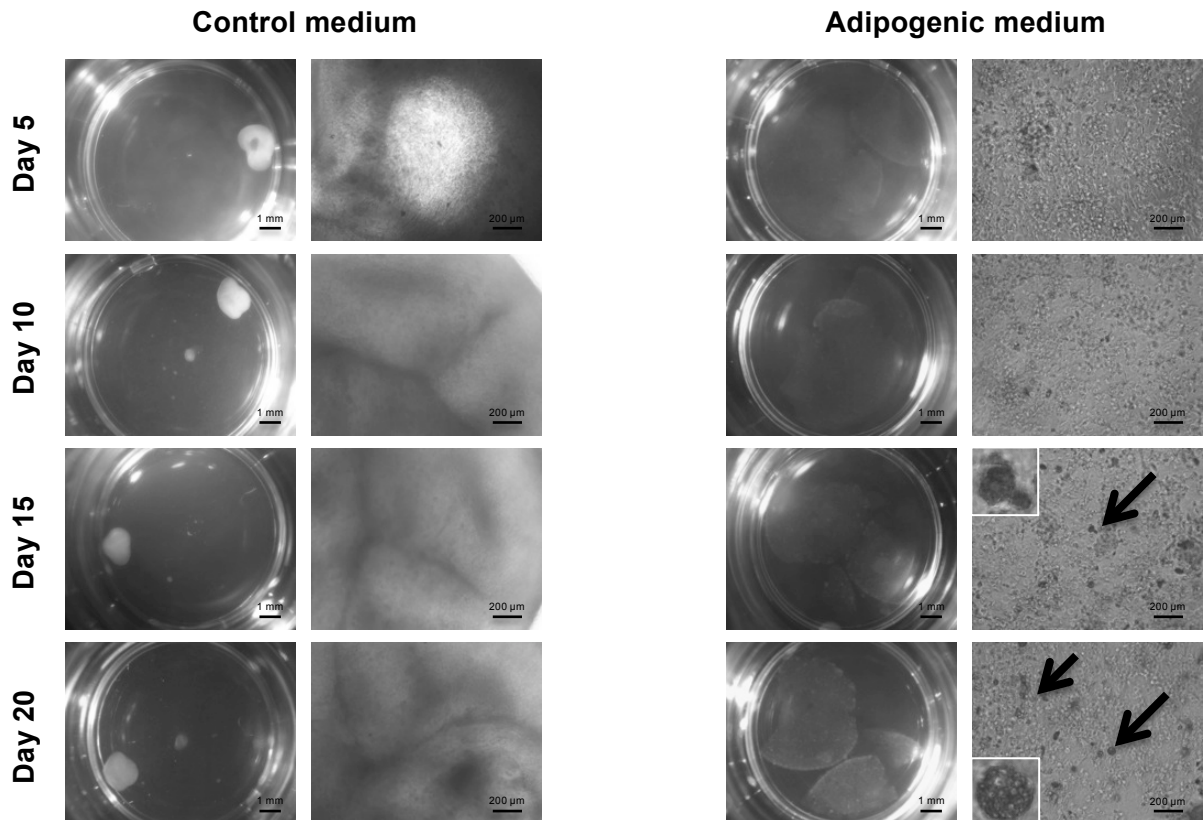


**Figure 17.** Stereoscopic (left column) and microscopic (right column) observation of hNDFs cultured for 20 days in RAD16-I with control and adipogenic media. Arrows point at intracellular lipid droplets, which confirmed the adipocyte-like phenotype of the cells when induced into adipogenic lineage.

Moreover, cellular viability of hNDFs in RAD16-I cultured in adipogenic induction medium was assessed and compared to cells cultured in control medium (**Figure 14**). Indeed, cells appeared rounded and dispersed when induced with chemical components. In terms of cell survival, almost all the cells were alive (green cells) in both conditions (control and adipogenic media). Some cells were dead (red cells) in adipogenic induction whereas cell death was negligible in control constructs.

After having observed lipid droplet formation in hNDFs, it was decided to specifically stain lipids with Nile red dye (red). The localization of lipids was compared in cells cultured in 2D, 3D with control and with adipogenic media. **Figure 18** shows that hNDFs cultured in 2D contained multiple lipids (red), which were homogeneously localized in their cytoplasm. It is important to point out that lipids are extremely abundant in cells: they are a major component of membranes and they are also present throughout the cytoplasm as different categories of lipids (vitamins, glycerolipids, sterols, etc.). Similarly, hNDFs cultured in RAD16-I with control medium had a diffuse and homogenized localization of lipids. Control cells contained lipids in

the cytoplasm (**Figure 18**) although the picture does not illustrate it properly due to the difficulty to focus on one single optical layer in the 3D construct volume. Conversely, hNDFs induced to adipogenic lineage in 3D enclosed defined clusters of lipid droplets that can be perfectly distinguished in the **Figure 18** (pointed by the arrows and magnified). Hereby, the important point was the localization of the lipids: diffused in 2D and 3D control constructs and very localized in 3D induced ones. The clusters observed in hNDFs induced in 3D with chemical inductors were the functional proof that the differentiated hNDFs were adipocyte-like cells, able to secrete fat.

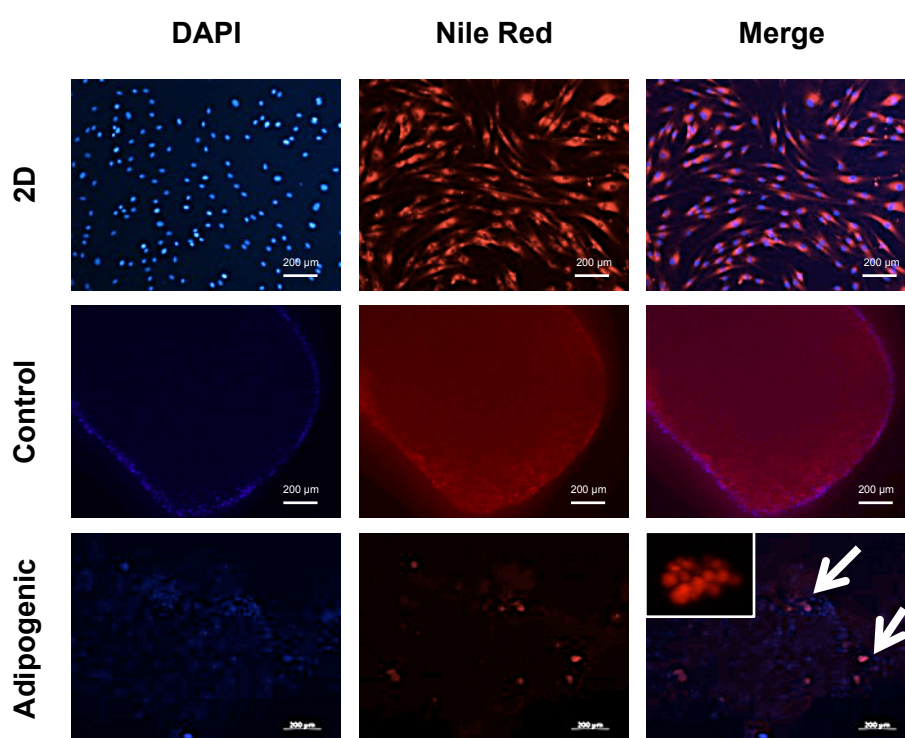


**Figure 18.** DAPI (nuclear dye) and Nile red (lipidic dye) staining of hNDFs cultured in 2D and in RAD16-I for 20 days with control and adipogenic media. Arrows point at lipid droplets specifically stained with Nile red.

Likewise, the adipogenic potential of hNDFs was analyzed at a molecular level. Total RNA was extracted and the expression of a typical adipogenic gene PPAR $\gamma$  (Peroxisome Proliferator-Activated Receptor  $\gamma$ ) was checked with the Polymerase Chain Reaction (PCR) technique. PPAR $\gamma$  is involved in extracellular matrix alterations and cytoskeletal remodeling during the differentiation of pre-adipocytes into mature adipocytes. Cells were cultured in 2D (d0 means day 0 at cell confluence), 3D for 20 days in control and adipogenic induction media. The ribosomal gene 18S was used as a housekeeper gene to confirm that the reaction

worked properly and to verify that all the samples loaded in the agarose gel had the same quantity of cDNA (loading control). It appeared that hNDFs expressed the gene in all cases, including in 2D cultures at day 0. **Figure 19** illustrates the agarose gel and it can be observed that a predicted size band displayed in all the samples. Therefore, it can be suggested that hNDFs expressed PPAR $\gamma$  when cultured in 2D at day 0 and in 3D after 20 days in control and adipogenic induction media. No obvious differences between the three samples could be observed.

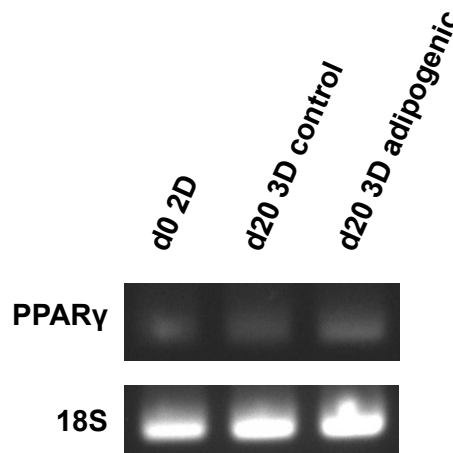


**Figure 19.** Agarose gel of specific bands for PPAR $\gamma$  amplified with PCR from hNDFs cultured in 2D and in RAD16-I for 20 days with control and adipogenic media.

### 3.3.5. *Cardiogenic lineage commitment of hNDFs cultured in RAD16-*

*I*

On the other hand, human Normal Dermal Fibroblasts (hNDFs) were chemically induced to cardiac lineage. For this, cells were embedded in RAD16-I in order to create a real 3D environment and then cultured for 20 days with cardiogenic induction medium. In parallel, hNDFs were cultured with control medium lacking any chemical inductor. The photographs taken under the stereoscope (left column of each block in the **Figure 20**) show that induced cells contracted faster the construct than the control ones. Nevertheless, both constructs (control and induced) looked very similar at day 20. Regarding the cell morphology, observation under the microscope (right column of each block in the **Figure 20**) showed that hNDFs underwent a few apparent morphologic changes when cultured in cardiogenic induction medium compared to control medium. Induced cells appeared rounded,



## MESENCHYMAL POTENTIAL OF HUMAN NORMAL DERMAL FIBROBLASTS IN THE THREE-DIMENSIONAL PEPTIDE SCAFFOLD RAD16-I

compacted and dense from day 3 to 10. Conversely, control hNDFs were stretched and elongated. For the last 10 days of the experiment, cells cultured in induction medium seemed to create clusters with dense cellular network whereas the cells in control medium organized themselves more linearly.

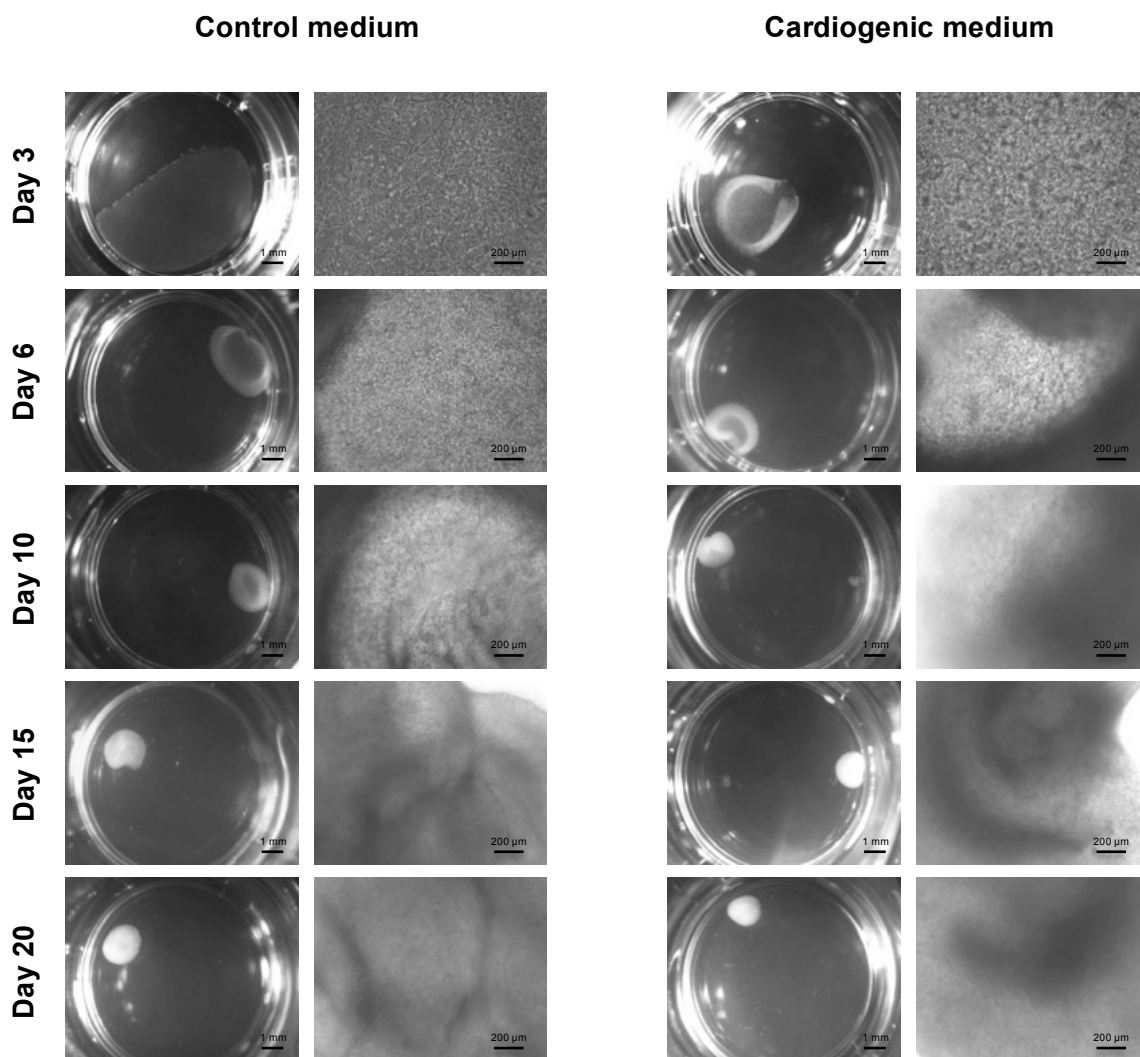


**Figure 20.** Stereoscopic (left column) and microscopic (right column) observation of hNDFs cultured in RAD16-I with control and cardiogenic media for 20 days.

The cell viability assay illustrated in **Figure 14** compared the cell survival of hNDFs cultured in 3D with control and cardiogenic induction media. Almost all of the cells were alive (green on the **Figure 14: 15% FBS and Cardiogenic and Calcein**), which also implied that very few cells were dead (red on the **Figure 14: 15% FBS and Cardiogenic and EthD-1**) in both culture conditions. As observed under the phase contrast microscope during the course of the experiment, hNDFs organized

differently in the peptide scaffold. Thus, hNDFs cultured with control medium appeared aligned while the cells maintained with cardiogenic medium created clusters (**Figure 14**).

Besides, the staining of nucleus and cytoskeleton of hNDFs in 3D cultured with control *versus* cardiogenic media confirmed the previous observations. Actin filaments (red staining on the **Figure 15**) of control hNDFs were stretched and long (elongated cells) while induced cells had wide and short (rounded cells) actin filaments. Also, nothing unusual could be observed regarding the nuclei (blue staining on the **Figure 15**): around 15-20  $\mu\text{m}$  and perfectly rounded.

Furthermore, the PCR technique revealed the gene profile of hNDFs embedded in RAD16-I and cultured with control and cardiogenic media for 20 days. The time points chosen to follow the trend of the cells in terms of mRNA expression were: day 0 (corresponding to hNDFs brought to confluence in 2D cultures before generating the 3D constructs), 3, 6, 10, 15 and 20 (hNDFs cultured in the bioscaffold with both media). Thus, **Figure 21** pictures the bands of the amplicons obtained in each condition. The primer pairs amplified cardiac progenitor (Mef2c and Tbx5) and mature cardiomyocyte (ACTC1) genes. The ribosomal 18S gene was used as a housekeeper gene to ensure that the PCR ran properly and to verify that all the samples loaded in the agarose gel had the same quantity of cDNA (loading control). As it can be observed in the **Figure 21**, hNDFs did express cardiac progenitor markers independently of the culture medium (control or cardiogenic) and the environment (2D or 3D). Indeed, all the samples displayed a band. Thus, hNDFs expressed cardiac progenitor genes (Mef2c and Tbx5) when cultured in 2D and in 3D with and without chemical cardiac induction. Nevertheless, it appeared that the intensity of the bands was slightly higher in the samples cultured with cardiogenic medium than with control one. Regarding ACTC1, it seemed that this gene was more expressed in control cells than in induced cells. Indeed, bands seemed more intense from day 3 to 20 in 3D culture samples with control medium than with induction one. However, bands got brighter in cardiogenic conditions at day 15 and 20. Nonetheless, hNDFs did not express the mature cardiomyocyte marker (ACTC1) when cultured in 2D at day 0.

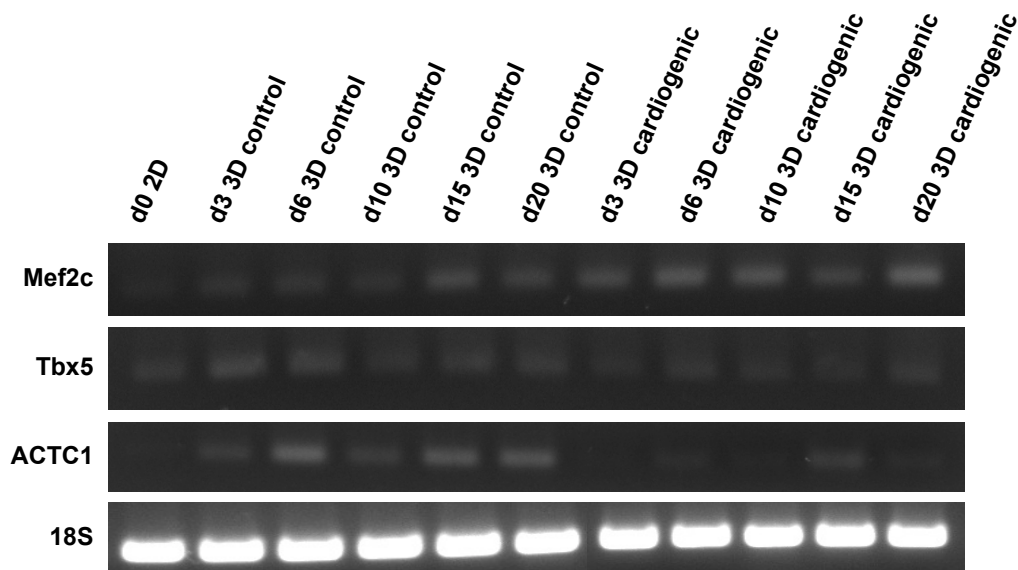


**Figure 21.** Agarose gel of specific bands for cardiac progenitor (Mef2c and Tbx5) and mature cardiomyocyte (ACTC1) genes amplified with PCR from hNDFs cultured in 2D and in RAD16-I for 20 days with control and cardiogenic media.

In addition, the presence of proteins was analyzed with immunocytochemistry (ICC) staining. Primary antibodies detected cardiac progenitor (Tbx5, Nkx2.5) and mature cardiomyocyte (Connexin 43, Cardiac Heavy Myosin (MYH)) proteins. Although the assay was qualitative, it could be determined presence or absence of target proteins. The results provided a relative idea of protein translation. It can be observed on the **Figure 22** that Nkx2.5 was vaguely translated in the cells forming the outer layer of induced 3D constructs at day 6. Moreover, Tbx5 was massively translated in hNDFs cultured with cardiogenic medium from day 3 to day 20. Control fibroblasts slightly expressed Tbx5 during the same time period. Connexin 43 (Cx43) was only observed in induced hNDFs at day 6, more precisely in the cells forming the outer layer of the construct. The cardiac heavy myosin (MYH) was similarly present in cells maintained in both culture media from day 3 to day 10. However, it appeared more intense in control cells than in induced cells from day 10 to day 20.



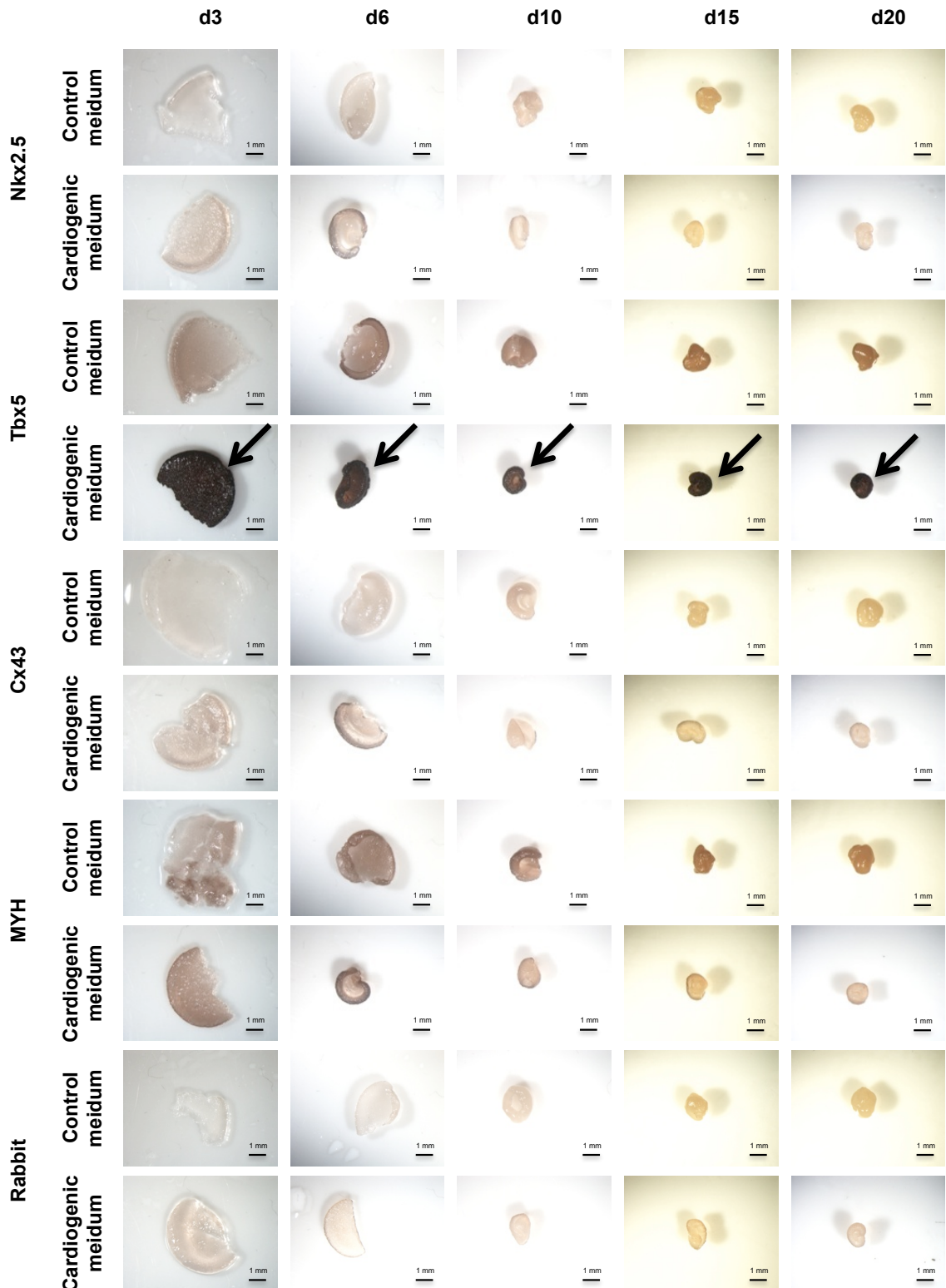


**Figure 22.** Immunostaining for cardiac progenitor (Nkx2.5 and Tbx5) and mature cardiomyocyte (Cx43 and MYH) proteins of hNDFs cultured in RAD16-I with control (15% FBS) and cardiogenic media for 20 days. Secondary antibodies were bound to HRP and the samples were positive when a brown precipitate appeared. Arrows point at highly positive samples. Secondary antibody anti-Rabbit represents negative controls, which were white in all cases.

### 3.4. Discussion

The use of human Normal Dermal Fibroblasts (hNDFs) in this chapter was not a random choice. A requirement for successful personalized therapy is to be able to explant large amounts of the individual's own cells to be reprogrammed: fibroblasts are the most abundant and least specialized cellular component of the connective tissue, widely abundant in the body. Fibroblasts are commonly used in regenerative research due to their role in skin wound healing. Also, this type of cells has a high proliferative potential and can be easily expanded *in vitro*. All in all, it is possible to quickly obtain millions of fibroblasts from a single patient and create a bank of early to mid passage stable diploid fibroblasts from a single primary culture derived from a biopsy<sup>9</sup>. Moreover, previous experience in Dr. Semino's laboratory proved that Mouse Embryonic Fibroblasts (MEFs) could be de-differentiated *in vitro* into a more primitive stage resembling stem cells<sup>4,10</sup>. These results encouraged us to reproduce these experiments with human adult fibroblasts. First of all, hNDFs were characterized in classical two-dimensional (2D) cultures on plastic surfaces (flasks, wells). The morphology of hNDFs was defined as normal: mono-nucleated cells with a spread shape and high number of filopodia (cytoplasmic projections of actin filaments). It is thought that the plasmatic membrane of the cellular mobile edge organizes the actin filaments of the filopodia. The staining of actin filaments showed that the cytoskeleton of hNDFs in 2D was dense, elongated and parallel. Furthermore, the actin cytoskeleton has important roles in cell morphology and migration through cell adhesions<sup>11</sup>. Moreover, hNDFs in 2D cultures did not express any early differentiation markers such as primitive (Brachyury, Gata4) or cardiac ones (Nkx2.5, Tbx5, Cx43, MYH). Hence, 2D cultures were used as reference to compare cellular behavior of hNDFs in 2D *versus* 3D environments.

Accordingly, hNDFs changed their morphology when cultured in 3D. On rigid substrate (flask), they appeared flattened and spread while in the peptide scaffold, they were elongated. Cellular extensions, creating a dense network between the cells embedded in RAD16-I and contributing to contraction forces generated by cell-cell interactions, could be appreciated under the microscope. The peptide scaffold mimics a malleable membrane similar to the extracellular matrix (ECM) and can yield to cytoskeletal tensions, resulting in less spread-shaped cells in 3D than in 2D<sup>12</sup>. Cells seemed to act as a whole and collaborate in contracting the construct. But, for some reason (differences in the oxygen pressure, nutrients availability or cellular density itself) the construct had an irregular shape reminding a disc. The outer layer

appeared denser and due to mechanical forces, it developed into a dome-like structure. This process happened at approximately day 5 of 3D culture. Probably, fibroblasts initially required cell proliferation until a high cellular density was reached, to generate matrix and therefore evolve 3D-matrix adhesions. This would result in the construct contraction<sup>13</sup> indicating that cells and matrix were mechanically coupled. Thus, matrix deformation is considered the main cause of mechanical signalling. Furthermore, cells modify their microenvironment depending on how rigid or soft they want it to be. Normal tissue cells anchor to the matrix and pull on their surroundings, test the force they had to apply to deform the matrix and respond through cytoskeleton organization to the resistance sensed. Cross-bridging interactions of actin and myosin filaments generate contractile forces. There is a “tactile” sensing of the environment and cells detect the tactile set-point as it happens in other responses as extracellular ion or optimal growth factor concentration detection<sup>14</sup>.

On the other hand, it was found that the RAD motif had a vast similarity to the RGD motif used in many experiments to render the matrix cell-friendly. Moreover, the RAD16-I is composed by repetitions of this motif. So, it would not be unusual to think that this property is responsible for attaching cells in the matrix. This would discard the theory that cells are cultured in a 3D neutral milieu in the peptide scaffold, as they would be anchored and not floating. Nevertheless, it has been proven that RAD motif by itself was not recognized by the ECM receptor repertoire when cells were cultured in RAD16-I scaffolds<sup>12</sup>. Therefore, the results presented above indicate that cells were cultured in a real and neutral 3D microenvironment and that the matrix was neither functionalized nor instructive. Nevertheless, the presence of serum in the medium and the cell conditioning activity would decorate the synthetic scaffold with proteins such as serum fibronectin and cell-secreted collagens and proteoglycans. Cells support themselves in the matrix thanks to cell-ECM (indirectly attached to the RAD16-I through protein decoration of the nanofibers) and cell-cell interactions, as they do not attach apparently to the RAD16-I nanofibers. Relatively little is known about how cells adhere to the matrix in living tissues but it is clear that integrins play a key role in this process<sup>13</sup>.

Conversely, Collagen I is defined in the literature as the gold standard of the 3D cultures. Collagen fibers (80% Collagen I) constitute the major structural component of the cardiac extracellular matrix (ECM)<sup>15</sup>. Consequently, it appears to be an excellent candidate for embedding cells, recreating a 3D environment and mimicking the natural scaffold surrounding the cells *in vivo*. Many attempts have been

addressed to create 3D constructs based on Collagen I scaffolds and used as cardiac patches<sup>15</sup>, bone grafts<sup>16</sup>, etc. Other combined cardiogenic engineered scaffolds aimed to restore the cardiac integrity after a myocardial infarction (MI) have been designed: gelatin and collagen<sup>17</sup>, native heart matrix and collagen<sup>18</sup>, adhesion peptides and collagen<sup>19</sup>, etc. However, the main drawback is that collagen is a natural extract from animal sources implying that it is an extremely instructive material. Anyhow, hNDFs were embedded in RAD16-I and in the well-defined Collagen I (benchmark). Collagen scaffolds have been shown to allow migration, proliferation and differentiation of cells. Hence, presence of early differentiation proteins was evaluated in hNDFs cultured in Collagen I and in RAD16-I. It was found that hNDFs did not express any early differentiation marker (Brachyury, FoxA2 and Gata4) when cultured in Collagen I whereas they did express them in RAD16-I. Hence, cells might undergo a mesenchymal potentiation when cultured in the peptide scaffold RAD16-I. The neutrality of the scaffold seems to be the signal for the cells to “de-differentiate” into a primitive stage. Probably, instructive scaffolds would present signals that would induce the embedded cells to behave in a certain way rather than taking them in a situation where they can have more options. In resume, this could explain why hNDFs cultured in 3D neutral peptide scaffolds present MSC-like phenotype, which is in fact the working hypothesis of this chapter.

Additionally, the importance of the Fetal Bovine Serum (FBS) was assessed in hNDFs cultured in RAD16-I. It has been reported in the literature that the engraftment of human cells cultured with FBS can lead to malignant ventricular arrhythmias and sudden deaths in patients due to fixation of animal proteins on the cell surface, which causes immunological adverse events<sup>20</sup>. Therefore, it should be considered to culture human cells with either autologous human serum or none (this chapter). Herein, the presence of serum in 2D cultures appeared to be critical for the cell survival: cells cultured without FBS detached and died despite the presence of PDGF. Conversely, cells embedded in RAD16-I survived no matter the composition of the culture medium. This means that the nature of the 3D scaffold is extensively more important than the composition of the culture medium. Indeed, the nutrients in the serum contribute to higher cell survival whereas they are not the critical factor for hNDFs to survive, the 3D environment is. Human NDFs cultured in 3D might secrete more necessary ECM to establish cell-ECM interactions than in 2D, decorating the neutral nanofibers. Consequently, cells equilibrate their surroundings with proteins needed to create the cellular network. Cells maintained without FBS but with PDGF created a weaker cellular network that caused a lower construct contraction.

Nevertheless, cells in defined medium (complemented with PDGF) survived because of cell interaction, even if there was less interaction than in cells cultured with FBS. Therefore, the cellular network created in 3D environments plays a key role in cell survival and not the composition of the medium. Moreover, hNDFs cultured in 2D expose adhesions receptors (mostly integrins) mainly in the ventral part of the cell in contact with the surface whereas in 3D, fibroblasts present them all over the cell surface<sup>21</sup>. Additionally, immunocytochemistry staining revealed the expression of early differentiation markers (Brachyury and FoxA2). Surprisingly, hNDFs underwent a similar mesenchymal potential acquisition in both media although cells cultured only with PDGF expressed less embryonic-related proteins than cells with FBS. Thus, it is believed that it is the 3D environment based on RAD16-I that causes the cells to interact, contract the construct and ultimately potentiate cells into a primitive cellular stage independently of the culture medium. The finding of Brachyury and FoxA2 positive cells in our system may indicate the primitive character of the cells and support their newly capacity to differentiate into mesenchymal lineages such as chondrogenic<sup>6</sup> and osteogenic<sup>5</sup> as well as adipogenic and cardiogenic (this work).

Adipogenesis has been widely studied in order to obtain obesity models in the laboratory. In addition, understanding the process of fat formation is important because this cellular type is the major energy reserve in higher eukaryotes as mammals. Interestingly, it exists a cellular intermediate stage: pre-adipocytes, which are undifferentiated fibroblast-like cells that mature into round flat cells, adipocytes<sup>22</sup>. The morphology of pre-adipocytes (similar to fibroblasts) together with the previously described fibroblastic de-differentiation observations inspired the study of adipogenic differentiation of hNDFs in the present chapter. Indeed, fibroblasts have the same cellular ancestor as adipocytes: Mesenchymal Stem Cells (MSCs). Some authors define fibroblasts as mature mesenchymal cells due to their similar phenotypic and functional features. *Blasi et al.* have proven that hNDFs in 2D can differentiate into osteogenic and adipogenic-like cells likewise adipose-derived MSCs. Nevertheless, the multipotentiality of fibroblasts is considerably more limited than MSCs<sup>23</sup>. Due to how fascinating these discoveries were, it was decided to study the plasticity of fibroblasts in 3D to become another cellular type. Three-dimensional cultures contribute to the mimicking of ECM-like *in vivo* environments and of tissue-like structures. Cells embedded *in vitro* in a convenient biomaterial might recreate *in vivo* cellular behavior, which is critical for engrafting regenerative studies. Successful differentiation of cells in 2D cultures is extremely useful for extrapolation in 3D cultures, which simulate tissue-like structures. For this reason, experiments aimed to

evaluate the multipotential capacity of hNDFs in 3D. It has been previously demonstrated that hNDFs spontaneously engaged into a primitive cell stage probably similar to MSCs. Therefore, fibroblasts with MSC-like properties in RAD16-I were chemically induced into adipogenic lineage. The results showed that fibroblasts with this induction treatment created a reduced cellular network that caused a lower contraction of the construct than control samples. The vast majority of the cells survived in both conditions whereas their morphology highly differed: control cells were elongated whereas induced cells were rounded and similar to adipocyte-like cells. Only cells cultured in 3D with adipogenic medium created lipid droplets. This suggests that hNDFs in RAD16-I scaffolds underwent a de-differentiation-like process, which turned them into cells with MSCs properties able to further commit into adipocytes. Interestingly, the de-differentiation-like process seemed to be spontaneous (expression of early mesenchymal markers such as Brachyury, FoxA2 and Gata4) and independent of the culture medium. Instead, the adipogenic commitment required chemical induction. Nonetheless, hNDFs cultured in 2D also showed high expression of adipogenic gene PPAR $\gamma$  and elevated amounts of cytoplasmatic lipids. Lipid formation observed in early 2D cultures might correspond to the high lipidic content in plasmatic membrane and cytoplasmic proteins. Also, PPAR $\gamma$  might be similar to its variant  $\alpha$  and  $\beta$ , which are abundant in several cell types. Although PPAR $\gamma$  plays a key role in fat deposition, it is also involved in the metabolism of insulin action of other cells<sup>24</sup>. For all these reasons, in the present work PPAR $\gamma$  might be an inaccurate adipogenic marker although it is described to be vastly expressed in fat tissue. In our assays, PPAR $\gamma$  did not appear to be a specific adipogenesis marker. Therefore, the most reliable method to confirm adipogenesis is the observation of cytosolic lipid droplets under the microscope, which are unique of adipocytes.

Although it has been previously shown that fibroblasts cultured in 2D with adipogenic inductors differentiated into adipocyte-like cells<sup>2</sup>, the development of 3D tissues opens a new therapeutic strategy in regenerative medicine. This indicates that fibroblasts present an intrinsic capacity to undergo adipogenesis regardless of the culture environment (2D or 3D). Nonetheless, it seems that in 3D cultures the tissue development process is more complex than in 2D maybe due to the fact that three-dimensional tissues present a hierarchical complexity. Human NDFs cultured in RAD16-I became adipocyte-like cells similarly to previous approaches of 2D cultures although our platform mimics *in vivo* three-dimensional tissue-like structures.

Regarding cardiac differentiation, chemical inductors in the culture medium have shown to increase cardiogenic potential of hESCs *in vitro*<sup>25</sup>. Moreover, other studies have focused on the importance of the three-dimensional environment and have performed systems to compare the ability of hESCs to generate functional cardiomyocytes in 2D and 3D models<sup>26</sup>. Indeed, the differentiation is closely influenced by the scaffold and directed by the culture medium<sup>27</sup>. Interesting tracking strategies have also been developed to assess cardiac differentiation in real-time<sup>28,29</sup>. Herein, it is suggested that the 3D peptide scaffold RAD16-I combined to cardiogenic induction medium generates cardiomyocyte-like cells from hNDFs. Interestingly, cell morphology and organization in the scaffold was very distinct comparing control *versus* cardiogenic conditions. Regarding gene expression profile, control and induced hNDFs expressed progenitor cardiac genes. Unexpectedly, hNDFs expressed more ACTC1 (mature cardiomyocyte marker) in control conditions than in induced. It is important to consider that this gene is also involved in early embryonic development, which could reflect to the developmental-like process that these cells are undergoing in scaffolds *per se*. The expression of ACTC1 was null in 2D cultures. Apparently, the peptide scaffold is the one that plays a key role in the expression of ACTC1. Hence, hNDFs in 3D expressed cardiac progenitor genes independently of the culture medium. Contrariwise, the protein detection assays demonstrated that only hNDFs cultured in 3D and chemically induced with cardiogenic medium undoubtedly over expressed cardiac progenitors markers (Tbx5). So, the scaffold and the induction medium are critical for the cardiac differentiation of hNDFs. The scaffold is needed to generate flexible un-specialized cells whereas the inductors are needed to commit the cells into cardiac lineage. In the experimental system proposed in this chapter, 3D cultures offer tissue-like structures able to express cardiac progenitor markers.

Thus, the induction medium is critical for the detection of cardiac proteins in hNDFs cultured in 3D. All in all, it is believed that the neutrality of the 3D scaffold sends the signal to the cells to express or over express a battery of genes. Indeed, cells might open a gene frame when they cannot make any commitment. In other words, cells become less specialized in neutral conditions in order to be more plastic for further commitments. Differentiated cells (hNDFs) cultured in a neutral 3D scaffold based on RAD16-I might get into a more naïve stage, open-chromatin state marked by high epigenetic instability. Similarly to *Efe et al.*'s findings, cells might "relax" back into epigenetically more stable states and acquire mesenchymal potentiality<sup>30</sup>. Although *Efe et al.* use inductive signals to bring the cells back to an

unstable intermediate population of uncommitted cells, this chapter is based on creating three-dimensional cultures to spontaneously obtain MSC-like cells. Inductors in the medium stimulate either the translation of mRNAs to proteins or the maturation of naïf proteins to functional proteins. Herein, a reproducible technique is presented as an alternative to differentiate hNDFs into cardiomyocyte-like cells without applying any known reprogramming technique.

### 3.5. Concluding remarks

- Direct cell-cell and indirect cell-RAD16-I hydrogel (through ECM and protein decoration of the nanofibers) interactions were involved in cell survival of hNDFs in 3D cultures. Cells secreted ECM proteins that conditioned the synthetic scaffold and allowed hNDFs to support themselves independently of the presence of serum in the medium.
- Human NDFs only expressed embryonic-related proteins such as Brachyury, FoxA2 and Gata4 when cultured in RAD16-I hydrogels suggesting that cells underwent a mesenchymal potentiation. Matrices based on Collagen I did not offer the neutrality given by RAD16-I hydrogels, which was the signal for the cells to acquire primitive properties.
- The mesenchymal phenotype acquisition of hNDFs embedded in RAD16-I hydrogels was spontaneous and independent of the composition of the culture medium (presence or absence of FBS and PDGF). The peptide 3D environment induced hNDFs to interact, contract the construct and express proteins characteristic of the early embryonic development.
- Adipogenic induction medium promoted the differentiation of hNDFs with MSCs properties into adipocyte-like cells when cultured in RAD16-I hydrogels. The peptide scaffold, which contained functional hNDFs-derived adipocytes able to deposit lipid droplets, mimicked a tissue-like structure similar to the *in vivo* ECM environment.
- Human NDFs, cultured in RAD16-I hydrogels and induced with cardiogenic medium, acquired cardiac progenitor-like phenotype by expressing genes and proteins such as Tbx5.



## 3.6. References

1. Burridge, P. W., Keller, G. M., Gold, J. D. & Wu, J. C. Production of de novo cardiomyocytes: human pluripotent stem cells differentiation and direct reprogramming. *Natl. Institutes Heal.* **10**, 16–28 (2013).
2. Chen, F. G. *et al.* Clonal analysis of nestin(-) vimentin(+) multipotent fibroblasts isolated from human dermis. *J. Cell Sci.* **120**, 2875–83 (2007).
3. Lysy, P. A., Smets, F., Sibille, C., Najimi, M. & Sokal, E. M. Human Skin Fibroblasts: From Mesodermal to Hepatocyte-Like Differentiation. *Hepatology* **46**, 1574–1585 (2007).
4. Quintana, L. *et al.* Early Tissue Patterning Recreated by Mouse Embryonic Fibroblasts in a Three-Dimensional Environment. *Tissue Eng.* **15**, (2009).
5. Garreta, E., Genove, E., Borros, S. & Semino, C. E. Osteogenic differentiation of mouse embryonic stem cells and mouse embryonic fibroblasts in a three-dimensional self-assembling peptide scaffold. *Tissue Eng.* **12**, 1–14 (2006).
6. Busmann, B. M. *et al.* Chondrogenic potential of human dermal fibroblasts in a contractile , soft , self-assembling , peptide hydrogel. *J. Tissue Eng. Regen. Med.* (2013). doi:10.1002/term
7. Massignani, M. *et al.* Enhanced fluorescence imaging of live cells by effective cytosolic delivery of probes. *PLoS One* **5**, e10459 (2010).
8. Schussler, O. *et al.* 3-Dimensional Structures to Enhance Cell Therapy and Engineer Contractile Tissue. *Asian Cardiovasc. Thorac. Ann.* 188–198 (2010). doi:10.1177/0218492310361531
9. Pollard, J. W. & Walker, J. M. *Basic cell culture protocols.* (1997).
10. Johnstone, B. *et al.* Tissue engineering for articular cartilage repair-the state of the art. *Eur. Cell. Mater.* **25**, 248–67 (2013).
11. Hakkinen, K. M., Harunaga, J. S., Doyle, A. D. & Yamada, K. M. Direct comparisons of the morphology, migration, cell adhesions, and actin cytoskeleton of fibroblasts in four different three-dimensional extracellular matrices. *Tissue Eng.* **17**, (2011).
12. Zhang, S. *et al.* Self-complementary oligopeptide matrices support mammalian cell attachment. *Biomaterials* **16**, 1385–93 (1995).
13. Cukierman, E., Pankov, R., Stevens, D. R. & Yamada, K. M. Taking cell-matrix adhesions to the third dimension. *Science* **294**, 1708–12 (2001).
14. Discher, D. E., Janmey, P. & Wang, Y.-L. Tissue cells feel and respond to the stiffness of their substrate. *Science* **310**, 1139–43 (2005).

15. Cortes-Morichetti, M. *et al.* Association between a cell-seeded collagen matrix and cellular cardiomyoplasty for myocardial support and regeneration. *Tissue Eng.* **13**, 2681–7 (2007).
16. Hesse, E. *et al.* Collagen type I hydrogel allows migration, proliferation and osteogenic differentiation of rat bone marrow stromal cells. *Natl. Institutes Heal.* **94**, 442–449 (2011).
17. Chimenti, I. *et al.* Human cardiosphere-seeded gelatin and collagen scaffolds as cardiogenic engineered bioconstructs. *Biomaterials* **32**, 9271–9281 (2011).
18. Duan, Y. *et al.* Hybrid gel composed of native heart matrix and collagen induces cardiac differentiation of human embryonic stem cells without supplemental growth factors. *J. Cardiovasc. Transl. Res.* **4**, 605–15 (2011).
19. Schussler, O. *et al.* Use of arginine-glycine-aspartic acid adhesion peptides coupled with a new collagen scaffold to engineer a myocardium-like tissue graft. *Nat. Clin. Pract. Cardiovasc. Med.* **6**, 240–9 (2009).
20. Chachques, J. C. *et al.* Autologous human serum for cell culture avoids the implantation of cardioverter-defibrillators in cellular cardiomyoplasty. **1**, 29–33 (2004).
21. Larsen, M., Artym, V. V, Green, J. A. & Yamada, K. M. The matrix reorganized: extracellular matrix remodeling and integrin signaling. *Curr. Opin. Cell Biol.* **18**, 463–71 (2006).
22. Gregoire, F. M., Smas, C. M. & Sul, H. S. Understanding adipocyte differentiation. *Physiol. Rev.* **78**, 783–809 (1998).
23. Blasi, A. *et al.* Dermal fibroblasts display similar phenotypic and differentiation capacity to fat-derived mesenchymal stem cells, but differ in anti-inflammatory and angiogenic potential. *Vasc. Cell* **3**, 5 (2011).
24. Loviscach, M. *et al.* Distribution of peroxisome proliferator-activated receptors (PPARs) in human skeletal muscle and adipose tissue: relation to insulin action. *Diabetologia* **43**, 304–11 (2000).
25. Laflamme, M. A. *et al.* Cardiomyocytes derived from human embryonic stem cells in pro-survival factors enhance function of infarcted rat hearts. *Nat. Biotechnol.* **25**, 1015–24 (2007).
26. Pal, R., Mamidi, M. K., Das, A. K. & Bhonde, R. Comparative analysis of cardiomyocyte differentiation from human embryonic stem cells under 3-D and 2-D culture conditions. *J. Biosci. Bioeng.* **115**, 200–6 (2013).
27. Levenberg, S. *et al.* Differentiation of human embryonic stem cells on three-dimensional polymer scaffolds. *Proc. Natl. Acad. Sci. U. S. A.* **100**, 12741–6 (2003).
28. Dixon, J. E., Dick, E., Rajamohan, D., Shakesheff, K. M. & Denning, C. Directed differentiation of human embryonic stem cells to interrogate the cardiac gene regulatory network. *Mol. Ther.* **19**, 1695–703 (2011).

29. Huber, I. *et al.* Identification and selection of cardiomyocytes during human embryonic stem cell differentiation. *FASEB J.* **21**, 2551–63 (2007).
30. Efe, J. A. *et al.* Conversion of mouse fibroblasts into cardiomyocytes using a direct reprogramming strategy. *Nat. Cell Biol.* **13**, 215–22 (2011).



*Chapter 4: Comparison of the cardiac  
differentiation potential of human induced  
Pluripotent Stem Cells in 2D and 3D cultures  
based on RAD16-I hydrogels and the effect of  
ascorbic acid on cardiogenesis*



**CHAPTER 4: COMPARISON OF THE CARDIAC DIFFERENTIATION  
POTENTIAL OF HUMAN INDUCED PLURIPOTENT STEM CELLS IN 2D  
AND 3D CULTURES BASED ON RAD16-I HYDROGELS AND THE  
EFFECT OF ASCORBIC ACID ON CARIOGENESIS**

4.1. *Introduction*

Cardiogenesis is the establishment of the cardiac lineage in the early embryo via the process of gastrulation, during which mesoderm is established, the embryonic origin of cardiomyocytes. Distinct gene regulatory networks are first involved in mesoderm formation and later cardiac development during primitive embryonic stages<sup>1</sup> (**Figure 23**). Nevertheless, it is known that adult cardiomyocytes are terminally differentiated and cannot proliferate. Since intrinsic cardiac regeneration is limited, many efforts focus on improving it. Here, the main goal is to preserve and restore cardiac function after myocardial infarction (MI). Multiple sources of stem cells (adult and embryonic) have been used in order to differentiate cardiomyocytes *in vitro* and implant them into the cardiac necrotic scar generated after MI. Human Embryonic Stem Cells (hESCs) are a promising cell source for such differentiation strategies due to their unlimited proliferation potential and pluripotency. Interestingly, hESCs grow and differentiate *in vitro* forming flat colonies. Nonetheless, the organization of the tissue that they are derived from *in vivo*, the inner cell mass, is three-dimensional. This is the reason why researchers are working on creating an optimal three-dimensional culture capable of mimicking the natural environment of cell niches.

Different strategies combining 3D cultures and cardiac differentiation of hESCs have been described in the literature, including synthetic bioactive hydrogels based on Polyethylene Glycol PEG<sup>2</sup>, biodegradable polymers such as poly(lactic-co-glycolic acid) PLGA and poly(L-lactic acid) PLLA<sup>3</sup>. Other approaches use suspensions of cellular aggregates called embryoid bodies (EBs), which resemble 3D cultures<sup>4</sup>. These strategies have successfully differentiated hESCs into cardiomyocytes although the concern is that hESCs are not patient-specific cells and could generate immune rejection. Therefore, the discovery of human induced Pluripotent Stem Cells (hiPSCs) provided a new approach to personalized cell therapy. Due to their mode of derivation, it is possible to create a specific hiPSC line for each person treated. Similar to what has been described above, hiPSCs have also been cultured in 3D

**COMPARISON OF THE CARDIAC DIFFERENTIATION POTENTIAL OF HUMAN INDUCED PLURIPOTENT STEM CELLS IN 2D AND 3D CULTURES BASED ON RAD16-I AND THE EFFECT OF ASCORBIC ACID ON CARDIOGENESIS**

scaffolds mimicking the natural *in vivo* environment. Different co-cultures<sup>5</sup>, cell-friendly cushions (matrigel), bioreactors<sup>6</sup>, synthetic hydrogels<sup>7</sup> are just a few examples of 3D cultures that have been established to differentiate hiPSCs. Moreover, cell differentiation and organization is influenced by the 3D environment and directed by chemical cardiac inducers. There are several agents that have been proven to induce cardiogenesis (retinoic acid, growth factors<sup>3</sup>, dimethyl sulfoxide, ascorbic acid, oxytocin<sup>4</sup>). Herein, we studied the cardiogenic effect of ascorbic acid (AA) on 2D and 3D cultures of hiPSCs. AA seemed to play a key role in promoting the proliferation of cardiac progenitor cells from pluripotent stem cells<sup>8</sup>. The following diagram illustrates the different developmental stages of cardiogenesis with the specific markers analyzed in this chapter for each step (**Figure 23**). More primitive markers are expected to decrease over time while cardiac specific genes should be increasingly expressed as differentiation progresses.

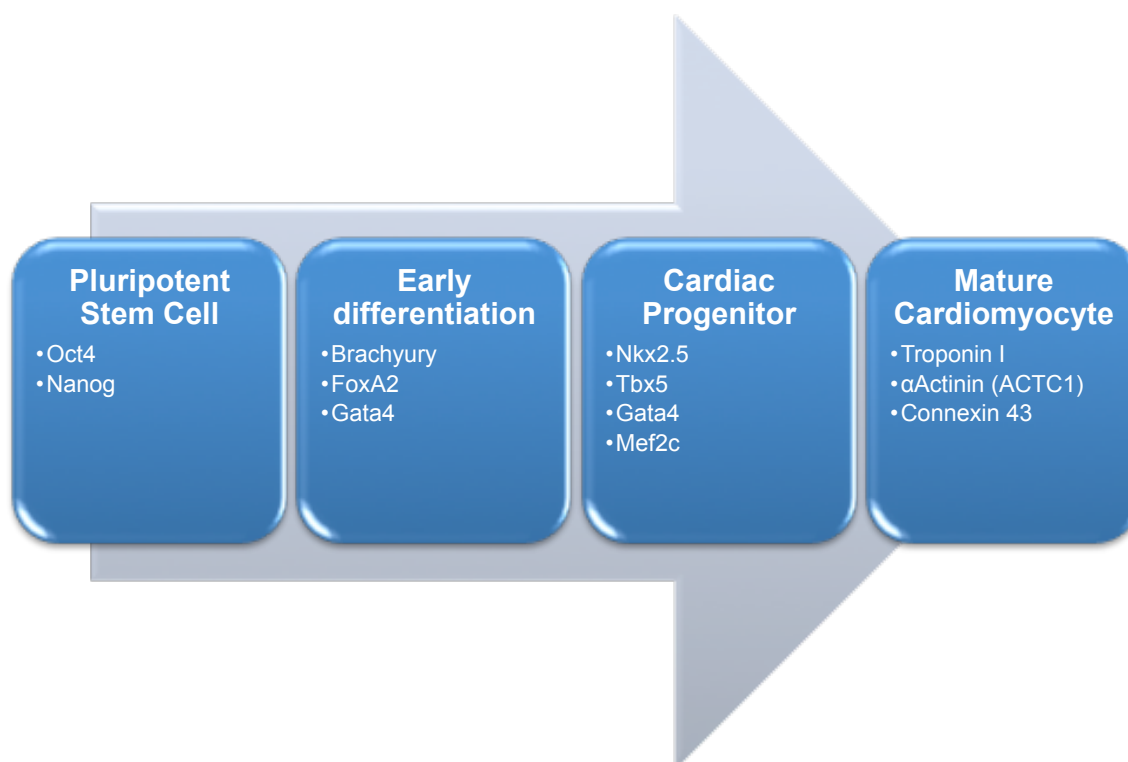


**Figure 23.** Diagram representing sequential steps in the cardiac differentiation of pluripotent stem cells as hiPSCs. Markers for each stage of development studied during this research are indicated<sup>40</sup>.



## 4.2. Hypothesis and specific aims

Cardiomyocytes derived from hiPSCs represent an excellent example of autologous cardiomyocyte transplantation therapy. Large quantities of patient-specific cardiomyocytes can be obtained with no political or ethical concerns of damaging human embryos. Therefore, it is important to design effective strategies to increase the yield of functional cardiomyocytes or progenitors thereof generated *in vitro* to be implanted *in vivo*. Herein, we compare three-dimensional (3D, based on RAD16-I) and two-dimensional (2D) cultures of differentiating hiPSCs and the effect of ascorbic acid (AA) on their cardiogenic differentiation.

Hypothesis: The 3D environment based on RAD16-I promotes better cardiogenic potential of hiPSCs than traditional 2D cultures despite the presence of AA in the medium.

Specific aim:

- Compare the cardiogenic commitment of hiPSCs in 2D and 3D cultures based on RAD16-I and assess the effect of AA on cardiogenesis.

## 4.3. Results

### 4.3.1. Cardiac induction of hiPSCs in 2D cultures and the effect of AA on cardiogenesis

Human induced Pluripotent Stem Cells (hiPSCs) have successfully been differentiated into cardiomyocytes *in vitro* although the efficiency remains very low. Only around 2% of the stem cells spontaneously differentiate into cardiomyocytes *in vitro*. Due to this low efficiency, cardiac tissue engineering aims to direct stem cell commitment into cardiac lineage. To improve cardiac differentiation of stem cells *in vitro*, differentiation pathways (endoderm, mesoderm and ectoderm) of hiPSCs should be narrowed to cardiac mesoderm. Indeed, several efforts have focused on designing a reproducible, cheap and robust system to increase the yield of differentiated cardiac cells *in vitro*. During the screening of cytokines and other chemical compounds it was shown that AA might be a suitable cardiac inducer<sup>8</sup>. Herein, we compared the cardiac potential of hiPSCs cultured in 2D with and without AA. The cells were seeded on matrigel pre-coated plastic in order to render the surface cell-friendly. The medium used contained Dulbecco's modified Eagle's

## COMPARISON OF THE CARDIAC DIFFERENTIATION POTENTIAL OF HUMAN INDUCED PLURIPOTENT STEM CELLS IN 2D AND 3D CULTURES BASED ON RAD16-I AND THE EFFECT OF ASCORBIC ACID ON CARDIOGENESIS

medium, fetal bovine serum, non-essential amino-acids, antibiotics,  $\beta$ -mercaptoethanol and plus or minus AA. The experiment was carried out for 25 days (**Figure 24**). The cells were observed under the phase microscope every day. Thus, the main goal was to compare the results obtained in the present chapter with other approaches in the literature and with 3D tissue-like cultures. Currently, very little is published on cardiac induction of hiPSCs.

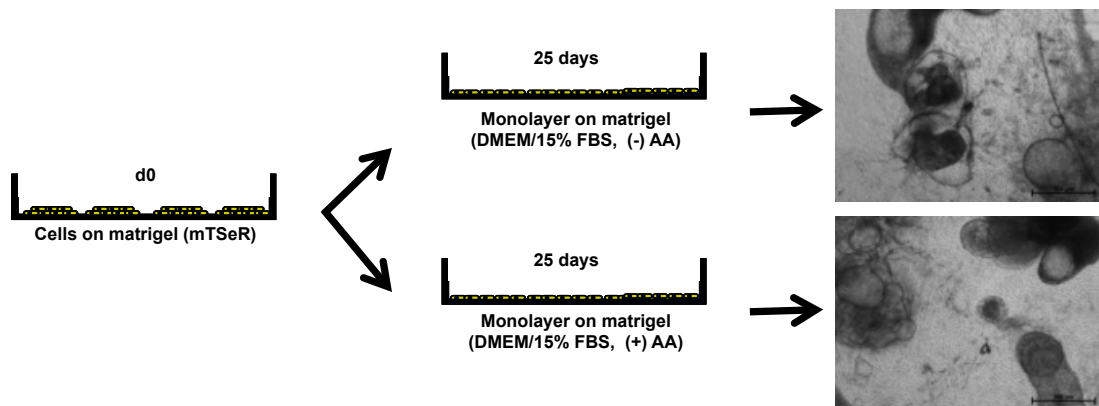


**Figure 24.** Schematic representation of the induced cardiac differentiation protocol used with hiPSCs in 2D cultures. Cells have been cultured with and without AA in order to assess its effect on cardiogenesis.

Therefore, hiPSCs were cultured and maintained pluripotent in 2D (on matrigel pre-coated plastic wells). At confluence (day 0), cells had large nuclei with multiple nucleoli, scant cytoplasm and formed tightly packed and flat colonies (**Figure 25**). Indeed, hiPSCs have an extremely similar morphology to hESCs. The size of the colony is critical to maintain the pluripotency of hiPSCs: the bigger it is, the more differentiated are the cells with the differentiation starting at the outer edge of the colony.

### hiPSCs in 2D culture

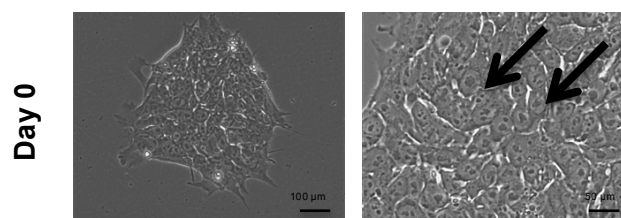


**Figure 25.** Microscopic observation of hiPSCs at confluence in 2D cultures. Arrows point at nucleoli.

As explained above and illustrated in **Figure 24**, hiPSCs were cultured in 2D with and without ascorbic acid (AA) for 25 days. The cultures were observed in detail under the microscope every day (**Figure 26**). The first obvious change was the morphology of the cells during the course of the experiment. At day 3, the amount of cytoplasm increased and cells started to aggregate, such that the colonies were not flat anymore. From day 6 onwards, cells clustered in dense three-dimensional, cyst-shaped structures reminiscent of bubbles. The size of these arrangements and the number of cells in them increased over time. Not only did the clusters become denser but the number of agglomerations also increased in both culture conditions (plus and minus AA). Interestingly, from day 14 onwards an increased number of beating clusters was observed in the cultures. The beating cells were located in the center of the 3D cyst-shaped structures. Cells randomly started to beat independently of the size, location and density of the cluster. The size of the bundles ranged from 500 to 1000  $\mu\text{m}$ . It is important to point out that there were no visible morphological differences in cells cultured with or without AA whereas there were considerably more beating clusters in induced cells with AA than without.

COMPARISON OF THE CARDIAC DIFFERENTIATION POTENTIAL OF HUMAN INDUCED PLURIPOTENT STEM CELLS IN 2D AND 3D CULTURES BASED ON RAD16-I AND THE EFFECT OF ASCORBIC ACID ON CARDIOGENESIS

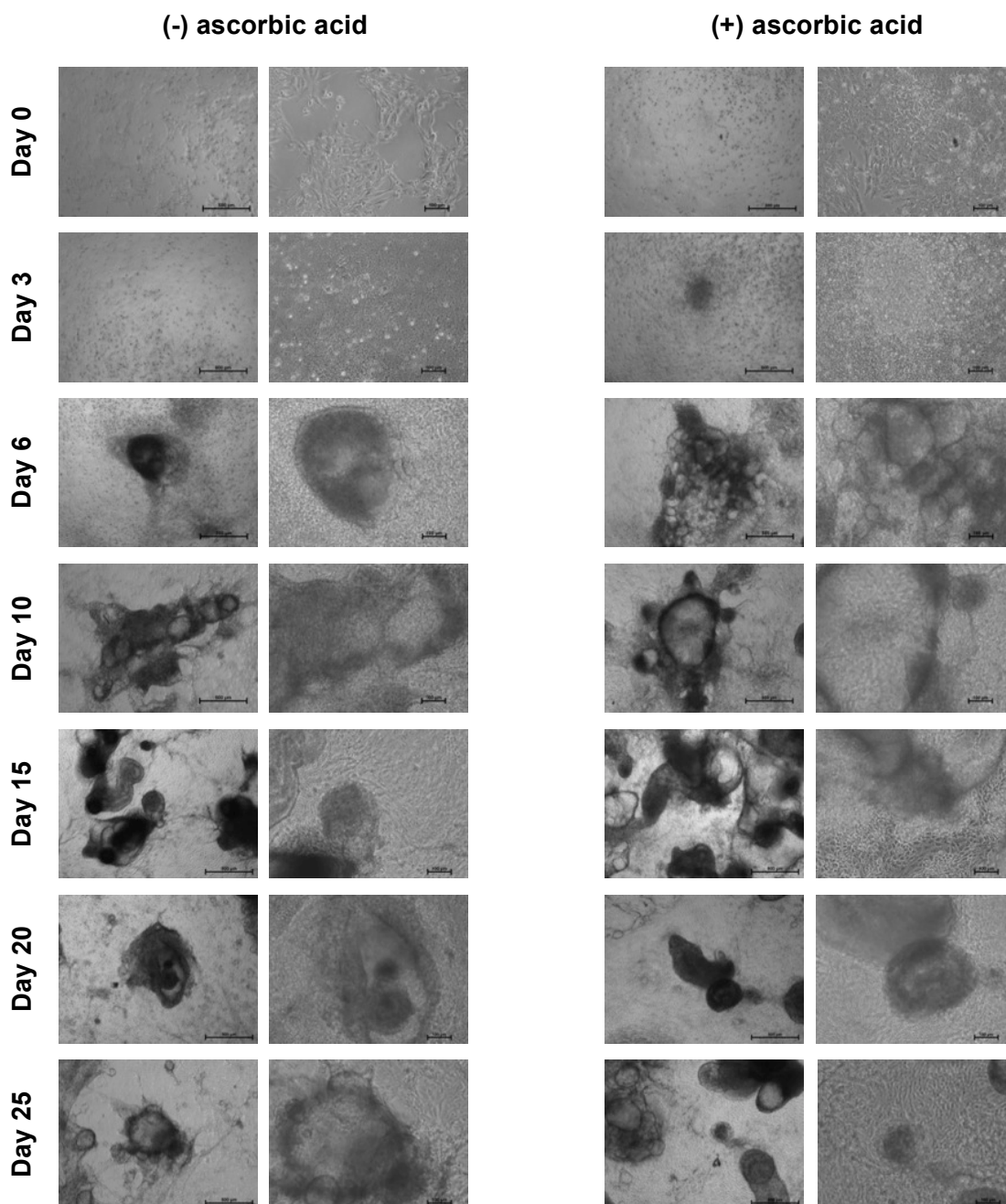


**Figure 26.** Cellular morphology of hiPSCs differentiated in 2D cultures into cardiac lineage in a medium with and without AA over 25 days. Cells created three-dimensional cyst-like structures from day 6 onwards, and these structures hosted beating clusters from day 14 onwards.

Furthermore, total RNA from cells cultured with and without AA was extracted at different time points (day 0, 3, 6, 10, 15, 20 and 25). The samples were treated with reverse transcriptase to obtain cDNA. Specific pluripotency (Oct4), early differentiation (FoxA2, Brachyury, Gata4), cardiac progenitor (Mef2c, Tbx5) and mature cardiomyocyte (ACTC1) genes were amplified with designed primer pairs (for choice of genes refer to **Figure 23**). The ribosomal gene 18S was used as a housekeeper gene. Indeed, 18S was used as a PCR control to confirm that the

reaction worked properly and as a loading control to verify that all the samples loaded in the agarose gel had the same quantity of cDNA. An agarose gel electrophoresis revealed the trend of gene expression of hiPSCs with and without AA (**Figure 27**). According to 18S amplification, none of the samples were degraded and they had approximately the same amount of cDNA. This observation was critical as it ensured that the observed gene expression profile was a result of AA and not a variable DNA concentration.

Although the PCR technique is semi-quantitative, it is still a powerful tool to observe changes in gene expression. Thus, Oct4 expression was very high at day 0 because cells were initially pluripotent. Afterwards, it decreased over time in both cases, AA present or absent, although the decrease was more accentuated in cells cultured with AA (induced cells) than without AA (control cells). Early differentiation genes (FoxA2 and Brachyury) were expressed from day 3 to 10 in both cases and there were no major differences between them. In addition, hiPSCs seemed to express genes related to pluripotency, early differentiation, cardiac progenitor and mature cardiomyocyte at day 0. Contrary, Gata4, which is also representative of early differentiation, displayed a completely different trend. Its expression was constant in control cells over the course of the experiment while its expression decreased in induced cells. At day 25 for example, its expression in control cells was noticeably higher than in induced cells. The expression of cardiac progenitor genes (Mef2C and Tbx5) increased over time under both experimental conditions. In fact, the expression was especially high from day 10 to 25. Finally, ACTC1 had a peak from day 3 to 10 and then declined from day 15 to 25 in cells cultured with and without AA. This decrease appeared more emphasized in induced cells compared to control cells.

COMPARISON OF THE CARDIAC DIFFERENTIATION POTENTIAL OF HUMAN INDUCED PLURIPOTENT STEM CELLS IN 2D AND 3D CULTURES BASED ON RAD16-I AND THE EFFECT OF ASCORBIC ACID ON CARDIOGENESIS

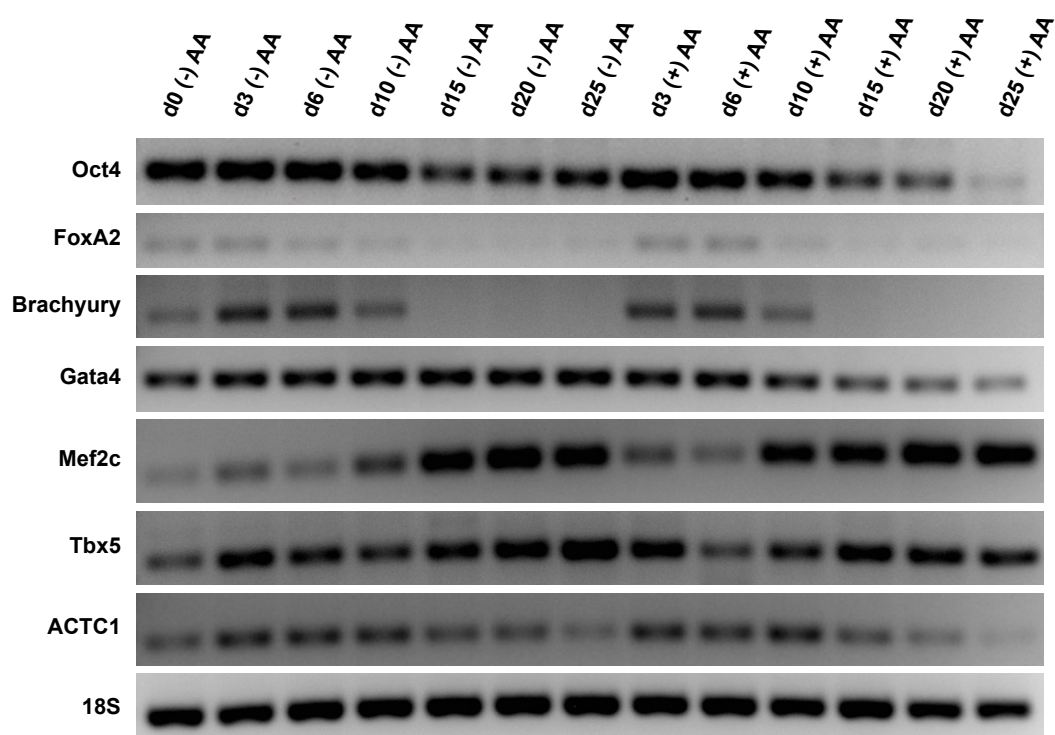


**Figure 27.** Agarose gel showing the PCR amplicons of RNA extracts from hiPSCs cultured with and without AA from day 0 to 25. The markers investigated were: Oct4 (pluripotency); FoxA2, Brachyury and Gata4 (early differentiation); Mef2c and Tbx5 (cardiac progenitors); ACTC1 (mature cardiomyocyte); 18S (ribosomal housekeeper).

Pursuing the analysis of gene expression, the gene profile of hiPSCs with and without AA from day 0 to 25 was analyzed with real time PCR (**Figure 28**). The same specific primer pairs given above were used. This technique is extremely useful in quantifying gene expression relative to a control. In this case, the expression of each gene at each time point was calculated relative to the expression of the same gene at day 0 (i.e. the control). All the values were normalized to 18S using the  $\Delta\Delta C_T$  technique<sup>9</sup>. As was expected, the expression of Oct4 dramatically decreased over the experimental period both in the presence and absence of AA because the cells lost pluripotency and displayed increased differentiation. Regardless of whether AA was present or absent FoxA2 had a peak of expression at day 6 although it was longer (day 3 to 6) and slightly higher in induced cells (plus AA). In the presence of AA, the early differentiation stage started sooner (day 3) and the expression of the genes related to this phase decreased more sharply than with control cells (minus AA). In addition, Gata4 also had an expression peak at day 3 to 6 in both scenarios while it was noticeably more accentuated in induced cells than in control cells. As mentioned above, Gata4 was up-regulated in the presence of AA. Moreover, the

expression of Gata4 was very high at day 3 and 6 but almost negligible for the remainder of the experimental period.

The two cardiac progenitor markers had different trends. On the one hand, Tbx5 expression increased over the course of the experiment. In the absence of AA, it peaked at day 10 while in the presence of AA the peak occurred at day 15. Again, the greatest expression level for induced cells was approximately twice that for control cells. On the other hand, Mef2c displayed the same trend with and without AA. Although its expression reached its maximum at day 25 in both cases, the peak was greater than 4-fold higher in the presence of AA. Unexpectedly, the expression of both cardiac progenitor genes peaked at different time points: Tbx5 at day 10 to 15 and Mef2c at day 15 to 25. This delay in the gene expression suggested that Tbx5 and Mef2c played different roles in the cardiac differentiation of hiPSCs in 2D cultures: the markers stood for early and late cardiac progenitors respectively.

Finally, the expression of ACTC1 reached its maximum at day 10 in control cells. In the presence of AA, the peak of expression was longer (day 6 to 10) and approximately twice that for control cells. The expression of ACTC1 was minor for the remainder of the experimental period in both scenarios (minus and plus AA). Surprisingly, the expression of ACTC1, which is a mature cardiomyocyte marker, peaked at early stages of the differentiation experiment. The correlation between the results obtained with PCR (**Figure 27**) and qPCR (**Figure 28**) suggested that, in this case, ACTC1 did not act as a mature cardiomyocyte gene but as a gene involved in cardiac mesoderm formation.

**COMPARISON OF THE CARDIAC DIFFERENTIATION POTENTIAL OF HUMAN INDUCED PLURIPOTENT STEM CELLS IN 2D AND 3D CULTURES BASED ON RAD16-I AND THE EFFECT OF ASCORBIC ACID ON CARDIOGENESIS**

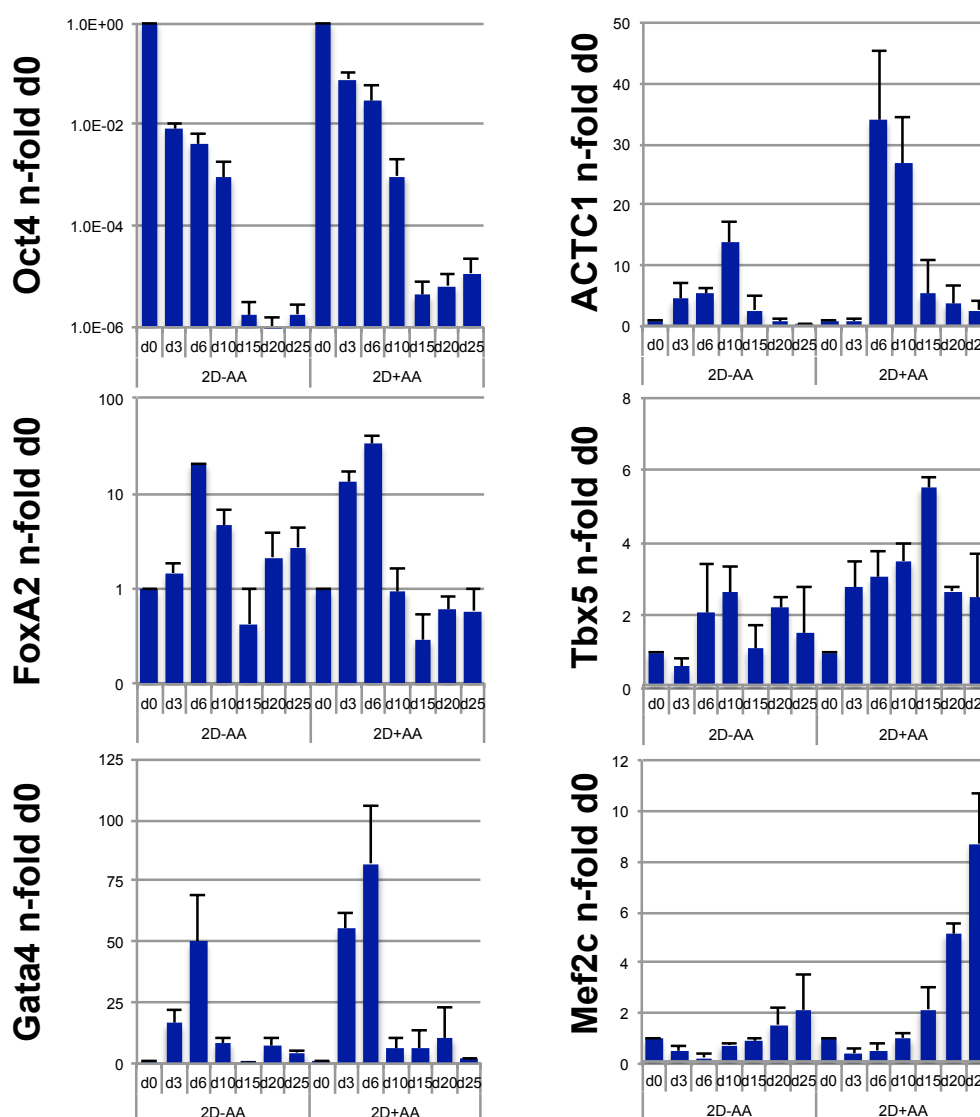


**Figure 28.** Quantitative PCR analysis for pluripotent (Oct4), early differentiation (FoxA2, Gata4), cardiac progenitor (Tbx5, Mef2c) and mature cardiomyocyte (ACTC1) markers of hiPSCs cultured in 2D with and without AA for 25 days. The assay was performed using SYBR Green and the n-fold expression of genes of interest was calculated according to the  $\Delta\Delta C_T$  method<sup>9</sup> using correction for PCR efficiency. Values represent n-fold expression over undifferentiated cells (d0) normalized to 18S.

The presence of proteins specific for early differentiation (Brachyury and Gata4), cardiac progenitor (Nkx2.5) and mature cardiomyocyte (MHC, Cx43 and Trop I) stages was also assessed. The same fluorescent conditions (i.e. concentration of antibodies, protocol, exposure time of fluorescence) were fixed for each targeted protein with and without AA. The ICCs showed that the fluorescent signal of hiPSCs cultured with AA was generally brighter than without AA (**Figure 29**). This suggests



that cells expressed higher levels of proteins when they were chemically induced than under control conditions. Indeed, there was a cellular differentiation time course: first, early differentiation proteins (Brachyury and Gata4) at day 3-6; second, cardiac progenitor proteins (Nkx2.5) at day 6; third, mature cardiomyocyte proteins (MHC, Cx43 and Trop I) at day 10-15. Furthermore, the localization of the proteins was highly specific depending on their nature and function. Brachyury, Gata4 and Nkx2.5 are transcription factors (TFs), proteins that specifically bind to DNA sequences forming complexes and regulating gene expression. Therefore, the localization of TFs is exclusively in the nucleus. The images taken under the fluorescent microscope showed that the TFs studied only appeared in the nucleus i.e. the blue dye (DAPI) that stained the nuclei and the green fluorescence of the secondary antibodies overlapped. Conversely, MHC, Cx43 and Trop I are cytosolic proteins. These markers were detected exclusively in the cytoplasm of the hiPSCs.

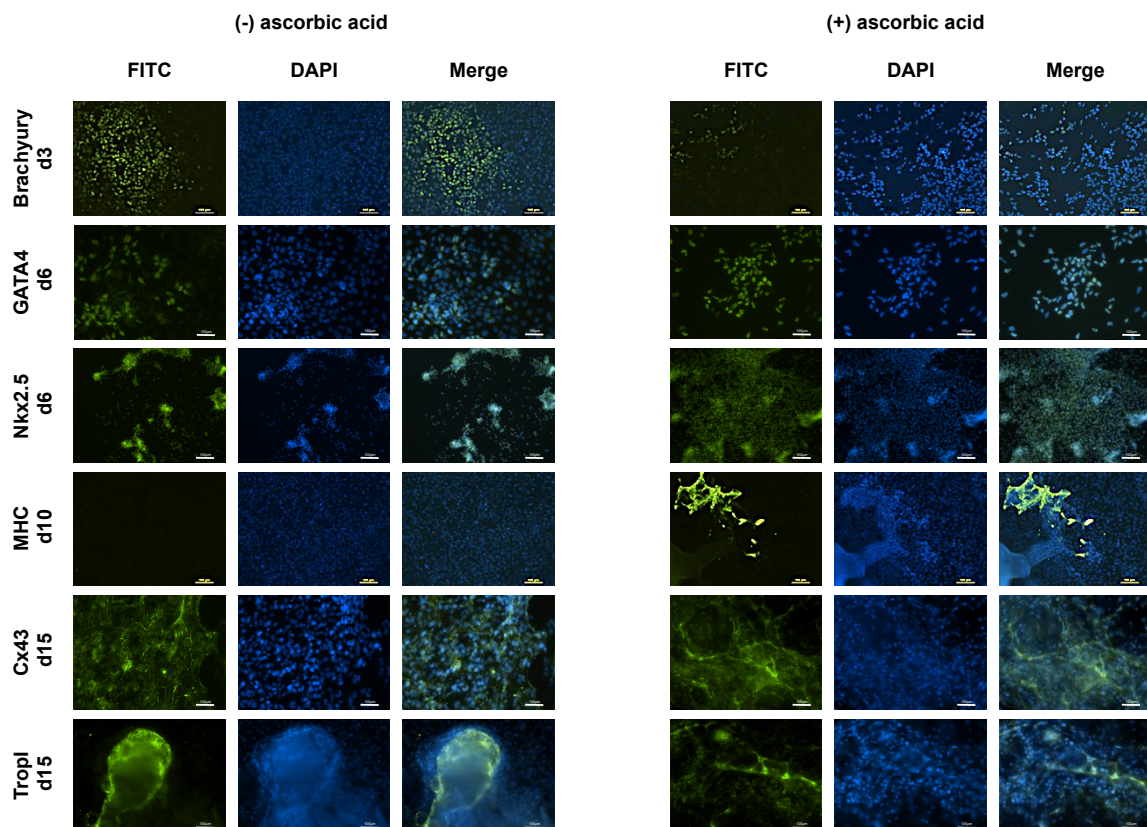


**Figure 29.** Immunostaining with FITC-conjugated secondary antibodies of hiPSCs cultured in 2D with and without AA. The proteins studied were related to early differentiation (Brachyury, Gata4), cardiac progenitor (Nkx2.5) and mature cardiomyocyte (MHC, Cx43, Trop I).

## COMPARISON OF THE CARDIAC DIFFERENTIATION POTENTIAL OF HUMAN INDUCED PLURIPOTENT STEM CELLS IN 2D AND 3D CULTURES BASED ON RAD16-I AND THE EFFECT OF ASCORBIC ACID ON CARDIOGENESIS

Finally, the absolute number of beating clusters with and without AA was determined. Cells were observed under the phase microscope. As mentioned above, cells clustered, created cystic aggregates and started beating when cultured in 2D. Exactly the same number of cultures of hiPSCs with and without AA was maintained in parallel. Beating clusters were counted every day and the data was plotted (**Figure 30**). The first beating clusters noticed were from hiPSCs cultured with AA at day 14. During the course of the experiment, the number of bundles containing functional cardiomyocytes increased under both conditions (minus/plus AA). By the end of the experiment (day 25), almost double the number of beating clusters was counted in induced cells than in control cells. Interestingly, functional cardiomyocytes did not beat rhythmically. There were differences in beating frequency among the plated cells.

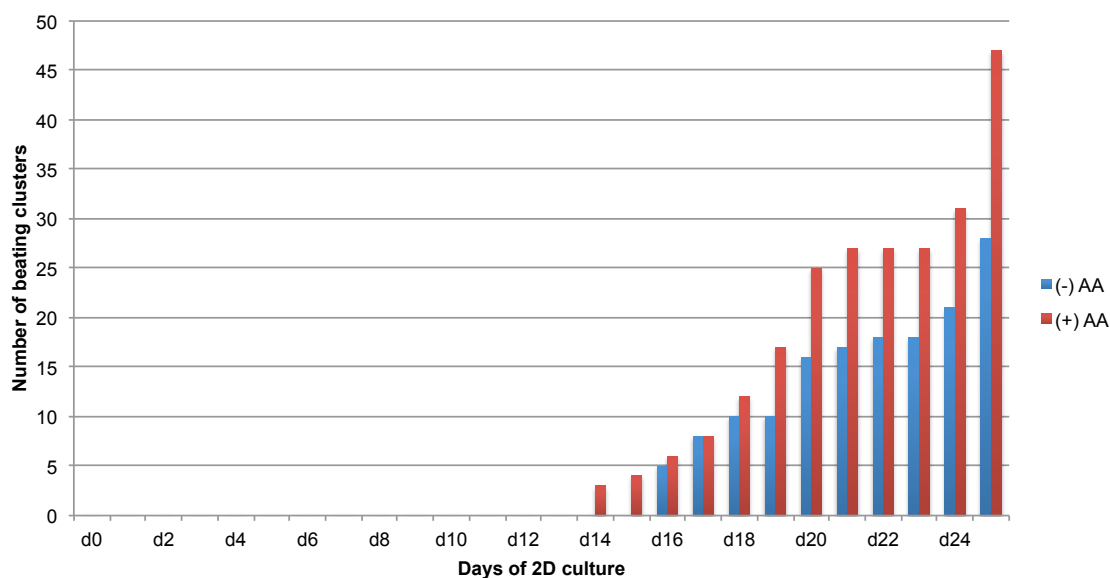


**Figure 30.** Comparison of the number of functional cardiomyocytes (beating clusters) obtained from hiPSCs with and without AA in 2D.

### 4.3.2. Setting up the 3D culture protocol based on RAD16-I with hESCs

Cardiac differentiation experiments in 2D cultures were carried out with both hESCs and hiPSCs. Parallel assays showed that hiPSCs committed to cardiomyocyte-like cells quicker and more efficiently than hESCs. Therefore, the cardiac potential of hiPSCs was investigated in both 2D and 3D cultures, the latter based on RAD16-I.

However, hESCs appeared to expand readily *in vitro* and were available in the laboratory at the time. Since there is no evidence in the literature that hESCs or hiPSCs differentiated into the cardiac lineage in RAD16-I, the conditions for the 3D culture had to be established. Consequently, only hESCs were used for this purpose. Cells were cultured in 3D and in a control medium for three days. Different cell concentrations were investigated:  $2 \cdot 10^6$  cells/mL,  $4 \cdot 10^6$  cells/mL and  $8 \cdot 10^6$  cells/mL. Human ESCs in RAD16-I had a rounded morphology and appeared as single cells (**Figure 31**). They did not cluster in 3D as they did in 2D cultures. The conditions used to decide the cellular concentration in 3D were: cells had to be in contact to avoid cell death but not extremely close to avoid accelerated differentiation and that there was sufficient space for them to proliferate and migrate. After three days, it appeared as if there were more cells in the tested cell concentrations than at day 1 although cells could not be counted. With the first concentration (80000 cells/construct) cells were very sparse at day 3. With the second concentration (160000 cells/construct), hESCs were separated on the first day whereas the cell density seemed higher at day 3. The final concentration (320000 cells/construct) indicated that the 3D culture was crowded the first day and extremely dense at day 3 (**Figure 31**).

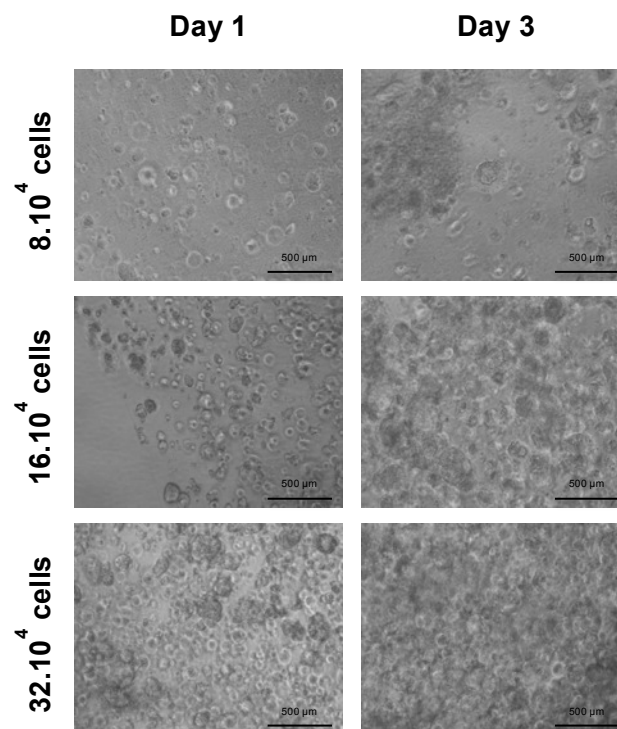


**Figure 31.** Observation under the phase microscope of 3D cultures of hESCs embedded in RAD16-I at three different cell densities for 1 and 3 days.

## COMPARISON OF THE CARDIAC DIFFERENTIATION POTENTIAL OF HUMAN INDUCED PLURIPOTENT STEM CELLS IN 2D AND 3D CULTURES BASED ON RAD16-I AND THE EFFECT OF ASCORBIC ACID ON CARDIOGENESIS

In addition, cellular survival was also checked for the previous three cell concentrations. Survival appeared to be very high; almost all cells were alive in the 3D scaffold independently of concentration. However, at low concentration the cell number did not seem to increase; at medium concentration the cells not only survived but they seemed to proliferate and cluster; at the highest concentration living cells were already grouped at day 1 and were extremely clustered and packed at day 3 (**Figure 32**).

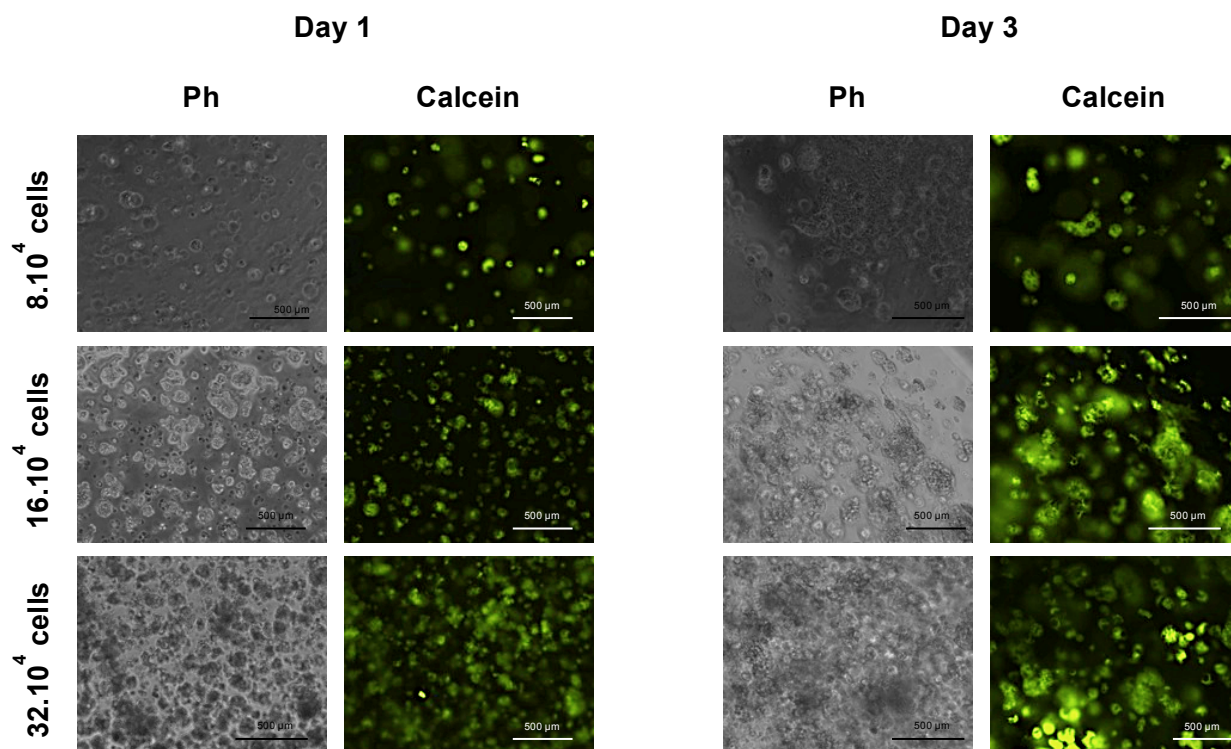


**Figure 32.** Viability assay of hESCs cultured in 3D at three different cell concentrations for 1 and 3 days. Calcein acetoxyethyl is a cell-permeable and non-fluorescent compound that in contact with intracellular esterases of live cells becomes intensely green fluorescent.

In order to obtain single hiPSCs from 3D constructs for cytospin experiments, hESCs were used to establish the protocol. Different enzymatic treatments were applied to hESCs with the aim of choosing the most effective one to obtain single cells out of the construct. The cleavage enzymes used were: accutase, collagenase IV and trypsin (**Figure 33**). Indeed, cells were alive in the three cases after disruption of the construct (viability assay). Most of the cells treated with accutase appeared grouped immediately after the treatment (suspension) and they clustered when seeded in 2D cultures. Apparently, the enzyme was not strong enough to cleave all the intercellular connections and release single cells with minimal surrounding



extracellular matrix. Collagenase IV had the same effect as accutase although very few cells were recovered after the treatment. It was likely that large bundles of cells were entrapped in the scaffold because the enzyme could not digest the connections. Therefore, cell sheets precipitated during the centrifugal rounds and were discarded. Finally, trypsin generated single cells and small cell clusters that also grouped in 2D cultures. Despite the high agglomeration rate in 2D, single cells were observed. Thus, the highest number of cells was obtained with the trypsin treatment. Indeed, this might be due to the explanation given above: trypsin digested more connections, generated more single cells and smaller cell clusters and consequently more cells were recovered from the centrifugal rounds.

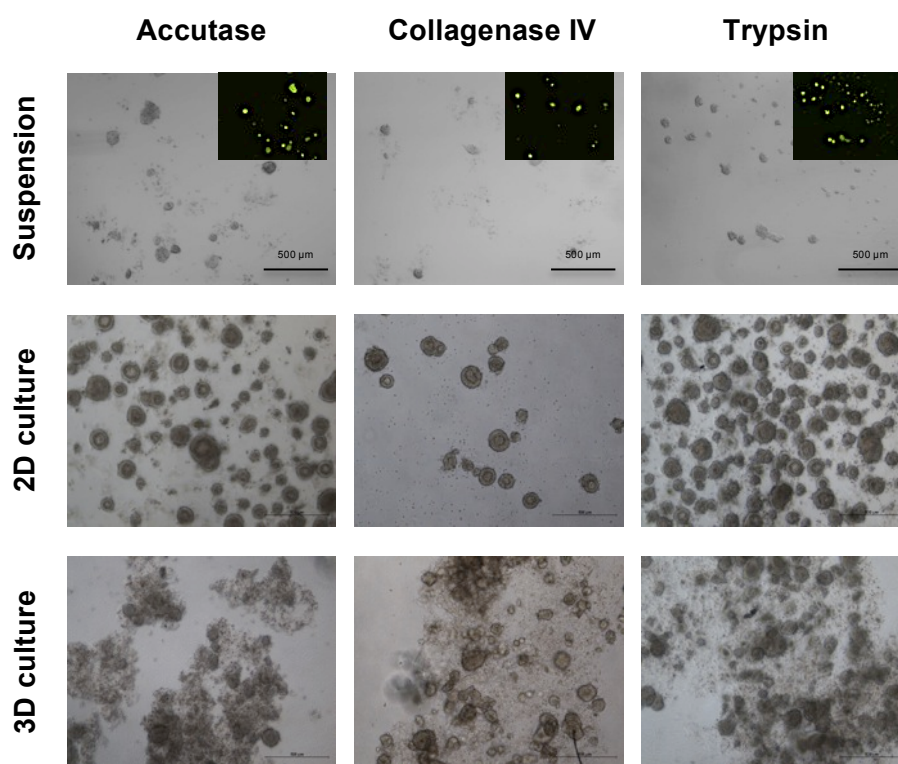


**Figure 33.** 3D constructs of hESCs disrupted with accutase, collagenase IV and trypsin. Microscopic observations after disruption: cells in suspension after the enzymatic treatment (suspension) and viability assay; cells seeded on 2D for one day after the disruption (2D culture); cells embedded in RAD16-I and cultured for one day after the disruption (3D culture).

#### 4.3.3. Cardiac induction of hiPSCs cultured in RAD16-I and the effect of AA on cardiogenesis

After having determined the conditions to culture human pluripotent stem cells in 3D, hiPSCs were embedded in RAD16-I. Cells were maintained in cardiogenic

**COMPARISON OF THE CARDIAC DIFFERENTIATION POTENTIAL OF HUMAN INDUCED PLURIPOTENT STEM CELLS IN 2D AND 3D CULTURES BASED ON RAD16-I AND THE EFFECT OF ASCORBIC ACID ON CARDIOGENESIS**

medium with and without AA to assess its effect on cells in 3D. Cells were cultured in 3D for 20 days. From day 3 to 20, cells appeared rounded and had an approximate diameter of 30  $\mu\text{m}$  (**Figure 34**). There were no obvious differences in cell morphology throughout the course of the experiment or between the cells cultured with or without AA. There was some slight clustering of human iPSCs in the scaffold during the first three days but there were no obvious changes after this point for both conditions. No beating clusters were found at any time.

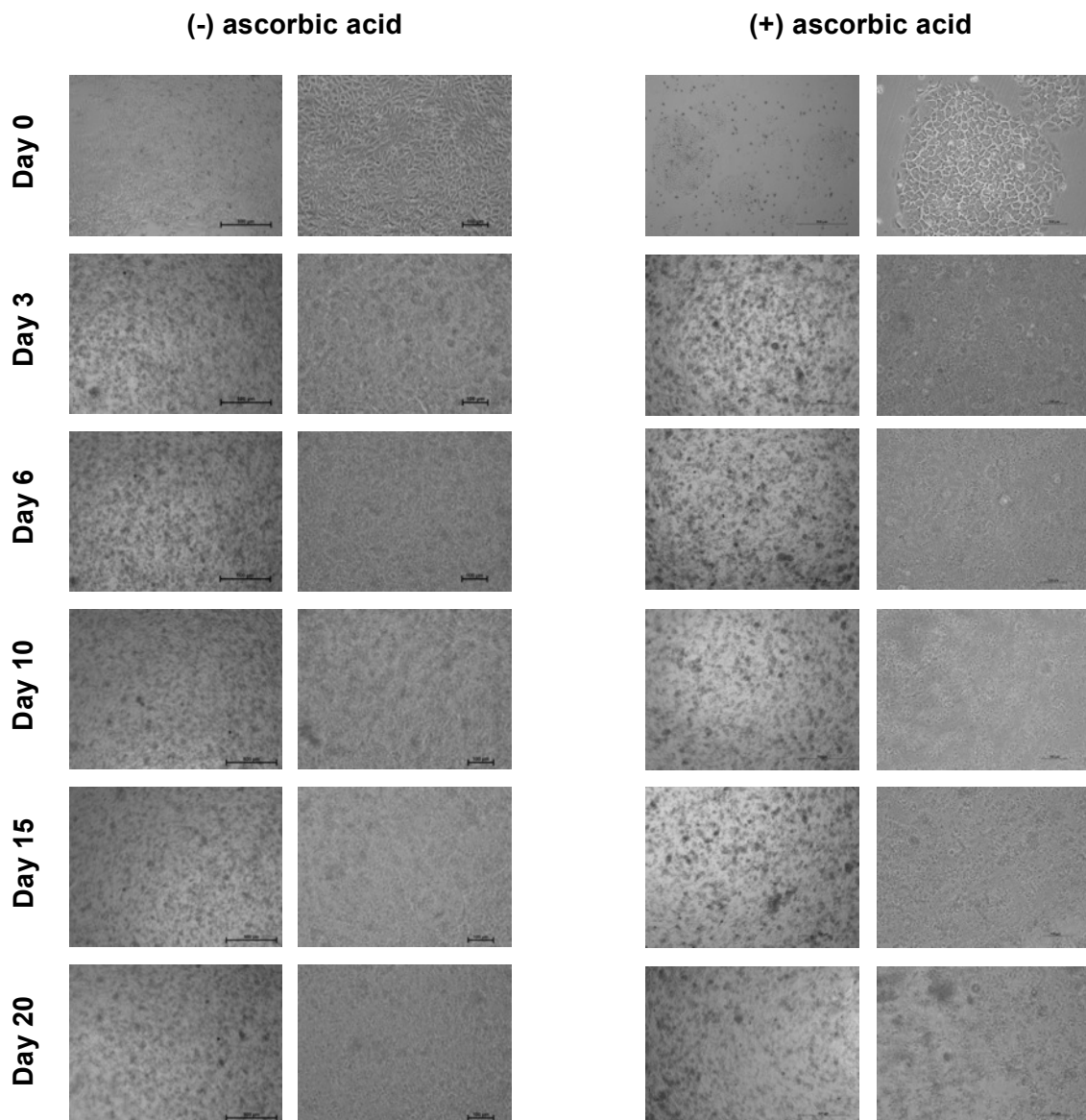


**Figure 34.** Observation under the phase microscope of hiPSCs cultured in RAD16-I with and without AA for 20 days. Cells remained static in the peptide bioscaffold.

As there was no variation in cell morphology during the experiment, it was hypothesized that cells were dead or senescent. Therefore, a live/dead assay was carried out with hiPSCs cultured in RAD16-I with and without AA for 20 days, which was the last time point of the cardiogenic experiment. The results suggested that approximately half of the cells were alive (green cells) when cultured in 3D with and without AA for 20 days (**Figure 35**). Dead cells (red cells) seemed to be entrapped throughout the matrix and were not localized in any specific part of the construct. Living cells (green cells) were either single or in clusters.

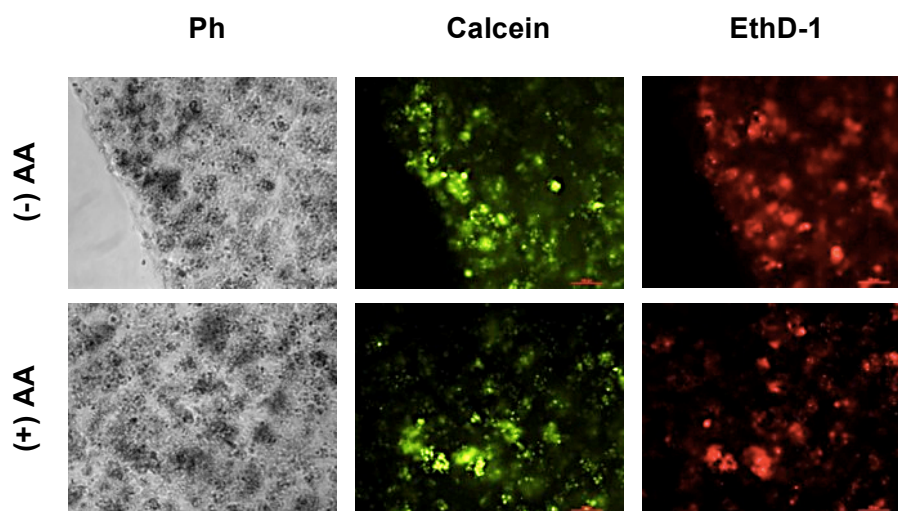


**Figure 35.** Live/Dead assay of hiPSCs cultured in 3D for 20 days with and without AA. Calcein acetoxymethyl detects living cells (green). Ethidium homodimer-1 (red) binds to nucleic acids of dead cells, which have a damaged plasmatic membrane.

Additionally, morphology of the nuclei and the cytoskeleton of hiPSCs in 3D was checked from day 0 to 20 (**Figure 36**). At day 0 (corresponding to 2D confluent culture) hiPSCs had short and thick actin filaments (red) that created a network around the nuclei (blue), which were rounded and turgescient. However, from day 3 onwards the nuclei adopted a kidney-shape in cells cultured in 3D. The cytoskeleton was unorganized and spread throughout the matrix surrounding the nuclei. No orientation of actin filaments was distinguished and the cytoskeleton became denser and more scattered over time. In fact, the cytoskeleton created a mass (red staining) with nuclei (blue dots) anchored in the free spaces. There were no differences between cells cultured with or without AA in terms of the morphology of the nuclei and cytoskeleton.



COMPARISON OF THE CARDIAC DIFFERENTIATION POTENTIAL OF HUMAN INDUCED PLURIPOTENT STEM CELLS IN 2D AND 3D CULTURES BASED ON RAD16-I AND THE EFFECT OF ASCORBIC ACID ON CARDIOGENESIS

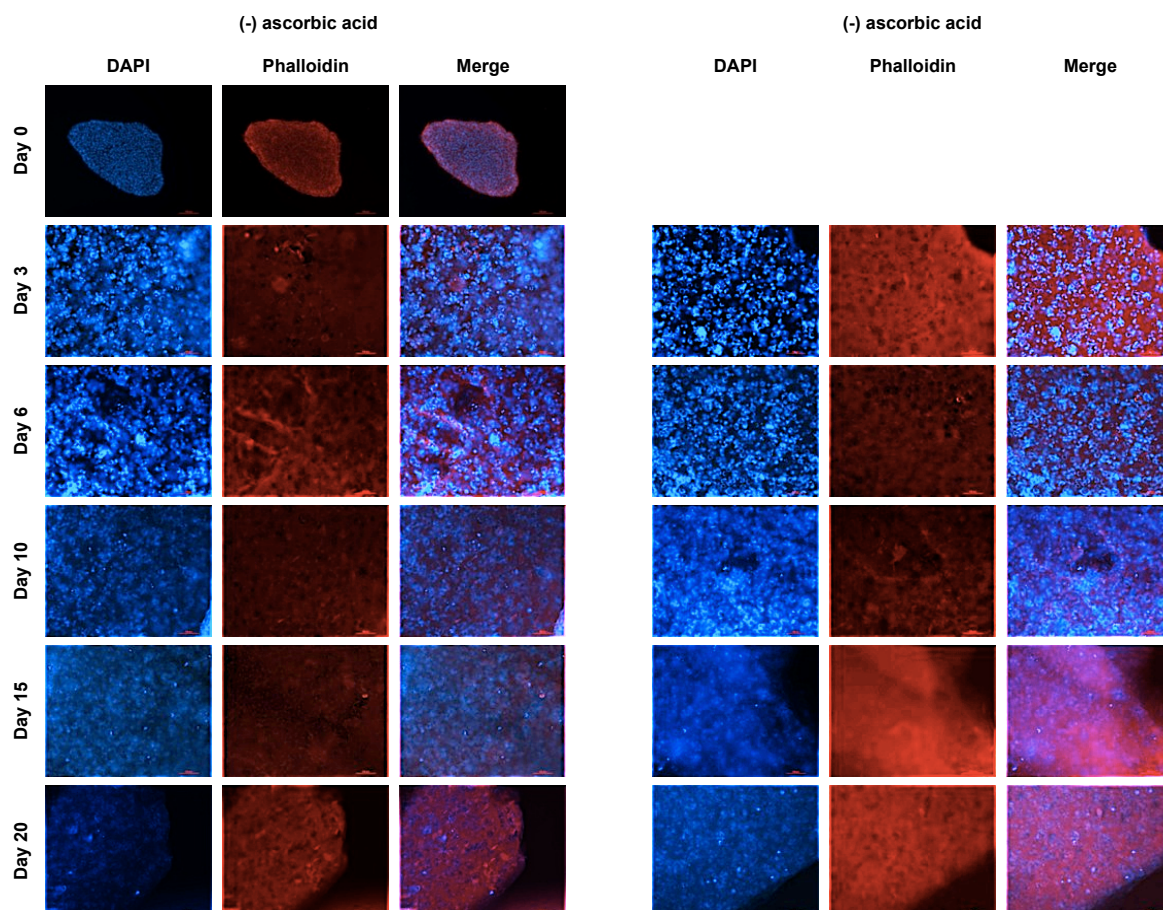


**Figure 36.** DAPI/Phalloidin staining of hiPSCs cultured in 3D with and without AA for 20 days. DAPI (blue) binds to DNA localized in the nucleus of the cells. Phalloidin (red) binds to the actin filaments of the cytoskeleton of the cells. Day 0 of the experiment corresponds to 2D cultures of hiPSCs at confluence.

Moreover, real time PCR was used to quantify the gene expression of differentiating hiPSCs cultured in 3D with and without AA (**Figure 37**). Cells were embedded in RAD16-I and maintained *in vitro* for 20 days. Cardiac commitment was tracked using the pluripotent (Oct4), early differentiation (FoxA2) and cardiac progenitor (Tbx5) markers. Each value was normalized to the correspondent value at day 0 (2D culture at confluence). The ribosomal gene 18S was used as a housekeeper gene to adjust the results by applying the  $\Delta\Delta C_T$  technique<sup>9</sup>. Although generally metabolic housekeeper genes (GAPDH, GUSB, etc.) are used to normalize qPCR results, it is thought that cells vary their metabolism in 3D cultures and this was why a ribosomal housekeeper gene was used. **Figure 37** shows that hiPSCs had an increased expression of Oct4 compared to 2D cultures (day 0). In the absence of AA, Oct4 expression reached its maximum at day 3 and then it remained constant from day 6 to 20. Similarly, hiPSCs cultured with AA had a peak of Oct4 expression at day 3 to 6 followed by a decline from day 10 to 15 and an increase at day 20. One possible explanation is that cells in 3D up-regulated and maintained



high levels of pluripotency for longer than in 2D cultures. For the early differentiation marker FoxA2, its expression increased from day 3 to 20 in hiPSCs cultured in 3D without AA. Contrary, cells maintained with AA had a decreasing expression of FoxA2 from day 3 to 20. Human iPSCs expressed  $10^3$  to  $10^5$  times more FoxA2 in 3D than in 2D (d0). Also, the expression was 10 to 100-fold higher in cells cultured in 3D without AA than with AA. Finally, the expression of the cardiac progenitor gene Tbx5 was similar in hiPSCs cultured with and without AA over the course of the experiment. Furthermore, its expression was around  $10^5$ -fold higher in 3D than in 2D (d0).

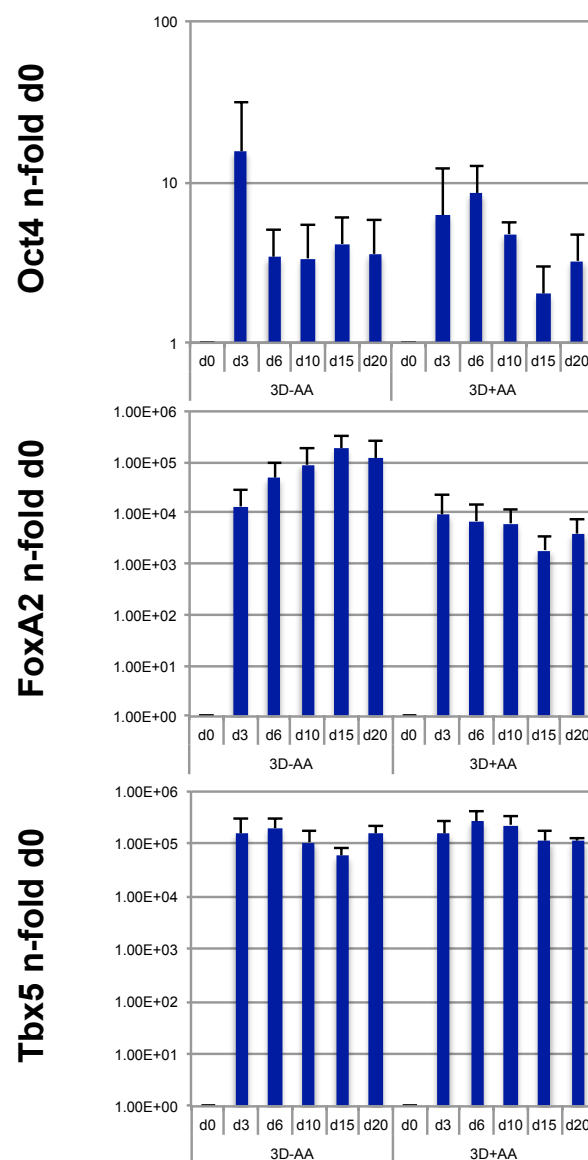


**Figure 37.** Quantitative PCR for pluripotent (Oct4), early differentiation (FoxA2) and cardiac progenitor (Tbx5) markers showing gene expression in 3D cultures of hiPSCs with and without AA. Analysis was performed as described in **Figure 28**.

#### COMPARISON OF THE CARDIAC DIFFERENTIATION POTENTIAL OF HUMAN INDUCED PLURIPOTENT STEM CELLS IN 2D AND 3D CULTURES BASED ON RAD16-I AND THE EFFECT OF ASCORBIC ACID ON CARDIOGENESIS

Taking into account the high expression of the pluripotent gene (Oct4) observed in the qPCR, further experiments were designed to confirm the pluripotency of hiPSCs in 3D over time. Firstly, hiPSCs were cultured in 3D without AA for 10 days. Then, constructs were disrupted with trypsin and the mixture was gently pipetted to homogenize the cellular suspension. The cells were seeded back in 2D on matrigel pre-coated wells. Interestingly, it was observed that cells did not attach the following day. This was possibly due to the cells being surrounded by remains of ECM, which prevented their attachment to the surface. Other possible explanations were that the trypsin treatment removed critical surface cell receptors or perhaps cells were simply dead. Conversely, the same experiment was carried out in parallel but instead cells were treated with ROCK inhibitor before disrupting the construct with trypsin. After one day in 2D culture, cells attached to the surface and survived (data not shown). Indeed, cells did survive the enzymatic treatment but needed to be treated with ROCK inhibitor to grow as single cells because they were pluripotent. Human iPSCs seemed to be pluripotent in 3D despite the presence of AA. The following experiments aimed to confirm the pluripotency of hiPSCs in 3D with and without AA at day 10. This specific time point was selected because qPCR showed that the gene expression peak of Oct4 was at day 3 to 6, so the following time point was chosen (day 10) to analyze functionality and protein translation.

Next step was to find and localize proteins using ICC assays. Results suggested that hiPSCs in 3D with and without AA contained pluripotent proteins such as Nanog at day 3 and 10 (**Figure 38**). The presence or absence of AA seemed to make no difference in terms of protein expression of Nanog. The staining was clearly positive: the secondary antibody bound to the enzyme HRP, which was highly reactive with the substrate, created a dark brown precipitate. The presence of proteins was homogeneous throughout the construct. Unfortunately, constructs at day 10 are extremely soft thereby making them difficult to manipulate. That was why the constructs were broken at day 10 (**Figure 38**). Despite our experience in 3D cultures, it was difficult to maintain intact constructs using ICC.

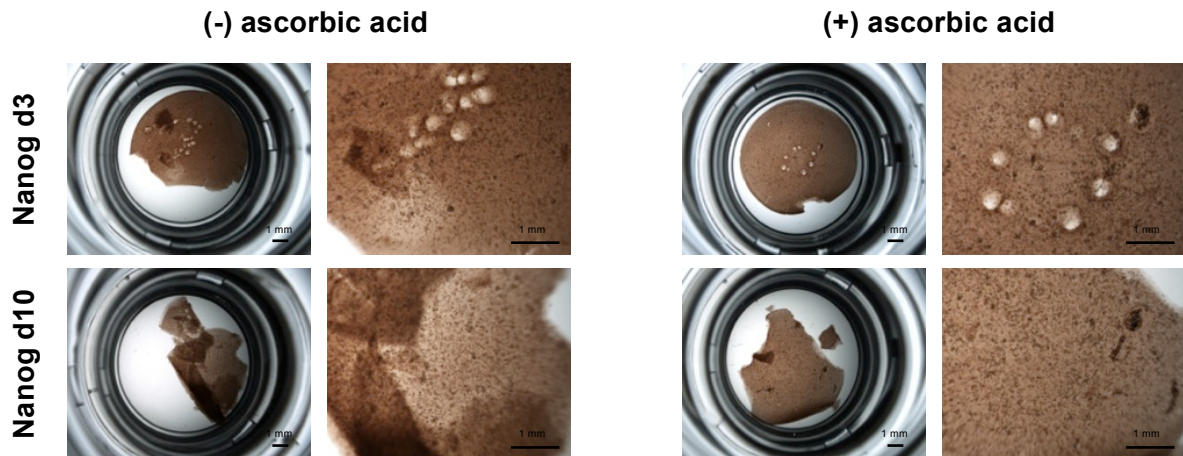


**Figure 38.** Immunostaining of hiPSCs in 3D cultured with and without AA for 3 and 10 days. HRP-conjugated secondary antibodies (brown precipitate) highlighted the localization of the pluripotent protein Nanog in the 3D constructs.

Additional ICC staining assays were run on hiPSCs to check the presence of other differentiation markers. Antibodies for early differentiation (FoxA2 and Gata4) and cardiac progenitor (Nkx2.5 and Tbx5) proteins were chosen to assess the cardiac commitment of hiPSCs. Cells were cultured in 3D with cardiogenic medium plus and minus AA from day 0 to 15. Immunological staining was achieved with HRP's substrate, which reacted with the enzyme linked to the secondary antibody. Surprisingly, all the samples appeared negative (white as opposed to brown precipitate). Indeed, none of the constructs were positive for any target protein (**Figure 39**). Also, as mentioned before, the constructs were very soft and fragile, which explained why some of the constructs were broken at the end of the ICCs.

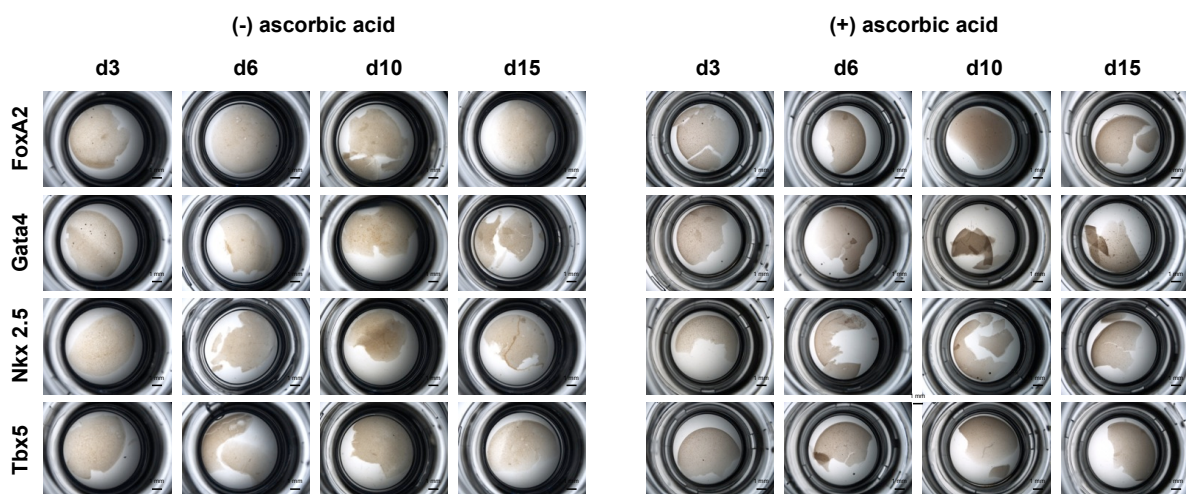


**Figure 39.** Immunostaining with HRP-conjugated secondary antibodies of hiPSCs cultured in 3D for 15 days with and without AA. The constructs appeared white i.e., negative for all the target proteins (early differentiation [FoxA2, Gata4] and cardiac progenitor [Nkx2.5, Tbx5] markers).

**COMPARISON OF THE CARDIAC DIFFERENTIATION POTENTIAL OF HUMAN INDUCED PLURIPOTENT STEM CELLS IN 2D AND 3D CULTURES BASED ON RAD16-I AND THE EFFECT OF ASCORBIC ACID ON CARDIOGENESIS**

The presence of cardiac differentiation proteins was double-checked with a second ICC technique, which would also give a closer observation of their localization in the cells. The protocol included cytospin and fluorescent ICC on glass slides. Indeed, the results confirmed that all the markers (FoxA2, Nkx2.5 and Tbx5, data not shown) were negative in hiPSCs cultured in 3D with cardiogenic medium both with and without AA for 15 days. Nevertheless, the samples that showed a very bright fluorescent signal under the microscope demonstrating that the target protein was present were: Nanog (pluripotency) at day 6 and 10 with and without AA (**Figure 40**). Gata4 (early differentiation) was also slightly positive at the same time points and conditions. Unfortunately, it was not possible to determine if the proteins were located in the nucleus or the cytoplasm. Indeed, the difficulties faced with these samples were that the cells had kidney-shaped nuclei and little cytoplasm which made it difficult to distinguish the localization of the proteins; there were remainders of extracellular matrix and RAD16-I that interfered in the staining and contributed to fluorescent background; and focusing the microscope image in 3D cultures was challenging. Despite these limitations, the results hinted that hiPSCs continuously expressed pluripotent markers when induced to cardiogenesis with and without AA at early (day 6) and late (day 10) stages of the 3D culture.

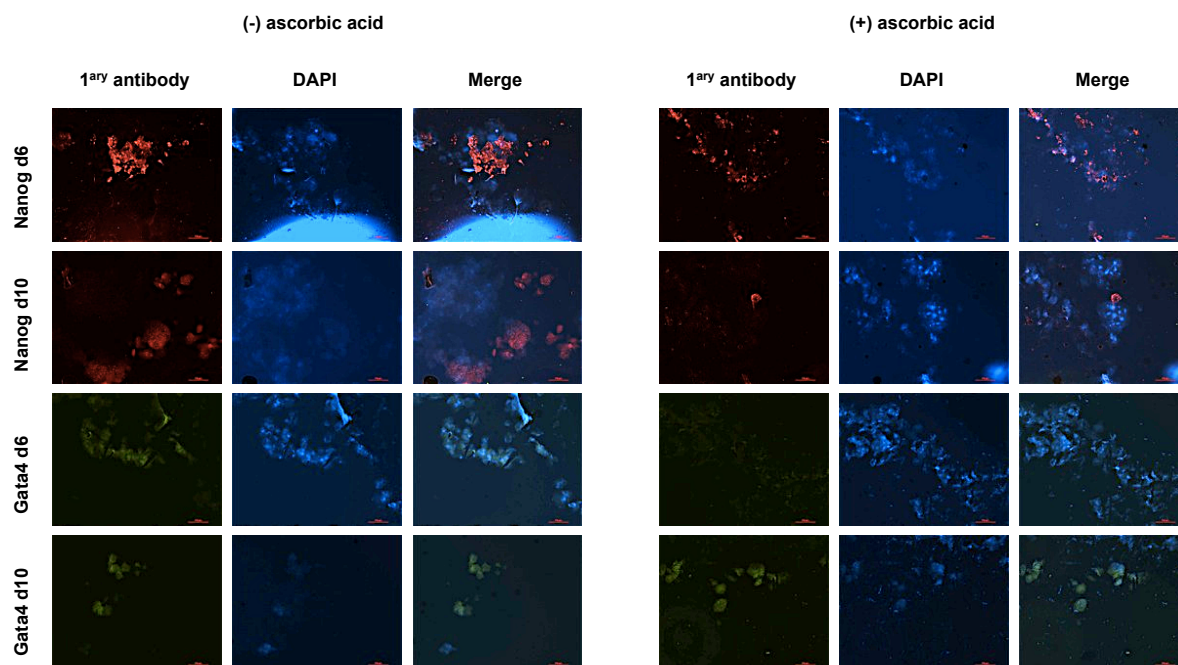


**Figure 40.** Fluorescent immunocytochemistry of cytospin samples of hiPSCs cultured in 3D with and without AA. Primary antibodies are bound to TRITC (red, Nanog) or FITC (green, Gata4).

#### 4.4. Discussion

Cardiac commitment of hiPSCs might become an unlimited source of patient-specific cardiomyocytes for regenerative medicine. Cardiogenesis studies with hiPSCs *in vitro* would also clarify human cardiac development, would allow cardiotoxicity studies<sup>10</sup> and would facilitate the testing of novel drugs to treat cardiac disease<sup>11-13</sup>. There are three main strategies for directed cardiac differentiation of hiPSCs and hESCs *in vitro*: (1) formation of contracting embryoid bodies although the efficiency is very low (0.1-25%) and the protocol takes at least 30 days<sup>14</sup>; (2) co-cultures with END2 (mouse visceral endoderm-like cells) stromal layers because it is known that endoderm influences cardiac differentiation during embryogenesis; (3) monolayer culture (2D) at high density seeded on Matrigel with treatment with induction proteins (activin A, bone morphogenetic protein 4) and growth factors<sup>15</sup>. Other approaches describe two-step procedures for the myogenic conversion of hESCs, which consist of culturing hESCs with myogenic medium and then infecting them with an adenovirus that expresses a myogenic master gene<sup>16</sup>. Additionally, researchers have suggested augmenting cardiac muscle cell number by antagonizing cell death (inhibiting machinery for apoptosis and necrosis) or by enhancing cell survival pathways. Despite the striking results, the number of cardiac muscle cells could not be reconstituted once cell death had occurred. For this reason, cardiac regeneration assays focus on restoring the damaged tissue by mobilizing endogenous SCs or supplying pre-differentiated progenitor cells<sup>17</sup>. The yields of *in vitro* cardiac commitment of hESCs can be up to 60% of contracting cells although the techniques are unsuitable to scale-up due to inherent low-throughput design, poor differentiation yields, low purity of the population of hiPSCs-derived cardiomyocytes (CM) acquired (1-50%), and the use of expensive reagents. Moreover, there exists a great inconsistency in differentiation efficiency among hESC and hiPSC lines due to genetic and epigenetic differences that directly impact their capacity to commit into cardiomyocytes. Human iPSCs exhibit superior epigenetic diversity, which is why no cardiac differentiation strategy has been optimized to date. Also, it is thought that hiPSCs retain an epigenetic memory of their somatic ancestor that affects their lineage-specific commitment capacity<sup>14</sup>. Importantly, SCs-derived CM should be carefully isolated before *in vivo* implantation in order to avoid tumor formation due to remaining pluripotent cells in the culture. Strategies to sort CM out of cultures include manual dissection of beating areas, Percoll density gradient sedimentation, genetic selection of stable clonal lines of cells and FACS (or MACS<sup>18</sup>) of cells expressing fluorescent reporters under cardiomyocyte gene promoters<sup>19,20</sup>.

## COMPARISON OF THE CARDIAC DIFFERENTIATION POTENTIAL OF HUMAN INDUCED PLURIPOTENT STEM CELLS IN 2D AND 3D CULTURES BASED ON RAD16-I AND THE EFFECT OF ASCORBIC ACID ON CARDIOGENESIS

Herein, hiPSCs were cultured in 2D and stimulated to commit into cardiomyocytes with ascorbic acid (AA). AA is a water-soluble vitamin involved in many biological reactions as a cofactor. It had previously been proven to promote cardiac differentiation of hESCs among others cytokines and chemical compounds reported to facilitate cardiac commitment. It appeared to be a robust, consistent and reproducible cardiac inducer among different hiPSCs lines including those without spontaneous cardiogenic potential<sup>21</sup>. Although it plays an antioxidative role in mammalian enzymatic reactions, its mechanism in cardiac differentiation remains unclear. Tests with other antioxidants suggest that the promoting effect of AA on cardiac differentiation is independent of its antioxidative property or that its antioxidative effect is insufficient to induce ESC-derived cardiomyocytes<sup>22</sup>. Researchers have proven that AA influences the initiation of cardiac differentiation of ESCs by modulating the synthesis of collagens (ECM)<sup>23</sup>. Here, results suggest that AA accelerates and improves the cardiac commitment of hiPSCs in 2D cultures. Indeed, gene expression of cardiac markers was significantly higher in cells treated with AA than without. The Oct4 expression decreased markedly during the first 15 days of the experiment in control (minus AA) and induced (plus AA) cells. Indeed, a strong down-regulation in total Oct4 gene expression also occurs during cardiogenesis of hiPSCs cultured in EBs, which confirms that there is a reduction in pluripotency<sup>24</sup>. The gastrulation seemed to take place from day 3 to 10, when there was a peak of expression of FoxA2 and Brachyury. Gata4 is thought to act as an early cardiac progenitor involved in early myocardial development, an intermediate between mesodermal formation and cardiac commitment<sup>22</sup>. Gata4 diminished faster in cells treated with AA, which implies that cardiac differentiation was more accentuated in induced cells than in control ones. Cardiac progenitor genes (Mef2c and Tbx5) were increasingly expressed from day 10 onwards. Tbx5 might be an early cardiac progenitor (expressed from day 6 to 15 approximately) whereas Mef2c might be a late cardiac progenitor (day 15 to 25). Conversely, ACTC1 is a mature cardiomyocyte gene although it has also been reported in gastrulation processes, mesoderm and pre-cardiac cells. Based on the results of this research, it may act as an early differentiation marker (peak of expression from day 3 to 10, similar to FoxA2 and Brachyury) and it may be involved in cardiac mesodermal formation. All in all, cardiac differentiation of hiPSCs cultured in 2D with and without AA appeared to be a stepwise process:



- (1) Pluripotency: Oct4 (day 0)
- (2) Early differentiation: FoxA2 and Brachyury (day 3 to 6)
- (3) Mesodermal and pre-cardiac formation: Gata4 and ACTC1 (day 6 to 10)
- (4) Early cardiac progenitor: Tbx5 (day 10 to 15)
- (5) Late cardiac progenitor: Mef2c (day 15 to 25).

Nevertheless, the gene expression of all the differentiation markers was always higher in cells treated with AA than without. AA appeared to accelerate the cardiac differentiation process. An interesting observation on the agarose gel (**Figure 27**) was that hiPSCs at day 0 expressed all the cardiac differentiation markers. Perhaps cells were not synchronized at confluence or maybe pluripotent cells constitutively express genes that they do not need. In any case, mRNA expression levels may not reflect the level of protein translation in stem cells. Cells (at pluripotent stage) transcribe unnecessary mRNAs, which can be translated into functional proteins during cell differentiation. It is thought that stem cells produce mRNA for a large number of genes to offer multiple options for development. Cells choose a path depending on what battery of mRNAs they translate into proteins<sup>25</sup>. Human iPSCs in the present study expressed cardiomesoderm-specific markers (Brachyury and Gata4) at day 3 to 6; cardiac-specific transcription factors (Nkx2.5) at day 6; and mature cardiomyocyte structural proteins (MHC, Cx43 and Trop I) at day 10 to 15<sup>26</sup>. The timing of cardiac commitment of hiPSCs in 2D was consistent in terms of gene and protein expression. Similarly to hiPSCs-based EBs, hiPSCs cultured in 2D also followed a temporal gene expression pattern associated with cardiomyogenesis and acquired necessary molecular, structural and functional cardiac properties that generated beating syncytia<sup>26,27</sup>. However, very little is known about the process involved in promoting mesendoderm to form committed cardiac mesendoderm<sup>28</sup>. In addition, cell morphology suggested that cells underwent a three-dimensional organization that caused the beating of cellular clusters from day 14 onwards. It has previously been shown that hiPSCs co-cultured on END2 endodermal cells started beating at day 10 of cardiac induction<sup>29</sup>. Although functional syncytia appeared four days later in the present work, the protocol used here is simpler, easier to reproduce and purer because it only involves one cell type. Likewise previous data, differentiating hiPSCs-derived cardiomyocytes had a non-rhythmical beating behavior: clusters of cells beat at different frequencies. The high variability in beating frequency among the cells indicated different stages of the maturation and phenotype of the CMs derived from hiPSCs. Indeed, acceleration of beating frequency may suggest ongoing maturation<sup>29</sup>. Moreover, the medium played a key

role i.e. FBS supplementation was essential for cardiac differentiation and AA promoted the contraction of cells. It has been shown that hiPSCs require FBS to start contraction and that hEBs could be maintained in a simple medium for long periods of time<sup>14</sup>. Therefore, the knowledge obtained from the efficient cardiac commitment of hiPSCs in 2D cultures could be used to understand the process in tissue-like 3D cultures.

To date, the most used 3D culture technique of hiPSCs is the formation of EBs, which are 3D aggregates of cells<sup>20</sup>. Many approaches show that cardiac differentiation of hiPSCs in EBs is more efficient than in monolayer cultures (2D). The combination of cells and a support scaffold provides hierarchical organization to the cells and sustains the development of functional tissue. Cardiac TE offers many strategies ranging from fabricated polymer scaffolds<sup>30</sup> to decellularized whole organs<sup>20</sup>. In this chapter, we propose a novel method to generate 3D cultures of hiPSCs based on hydrogel RAD16-I and assess their cardiac commitment in a tissue-like environment. Surprisingly, it was observed over the course of the experiment that the morphology of the cells did not vary in the 3D constructs. Cells appeared rounded and slightly clustered. The nuclear staining was not very accurate but bright-blue dots could be observed against the amorphous blue background of the RAD16-I scaffold<sup>31</sup>. Viability assays proved that nearly half of the population of hiPSCs embedded in RAD16-I was alive, which may have been due to cells in the hydrogel proliferating and dying at approximately the same rate. Therefore, cell morphology and proliferation rate of hiPSCs in 3D were similar to pluripotent cells. Gene expression profiles showed that hiPSCs cultured in 3D up-regulated genes of pluripotency (Oct4), early differentiation (FoxA2) and early cardiac progenitor (Tbx5) independently of the presence of AA. FoxA2 and Tbx5 were expressed up to 10<sup>5</sup> times more in 3D than in 2D cultures. Nevertheless, ICC indicated that cells did not contain any protein related to early differentiation (FoxA2) nor to cardiac progenitor (Gata4, Nkx2.5 and Tbx5). Human iPSCs cultured in 3D with and without AA only translated pluripotent proteins such as Nanog at day 3, 6 and 10. A possible explanation might be that cells embedded in RAD16-I and induced with cardiogenic media (with and without AA) were pluripotent-like cells because they contained high levels of pluripotent genes and proteins. Furthermore, the expression of the pluripotent gene Oct4 in 3D cultures was high for 20 days whereas in 2D cultures it dropped markedly after the third day of cardiac differentiation. Retention of Oct4 expression has been reported in neural progenitor populations whereas its rapid down-regulation is linked to the formation of primitive endoderm that is essential for



mesodermal differentiation (and later cardiac commitment)<sup>5</sup>. Human iPSCs cultured in RAD16-I might acquire an increased potentiality to commit into any germ layer-derived lineage although AA directs their differentiation into cardiomyocyte-like cells. Moreover, hiPSCs 3D-constructs expressed high levels of differentiation genes (FoxA2 and Tbx5) that were not translated into functional proteins. The persistent mRNA expression might be due to a variety of downstream regulators such as microRNA, which are especially important for pluripotency genes. The discrepancy between mRNA and protein expression has been previously observed in other cardiac differentiation assays<sup>24</sup>. The reasons why gene expression at the transcript level does not correlate well with its expression at the protein level might be related to alternative splicing, mRNA degradation and post-translational modifications. Differentiation assays with hESCs showed that the correlation between RNA and protein abundance levels is often low due to post-translational regulation of the proteome in stem cell populations<sup>32</sup>. It is hypothesized that protein degradation is higher than mRNA degradation because genes/transcripts can be switched off<sup>33</sup>. Therefore, proteomics and transcriptomics data are complementary rather than duplicative in human pluripotent SCs. The mRNA levels are only a partial reflection of the functional state of an organism and the amount of protein is often not predictable from mRNA abundance<sup>34</sup>. *Unwin et al.* demonstrated that 54% of protein changes are not observed at the transcriptional level<sup>35,36</sup>. Indeed, SCs seem to transcribe a large number of genes whereas they diminish the transcription with differentiation. Researchers suggest that SCs generate mRNA species that are not directly linked to proteins in order to offer multiple options for development<sup>25</sup>.

Nevertheless, another approach sustains the contrary to the description previously stated: high levels of Oct4 expression might indicate that hiPSCs cultured in 3D have an increased level of differentiation. *Niwa et al.* showed that up-regulation of Oct4 induced commitment into extra-embryonic endoderm and mesoderm lineages. They found that both loss and gain of target gene expression contributed to induction of differentiation. Therefore, Oct4 function seems to be a requirement for maintenance of ESC identity although any variation of its expression levels triggers differentiation<sup>37</sup>. This approach is coherent with the results presented in this chapter and it might justify why hiPSCs expressed astonishing high levels of differentiation genes (FoxA2 and Tbx5). Cells cultured in RAD16-I acquired an increased potentiality to commit into cardiac lineage.

The suggested 3D protocol offers a strong pre-differentiation of hiPSCs into cardiomyocyte-like cells with high potential to commit to cardiac lineage (up to  $10^5$  times more than cells cultured in 2D). Recently, *Hudson et al.* demonstrated that hESCs passaged as single-cell suspensions before cardiac differentiation reduced the heterogeneity of the cell population and enhanced the cardiac commitment<sup>38</sup>. The present protocol includes a disaggregation step where hiPSCs clusters are totally disrupted into single-cells prior to encapsulation in RAD16-I. This might correlate with previous reports and explain the increased potentiality of hiPSCs to commit into cardiac lineage (spontaneous up-regulation of cardiac genes in 3D with and without AA). Thus, cells differentiated in 3D might be partially committed but not totally functional, as they do not create contracting syncytia. It has been previously shown that the stiffness of the substrate influences the contraction stress of the cells i.e. hPSCs-derived CMs on stiff substrates generated more contraction stress than those on soft ones<sup>7</sup>. Perhaps in the current study the peptide scaffold was too soft to promote cell beating of hiPSCs. Therefore, future experiments should focus on adjusting the stiffness of the scaffold by increasing and testing different RAD16-I concentrations. It would be interesting to characterize functional CMs derived from hiPSCs cultured in RAD16-I and compare yields of cardiac differentiation with other approaches. Nevertheless, the implantation of beating cells into cardiac damaged tissue would seriously compromise the endogenous electrical properties of the heart and its coordinated contraction. As a result, atrial syncytium would be de-synchronized, which would lead to major consequences. This chapter describes the generation of a tissue-like 3D culture of pre-differentiated hiPSCs, with an extremely high potential to commit into CM but with no contracting properties.

To avoid tumor formation, pluripotent cells cannot be directly injected into patients but need to be pre-differentiated into a desired cell type prior to *in vivo* transplantation<sup>39</sup>. Although undifferentiated cells could lead to tumorigenesis, heterogenic cell populations may be beneficial because of the variety of stages of pre-differentiated cells (nodal, atrial, ventricular), which could regenerate and repopulate the heart<sup>24</sup>. In the present study, hiPSCs seemed to express increased levels of Oct4 when cultured in 3D scaffolds based on RAD16-I. Therefore, future approaches should focus on characterizing the degree of pluripotency of these cells (teratoma formation assays). As mentioned above, fully differentiated and beating cardiomyocytes should not be engrafted *in vivo* because they would dangerously compromise the electromechanical properties of the living cardiac tissue and cause pro-arrhythmias.

#### 4.5. Concluding remarks

- Cardiac differentiation of hiPSCs cultured in 2D with and without AA appeared to be a stepwise process in terms of gene and protein expression. First, pluripotent cells differentiated into mesendodermal cells (day 3 to 6); second, mesodermal cells committed to pre-cardiac cells (day 6 to 10); third, hiPSCs went through an early cardiac progenitor stage (day 10 to 15); and finally, cells acquired late cardiac progenitor properties (day 15 to 25).
- Gene expression of cardiac markers was significantly higher in cells treated with AA than without, which suggests that AA accelerated and improved the cardiac commitment of hiPSCs in 2D cultures.
- The high variability in beating frequency among hiPSCs differentiated in 2D cultures indicated different stages of phenotype of the CMs derived from them and thus, ongoing cardiac maturation.
- Human iPSCs cultured in 3D up-regulated and retained expression of Oct4 despite the presence or absence of AA for at least 10 days. High levels of the target gene indicated that hiPSCs displayed an increased level of differentiation.
- Gene expression profiles showed that hiPSCs cultured in 3D with and without AA up-regulated  $10^5$ -fold more genes related to early differentiation (FoxA2) and early cardiac progenitor (Tbx5) than cells cultured in 2D.
- The suggested 3D protocol offered a strong pre-differentiation of hiPSCs into cardiomyocyte-like cells with high potential to commit into cardiac lineage.
- Human iPSCs embedded in RAD16-I did not create contracting syncytia, which might be crucial for *in vivo* engraftment purposes to not compromise the electromechanical properties of the heart.

#### 4.6. References

1. Burridge, P. W., Keller, G. M., Gold, J. D. & Wu, J. C. Production of de novo cardiomyocytes: human pluripotent stem cells differentiation and direct reprogramming. *Natl. Institutes Heal.* **10**, 16–28 (2013).
2. Kraehenbuehl, T. P. *et al.* Human embryonic stem cell-derived microvascular grafts for cardiac tissue preservation after myocardial infarction. *Biomaterials* **32**, 1102–9 (2011).
3. Levenberg, S. *et al.* Differentiation of human embryonic stem cells on three-dimensional polymer scaffolds. *Proc. Natl. Acad. Sci. U. S. A.* **100**, 12741–6 (2003).
4. Pal, R., Mamidi, M. K., Das, A. K. & Bhone, R. Comparative analysis of cardiomyocyte differentiation from human embryonic stem cells under 3-D and 2-D culture conditions. *J. Biosci. Bioeng.* **115**, 200–6 (2013).
5. Ojala, M. *et al.* Culture conditions affect cardiac differentiation potential of human pluripotent stem cells. *PLoS One* **7**, e48659 (2012).
6. Kehoe, D. E., Jing, D., Lock, L. T. & Tzanakakis, E. S. Scalable stirred-suspension bioreactor culture of human pluripotent stem cells. *Tissue Eng. Part A* **16**, 405–421 (2010).
7. Hazeltine, L. B. *et al.* Effects of substrate mechanics on contractility of cardiomyocytes generated from human pluripotent stem cells. *Int. J. Cell Biol.* **2012**, 508294 (2012).
8. Cao, N. *et al.* Ascorbic acid enhances the cardiac differentiation of induced pluripotent stem cells through promoting the proliferation of cardiac progenitor cells. *Cell Res.* **22**, 219–36 (2012).
9. Zhang, J. D., Ruschhaupt, M. & Biczok, R. ddCt method for qRT – PCR data analysis. *Bioconductor* 1–8 (2013).
10. Wobus, A. M. & Löser, P. Present state and future perspectives of using pluripotent stem cells in toxicology research. *Arch. Toxicol.* **85**, 79–117 (2011).
11. Matsa, E. *et al.* Drug evaluation in cardiomyocytes derived from human induced pluripotent stem cells carrying a long QT syndrome type 2 mutation. *Eur. Heart J.* **32**, 952–62 (2011).
12. Park, I. *et al.* Disease-specific induced pluripotent stem (iPS) cells. *Natl. Institutes Heal.* **134**, 877–886 (2009).
13. Saha, K. & Jaenisch, R. Technical challenges in using human induced pluripotent stem cells to model disease. *Natl. Institutes Heal.* **5**, 584–595 (2010).
14. Burridge, P. W. *et al.* A universal system for highly efficient cardiac differentiation of human induced pluripotent stem cells that eliminates interline variability. *PLoS One* **6**, e18293 (2011).
15. Hoekstra, M., Mummery, C. L., Wilde, A. A. M., Bezzina, C. R. & Verkerk, A. O. Induced pluripotent stem cell derived cardiomyocytes as models for cardiac arrhythmias. *Front. Physiol.* **3**, 346 (2012).

16. Goudenege, S. *et al.* Myoblasts derived from normal hESCs and dystrophic hiPSCs efficiently fuse with existing muscle fibers following transplantation. *Mol. Ther.* **20**, 2153–67 (2012).
17. Mercola, M., Ruiz-lozano, P. & Schneider, M. D. Cardiac muscle regeneration : lessons from development. 299–309 (2011). doi:10.1101/gad.2018411.GENES
18. Uosaki, H. *et al.* Efficient and scalable purification of cardiomyocytes from human embryonic and induced pluripotent stem cells by VCAM1 surface expression. *PLoS One* **6**, e23657 (2011).
19. Kita-Matsuo, H. *et al.* Lentiviral vectors and protocols for creation of stable hESC lines for fluorescent tracking and drug resistance selection of cardiomyocytes. *PLoS One* **4**, e5046 (2009).
20. Shiba, Y., Hauch, K. D. & Laflamme, M. A. Cardiac applications for human pluripotent stem cells. *Natl. Institutes Heal.* **15**, 2791–2806 (2010).
21. Cao, N. *et al.* Ascorbic acid enhances the cardiac differentiation of induced pluripotent stem cells through promoting the proliferation of cardiac progenitor cells. *Cell Res.* **22**, 219–36 (2012).
22. Takahashi, T. *et al.* Ascorbic acid enhances differentiation of embryonic stem cells into cardiac myocytes. *Circulation* **107**, 1912–6 (2003).
23. Sato, H. *et al.* Collagen synthesis is required for ascorbic acid-enhanced differentiation of mouse embryonic stem cells into cardiomyocytes. *Biochem. Biophys. Res. Commun.* **342**, 107–12 (2006).
24. Zhang, J. *et al.* Functional cardiomyocytes derived from human induced pluripotent stem cells. *Natl. Institutes Heal.* **104**, (2010).
25. Williamson, A. J. K. *et al.* Quantitative proteomics analysis demonstrates post-transcriptional regulation of embryonic stem cell differentiation to hematopoiesis. *Mol. Cell. Proteomics* **7**, 459–72 (2008).
26. Zwi, L. *et al.* Cardiomyocyte differentiation of human induced pluripotent stem cells. *Circulation* **120**, 1513–23 (2009).
27. Jameel, M. N. & Zhang, J. Stem cell therapy for ischemic heart disease. *Antioxid. Redox Signal.* **13**, 1879–97 (2010).
28. Willems, E., Bushway, P. J. & Mercola, M. Natural and synthetic regulators of embryonic stem cell cardiogenesis. *Natl. Institutes Heal.* **30**, 635–642 (2012).
29. Sheng, X. *et al.* Human pluripotent stem cell-derived cardiomyocytes: response to TTX and lidocain reveals strong cell to cell variability. *PLoS One* **7**, e45963 (2012).
30. Ye, L. *et al.* Effective cardiac myocyte differentiation of human induced pluripotent stem cells requires VEGF. *PLoS One* **8**, e53764 (2013).
31. Piao, H. *et al.* Effects of cardiac patches engineered with bone marrow-derived mononuclear cells and PGCL scaffolds in a rat myocardial infarction model. *Biomaterials* **28**, 641–9 (2007).
32. Jadaliha, M. *et al.* Quantitative proteomic analysis of human embryonic stem cell differentiation by 8-plex iTRAQ labelling. *PLoS One* **7**, e38532 (2012).

**COMPARISON OF THE CARDIAC DIFFERENTIATION POTENTIAL OF HUMAN INDUCED PLURIPOTENT STEM CELLS IN 2D AND 3D CULTURES BASED ON RAD16-I AND THE EFFECT OF ASCORBIC ACID ON CARIOGENESIS**

33. Unwin, R. D. & Whetton, A. D. Systematic proteome and transcriptome analysis of stem cell populations. *Cell cycle* **5**, 1587–91 (2006).
34. Fathi, A. *et al.* Comparative proteome and transcriptome analyses of embryonic stem cells during embryoid body-based differentiation. *Proteomics* **9**, 4859–70 (2009).
35. Unwin, R. D. *et al.* Quantitative proteomics reveals posttranslational control as a regulatory factor in primary hematopoietic stem cells. *Blood* **107**, 4687–94 (2006).
36. Unwin, R. D., Pierce, A., Watson, R. B., Sternberg, D. W. & Whetton, A. D. Quantitative proteomic analysis using isobaric protein tags enables rapid comparison of changes in transcript and protein levels in transformed cells. *Mol. Cell. Proteomics* **4**, 924–35 (2005).
37. Niwa, H., Miyazaki, J. & Smith, A. G. Quantitative expression of Oct-3/4 defines differentiation, dedifferentiation or self-renewal of ES cells. *Nat. Genet.* **24**, 2–6 (2000).
38. Hudson, J., Titmarsh, D., Hidalgo, A., Wolvetang, E. & Cooper-White, J. Primitive cardiac cells from human embryonic stem cells. *Stem Cells Dev.* **21**, 1513–23 (2012).
39. Ao, A., Hao, J. & Hong, C. C. Regenerative chemical biology: current challenges and future potential. *Natl. Institutes Heal.* **18**, 413–424 (2012).
40. Rajala, K., Pekkanen-Mattila, M. & Aalto-Setälä, K. Cardiac differentiation of pluripotent stem cells. *Stem Cells Int.* **2011**, 383709 (2011).

*Chapter 5: Development of biological scaffolds  
for post-infarction scar repair*





## **CHAPTER 5. DEVELOPMENT OF BIOLOGICAL SCAFFOLDS FOR POST-INFARCTION SCAR REPAIR**

### *5.1. Introduction*

Myocardial infarction (MI) treatment has been a target of research for over 50 years. Since the first cardiac surgery in 1893, technical approaches have dramatically evolved with the incorporation of chemical drugs and the widespread use of coronary stents for occluded coronary arteries. The post-infarction scar can successfully be minimized thanks to technological advances although there is still a portion of the heart that becomes hypo- or akinetic following MI. Cardiac tissue engineering offers the advantage of combining progenitor cells with delivery vehicles to restore damaged myocardial tissue. Indeed, engineered tissue grafts and myocardial bioprotheses aim to improve cellular engraftment and viability, combining cellular components with supporting materials. A myocardial bioprosthesis is a *smart patch*, which function is to mimic structural cardiac muscle architecture. Therefore, the engineered scaffold should be deformable to support cardiac contraction, biomimetic to encourage cell coupling with host tissue and pro-angiogenic to promote vascularization of the new-formed tissue<sup>1</sup>.

New directions in cardiac regeneration research point at devices that monitor the effect of the cardiac graft on the infarcted heart. Indeed, telemedicine is the transmission of information from patients directly to attending cardiologists. Hence, it is an online monitoring technology of biological parameters as electrocardiograms. The main goal of telemedicine is to reduce the delay in the treatment of MI and allow cardiologists to react quickly (up to 60 critical minutes can be saved from symptom onset to reperfusion therapy)<sup>2</sup>. Tele-health systems are also under development and validation for a closer monitoring of post-infarction patients<sup>3,4</sup>. Concretely, it is possible to identify healthy from necrotic myocardium by means of Electrochemical Impedance Spectroscopy (EIS)<sup>5-8</sup>. Herein, we established a new 3D cell-based myocardial bioprosthesis model based on human decellularized pericardium refilled with a mixture of RAD16-I hydrogel and adult stem cells, together with an implantable EIS measurement system for *in vivo* online monitoring of post-infarction scar formation in swine. *La Marató de TV3* funded this project (*Development of biological scaffolds for post-infarction scar repair: local delivery of stem cells, angiogenic factors and on line monitoring of myocardial regeneration* – 080330). Thus, three

research groups collaborated to develop the *smart patch*: Institut Químic de Sarrià (IQS, Dr. Semino's laboratory: we established the 3D cultures of porcine adult stem cells, we prepared the human pericardia to be used as macro-scaffold of the patch, we tailored RAD16-I nanofibers with NanoGold particles and we collaborated with the microsurgeries on swine), Institut Germans Trias i Pujol (IGTP, Dr. Bayés-Genís' laboratory: they characterized the porcine stem cell line, they were in charge of the microsurgeries on swine and the *posteriori* analysis of the samples collected after porcine sacrifice) and Universitat Politècnica de Catalunya (UPC, Dr. Bragós' laboratory: they designed the monitoring device based on EIS, they collaborated with us improving the electrical potential of the patch (NanoGold) and they analyzed the data obtained on line from the EIS).

### 5.2. Hypothesis and specific aims

Human cardiac tissue has very limited regenerative potential. Novel cell and tissue therapies based on the use of adipose tissue-derived stem cells may be useful alternatives to limit the size of myocardial infarction. The main goal of this project was to develop and validate a bioactive implant consisting in electronic sensors within a microporous membrane filled with stem cells to regenerate myocardial infarction in swine.

Hypothesis: Human pericardium may be a convenient macro-scaffold to support 3D cultures of porcine Mediastinal Adipose Tissue Progenitor Cells (pMATPCs) embedded in the peptide hydrogel RAD16-I. Thus, tailored nanofibers with NanoGold may help to facilitate the propagation of electrical current through the bioactive patch by reducing the electrode impedance.

#### Specific aims:

- Study of the cardiogenic potential of pMATPCs in 3D cultures based on RAD16-I.
- Decellularization and characterization of human pericardium as a macro-scaffold for the *smart patch*.
- Tailoring of RAD16-I nanofibers with NanoGold in order to improve the electrical conductivity of the *smart patch*.
- Implantation of the *smart patch* in swine.

### 5.3. Results

#### 5.3.1. Cardiogenic potential of pMATPCs in 2D and 3D cultures based on RAD16-I

The group of Dr. Bayés-Genís has successfully established and characterized primary cell cultures from porcine Mediastinal Adipose Tissue Progenitor Cells (pMATPCs)<sup>9</sup>. They identified a few elongated fibroblast-like cells that attached after 3 – 4 days and could be maintained in culture (~ 15 passages) with a duplication time of 3 – 4 days. Immunophenotypical characterization revealed a homogenous Mesenchymal Stem Cell-like profile. Porcine MATPC were successfully differentiated into osteogenic, adipogenic and chondrogenic lineages, which demonstrated that these cells were multipotent. The gene expression analysis revealed high expression of Connexin 43 (Cx43) and traces of Gata4 in 2D cultures. At protein level, pMATPCs expressed Cx43 and Gata4, and were negative for cardiac Troponin I (cTnI) when cultured in traditional plastic flasks (performed by the group IGTP)<sup>9</sup>. As observed in 2D cultures, there was presence of proteins Cx43 and Gata4 in 3D-pMATPCs constructs whereas there was no expression of cTnI (**Figure 41**). Indeed, it was shown by immunocytochemistry that pMATPCs cultured in RAD16-I for 7 days slightly expressed Gata4 (cardiac progenitor marker) and highly expressed Cx43 (mature cardiomyocyte marker). Up to now, porcine-derived MSCs have been isolated from bone marrow<sup>10</sup>, subcutaneous adipose tissue<sup>11</sup>, umbilical cord blood and peripheral blood<sup>12</sup>. Our collaborator's data (IGTP) showed that pMATPCs could be easily isolated from mediastinal adipose tissue. Cells were expanded in 2D cultures forming a homogenous cell population with MSC-like phenotype, denoting standard multipotency as well as expression of some cardiac and endothelial markers. The results presented in this chapter suggest that pMATPCs behaved similarly to 2D cultures when cultured in 3D based on the RAD16-I hydrogel. Anyhow, the expression of Cx43 and Gata4 proteins in cells embedded in 3D seemed to be enhanced compared to 2D cultures.

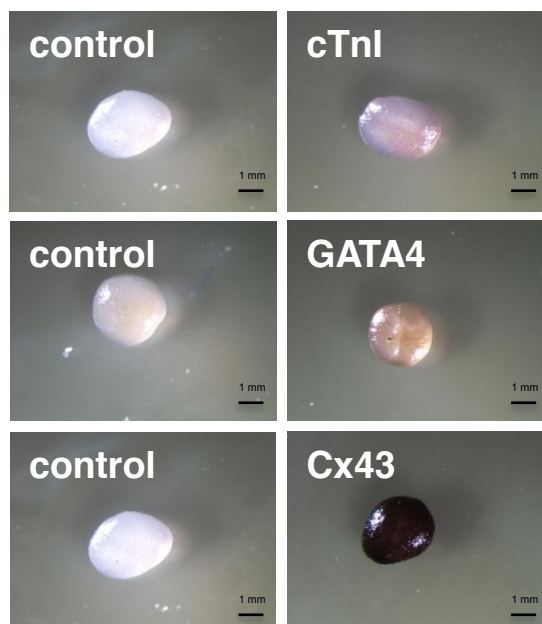


**Figure 41.** Immunocytochemistry for mesenchymal (Gata4) and mature cardiomyocyte (cTnI and Cx43) markers of pMATPCs cultured in RAD16-I for 7 days. Secondary antibodies were bound to HRP enzyme, which reacted with its substrate creating a brown precipitate. Control samples represent negative control for each primary antibody.

### 5.3.2. Preparation of the biological macro-scaffold based on decellularized human pericardium

The aim of obtaining totally decellularized pieces of pericardium was to use the mechanical and morphological properties of these macro-scaffolds to support the bioengineered cardiac patch. Other approaches have applied acellular extracellular scaffolds for tissue engineering or regeneration purposes<sup>13–17</sup>. It was of critical importance to remove all the endogenous pericardial cells in order to avoid any immunological rejection during the implantation of the patch: the pericardium was explanted from human hearts and the final implant was in a porcine model. Several decellularization protocols have been described in literature including physical, chemical and enzymatic approaches<sup>18</sup>. Hereby, an effective chemical decellularization based on ionic detergents was successfully established. After an exhaustive process of washing out cell debris using detergents and a perfusion method, pericardia appeared totally white, clean of blood remains (**Figure 42**). In addition, pericardia were lyophilized in PBS solution to induce the self-assembling of

RAD16-I. Indeed, the peptide nanofibers spontaneously self-assemble at high ionic strength. The salts contained in PBS got entrapped into the pericardium after exhaustive de-hydration and promoted the self-assembling of RAD16-I nanofibers inside the pericardium. After lyophilization at low temperature, pericardia were re-hydrated with a solution of RAD16-I at 0.15%. Entirely wet structures were obtained, indicating that pericardium was hydrophilic and could be easily hydrated after lyophilization (**Figure 42**). Indeed, the biomaterial had to be hydrophilic to host and retain cells inside the cardiac patch.

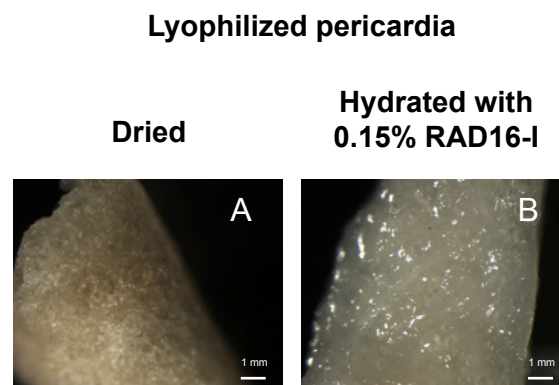


**Figure 42.** Macroscopic morphology of lyophilized human pericardia under stereoscope. A) Dried lyophilized pericardium. B) Re-hydrated lyophilized pericardium with RAD16-I 0.15%. Note that rehydration with RAD16-I peptide solution was highly efficient and fast.

Then, decellularized and lyophilized pericardia were impregnated with: (1) 0.15% RAD16-I solution; and (2) water (control). The samples were stained with Congo red, which specifically marks  $\beta$ -sheet structures generated by self-assembled RAD16-I (**Figure 43**). There was positive bright red-colored Congo red staining in the pericardium embedded with RAD16-I but not in the control pericardium (water). The pericardium's extracellular matrix (ECM) is mainly composed of collagen fibers, which have  $\alpha$ -helix structure but not  $\beta$ -sheet. Therefore, the  $\beta$ -sheets observed corresponded to the scaffold generated by RAD16-I peptide. The 3D scaffold based on  $\beta$ -sheet layers of nanofibers was spontaneously generated inside the pericardium and in between its filaments. The self-assembling process occurred normally and the filaments of the pericardium did not interfere in the process.

### Congo Red staining on decellularized pericardia

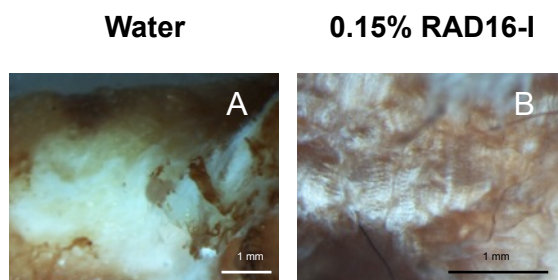


**Figure 43.** Congo red staining of decellularized and lyophilized human pericardia. A) Pericardium embedded with water. B) Pericardium embedded with RAD16-I 0.15%.

Additionally decellularized and lyophilized pericardia were stained with the blue nuclei dye DAPI in order to evaluate the presence of endogenous pericardial cells (**Figure 44**). As mentioned above, it was of critical importance to obtain cell-free matrices to avoid any immune rejection of the patch implanted *in vivo*. Thus, no nuclei were observed in the pericardium's matrix although the collagen fibers themselves appeared auto-fluorescent under the microscope. Pericardia did not contain pericardial endogenous cells after the decellularization process.

### Decellularized and lyophilized pericardia

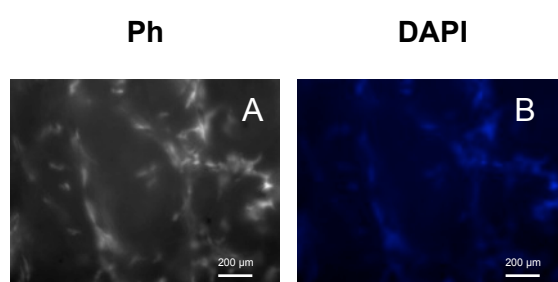


**Figure 44.** DAPI staining of decellularized and lyophilized human pericardia. A) Observation under phase contrast. B) Photograph under fluorescent excitation at UV wavelength.

At a closer inspection using Scanning Electron Microscopy (SEM), it was confirmed that pericardia did not contain any endogenous cell or cell debris. Moreover, pericardial matrix was rich in filaments (**Figure 45**). After the aggressive

chemical decellularization, the pericardium's fibers appeared intact and not damaged. The inner structure of the pericardium was maintained. The filament structures observed corresponded to collagen fibers characteristic of the pericardium's ECM but no endogenous cells were detected.

### SEM of decellularized and lyophilized pericardia

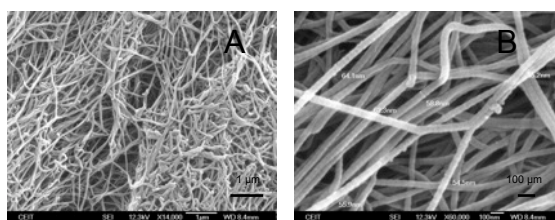


**Figure 45.** Scanning Electron Microscopy photographs of human decellularized pericardium. A) structure of pericardium's filaments. B) closer observation of filaments.

#### 5.3.3. Tailoring of RAD16-I with NanoGold particles

Nanoparticles have been increasingly used in the design of hybrid nanomaterials for diverse fields. Combination of nanosized inorganic particles, such as NanoGold, with materials or biomolecules optimizes the properties of the tailored product. Applications range from electrochemical immunosensors<sup>19</sup> to conductometric immunoassays<sup>20</sup>. In this study, NanoGold particles were combined to the self-assembling peptide RAD16-I to render the scaffold more conductive (**Figure 46**). To attach conductive metal nanocrystals to a peptide is one of the greatest challenges in electronics industry<sup>21</sup>. Herein, the nanofibers tailored were based on pre-synthesized RAD16-I cross-linked to biotin motifs. Taking advantage of the high affinity of biotin to streptavidin, biotin-RAD16-I was mixed with a suspension of streptavidin-NanoGold. After self-assembling at high ionic strength, the scaffold enclosed particles of gold in its tertiary structure (**Figure 46**). Tests of impedance suggested that the tailored scaffold showed higher conductivity than the control scaffold RAD16-I (collaborator group UPC).

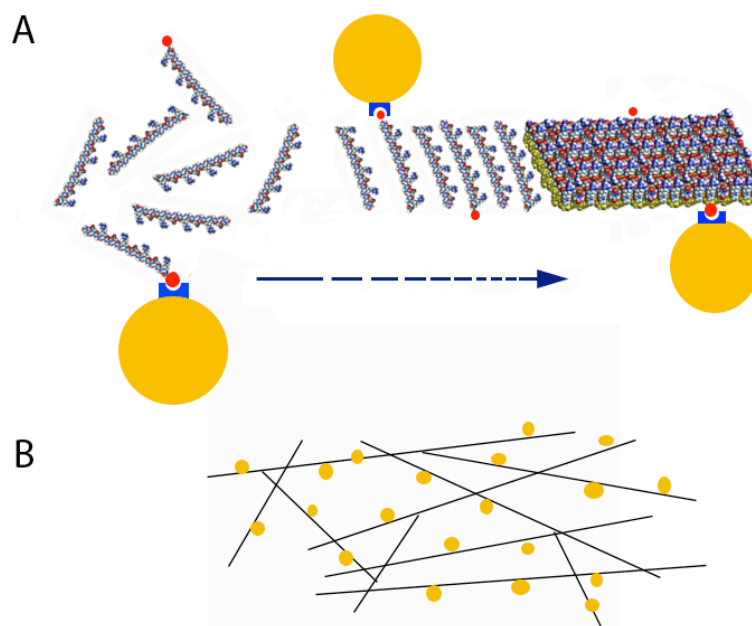


**Figure 46.** Scheme of Biotin-RAD16-I binding to Streptavidin-NanoGold. A) 3D scaffold RAD16-I containing nanoparticles of Gold. B) Nanofibers enclosing NanoGold.

#### 5.3.4. *Implant in vivo of the cardiac smart patch into swine*

There are interesting approaches in literature illustrating examples of reseeded acellular scaffolds as engineered patches for cardiac regeneration<sup>22–24</sup>. The present study includes previous proof-of-concept of each component of the patch *in vitro* and the application of the patch *in vivo* in swine. After analyzing independently all the variables of the implant (characterization of pMATPCs cultured in 2D and 3D, obtaining decellularized human pericardia, conductivity assays of NanoGold-RAD16-I and design of EIS), the pieces were combined and implanted *in vivo* in a porcine model. The final patch consisted in a rectangular decellularized human pericardium (IQS) containing a mixture of GFP-labeled pMATPCs (IGTP) embedded in RAD16-I (IQS) and connected to two Lead Coupler stainless steel electrodes with high increased conductivity using NanoGold particles<sup>5</sup> (IQS and UPC) that were plugged to a measurement system device coated with biocompatible silicone (UPC) (**Figure 47**). The group of Dr. Bayés-Genís conducted the microsurgeries on swine.

Steps for electrode assembling, NanoGold loading and hydrogel RAD16-I with pMATPCs refilling of pericardial scaffold are shown in **Figure 47**. First of all, two stainless steel electrodes were assembled at both extremes of the lyophilized



pericardium. Then, the joints were wetted with RAD16-I rich in NanoGold<sup>5</sup>. Afterwards, the mixture of RAD16-I 0.15% and pMATPCs was loaded into the pericardium, which appeared completely soaked. Culture medium was added at the periphery of the patch to increase the ionic strength and induce hydrogel self-assembling (**Figure 47 E**). At the same time, coronary artery ligation was generated to induce acute MI in swine. Then, the *smart patch* was implanted over the ischemic myocardium (**Figure 47 F-G** and **Figure 48 A-B**). The veterinary connected the cardiac patch to the EIS device coated with biocompatible silicone, which was implanted into the back of the porcine neck. The experiment lasted for 30 days and the data was sent via Zigbee to a computer and monitored online. Cardiac examination upon sacrifice showed myocardial *smart patch* covering the infarct area in all pigs (**Figure 48 D-F**). All in all, further results showed that left ventricular infarction area was considerably smaller in treated pigs (with implanted *smart patch* containing pMATPCs) than in control pigs (with implanted *smart patch* without cells). In addition, our collaborator group (IGTP) observed after sacrifice that cells not only proliferated but also migrated from the *smart patch* into the infarct core and border zones. Interestingly, they found vascularization inside the myocardial *smart patch*. In terms of impedance analysis (UPC), treated and control animals had a similar frequency pattern.

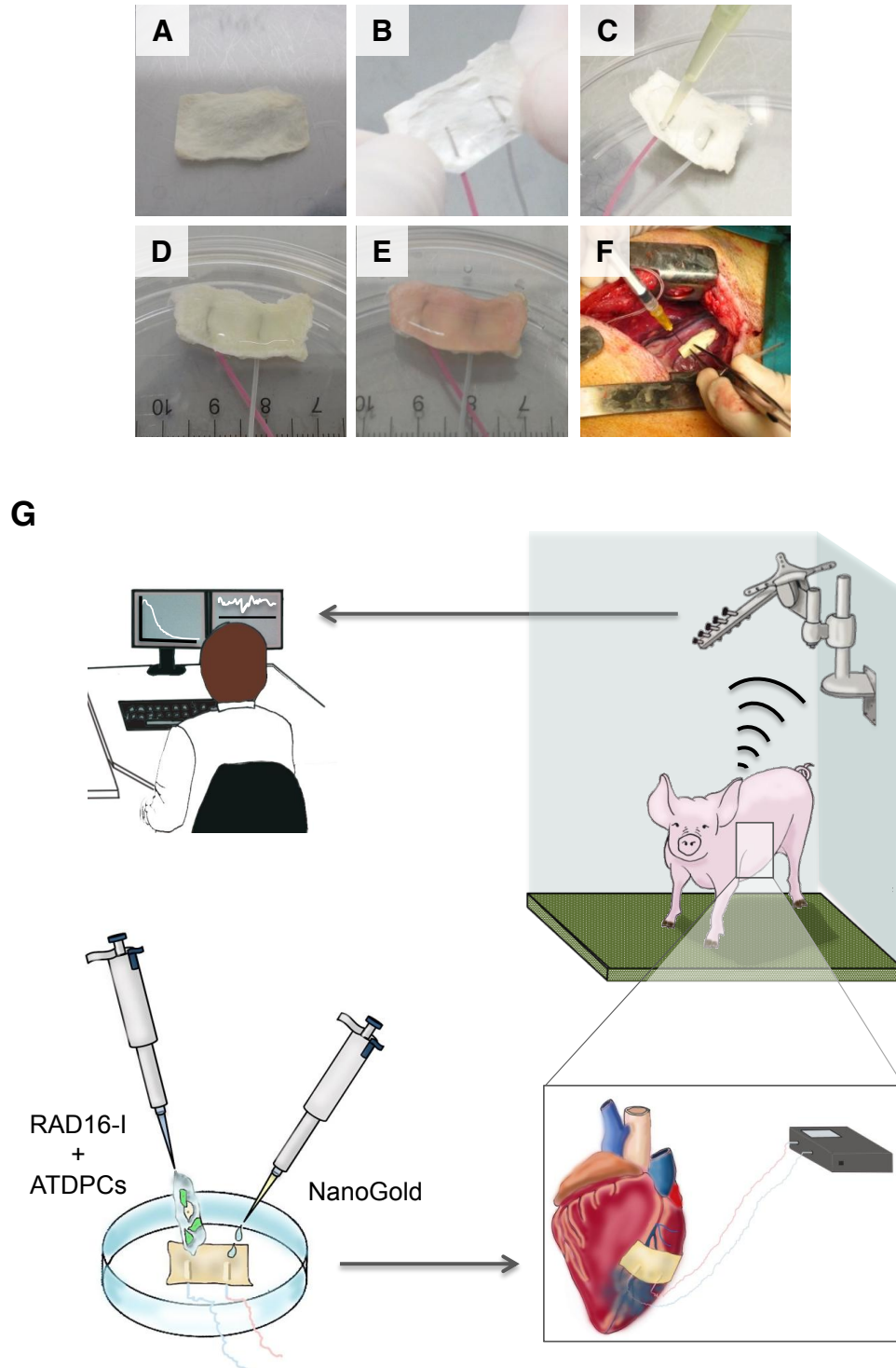


**Figure 47.** Myocardial bioprosthesis assembling and implantation. A) Pericardial scaffold after being decellularized, lyophilized, and sterilized. B) Anchoring of stainless steel electrodes. C) Loading of RAD16-I rich in NanoGold in the joints. D) Loading of the mixture RAD16-I and pMATPCs. E) Addition of culture medium. F) Implantation of a myocardial bioprosthesis with surgical glue over an infarcted pig heart. G) Schematic illustration showing the main parts of the implemented EIS measurement system: an electronic device connected to the myocardial bioprosthesis which enables impedance measurement of the infarcted tissue, a wireless link to transmit impedance data via a transmitting aerial and a computer to log, process and display data.

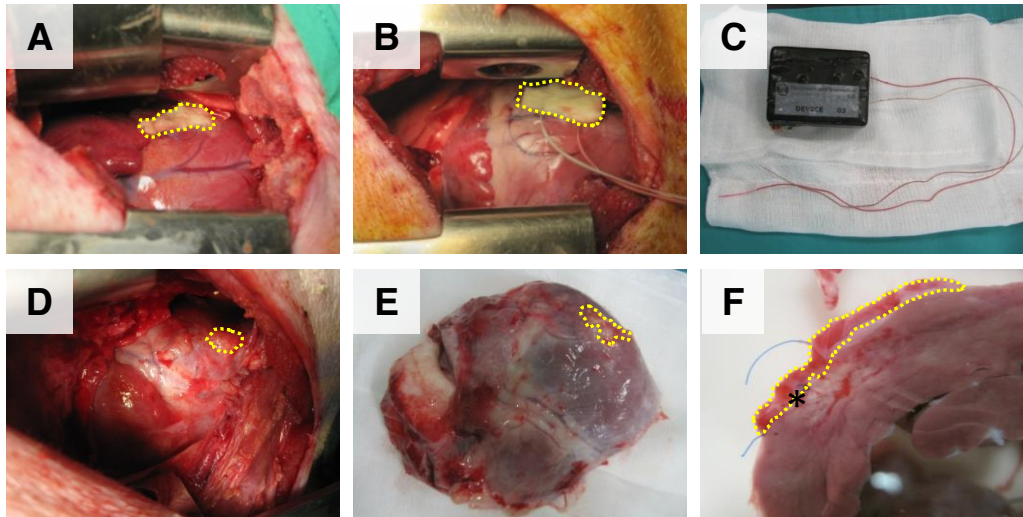


**Figure 48.** Macroscopic appearance and histological examination of myocardial bioprostheses in porcine hearts. A) Myocardial bioprosthesis implanted on the porcine infarcted myocardium. B) Myocardial bioprosthesis with anchored stainless steel electrodes implanted in a heart. C) Implantable system sealed with biocompatible silicone. D) Bioprosthesis placed over the infarcted myocardium in a control pig at sacrifice. E) Myocardial bioprosthesis residues remained 1 month post-implantation over the explanted heart surface. F) Transversal heart section of a treated pig with the attached bioprosthesis indicated.

#### 5.4. Discussion

Cardiac tissue engineering aims to restore damaged myocardial tissue. Many efforts focus on designing a suitable biomaterial to engraft cells onto the post-infarction scar and improve cardiac regeneration. Scaffolds should mimic the native extracellular matrix (ECM), which guides cellular attachment, survival, migration, proliferation and differentiation<sup>25</sup>. An interesting example of bioprosthesis is the clinical trial called MAGNUM (Myocardial Assistance by Grafting a New bioartificial Upgraded Myocardium), which is based on a biodegradable 3D collagen patch seeded with bone marrow cells<sup>26</sup>. Other approaches combine adipose-derived stem cells seeded on collagen 3D scaffolds with ventricular constraint devices (CorCap)<sup>27</sup>. Indeed, the cardiac connective tissue is mainly composed of collagen and this is why many strategies focus on designing biocompatible patches that mimic the *in vivo* cardiac environment. In the present study, the idea arose to use natural collagen matrices, such as pericardium, to create a bioprosthesis hosting stem cells. Since 1963, pericardium has been used to replace aortic valve and so, treat aortic insufficiency. Fifty years ago, researchers suspected that endogenous tissue could be “recycled” and used as bioscaffolds for cardiac therapy, which is the base of cardiac tissue engineering defined in the 1980’s. The use of pericardium as biological

scaffold for autologous engraftment has many advantages including ready availability, ease of handling and low cost<sup>28</sup>. Herein, human pericardium was used as a macro-scaffold of the *smart patch* because of its mechanical properties: relatively thick and elastic membrane that can easily host exogenous cells thanks to its porosity. Although pericardial matrix is not an exact match for ventricular myocardium matrix, the pericardium is thought to influence myocardial contraction and epicardial vessel properties. Despite the structural support that the pericardium provides to the heart, it is routinely unsutured, cut or even removed during cardiothoracic surgery without any adverse consequence. Thus, this work describes a successful protocol to decellularize human pericardia, which were obtained from consenting patients undergoing cardiothoracic surgery. After extensive detergent treatment, human pericardia appeared completely washed out of any blood remain. By visual inspection, the membranes looked soft and white due to the high content of collagen fibers in the pericardial ECM. The decellularization protocol was successfully established. The collagen scaffolds were free of endogenous cell debris (**Figure 44**) and very rich in filaments (**Figure 45**). Indeed, natural acellular ECM-based scaffolds seem to be excellent candidates for allograft tissue engineering<sup>13</sup>. Some decellularized allogenic medical products (most of them derived from animals or cadavers) are now being commercialized for use in human patients<sup>29</sup>. Nevertheless, the *condicio sine qua non* herein was that the membranes had to be acellular to avoid any inflammatory response after xenotransplantation of the *smart patch* into swine myocardium.

RAD16-I hydrogel provides suitable nanostructural and biochemical properties to culture cells embedded into it. This self-assembling peptide can promote growth and proliferation of a wide variety of cells. Indeed, it creates a favorable milieu for cell adhesion, spreading, migration, growth and differentiation<sup>30</sup>. Three-dimensional cultures of pMATPCs in RAD16-I showed that porcine adult stem cells could easily be embedded in the peptide scaffold. Cells behaved similarly in 3D and in 2D cultures. No apparent differences in gene profile or protein expression were observed although the expression of cardiac proteins in cells cultured in RAD16-I seemed to be higher than in cells in 2D. Porcine MATPCs slightly enhanced their cardiogenic potential in 3D cultures. Therefore, it was assumed that *in vitro* 3D constructs of pMATPCs in RAD16-I hydrogels would be similar to 3D cultures of the same mixture inside pericardial membranes. Thus, pericardia were lyophilized in PBS solution to entrap salts into the membrane. The salts increased the ionic strength and promoted the self-assembling of RAD16-I nanofibers when the peptide-

cell mix solution was loaded in the pericardium. Therefore, the hydrogel created a micro-3D environment for the cells and the pericardium offered a macro-support membrane to the mixture. The combination of pMATPCs and RAD16-I generated an optimal cellular 3D network inside the scaffold. Indeed, Congo red staining showed that the nanofibers created  $\beta$ -sheet tapes in between the pericardial fibers, entrapping the cells inside the scaffold. The membrane appeared to be hydrophilic and cell-friendly.

In summary, proof of concept has been established for the use of a new myocardial *smart patch* for cardiac repair. Porcine MATPCs may be promising candidates for cardiac regeneration pre-clinical studies. The pericardium-based patch could be implanted with minimally invasive methods to promote neovascularization and progenitor cell homing into damaged myocardium *in vivo*, with the EIS system serving as an online audit of scar evolution. Novel myocardial patch with online monitoring of cardiac repair may accelerate clinical translation. The engineered patch seemed to improve the cardiac regeneration. The results of this section have been included in a recently submitted manuscript to a peer-reviewed journal.

### 5.5. Concluding remarks

- Human pericardium was successfully decellularized using an exhaustive chemical method based on ionic detergents. An appropriate protocol was established to eliminate pericardial endogenous cells without disrupting the structure of the internal pericardial fibers.
- NanoGold tailoring of RAD16-I nanofibers seemed to increase the conductivity of the scaffold, which would help the propagation of electrical current from resident cardiac cells to the engrafted pMATPCs and improve the global syncytium. Therefore, human pericardium was used as a highly conductive biological macro-scaffold for the *smart patch*.
- Porcine MATPCs had a similar protein expression profile in 2D and in 3D cultures based on RAD16-I hydrogel. Nevertheless, detection of high levels of protein Connexin 43 in 3D constructs suggested that the cardiogenic potential was slightly increased in cells cultured in 3D.
- The designed *smart patch* was successfully implanted *in vivo* and seemed to promote cell migration to the infarcted area in swine. The technique

proposed in the current project was an applicable cell-delivery scaffold to improve cardiac regeneration by release of pMATPCs into the infarcted area with an online audit of scar evolution based on EIS.

### 5.6. References

1. Vunjak-Novakovic, G., Lui, K. O., Tandon, N. & Chien, K. R. Bioengineering heart muscle: a paradigm for regenerative medicine. *Annu. Rev. Biomed. Eng.* **13**, 245–67 (2011).
2. Clemmensen, P., Loumann-Nielsen, S. & Sejersten, M. Telemedicine fighting acute coronary syndromes. *J. Electrocardiol.* **43**, 615–8 (2010).
3. Shah, B. R. *et al.* Secondary prevention risk interventions via telemedicine and tailored patient education (SPRITE): a randomized trial to improve postmyocardial infarction management. *Circ. Cardiovasc. Qual. Outcomes* **4**, 235–42 (2011).
4. De Waure, C., Cadeddu, C., Gualano, M. R. & Ricciardi, W. Telemedicine for the reduction of myocardial infarction mortality: a systematic review and a meta-analysis of published studies. *Telemed. J. E. Health.* **18**, 323–8 (2012).
5. Sanchez, B. *et al.* Towards on line monitoring the evolution of the myocardium infarction scar with an implantable electrical impedance spectrum monitoring system. *34th Annu. Int. Conf. IEEE Eng. Med. Biol. Soc.* **2012**, 3223–6 (2012).
6. Casas, O. *et al.* In vivo and in situ ischemic tissue characterization using electrical impedance spectroscopy. *Ann. N. Y. Acad. Sci.* **873**, 51–8 (1999).
7. Salazar, Y., Bragos, R., Casas, O., Cinca, J. & Rosell, J. Transmural versus nontransmural in situ electrical impedance spectrum for healthy, ischemic, and healed myocardium. *IEEE Trans. Biomed. Eng.* **51**, 1421–7 (2004).
8. Sanchez, B., Schoukens, J., Bragos, R. & Vandersteen, G. Novel estimation of the electrical bioimpedance using the local polynomial method. Application to in vivo real-time myocardium tissue impedance characterization during the cardiac cycle. *IEEE Trans. Biomed. Eng.* **58**, 3376–85 (2011).
9. Prat-Vidal, C. *et al.* Online monitoring of myocardial bioprosthesis for cardiac repair. submitted (2013).
10. Ock, S.-A., Jeon, B.-G. & Rho, G.-J. Comparative characterization of porcine mesenchymal stem cells derived from bone marrow extract and skin tissues. *Tissue Eng. Part C* **16**, 1481–1491 (2010).
11. Rigol, M. *et al.* Effects of adipose tissue-derived stem cell therapy after myocardial infarction: impact of the route of administration. *J. Card. Fail.* **16**, 357–66 (2010).

12. Wang, X. & Moutsoglou, D. Osteogenic and adipogenic differentiation potential of an immortalized fibroblast-like cell line derived from porcine peripheral blood. *In Vitro Cell. Dev. Biol. Anim.* **45**, 584–91 (2009).
13. Chen, F., Yoo, J. J. & Atala, a. Acellular collagen matrix as a possible “off the shelf” biomaterial for urethral repair. *Urology* **54**, 407–10 (1999).
14. Lichtenberg, A. *et al.* In vitro re-endothelialization of detergent decellularized heart valves under simulated physiological dynamic conditions. *Biomaterials* **27**, 4221–9 (2006).
15. Lichtenberg, A., Breyman, T., Cebotari, S. & Haverich, A. Cell seeded tissue engineered cardiac valves based on allograft and xenograft scaffolds. *Prog. Pediatr. Cardiol.* **21**, 211–217 (2006).
16. Seif-Naraghi, S. B., Salvatore, M. a, Schup-Magoffin, P. J., Hu, D. P. & Christman, K. L. Design and characterization of an injectable pericardial matrix gel: a potentially autologous scaffold for cardiac tissue engineering. *Tissue Eng. Part A* **16**, 2017–27 (2010).
17. Seif-Naraghi, S. B., Horn, D., Schup-Magoffin, P. J. & Christman, K. L. Injectable extracellular matrix derived hydrogel provides a platform for enhanced retention and delivery of a heparin-binding growth factor. *Acta Biomater.* **8**, 3695–703 (2012).
18. Gilbert, T. W., Sellaro, T. L. & Badylak, S. F. Decellularization of tissues and organs. *Biomaterials* **27**, 3675–83 (2006).
19. Su, B., Tang, D., Li, Q., Tang, J. & Chen, G. Gold-silver-graphene hybrid nanosheets-based sensors for sensitive amperometric immunoassay of alpha-fetoprotein using nanogold-enclosed titania nanoparticles as labels. *Anal. Chim. Acta* **692**, 116–24 (2011).
20. Liang, K.-Z., Qi, J.-S., Mu, W.-J. & Liu, Z.-X. Conductometric immunoassay for interleukin-6 in human serum based on organic/inorganic hybrid membrane-functionalized interface. *Bioprocess Biosyst. Eng.* **32**, 353–9 (2009).
21. Zhang, S. Fabrication of novel biomaterials through molecular self-assembly. *Nat. Biotechnol.* **21**, 1171–1178 (2003).
22. Galvez-Monton, C., Prat-Vidal, C., Roura, S., Soler-Botija, C. & Bayes-Genis, A. Ingenieria tisular cardiaca y corazon bioartificial. *Rev. Esp. Cardiol.* **820**, (2013).
23. Wang, B. *et al.* Fabrication of cardiac patch with decellularized porcine myocardial scaffold and bone marrow mononuclear cells. *Natl. Institutes Heal.* **94**, 1100–1110 (2011).
24. Ota, T., Gilbert, T. W., Badylak, S. F., Schwartzman, D. & Zenati, M. A. Electromechanical characterization of a tissue-engineered myocardial patch derived from extracellular matrix. *J. Thorac. Cardiovasc. Surg.* **133**, 979–85 (2007).

25. Midwood, K. S., Williams, L. V. & Schwarzbauer, J. E. Tissue repair and the dynamics of the extracellular matrix. *Int. J. Biochem. Cell Biol.* **36**, 1031–7 (2004).
26. Chachques, J. C. *et al.* Myocardial Assistance by Grafting a New Bioartificial Upgraded Myocardium (MAGNUM trial): clinical feasibility study. *Ann. Thorac. Surg.* **85**, 901–8 (2008).
27. Shafy, A. *et al.* Development of cardiac support bioprostheses for ventricular restoration and myocardial regeneration. *Eur. J. Cardiothorac. Surg.* **43**, 1211–9 (2013).
28. Duran, C. M. G., Gometza, B., Kumar, N., Gallo, R. & Martin-Duran, R. Aortic valve replacement with freehand autologous pericardium. *J. Thorac. Cardiovasc. Surg.* **110**, 511–6 (1995).
29. Choi, J. S. *et al.* Decellularized extracellular matrix derived from human adipose tissue as a potential scaffold for allograft tissue engineering. *J. Biomed. Mater. Res. A* **97**, 292–9 (2011).
30. Semino, C. E. Self-assembling Peptides: From Bio-inspired Materials to Bone Regeneration. *J. Dent. Res.* **87**, 606–616 (2008).



*Conclusions*



## **CONCLUSIONS**

1. Direct cell-cell and indirect cell-RAD16-I hydrogel (through ECM and protein decoration of the nanofibers) interactions were involved in cell survival of hNDFs in 3D cultures. Cells secreted ECM proteins that conditioned the synthetic scaffold and allowed hNDFs to support themselves independently of the presence of serum in the medium.
2. Human NDFs only expressed embryonic-related proteins such as Brachyury, FoxA2 and Gata4 when cultured in RAD16-I hydrogels suggesting that cells underwent a mesenchymal potentiation. Matrices based on Collagen I did not offer the neutrality given by RAD16-I hydrogels, which was the signal for the cells to acquire primitive properties.
3. The mesenchymal phenotype acquisition of hNDFs embedded in RAD16-I hydrogels was spontaneous and independent of the composition of the culture medium (presence or absence of FBS and PDGF). The peptide 3D environment induced hNDFs to interact, contract the construct and express proteins characteristic of the early embryonic development.
4. Adipogenic induction medium promoted the differentiation of hNDFs with MSCs properties into adipocyte-like cells when cultured in RAD16-I hydrogels. The peptide scaffold, which contained functional hNDFs-derived adipocytes able to deposit lipid droplets, mimicked a tissue-like structure similar to the *in vivo* ECM environment.
5. Human NDFs, cultured in RAD16-I hydrogels and induced with cardiogenic medium, acquired cardiac progenitor-like phenotype by expressing genes and proteins such as Tbx5.
6. Cardiac differentiation of hiPSCs cultured in 2D with and without AA appeared to be a stepwise process in terms of gene and protein expression. First, pluripotent cells differentiated into mesendodermal cells (day 3 to 6); second, mesodermal cells committed to pre-cardiac cells (day 6 to 10); third, hiPSCs went through an early cardiac progenitor stage (day 10 to 15); and finally, cells acquired late cardiac progenitor properties (day 15 to 25).
7. Gene expression of cardiac markers was significantly higher in cells treated with AA than without, which suggests that AA accelerated and improved the cardiac commitment of hiPSCs in 2D cultures.
8. The high variability in beating frequency among hiPSCs differentiated in 2D cultures indicated different stages of phenotype of the CMs derived from them and thus, ongoing cardiac maturation.

9. Human iPSCs cultured in 3D up-regulated and retained expression of Oct4 despite the presence or absence of AA for at least 10 days. High levels of the target gene indicated that hiPSCs displayed an increased level of differentiation.
10. Gene expression profiles showed that hiPSCs cultured in 3D with and without AA up-regulated  $10^5$ -fold more genes related to early differentiation (FoxA2) and early cardiac progenitor (Tbx5) than cells cultured in 2D.
11. The suggested 3D protocol offered a strong pre-differentiation of hiPSCs into cardiomyocyte-like cells with high potential to commit into cardiac lineage.
12. Human iPSCs embedded in RAD16-I did not create contracting syncytia, which might be crucial for *in vivo* engraftment purposes to not compromise the electromechanical properties of the heart.
13. Human pericardium was successfully decellularized using an exhaustive chemical method based on ionic detergents. An appropriate protocol was established to eliminate pericardial endogenous cells without disrupting the structure of the internal pericardial fibers.
14. NanoGold tailoring of RAD16-I nanofibers seemed to increase the conductivity of the scaffold, which would help the propagation of electrical current from resident cardiac cells to the engrafted pMATPCs and improve the global syncytium. Therefore, human pericardium was used as a highly conductive biological macro-scaffold for the *smart patch*.
15. Porcine MATPCs had a similar protein expression profile in 2D and in 3D cultures based on RAD16-I hydrogel. Nevertheless, detection of high levels of protein Connexin 43 in 3D constructs suggested that the cardiogenic potential was slightly increased in cells cultured in 3D.
16. The designed *smart patch* was successfully implanted *in vivo* and seemed to promote cell migration to the infarcted area in swine. The technique proposed in the current project was an applicable cell-delivery scaffold to improve cardiac regeneration by release of pMATPCs into the infarcted area with an online audit of scar evolution based on EIS.

## Appendix



# *Self-assembling peptide scaffolds as innovative platforms for drug and cell delivery systems in cardiac regeneration*

**Veronica A. C. Puig-Sanvicens & Carlos E. Semino**

## **Drug Delivery and Translational Research**

An Official Journal of the Controlled Release Society

ISSN 2190-393X

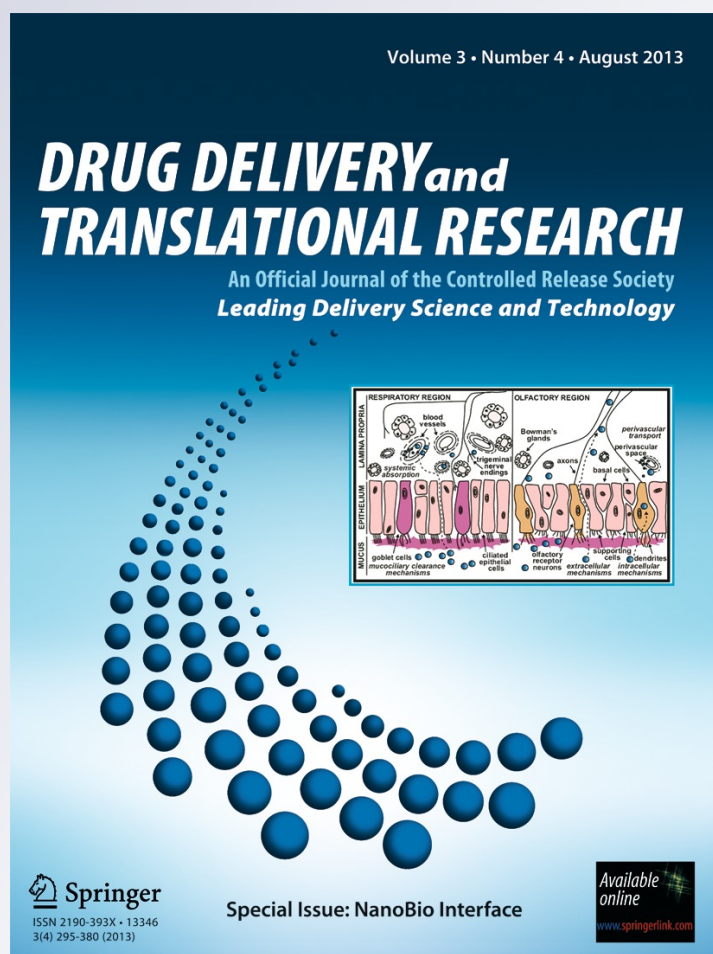
Volume 3

Number 4

Drug Deliv. and Transl. Res. (2013)

3:330-335

DOI 10.1007/s13346-012-0125-8



**Your article is protected by copyright and all rights are held exclusively by Controlled Release Society. This e-offprint is for personal use only and shall not be self-archived in electronic repositories. If you wish to self-archive your article, please use the accepted manuscript version for posting on your own website. You may further deposit the accepted manuscript version in any repository, provided it is only made publicly available 12 months after official publication or later and provided acknowledgement is given to the original source of publication and a link is inserted to the published article on Springer's website. The link must be accompanied by the following text: "The final publication is available at [link.springer.com](http://link.springer.com)".**



# Self-assembling peptide scaffolds as innovative platforms for drug and cell delivery systems in cardiac regeneration

Veronica A. C. Puig-Sanvicens ·  
Carlos E. Semino

Published online: 8 January 2013  
© Controlled Release Society 2013

**Abstract** Today, the use of biomaterials in many biomedical platforms is becoming increasingly popular due to their high diversity, infinite mimicking capacity, and emerging functions. Applications currently cover diverse areas in biomedicine including systems for cell isolation, expansion and maintenance, platforms for drug and cell delivery, scaffolds for tissue engineering, tissue regeneration and repair, cancer therapy, etc. Biomaterials in general can be: (1) natural in origin such as many proteins from the extracellular matrix, natural polysaccharides or scaffolds presented in a blood clot or (2) synthetic, including polymers, ceramics, or peptides. In this review, we focus on the use of self-assembling peptide scaffolds as an innovative and reliable strategy to obtain platforms for cell and drug delivery to injured or diseased tissues and organs. This type of material is molecular by design and it develops spontaneously into nanofiber scaffolds with multiple uses. In particular, examples are given for applications in the area of cardiac repair and regeneration.

**Keywords** Self-assembling peptide scaffold · Drug delivery · Cell delivery · Cardiac regeneration

## Introduction

Tissue engineering (TE) combines biomaterials with cell biology in order to generate biological substitutes for damaged organs or tissues. By definition, an engineered tissue includes some or all of these: cells, chemical factors, and a biomaterial to provide physical support [1]. Thus, TE has

been shown to be a powerful tool to replace or rebuild damaged tissues and organs [2]. During the past decades, several types of biomaterials have been tested to elucidate the best 3D scaffold for TE. These artificial microenvironments can be divided into two groups depending on their origin: natural (collagen [3], alginate, matrigel [4], fibrin, etc.) and synthetic (polyglycolic acid, polylactic acid, poly(lactic-co-glycolic acid) [5], poly lactide-co-glycolide, poly(ethylene glycol), etc.) [5, 6]. Moreover, polymer tensile strength can be adjusted for hard or soft tissue regeneration therapy [7]. Rapidly, researchers focused on using them as cell carriers for different applications [8]. Despite their promising characteristics, major drawbacks had to be overcome: natural materials are undefined and instructive structures whereas synthetic ones are not sufficiently bioactive. Indeed, an interesting approach is to create “smart” synthetic biomaterials in order to render them more cell-friendly.

Tissue engineering of vascular grafts and valves restoration can be achieved by transplanting autologous cells into biocompatible and biomechanically stable scaffolds, which represents an advantage over the classical use of prostheses, allografts, or nonliving xenografts. Thus, since blood is in intimate contact to non-adequate surfaces due to the poor endothelial layer development the common issues related to this classical approach include thrombosis, blood thinner related hemorrhage, aneurysm, etc. For instance, problems associated with biological reactions at the blood–material or tissue–material interface have been detected when polymeric scaffolds, such as Dacron or expanded polytetrafluoroethylene, are used to obtain vascular grafts [9–12]. Thus, a new approach is to develop vascular grafts, and eventually bioengineered valves, combining human cells (autologous) and new biomaterials such as biodegradable polyglycolic acid–poly-L-lactide and polyglycolic acid– $\epsilon$ -caprolactone matrices, with good engraftment, biomechanical properties, and biocompatibility performance [13].

V. A. C. Puig-Sanvicens · C. E. Semino (✉)  
Department of Bioengineering, IQS-School of Engineering,  
Ramon Llull University (IQS-URL), Via Augusta 390,  
08017 Barcelona, Spain  
e-mail: semino.c@gmail.com

Although cardiovascular tissue engineering is an extensive field in this review, we specifically focus on tailored biomaterials designed to restore cardiac tissue after myocardial infarction (MI) [14]. Heart failure is one of the main causes of mortality in the world and currently the only solution for end-stage patients is cardiac transplantation. For example, in 2005 the American Heart Association reported 850,000 cases of MI in the USA and US\$170 billion was invested in heart disease management that year [15]. In the past decade, various strategies for cardiac reparative medicine have been investigated, from TE to stem cell-based therapy [16]. Initially, researchers attempted to inject cells directly into the damaged tissue but the cellular loss was greater than 85 % and few of the remaining cells survived. As a result, injectable scaffolds releasing cells, drugs, or growth factors (GFs) have potential for cardiac regenerative therapy [17]. The goal is to increase survival of engrafted cells, guide cell differentiation, and migration. To accomplish it, scaffolds should be noncytotoxic, biodegradable, porous, permeable, and flexible [18]. First attempts of drug and cell delivery for MI repair [19] were based on tailoring natural and synthetic biomaterials with the integrin adhesion peptide sequence arginine–glycine–aspartic acid (RGD), GFs [20], hormones, and other proteins (Fig. 1). Furthermore, GFs are worthy of further attention because they are involved in cell survival, growth, differentiation, mobility, and communication processes. Therefore, controlled release of GFs to the target tissue can be via diffusion, cell-mediated proteolysis or in response to a mechanical stimulus [21]. For instance, the gold standard collagen, which has convenient mechanical properties, has been conjugated with polysaccharides [22–24], RGD [25], GFs (vascular endothelial growth factor (VEGF) [26]), and

specific antibodies [27]. Additional examples reported in the literature are based on gelatin [28], alginate (functionalized with RGD [29], extracellular matrix peptides [30], placental GF [31], insulin-like GF-1 [32], hepatocyte GF [32]), and chitosan [33]. Other attempts include b-fibroblast GF-loaded NIPAAm thermosensitive hydrogels [34] and modified PEG [34, 35]. All of these scaffolds have been seeded with cells in order to promote cardiac regeneration (Table 1).

Finally, a novel and promising strategy combines self-assembling peptides with functional motifs. By definition, molecular self-assembly is the spontaneous organization of molecules under thermodynamic equilibrium conditions into regular structures linked by noncovalent interactions. Indeed, oligopeptides self-assemble at physiological conditions into nanofibers recreating biological *in vivo* processes [36]. The peptidic chains form  $\beta$ -sheet structures due to internal periodic repeats of alternating ionic hydrophilic and hydrophobic amino acids [37]. There are three different types of self-assembling peptides (SAPs): type I (form  $\beta$ -sheet structures), type II (form both  $\beta$ -sheet and  $\alpha$ -helix), and type III (form monolayers on surfaces). The interactions are weak and noncovalent. Self-assembling peptides have been widely used for cell delivery and because of their neutrality, they appeared to be suitable scaffolds for cell differentiation and dedifferentiation [38]. Nevertheless, biomaterial science has advanced with the design of nanofibers to render the scaffold more biomimetic. SAPs can be easily modified by chemical reactions in order to integrate biological motifs within them [39]. This technology has been applied in neural regeneration [40], chondrogenesis [37, 38], vascularization [41], etc. These hydrogels have been modified with dextran macromolecules [42], laminin and collagen motifs [41], integrin-binding sequence, laminin receptor binding sequence, and heparin binding sequence [43]. Interestingly, self-assembling materials have been shown to be an excellent vehicle for therapeutic drug delivery in cancer [16, 17], female birth control, and for pain relief [44]. Whereas many other novel polymeric biomaterials have been developed for drug delivery (micelles and vesicles), hydrogel delivery vehicles based on SAPs (RADA16, peptide–amphiphiles [45], MAX1 and MAX8 [39], and Q11 [46]) are currently used in tissue regeneration studies. Here, we review some examples of tailored self-assembling peptides, most based on RADA16-I, for cardiac regeneration therapy (Table 1). RADA16 was the first SAPs commercially available (PuraMatrix™) and that is why it has been widely used in regeneration studies. Indeed, RADA16 appeared to be a more cell-friendly environment for endothelial cells (ECs) than other SAPs (KFE-8 and KLD-12) [47]. RADA16 is hydrophilic and can be formulated in water. We believe that this specific SAP has the potential to be an excellent “smart” synthetic biomaterial.

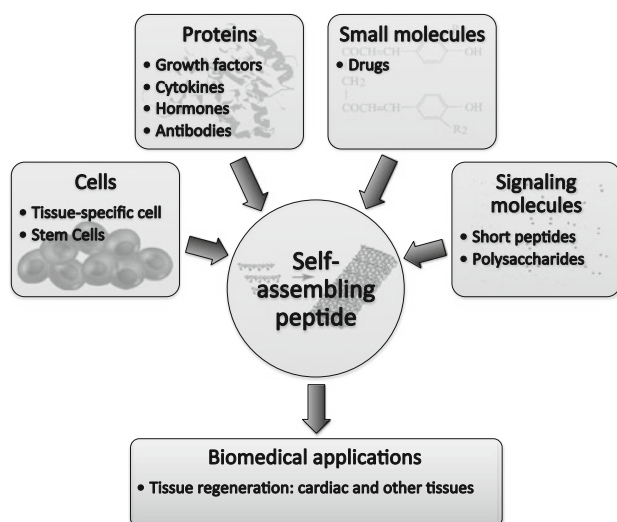


**Fig. 1** Main drug and cell delivery systems using self-assembling peptide scaffold platform

**Table 1** Biomaterials used to restore cardiac function after myocardial infarction

	Biomaterial platform	Biological activity	References
Natural	Peptide-modified chitosan-collagen hydrogel	Cardiac cell delivery onto myocardial infarcts	[22]
	Collagen-glycosaminoglycans	Mesenchymal stem cell delivery onto myocardial infarcts	[23]
	Collagen-chitosan composite hydrogel	Thymosin $\beta$ 4 release promotes epicardial cell migration and angiogenesis	[24]
	Collagen myocardial patch membranes	Collagen-binding VEGF release accelerates heart healing	[26]
	Alginate with immobilized RGD peptides	Promotes cardiac regeneration	[29]
	Alginate containing IGF-1 and HGF	Enhances myocardial repair	[32]
	Chitosan hydrogel	Promotes stem cell engraftment, survival and homing in ischemic cardiac tissue	[33]
Synthetic	Cell-responsive PEG-hydrogel	Enhances cardioprogenitor differentiation	[65]
	Self-assembling peptide (SAP) nanofibers	Promotes intramyocardial angiogenesis	[49]
	SAP nanofibers	Improves cardiac function	[50]
	SAP nanofibers	Intramyocardial delivery of PDGF improves postinfarction ventricular function	[54]
	VEGF associated SAP nanofibers	Improves cardiac function	[52]
	Biotinylated SAP nanofibers	Myocardial IGF-1 delivery improves cell therapy for myocardial infarction	[57]
	SAP nanofibers	Skeletal myoblast transplantation in infarcted myocardium.	[59]

#### Strategies to restore myocardial infarction using designed self-assembling peptides

Cell therapy is crucial in cardiac repair attempts. Indeed, massive cell death occurs after infarction leading to a necrotic area that generates a scar. Cardiac progenitor cells (CPCs) are tissue-specific progenitors that reside in the heart and are responsible for its regeneration. Thus, cardiac tissue self-regenerates although it does so very slowly [48]. It is thought that resident CPCs require a stimulus to migrate to the damaged area. Attempts have been made to accelerate this natural regeneration led by the migration of CPCs and restoration of cardiomyocytes loss and vascular structures in the infarcted zone. The major concern is that few transplanted cells can survive injection into the myocardium probably due to paracrine effects, transdifferentiation, or high oxidative stress. A solution would be to design a beneficial scaffold that recruits endogenous cells and induces survival of the engrafted cells in the injected scaffold.

Microenvironments themselves, without any coupled biological signal, can promote vascular cell recruitment in the myocardium. Indeed, ECs are able to invade the injected scaffold, self-organize, and mature inside it. Although it is not well understood, ECs seem to somehow preserve cardiac function after MI [47, 48]. Moreover, it has been observed that potential myocyte progenitors can populate the engrafted microenvironment. In spite of their innate potential to attract cells of the peptide scaffold, the combination of the self-assembling microenvironment with exogenous cells (neonatal cardiac myocytes or embryonic stem cells) increases the recruitment of

endogenous cardiac progenitors and promotes the spontaneous differentiation into myocytes. It is thought that nonsurviving injected cardiomyocytes release recruitment signals for endogenous cardiac progenitors [49].

Nevertheless, it is strongly believed that the attachment of functional motifs to the nanofibers of the engrafted scaffold combined with cell delivery could have a beneficial effect on cardiac regeneration after MI. The best-established system involves the attachment of the cell adhesion motif RGD. Thus, modified self-assembling peptide RADA16 presenting RGDSP (adhesion sequence) promotes survival, growth, and differentiation of encapsulated marrow-derived cardiac stem cells. This is an excellent approach for stem cell transplantation into damaged tissue [50]. Another example describes the co-assembly of the peptide hydrogel Q11 to ligands RGDS and IKVAV for endothelial cells and vascularization [46].

Furthermore, the most promising studies combine self-assembling peptides with GFs, which have crucial function during cardiogenesis (fibroblast GF (FGF) [51], VEGF [52], angiopoietin-1, and platelet-derived GF (PDGF) [48, 53]). The major concern is to control the speed and concentration at which the GFs are released to obtain a sustained and prolonged delivery into the myocardial scar. Indeed, some GFs delivered systemically could have negative side effects on other organs [54]. It has been proven that RADA16 adsorbs GFs through noncovalent interactions. For instance, VEGF combined with RADA16-heparin-binding domain induces angiogenesis, recruitment, and differentiation of endogenous cardiac stem cells into cardiomyocytes [52]. Indeed, there seems to be a cross-talk between ECs and

myocytes through a VEGF-dependent mechanism that promotes an endothelium specific prosurvival effect on myocytes [55].

In vivo assays have proven that GF bound to SAPs are controllably released to the infarcted myocardium for up to 14 days. Indeed, PDGF-BB, which plays a key role in cardiovascular development, has been successfully linked to RADA16-II. Hsieh et al. have demonstrated that the endothelium protects cardiomyocytes through the PDGF-BB/PDGFR- $\beta$  pathway. Furthermore, PDGF seems to be a potential dose-dependent cardiomyocyte survival factor [48, 53].

Another GF widely used in cardiac regeneration with extraordinary results is the insulin-like growth factor 1 (IGF-1), which seems to induce cardiomyocyte and cardiac stem cell growth as well as survival. Indeed, the overexpression of this GF somehow inhibits myocyte apoptosis and ventricular dilation after infarction. IGF-1 is not only a survival factor but it also promotes differentiation of engrafted embryonic stem cells into myocardium. The main disadvantage is its short retention time in the target tissue because of its small size and rapid diffusion through tissues. An important advance in the field came when a nanofiber-mediated IGF-1-delivery was combined with CPC therapy to improve the recovery of myocardial function after infarction. Thus, CPCs expose IGF-1 receptors, which promote cell survival and growth. Self-assembling peptide nanofibers can be tethered to IGF-1 (NF-IGF-1) using the complex biotin–streptavidin in order to prolong its release to the myocardium. Injection of NF-IGF-1 with CPCs to the border zone of an induced infarcted model in rats promoted CPC division and avoided cell death caused by reactive oxygen species due to the high oxidative stress in the ischemic myocardium. The data suggested that injected cells released cytokines that activated resident progenitors to migrate and regenerate the infarcted heart. Both delivered and resident CPCs underwent lineage commitment and rapidly differentiated into myocytes and coronary vessels across the damaged area. Researchers concluded that the combination therapy was more regenerative (increased recovery of myocardial structure and ventricular performance) than implanting only CPCs or NF-IGF-1 [56]. Similarly, Davis et al. tethered IGF-1 to RADA16-II and created a “biotin sandwich” (biotin-IGF+streptavidin+biotin scaffold) aimed to deliver the GF specifically to local myocardial infarction. Therefore, streptavidin residues served as a bridge between the self-assembling peptide and the GF, leaving the IGF-1 tails available for the IGF-1 receptors of the engrafted neonatal cardiomyocytes. Functionalized scaffolds promoted cell survival, growth, and the expression of cardiac maturation markers. At short term, tethered IGF-1 seemed to prevent post-infarction ventricular systolic dysfunction and dilation. Experiments in vivo demonstrated that local delivery of IGF-1 increased cardiomyocyte growth

and maturation in induced myocardial infarction in rats. Moreover, it was speculated that embedded cells secreted proteases that degraded the peptide nanofibers allowing the local release of IGF-1 by diffusion. Only the combination of tethered IGF-1 scaffold together with cardiomyocytes protected cardiac function after MI. The growth factor had a beneficial effect on the injected cells (due to physical proximity) and on the surrounding resident myocytes (due to diffusion). This technique achieved improvement in systolic function after infarction and reduction of ventricular dilation [57]. Related to these experiments, many other options arose including linkage of more than one GF to the same self-assembling peptide matrix. For instance, combination of FGF-2 and PDGF-BB with RADA16-II acts synergistically to establish a functional angiogenic system. Thus, FGF-2 activates ECs and PDGF-BB stimulates vascular smooth muscle cells to mature and remodel vascular network. It was found that dual GF delivery was more effective and led to angiogenesis, fibrosis prevention and cardiomyocyte protection. As a result, an enormous variety of research avenues based on combinatorial factors could be explored in order to regenerate cardiac tissue after MI [58]. Nonetheless, the design of self-assembling peptides may be cell specific. Indeed, crucial features to be taken into account to succeed in cardiac regeneration are: adequate tailored scaffold (linkage technique, selection of GF) for a specific cell type and correct timing of graft injection [59].

In addition, chemotaxis is known to drive cell recruitment. Segers et al. have applied this concept to recruit stem cells to injured myocardium. For this, they designed a fusion protein consisting of RADA16-II linked to stromal cell-derived factor-1 (which is a chemokine involved in homing hematopoietic stem cells). After implanting the scaffold into the infarcted myocardium, they observed that it attracted endothelial progenitor cells to the heart thereby improving cardiac function after MI [60].

These examples illustrate a promising approach to cell therapy even though the tailoring of 3D scaffolds continues to be an ongoing area of research. Designing the local microenvironment improves the regenerative response of the injected and the endogenous cells. Whereas most of the attempts are based on tethering factors to self-assembling peptides using the biotin–streptavidin phenomenon, one potentially fruitful alternative could be to fuse growth factors directly to the scaffold. Thus, the protein could be covalently linked to the peptide motifs.

## Conclusions

All in all, self-assembling peptides seem to be an excellent candidate for cell and drug delivery. The characteristics of the nanofibers allow easy anchorage of functional biological



motifs. Advances in bioactive scaffolds allow controlled release of cells, proteins, small molecules, and signaling motifs. Thus, designed self-assembling peptides are widely used in TE whereas herein we focused on cardiac regeneration. Moreover, encouraging applications involve cartilage tissue regeneration [61, 62] and neural restoration via cytokines [63]. This review illustrates different techniques to tailor scaffolds. The data showed that the linkage method of the motif to the self-assembling peptide sequence plays a key role in the therapeutic effect. Indeed, many researchers conclude that the best option would be a covalent bond in order to limit and localize the delivery. Another proposal to promote cell migration is to attach chemo-attractants to the scaffold. Nevertheless, design of new biomaterials should be cell-specific and they will require extensive study of drug release (dose, timing, and spatial range) for a specific target tissue and disease [64].

**Acknowledgments** BTC2009/2010-0010-AND Fellowship Grant from the Government of Andorra to VACPS is greatly acknowledged. The authors of this work want to thank to the European Union, Seventh Framework Program (7FP/2007-2013) for funding received with the project RECATABI to CES under grant agreement no. 229239.

## References

1. Metallo CM, Azarin SM, Ji L, de Pablo JJ, Palecek SP. Engineering tissue from human embryonic stem cells. *Nat Inst Health*. 2009;12(3):709–29.
2. Atala A. Regenerative medicine strategies. *J Pediatr Surg*. 2012;47(1):17–28.
3. Valarmathi MT, Goodwin RL, Fuseler JW, Davis JM, Yost MJ, Potts JD. A 3-D cardiac muscle construct for exploring adult marrow stem cell based myocardial regeneration. *Biomaterials*. 2010;31(12):3185–200.
4. Naderi H, Matin MM, Bahrami AR. Review paper: critical issues in tissue engineering: biomaterials, cell sources, angiogenesis, and drug delivery systems. *J Biomater Appl*. 2011;26(4):383–417.
5. Huang C, Wei H, Yeh Y, Wang J, Lin W, Lee T, Hwang S, Choi S, Xia Y, Chang Y, Sung H. Injectable PLGA porous beads cellularized by hAFSCs for cellular cardiomyoplasty. *Biomaterials*. 2012;33(16):4069–77.
6. Chen Q-Z, Harding SE, Ali NN, Lyon AR, Boccaccini AR. Biomaterials in cardiac tissue engineering: ten years of research survey. *Mater Sci Eng*. 2008;59:1–37.
7. Venugopal JR, Prabhakaran MP, Mukherjee S, Ravichandran R, Dan K, Ramakrishna S. Biomaterial strategies for alleviation of myocardial infarction. *J Royal Soc Interface*. 2012;9(66):1–19.
8. Demirbag B, Huri PY, Kose GT, Buyuksungur A, Hasirci V. Advanced cell therapies with and without scaffolds. *Biotechnol J*. 2011;6(12):1437–53.
9. Langer R, Vancanti JP. *Tissue engineering*. Science. 1993;260:920–6.
10. Campbell CD, Goldfarb D, Roe R. A small arterial substitute: expanded microporous polytetrafluoroethylene: patency versus porosity. *Ann Surg*. 1975;182:138–43.
11. DeBakey ME, Jordan GL, Abbott JP, O'Neal RM. The fate of dacron vascular grafts. *Arch Surg*. 1964;89:757–82.
12. Molina JE, Carr M, Yarnoz MD. Coronary bypass with Gore-Tex graft. *J Thorac Cardiovasc Surg*. 1978;75:769–71.
13. Roh JR, Sawh-Martinez R, Brennan MP, Jay SM, Devine L, Rao DA, Yi T, Mirensky TL, Nalbandian A, Udelsman B. Tissue-engineered vascular grafts transform into mature blood vessels via an inflammation-mediated process of vascular remodeling. *Proc Natl Acad Sci*. 2010;107:4669–74.
14. Nelson DM, Ma Z, Fujimoto KL, Hashizume R, Wagner WR. Intramyocardial biomaterial injection therapy in the treatment of heart failure: materials, outcomes and challenges. *Nat Inst Health*. 2012;7(1):1–15.
15. Dib N, Menasche P, Bartunek JJ, Zeiher AM, Terzic A, Chronos NA, Henry TD, Peters NS, Fernández-Avilés F, Yacoub M, Sanborn TA, Demaria A, Schatz RA, Taylor DA, Fuchs S, Itescu S, Miller LW, Dinsmore JH, Dangas GD, Popma JJ, Hall JL, Holmes DR. Recommendations for successful training on methods of delivery of biologics for cardiac regeneration: a report of the International Society for Cardiovascular Translational Research. *JACC Cardio Int*. 2010;3(3):265–75.
16. Giraud M-N, Guex AG, Tevaearai HT. Cell therapies for heart function recovery: focus on myocardial tissue engineering and nanotechnologies. *Cardiol Res Pract*. 2012;2012:971614.
17. Ptaszek LM, Mansour M, Ruskin JN, Chien KR. Towards regenerative therapy for cardiac disease. *Series Stem Cells*. 2012;379:933–42.
18. Karam J-P, Muscari C, Montero-Menei CN. Combining adult stem cells and polymeric devices for tissue engineering in infarcted myocardium. *Biomaterials*. 2012;33(23):5683–95.
19. Nelson DM, Ma Z, Fujimoto KL, Hashizume R, Wagner WR. Intra-myocardial biomaterial injection therapy in the treatment of heart failure: materials, outcomes and challenges. *Acta Biomaterialia*. 2011;7(1):1–15.
20. Chiu LLY, Radisic M, Vunjak-novakovic G. Bioactive scaffolds for engineering vascularized cardiac tissues. *Macromol Biosci*. 2010;10:1286–301.
21. Hwang NS, Elisseeff J. Controlled differentiation of stem cells. *Nat Inst Health*. 2009;60(2):199–214.
22. Reis LA, Chiu LLY, Liang Y, Hyunh K, Momen A, Radisic M. A peptide-modified chitosan-collagen hydrogel for cardiac cell culture and delivery. *Acta Biomaterialia*. 2012;8(3):1022–36.
23. Xiang Z, Liao R, Kelly MS, Spector M. Collagen-GAG scaffolds grafted onto myocardial infarcts in a rat model: a delivery vehicle for mesenchymal stem cells. *Tissue Eng*. 2006;12(9):2467–78.
24. Chiu LLY, Radisic M. Controlled release of thymosin  $\beta$ 4 using collagen-chitosan composite hydrogels promotes epicardial cell migration and angiogenesis. *J Cont Rel*. 2011;155:376–85.
25. Chimenti I, Rizzitelli G, Gaetani R, Angelini F, Ionta V, Forte E, Frati G, Schussler O, Barbetta A, Messina E, Dentini M, Giacomello A. Human cardiosphere-seeded gelatin and collagen scaffolds as cardiogenic engineered bioconstructs. *Biomaterials*. 2011;32:9271–81.
26. Gao J, Liu J, Gao Y, Wang C, Zhao Y, Chen B, Xiao Z, Miao Q, Dai J. A myocardial patch made of collagen membranes loaded with collagen-binding human vascular endothelial growth factor accelerates healing of the injured rabbit heart. *Tissue Eng*. 2011;17(21–22):2739–47.
27. Shi C, Li Q, Zhao Y, Chen W, Chen B, Xiao Z, Lin H, Nie L, Wang D, Dai J. Stem-cell-capturing collagen scaffold promotes cardiac tissue regeneration. *Biomaterials*. 2011;32(10):2508–15.
28. Cheng K, Blusztajn A, Shen D, Li T-S, Sun B, Galang G, Zarebinski TI, Prestwich GD, Marbán E, Smith RR, Marbán L. Functional performance of human cardiosphere-derived cells delivered in an in situ polymerizable hyaluronan-gelatin hydrogel. *Biomaterials*. 2012;33(21):5317–24.
29. Shachar M, Tsur-gang O, Dvir T, Leor J, Cohen S. The effect of immobilized RGD peptide in alginate scaffolds on cardiac tissue engineering. *Acta Biomaterialia*. 2011;7(1):152–62.

30. Sapir Y, Kryukov O, Cohen S. Integration of multiple cell-matrix interactions into alginate scaffolds for promoting cardiac tissue regeneration. *Biomaterials*. 2011;32:1838–47.
31. Binsalamah ZM, Paul A, Khan AA, Prakash S, Shum-Tim D. Intramyocardial sustained delivery of placental growth factor using nanoparticles as a vehicle for delivery in the rat infarct model. *Int J Nanomed*. 2011;6:2667–78.
32. Ruvinov E, Leor J, Cohen S. The promotion of myocardial repair by the sequential delivery of IGF-1 and HGF from an injectable alginate biomaterial in a model of acute myocardial infarction. *Biomaterials*. 2011;32(2):565–78.
33. Liu Z, Wang H, Wang Y, Lin Q, Yao A, Cao F, Li D, Zhou J, Duan C, Du Z, Wang Y, Wang C. The influence of chitosan hydrogel on stem cell engraftment, survival and homing in the ischemic myocardial microenvironment. *Biomaterials*. 2012;33(11):3093–106.
34. Li Z, Guo X, Guan J. A thermosensitive hydrogel capable of releasing bFGF for enhanced differentiation of mesenchymal stem cell into cardiomyocyte-like cells under ischemic conditions. *Biomacromolecules*. 2012;13(6):1956–64.
35. Baumann L, Prokoph S, Gabriel C, Freudenberg U, Werner C, Beck-Sickingler AG. A novel, biased-like SDF-1 derivative acts synergistically with starPEG-based heparin hydrogels and improves eEPC migration in vitro. *J Cont Rel*. 2012;162(1):68–75.
36. Zhang S. Fabrication of novel biomaterials through molecular self-assembly. *Nat Biotechnol*. 2003;21(10):1171–8.
37. Zhang S, Gelain F, Zhao X. Designer self-assembling peptide nanofiber scaffolds for 3D tissue cell cultures. *Sem Cancer Bio*. 2005;15:413–20.
38. Quintana L, Fernandez Muinos T, Genove E, Olmos MDM, Borros S, Semino CE. Early tissue patterning recreated by mouse embryonic fibroblasts in a three-dimensional environment. *Tissue Eng*. 2009;15(1):45–54.
39. Kyle S, Aggeli A, Ingham E, McPherson MJ. Production of self-assembling biomaterials for tissue engineering. *Trends Biotechnol*. 2009;27(7):423–33.
40. Gelain F, Bottai D, Vescovi A, Zhang S. Designer self-assembling peptide nanofiber scaffolds for adult mouse neural stem cell 3-dimensional cultures. *PLoS one*. 2006;1(1):119.
41. Genové E, Shen C, Zhang S, Semino CE. The effect of functionalized self-assembling peptide scaffolds on human aortic endothelial cell function. *Biomaterials*. 2005;26:3341–51.
42. Branco MC, Pochan DJ, Wagner NJ, Schneider JP. Macromolecular diffusion and release from self-assembled b-hairpin peptide hydrogels. *Nat Inst Health*. 2010;30(7):1339–47.
43. Genové E, Schmitmeier S, Sala A, Borrós S, Bader A, Griffith LG, Semino CE. Functionalized self-assembling peptide hydrogel enhance maintenance of hepatocyte activity in vitro. *J Cell Mol Med*. 2009;XX:1–12.
44. Branco MC, Schneider JP. Self-assembling materials for therapeutic delivery. *Nat Inst Health*. 2009;5(3):817–31.
45. Standley SM, Toft DJ, Cheng H, Soukasene S, Chen J, Raja SM, Band V, Band H, Cryns VL, Stupp SI. Induction of cancer cell death by self-assembling nanostructures incorporating a cytotoxic peptide. *Nat Inst Health*. 2011;70(8):3020–6.
46. Jung JP, Nagaraj AK, Fox EK, Rudra JS, Devgun JM, Collier JH. Co-assembling peptides as defined matrices for endothelial cells. *Nat Inst Health*. 2010;30(12):2400–10.
47. Sieminski AL, Semino CE, Gong H, Kamm RD. Primary sequence of ionic self-assembling peptide gels affects endothelial cell adhesion and capillary morphogenesis. *J Biomed Mater Res*. 2008;87(2):494–504.
48. Bergmann O, Bhardwaj RD, Bernard S, Zdunek S, Barnabé-Heider F, Walsh S, Zupicich J, Alkass K, Buchholz BA, Druid H, Jovinge S, Frisén J. Evidence for cardiomyocyte renewal in humans. *Nat Inst Health*. 2010;324(5923):98–102.
49. Davis ME, Motion JPM, Narmoneva DA, Takahashi T, Hakuno D, Kamm RD, Zhang S, Lee RT. Injectable self-assembling peptide nanofibers create intramyocardial microenvironments for endothelial cells. *Nat Inst Health*. 2009;111(4):442–50.
50. Guo H, Cui G, Wang H, Tan Y. Transplantation of marrow-derived cardiac stem cells carried in designer self-assembling peptide nanofibers improves cardiac function after myocardial infarction. *Biochem Biophys Res Commun*. 2010;399(1):42–8.
51. Chan SS-K, Li H-J, Hsueh Y-C, Lee DS, Chen J-H, Hwang S-M, Chen C-Y, Shih E, Hsieh PCH. Fibroblast growth factor-10 promotes cardiomyocyte differentiation from embryonic and induced pluripotent stem cells. *PLoS One*. 2010;5(12):14414.
52. Guo H, Cui G, Yang J, Wang C, Zhu J, Zhang L, Jiang J, Shao S. Sustained delivery of VEGF from designer self-assembling peptides improves cardiac function after myocardial infarction. *Biochem Biophys Res Commun*. 2012;424:105–11.
53. Altunbas A, Lee SJ, Rajasekaran SA, Schneider JP, Pochan DJ. Encapsulation of curcumin in self-assembling peptide hydrogels as injectable drug delivery vehicles. *Nat Inst Health*. 2011;32(25):5906–14.
54. Hsieh PCH, MacGillivray C, Gannon J, Cruz FU, Lee RT. Local controlled intramyocardial delivery of platelet-derived growth factor improves postinfarction ventricular function without pulmonary toxicity. *Circulation*. 2006;114(7):637–44.
55. Narmoneva DA, Vukmirovic R, Davis ME, Kamm RD, Lee RT. Endothelial cells promote cardiac myocyte survival and spatial reorganization. *Nat Inst Health*. 2009;110(8):962–8.
56. Padin-Iruegas ME, Misao Y, Davis ME, Segers VFM, Esposito G, Tokunou T, Urbanek K, Hosoda T, Rota M, Anversa P, Leri A, Lee RT, Kajstura J. Cardiac progenitor cells and biotinylated IGF-1 nanofibers improve endogenous and exogenous myocardial regeneration after infarction. *Nat Inst Health*. 2010;30(7):1339–47.
57. Davis ME, Hsieh PCH, Takahashi T, Song Q, Zhang S, Kamm RD, Grodzinsky AJ, Anversa P, Lee RT. Local myocardial insulin-like growth factor 1 (IGF-1) delivery with biotinylated peptide nanofibers improves cell therapy for myocardial infarction. *PNAS*. 2006;103(21):8155–60.
58. Kim JH, Jung Y, Kim S-H, Sun K, Choi J, Kim HC, Park Y, Kim SH. The enhancement of mature vessel formation and cardiac function in infarcted hearts using dual growth factor delivery with self-assembling peptides. *Biomaterials*. 2011;32(26):6080–8.
59. Dubois G, Segers VFM, Bellamy V, Sabbah L, Peyrard S, Bruneval P, Hagège AA, Lee RT, Menasché P. Self-assembling peptide nanofibers and skeletal myoblast transplantation in infarcted myocardium. *J Biomed Mater Res*. 2008;87(1):222–8.
60. Segers VFM, Tokunou T, Higgins LJ, MacGillivray C, Gannon J, Lee RT. Local delivery of protease-resistant stromal cell derived factor-1 for stem cell recruitment after myocardial infarction. *Circulation*. 2007;116(15):1683–92.
61. Kopesky PW, Vanderploeg EJ, Kisiday JD, Frisbie DD, Sandy JD, Grodzinsky AJ. Controlled delivery of transforming growth factor b1 by self-assembling peptide hydrogels induces chondrogenesis of bone marrow stromal cells and modulates Smad2/3 signaling. *Tissue Eng*. 2011;17(1–2):83–92.
62. Miller RE, Kopesky PW, Grodzinsky AJ. Growth factor delivery through self-assembling peptide scaffolds. *Clin Orthop Relat Res*. 2011;469(10):2716–24.
63. Gelain F, Unsworth LD, Zhang S. Slow and sustained release of active cytokines from self-assembling peptide scaffolds. *J Cont Rel*. 2010;145(3):231–9.
64. Davis ME, Hsieh PCH, Grodzinsky AJ, Lee RT. Custom design of the cardiac microenvironment with biomaterials. *Nat Inst Health*. 2009;97(1):8–15.
65. Kraehenbuehl TP, Zammaretti P, Van der Vlies A, Schoenmakers RG, Lutolf MP, Jaconi ME, Hubbell JA. Three-dimensional extracellular matrix-directed cardioprogenitor differentiation: systematic modulation of a synthetic cell-responsive PEG-hydrogel. *Biomaterials*. 2008;29:2757–66.